UNIVERSITY OF SOUTHAMPTON

Faculty of Medicine, Health and Life Sciences

School of Medicine

The BOLD MRI Response of the Brain to Alterations in Arterial Blood Pressure

Angela Anagha Darekar

Submitted for the degree of Doctor of Philosophy

September 2009

UNIVERSITY OF SOUTHAMPTON

ABSTRACT

FACULTY OF MEDICINE, HEALTH AND LIFE SCIENCES

DEPARTMENT OF MEDICAL PHYSICS AND BIOENGINEERING

Doctor of Philosophy

THE BOLD MRI RESPONSE OF THE BRAIN TO ALTERATIONS IN ARTERIAL BLOOD PRESSURE

by Angela Anagha Darekar

The impact of blood pressure changes on cerebral blood flow is an important area of investigation. The cerebral autoregulation mechanism acts to maintain blood supply to the brain, despite changes in blood pressure. Blood flow alterations are closely linked to neuronal activation, and this activity can be visualised using blood oxygenation level dependent magnetic resonance imaging (BOLD MRI) – functional MRI. The aim of this project is to investigate the effect of dynamic blood pressure stimuli on the BOLD MRI signal in the brain.

Two blood pressure stimuli were employed; thigh cuff deflation and the Valsalva manoeuvre. BOLD MRI signal changes were measured throughout both challenges. Arterial and venous blood pressure and tympanic membrane displacement (TMD) measurements were also made during these challenges. Blood pressure data was used to drive two linked models. The first model represented cerebral vascular physiology (Ursino) and this fed into a second model (Buxton), which predicted the resulting BOLD signal changes. This allowed comparison with experimental BOLD data. TMD data was also compared to intracranial pressure changes predicted by the Ursino model.

The experimental BOLD data was found to agree reasonably well with the BOLD signal changes predicted by the modelling. BOLD signal changes are most influenced by deoxyhaemoglobin changes, predominantly as a result of blood flow alterations during the blood pressure challenges, which are not immediately compensated for by the autoregulation mechanism. TMD changes did not reflect intracranial pressure changes predicted by the modelling.

In conclusion, if such blood pressure changes do occur during a functional MRI experiment, they may cause changes in the BOLD signal that are not due to neuronal activation. These signal changes may be employed to investigate the cerebral autoregulation mechanism across the brain, or to correct for inaccuracies in functional MRI data in patients with impaired cerebral autoregulation.

Contents

List of figures

List of tables

Declaration of Authorship

I, Angela Anagha Darekar, declare that the thesis entitled: The BOLD MRI response of the brain to alterations in arterial blood pressure, and the work presented in the thesis are both my own, and have been generated by me as the result of my own original research. I confirm that:

- this work was done wholly or mainly while in candidature for a research degree at this University;
- where any part of this thesis has previously been submitted for a degree or any other qualification at this University or any other institution, this has been clearly stated. Small sections of this PhD thesis have been taken from the two MSc theses as described below:

  Section 2.1 Brain anatomy:

  > *Darekar AA (1998) Diffusion Tensor and Perfusion MRI Applied to Intra-axial Brain Tumours*, MSc thesis, King's College, University of London.

  Section 3.1 Basic theory of MRI:

  > *Darekar AA (1998) Diffusion Tensor and Perfusion MRI Applied to Intra-axial Brain Tumours*, MSc thesis, King's College, University of London.
  >
  > *Darekar AA (1996) NMR Relaxation Times of Articular Cartilage and the Effect of Impact Loading*, MSc thesis, University of Aberdeen.

  Section 3.2 Spatial encoding in MRI:

  > *Darekar AA (1998) Diffusion Tensor and Perfusion MRI Applied to Intra-axial Brain Tumours*, MSc thesis, King's College, University of London.

- where I have consulted the published work of others, the source is always clearly attributed;

- where I have quoted from the work of others, the source is always given. With the exception of such quotations, this thesis is entirely my own work;
- I have acknowledged all main sources of help;
- where the thesis is based on work done by myself jointly with others, I have made clear exactly what was done by others and what I have contributed myself;
- None of this work has been published before submission.

Signed:……

Date:……

Acknowledgements

First and foremost I would like to thank my main supervisor, Dr Tony Birch. Without him, this project would not have been initiated and it is due to his unfailing patience, enthusiasm and encouragement that it has progressed and that this thesis has been completed. His support, help and guidance over the many years that this PhD has been undertaken has never faltered, and I am immensely grateful to him, both as a supervisor and as my line manager for some of that time.

I feel privileged to have been given the opportunity to carry out this work and I appreciate the time and funding afforded to me to do so by the Department of Medical Physics and Bioengineering, Southampton University Hospitals NHS Trust. Thanks must go in particular to Dr Peter Jackson, who as Head of Department encouraged me to undertake this PhD and provided supervisory support. I would also like to express my appreciation to my other supervisors, Prof John Fleming and Dr Peter Garrard for their help and advice.

A big thank you to the Department of Radiology at Southampton University Hospitals NHS Trust, and in particular the MRI Superintendent Radiographer, Susan King, for allowing me to use the MRI scanner in the evenings and weekends to carry out my experimental work. In addition, I must express my huge gratitude to all my volunteers who patiently endured my experiments without complaint. Many thanks also to the volunteers who carried out the region of interest analysis on the jugular vein MRI data.

Also, Dr Robert Marchbanks' advice and expertise has been invaluable in enabling me to successfully carry out the experiments involving tympanic membrane displacement measurements.

Lastly, I would like to thank my friends and family, whose constant support and wise words are enormously appreciated. I would especially like to thank my parents for their unconditional support and most of all, my sister, Amanda Darekar, for helping me every step of the way.

Chapter 1 Introduction

1.1 The BOLD effect and functional MRI

The consequence of blood pressure changes on cerebral blood flow is an important area of investigation. Blood supply to the brain is preserved despite changes in blood pressure by means of the cerebral autoregulation mechanism[1], where vessels alter their resistance accordingly to maintain blood flow. This is vital as the brain is a highly metabolic organ and any interruption to this supply could lead to loss of function or brain injury, as is the case in ischaemic attacks. To this end, there have been many investigations into the relationship between blood pressure changes and the blood flow response[2]. Most recent studies have involved the use of transcranial Doppler to measure these flow changes. Magnetic resonance imaging (MRI) is a non-invasive imaging technique that can also be used to interrogate cerebral haemodynamics.

Changes in blood flow in the brain are closely linked to neuronal activation and this activity can be imaged using a technique known as functional MRI[3]. It is used widely in research to examine cerebral function in response to motor, sensory and cognitive tasks. This technique relies on the mechanism of neurovascular coupling, i.e. the coupling between neuronal activation and blood flow, to map cerebral metabolism changes across the brain in response to a neuronal stimulus. Clinical applications, such as language and memory function localisation prior to neurosurgery, are being developed. Functional MRI employs a phenomenon known as the BOLD (blood oxygenation level dependent) MRI effect to identify areas of the brain involved in specific tasks. This technique relies on the changes in blood oxygenation that occur during periods of brain activity to highlight the areas responsible for this activity. During activation, there is an increase in cerebral metabolism. However, there is also a disproportionately large increase in blood flow during activation. This results in an increase in oxyhaemoglobin and a decrease in deoxyhaemoglobin concentration in activated areas of the brain. The BOLD

effect results from a difference in magnetic susceptibility between deoxyhaemoglobin and the surrounding tissue, which leads to spin dephasing and a reduction in signal in a gradient echo MRI experiment. Conversely, oxyhaemoglobin has a similar magnetic susceptibility to brain parenchyma, and as such, there is little dephasing of the spins, and no reduction in signal. Hence, the deoxyhaemoglobin content of a voxel determines the BOLD signal intensity. By comparing the MRI signal across the brain during rest and activation, areas that are activated whilst carrying out a particular task have a reduced deoxyhaemoglobin content and an increased MRI signal and can be identified.

The vast majority of functional MRI studies are carried out using the BOLD technique. This technique describes the perfusion state of the brain at rest and during activation, but provides no information about the absolute value of perfusion in the brain. This can be assessed using a number of methods, for example using contrast agents (a blood volume technique) or a technique such as arterial spin labelling[4] (ASL, a blood flow technique). Contrast agents require several injections and thus have not been routinely used for functional imaging. ASL is mainly used for perfusion studies as an absolute measure of flow, but is also used to image regional brain function. ASL involves tagging blood outside the slice of interest (by applying a 180° radiofrequency inversion pulse), and then detecting this tagged blood as it flows into this slice a period of time later (TI). The experiment is repeated without tagging the blood, which creates a control image. The two sets of images are subtracted to provide an ASL difference image with the signal attributed to static spins subtracted out, leaving signal from just the flowing spins, i.e. signal from arterial blood delivered to the slice of interest during the time interval, TI. It acts as an endogenous contrast agent and reflects a change in arterial flow rather than venous oxygenation, which is the case in the BOLD method[5].

The advantage of ASL over BOLD is that it provides much better accuracy in the localisation of activation, as there are questions regarding the accuracy of the BOLD technique for this[6]. ASL also allows investigation into chronic

alterations in the perfusion state of the diseased brain, for example in stroke[7], whereas BOLD highlights the change in perfusion state during a task and provides no quantitative baseline perfusion information. There are, however, some disadvantages to the ASL technique; there are several sources of error in this method. The transit delay, i.e. the time it takes for blood to travel from the inversion slice to the slice of interest, varies across the brain, particularly in areas of disease such as stroke or stenosis. If this delay is too long, the inverted magnetisation will relax leading to a loss of signal from the labelled blood. There may be also issues regarding incomplete inversion of the tagged blood, variations in local T_1 values across the brain and signal contributions from large vessels that traverse the slice of interest[5]. The other issue with ASL and measuring functional activation is the much smaller signal change with activation induced in ASL imaging, 0.5-1.0%, compared with a 3-5% change in BOLD imaging[8].

Although there are advantages to detecting brain activation using ASL, dealing with the technical issues mentioned above is not simple and as such, the majority of activation studies employ the BOLD technique. This is the technique under investigation in this project. In addition, the technique of arterial spin labelling introduces a delay in acquisition between the tag and control image of at least 2 seconds, which is slightly too long to adequately sample the signal changes that are expected during the blood pressure stimuli applied in this project.

1.2 The Problem

It is assumed that blood pressure remains constant during functional MRI experiments; however this may not always be the case[9,10]. It is not clear how blood pressure changes affect functional MRI data. A change in blood pressure is likely to alter the flow and volume of intracranial blood, and this is postulated to alter the concentrations of oxyhaemoglobin and deoxyhaemoglobin within a voxel, thus affecting the BOLD signal. Blood flow

and volume changes that do not result from neuronal activation, but from blood pressure changes, may be a source of errors in functional MRI data. This could lead to inaccuracies in functional MRI data that may result in misinterpretation of functional MR images. The problem of impaired autoregulation and the effect on functional MRI studies has been mentioned by a number of authors relating to a number of conditions including stroke, cerebral artery disease and tumours[11,12,13,14,15,16]. However, no studies have addressed the issue using the same methodology used in this project, i.e. by examining the BOLD signal response to rapid, dynamic changes in blood pressure.

This is one of the motivations for this project; do blood pressure alterations lead to changes in the BOLD signal, and if this is the case, what causes these changes? The benefits of this are two-fold; firstly, the consequence of blood pressure changes on the BOLD signal and functional MRI data will be elucidated and secondly, it may lead on to new imaging data pertaining to the autoregulation mechanism, as it is this mechanism which modulates blood flow, and therefore, the BOLD signal, in response to blood pressure changes.

There are two main scenarios where this would be of particular concern. Firstly, in subjects with normal autoregulation this mechanism takes a few seconds to act during rapid blood pressure changes. If these blood pressure changes are coincident with the particular paradigm employed in a functional MRI experiment, blood flow and hence BOLD signal changes may result that are not due to neuronal activation, thus leading to erroneous results in such a study.

Secondly, in the case of impaired autoregulation, blood flow alteration as a result of blood pressure changes would not be adequately compensated for. For example, if blood pressure increases, blood flow would increase and in a functional MRI experiment, this could be interpreted as flow increases due to neuronal activation. This would particularly be a problem in specific areas of the brain that have impaired autoregulation. The converse result could also

occur leading to false negative or decreased demonstrations of brain activation. For example, this has been reported in the vicinity of brain tumours[11].

Thus, more specifically, the questions that are being addressed in this project are: what changes are observed in the BOLD signal as a result of rapid blood pressure changes and does the autoregulation mechanism influence these changes?

Other groups have investigated the effect of blood pressure changes on the BOLD signal, but most of these studies have imposed blood pressure changes over a much longer timescale than that used in this project. Even when changes have been imposed rapidly, the main focus of the investigation has been the cognitive functional MRI response of the brain to such changes[17,18,19], rather than explicitly trying to explain the signal changes as a results of flow, volume and deoxyhaemoglobin alterations during the blood pressure challenges. In other studies, challenges that do invoke blood pressure changes have been used, but the blood pressure involvement in the subsequent BOLD signal changes has not been considered[20,21,22]. Some modelling work has started to try and link vascular changes to BOLD signal changes after blood pressure provocation, but this has been carried out in a theoretical manner, with no experimental input[23].

The proposal is to predict the effect of a change in blood pressure on the BOLD MRI signal using mathematical modelling and compare this prediction with measured data. Experimental data will be acquired by invoking rapid blood pressure changes in healthy volunteers whilst measuring the BOLD signal. This work will enhance our understanding of cerebral haemodynamics and the origin of the BOLD signal. Once the BOLD response to dynamic blood pressure changes has been characterised, future work can assess the impact of both normal and pathological physiological variations across the brain on this response. It is hypothesised in the literature that blood pressure changes affect blood flow abnormally in regions of the brain affected by

disease or injury[11,12], and this can lead to artefacts in BOLD MRI data. Although this is detrimental in functional MRI, regional variations in the BOLD response to blood pressure changes could highlight areas of abnormal cerebral vascular physiology. If the MRI signal changes that are observed across the brain, due to a change in blood pressure, can be identified and analysed, it may be possible to generate maps of the brain that demonstrate aspects of vascular physiology related to autoregulation. This could be valuable clinically; abnormalities of the cerebral vascular system that are currently not shown on MRI could be highlighted using a non-invasive, whole brain imaging technique. In addition, it may be possible to use the resulting data to correct for errors, due to impaired autoregulation, in functional MRI studies on such patients.

1.3 Clinical relevance

Characterising the BOLD response to changes in blood pressure could be extremely valuable clinically. Novel MRI parameters could be derived from this data and these could provide new information about vascular physiology. This information could be useful in cases where the cerebral autoregulation mechanism is impaired, as it is hypothesised that this would have an impact on the BOLD response to blood pressure changes. Cerebral autoregulation is known to fail in a wide variety of circumstances. In chronic hypertension both the upper and lower limits of autoregulation are shifted towards higher pressures. In diabetes mellitus, one of the long-term effects is that CBF autoregulation is impaired[24,25] and blood flow becomes partially pressure passive. This could be due to some atherosclerosis of larger vessels and diabetic microangiopathy in the brain[26]. Head injury and sub-arachnoid haemorrhage are conditions where autoregulation can commonly become disturbed[27,28]; there can be both a loss of autoregulation and impaired autoregulation. Other neurological conditions where impaired autoregulation is a feature are intracranial tumours[11,12], ischaemic cerebrovascular

diseases[29], acute ischaemic stroke[30], epilepsy[31], infections and spreading depression and migraine[26]. Other pathologies have also been investigated with respect to cerebral autoregulation. This includes studies of premature and critically ill infants[32,33,34] and in cases of anaemia[35], hypertension[36,37], cardiac arrest[38], carotid artery disease[39,40,41] and hepatic disease[42]. Impairment of the autoregulation mechanism could lead to inaccuracies in the results when carrying out BOLD fMRI in patients with these conditions.

The ability to assess the brain's response to a change in blood pressure across the whole brain using MRI could be extremely valuable. At the moment, modalities such as MRI, SPECT and PET can measure blood flow and volume changes globally across the brain, but none of these can combine both the temporal resolution and whole brain coverage of BOLD MRI. It is hypothesised that the mechanism of blood flow regulation will fail before a decrease in blood flow to the brain is seen. Therefore, many conditions that are currently related to an impairment of blood flow to the brain, could be potentially diagnosed at an earlier stage if poor autoregulation, or an MRI parameter related to it, could be identified. This has begun to be investigated in cases of dementia[43,44]. TCD measurements of autoregulation are sometimes used to monitor conditions such as ischaemic stroke. It is envisaged that MRI could be used for monitoring disease progression, as a one off measurement, or as a pre and post surgical assessment tool. Some specific areas in which this type of technique could be useful include determining the cause of dizziness and balance problems, or as a diagnosis tool for clinical depression. Alzheimer's disease is another condition that could benefit from this technique, as impaired autoregulation could be an early indication of the disease[45,46,47]. It could also be used to monitor the treatment or progression of the disease.

Elucidation of the BOLD response to blood pressure changes should also allow a better understanding of the variations seen in functional MRI experiments, i.e. whether these variations are due to blood pressure changes as well as the effect of cerebral metabolism changes. In addition, if

autoregulation is impaired, blood flow changes may occur as a result of blood pressure alterations. This would mean that when comparing the BOLD signal during rest and activation two periods, identifying areas of the brain that are being activated could be more difficult. The difference in rest and activation BOLD signal (at magnet strengths of 1.5 T) is only approximately 3%[3], which means that this signal difference can easily be masked by additional variations in signal that are not purely due to functional activation. Impaired autoregulation may also affect the time course of signal changes in a functional MRI experiment. Hence, if impaired autoregulation can be detected, these errors in the functional MRI data could be recognised and maybe even be corrected for. This should increase the reliability and accuracy of the BOLD technique in functional MRI. This would be particularly important when carrying out functional MRI in patients with some of the conditions mentioned above.

If the changes in the BOLD signal that are observed in response to dynamic blood pressure changes can be characterised within both a normal population and in different categories of patients, this could lead to a novel method of using BOLD MR imaging to provide new physiological information. A similar approach is used in relation to cerebrovascular reactivity to CO_2 inhalation[48,49], but not as yet as a method to assess the brain's response to blood pressure changes.

1.4 Modelling aspects of the project

A significant component of this project will be to use mathematical modelling to try and elucidate the signal changes that are observed. Two models will be used to explain the signal changes. Firstly, an electrical circuit analogue of the cerebrovascular circulation will be set up. This is a model based on the work of Ursino[50], who has contributed a great deal to this field of investigation. This will enable inputs such as the arterial blood pressure and venous blood pressure to be incorporated, and these inputs will be derived from measured

data. This model will take into account the dynamic aspects of blood flow in the brain in response to transients in arterial blood pressure; in particular, the action of the autoregulation mechanism in response to these blood pressure changes. Pressure changes across the whole vascular tree will be able to be derived and also information regarding intracranial pressure changes. In addition, the dynamics of arterial and venous blood flow and venous blood volume will be able to be examined, in response to varying blood pressure challenges. Outputs from this model, namely venous blood flow and volume will be used as inputs into a model that describes the BOLD-MRI signal in terms of the deoxyhaemoglobin content of venous blood and venous blood volume. This is part of a model first described by Buxton[51], which was later amended and improved by Obata[52]. This will allow the comparison of predicted BOLD-MRI signal changes (in response to arterial blood pressure changes), to those that have been observed in 9 healthy volunteers. Another measurement that has been made is that of the tympanic membrane displacement (TMD) response to similar arterial blood pressure challenges. Measurements of TMD are thought to reflect ICP changes within the cranium, and this will also be able to be investigated by examining the ICP changes predicted by the model of the cerebrovascular circulation.

The models will predict the BOLD response to two blood pressure challenges, namely thigh cuff deflation and the Valsalva manoeuvre. These are commonly used to alter arterial blood pressure over a short timescale and in a non-invasive manner. They are also challenges that can be carried out easily and safely in the MRI scanner environment. These challenges are described more fully in Chapter 4.

1.5 The Experiments

The aim of this project is to improve our understanding of and to quantify the BOLD signal change in response to a fast, dynamic change in blood pressure. Two methods have been used to modify blood pressure in the

brain. The first involves inflating and suddenly deflating thigh blood pressure cuffs to achieve a step reduction in arterial blood pressure. The other method that has been employed is the Valsalva manoeuvre, that is, forced expiration against a closed glottis, which is a strong modulator of both arterial and venous blood pressure. We have hypothesised that BOLD signal changes will be seen due to arterial blood flow changes (resulting from the changes in blood pressure and the subsequent cerebral autoregulation response) propagating through the vascular tree in the brain. It is also questioned whether venous pressure changes influence the BOLD signal during these dynamic blood pressure challenges. This hypothesis has been investigated by carrying out experiments on a small cohort of healthy volunteers. The BOLD signal has been measured whilst imposing the two blood pressure stimuli in turn and this signal has then been compared with mathematical modelling predictions of this response to test our understanding of the origin of the observed signal changes. Additional measurements were carried out on the volunteers to obtain input data for the model. Angiographic MR images of the internal jugular vein were also acquired during the same blood pressure challenges. The resulting change in cross sectional area is used to derive the changes in jugular venous blood pressure occurring during these challenges. Continuous measurements of blood pressure, using a Finapres device, were made for each volunteer (outside the scanner environment) to record their blood pressure alterations during the thigh cuff deflations and Valsalva manoeuvres. The arterial and venous blood pressure data has been used in a two-stage model to predict the BOLD signal changes that are observed. Arterial and jugular blood pressures are used as inputs to the first stage of this model (which has been developed by Ursino) and used to predict cerebral venous flow and volume changes. The outputs from the Ursino model are incorporated into the second stage (developed by Buxton and Obata) to predict the BOLD MRI signal. The results from the modelling are compared to the measured BOLD data. The models will eventually allow predictions of BOLD signal changes in response to any blood pressure

variations, and enable the effect of physiological features, such as the autoregulation mechanism, to be examined. At the same time, tympanic membrane displacement (TMD) measurements were also made to investigate the intracranial pressure changes taking place. Changes in intracranial pressure determined from these measurements are compared to those derived from Ursino's model.

1.6 Outline of thesis and original contribution

The thesis comprises eight chapters. Each is summarised below:

Chapter 1 – Introduction

This chapter sets the scene for the project. There is a brief description of the BOLD technique and its application to functional MRI. The problem of the influence of blood pressure changes on BOLD data is defined and explored in terms of clinical relevance and there are descriptions of both the modelling and experimental aspects of the project.

Chapter 2 – Brain anatomy and physiology

This chapter covers anatomy and physiology of the brain relevant to this project. This includes basic brain anatomy, including that of the cerebral vasculature, vascular physiology, brain metabolism and the function of the cerebral autoregulation mechanism.

Chapter 3 – Overview of Magnetic Resonance Imaging

An introduction to MRI theory is provided in this chapter. This includes the fundamentals of the technique, and this description is extended to include echo planar imaging and the BOLD technique.

Chapter 4 – Background information

This chapter provides some more background information more specific to the project. This includes a literature review of the BOLD technique and previous investigations into the effects of blood pressure changes, the measurement of cerebral reactivity, the influence of the Valsalva manoeuvre and a brief consideration of resting state functional MRI. The next section deals with the mathematical modelling aspects of the project. The final section of this chapter describes the techniques used to alter and measure both blood pressure and intracranial pressure (ICP).

Chapter 5 – Methods

This chapter describes the methods for all aspects of the project, both experimental and modelling. The chapter starts with a description of the experimental study design, and then goes on to describe the application of the two blood pressure stimuli. Measurements of arterial and venous blood pressure and intracranial pressure are described next. The final two sections describe the methods relating to the BOLD MRI experiments and the modelling work respectively.

Chapter 6 – Experimental results

This chapter presents all the experimental results from all nine volunteers individually and a mean of all subjects. The data that is presented is the arterial blood pressure data, the venous blood pressure data, the tympanic membrane displacement data and the BOLD MRI data obtained from three regions of interest, two grey matter regions (cortical and one at the back of the brain) and one white matter region of interest. Some numerical data is derived from these plots and there is some discussion of the results.

Chapter 7 – Modelling results

The results from the modelling work are presented in this chapter. This includes two sets of plots, one pertaining to the BOLD modelling results and the corresponding inputs and outputs (arterial blood pressure, venous flow and volume, deoxyhaemoglobin and BOLD signal modelling prediction). This data is compared to the BOLD experimental data obtained from the grey matter (back of brain) region of interest. The other set of plots concerns the prediction of intracranial pressure changes occurring during the blood pressure challenges. These intracranial pressure changes (derived from the Ursino model) are compared to the tympanic membrane displacement results. Arterial blood pressure and jugular venous blood pressure data is also presented. Both sets of plots are presented for the mean data from nine volunteers, and for thigh cuff deflation and Valsalva manoeuvre experiments. Again, some numerical data is derived from these plots.

Chapter 8 – Discussion, conclusions and further work

This final chapter draws together the results from the experimental and modelling aspects of the project. The issues regarding the implementation of the two models, the Ursino and Buxton models, are considered. Errors and issues concerning the experimental data that has been acquired are also discussed and model outputs are compared to the experimental data. In the next section the physiological importance of these results is considered in the form of four questions:

1) *Which physiological factors dominate the BOLD signal changes observed in response to rapid blood pressure changes?*
2) *What are the implications of these changes on functional MRI studies?*
3) *Can information about the physiological processes occurring (i.e. autoregulation) be deduced from these studies?*

4) *Can any information about intracranial pressure be derived from this data?*

Further work is discussed in the next section, and the chapter ends with the final conclusions that can be made from the work carried out in this project.

Original contribution

The original contribution of this work has involved the investigation of fast, dynamic blood pressure changes and their impact on the BOLD MRI signal. The two blood pressure challenges that have been imposed are the inflation and then rapid deflation of thigh blood pressure cuffs, and the action of the Valsalva manoeuvre. Neither of these stimuli has been investigated in terms of the blood pressure change that is taking place and its subsequent effect on the BOLD MRI signal changes in the brain. The experimental data from the BOLD MRI experiments has been compared to predictions from modelling work. The models that have been used are the Ursino[50] model of the cerebral vasculature and BOLD signal changes described by Buxton[51] and Obata[52]. A similar approach has been used before[23], but no experimental work has been carried out to validate this modelling approach.

The measurement of jugular vein pressure is another new aspect of this project. There is little information the literature regarding *venous* pressure changes during such blood pressure alterations.

Another component of this project was to investigate the intracranial pressure (ICP) changes taking place during the blood pressure challenges. Tympanic membrane displacement measurements (which are thought to reflect ICP changes) were also made during the same blood pressure challenges described above. These measurements have not been carried out before. ICP changes were derived from the Ursino model and compared to the TMD data.

Chapter 2 Brain anatomy and physiology

2.1 Brain anatomy

For completeness, this section will give a brief overview of the gross anatomy of the brain[53,54].

The brain is a very delicate organ and as such must be adequately protected. It is encased within the skull and is furthermore protected by layers of connective tissue (the meninges) and cerebrospinal fluid (CSF). The outer layer of this tissue is the dura mater, the middle layer is the arachnoid mater and the inner layer is the pia mater. The dura mater is split into four sections and is separated by the falx cerebri (which separates the right and left hemispheres) and the tentorium cerebelli, which separates the cerebrum and the cerebellum. The venous sinuses are contained between the layers of the dura mater. The arachnoid mater is separated from the pia mater by the subarachnoid space, which contains cerebrospinal fluid. The pia mater is a very thin, delicate membrane and is penetrated by the pial vessels, which supply the brain cortex.

A longitudinal fissure separates the cerebral hemispheres. These consist of four lobes, the frontal, parietal, occipital and temporal lobes, which are named after the skull bones overlying each of them. Each lobe is responsible for different functions, for example the frontal lobe is important for motivation whereas the temporal lobe is responsible for some aspects of the speech mechanism and memory.

Between the cerebrum and the brain stem is the diencephalon, which contains the thalamus, subthalamus, hypothalamus and epithalamus. The majority of the diencephalon is made up of the thalamus.

The brain stem connects the spinal cord to the brain and is made up of the medulla oblongata, pons and mid-brain. Most cranial nerves enter the brain via the brain stem and it is responsible for many functions. The medulla oblongata is the most inferior section of the brain stem. Superior to the

medulla is the pons, and lastly, the mid-brain is most superior. White matter tracts traverse the mid-brain conducting motor and sensory commands.

The cerebellum is located posterior to the brain stem and consists of the superior and inferior vermis and the cerebellar hemispheres. There are three white matter tracts that connect the cerebellum to the brain stem. Different parts of the cerebellum are responsible for balance, muscle tone, coordination and fine movement.

The corpus callosum occupies the medial surface of the brain in the midline. This is a large white matter tract that connects the two hemispheres of the brain at the base of the longitudinal fissure. This is the main commisure that transmits sensory information from one hemisphere to the other.

The basal ganglia are nuclei situated in the inferior cerebrum, the diencephalon and the mid-brain. The main function of the basal ganglia is to coordinate smooth motor movements.

A large cavity, the lateral ventricle, is found in each cerebral hemisphere. Each lateral ventricle is separated by septa pellucida. They are connected to the third ventricle by interventricular foramen, in the diencephalon. This third ventricle is connected to the fourth by the cerebral aqueduct in the pons. This fourth ventricle is connected to the central canal of the spinal cord. Cerebrospinal fluid (CSF) is produced in and flows through the ventricles and is similar to plasma or interstitial fluid. Its function is to protect the spinal cord and brain and provide nutrients to the central nervous system.

2.2 Brain vascular anatomy

The brain is perhaps the most complex and important organ in the body. Brain cells must be supplied with a continuous source of oxygen and glucose and this is delivered via the blood supply. Because of this, it is imperative that blood flow is maintained, and at a constant level. The brain receives 20% of the cardiac output and consumes 20% of the oxygen used by the

body at rest, despite accounting for only 2% of the human body weight. If blood flow to the brain becomes impaired in any way, then a loss of consciousness may occur very rapidly and if this is not reversed then irreversible brain damage may arise within a few minutes[54]. This is the case in ischaemic stroke and loss of the autoregulation mechanism may be a precursor to this.

The human body has developed in such a way that blood flow is maintained despite various challenges to it. By examining cerebral vascular anatomy, as well as physiology, it is possible to understand how this works. Blood is delivered to the brain tissue by four arteries, the two internal carotid arteries and two vertebral arteries, and branches of these arteries give rise to the circle of Willis. This is a circuit of blood vessels that ensure that blood flow to the brain is maintained even if one of the supplying arteries becomes occluded or obstructed[54].

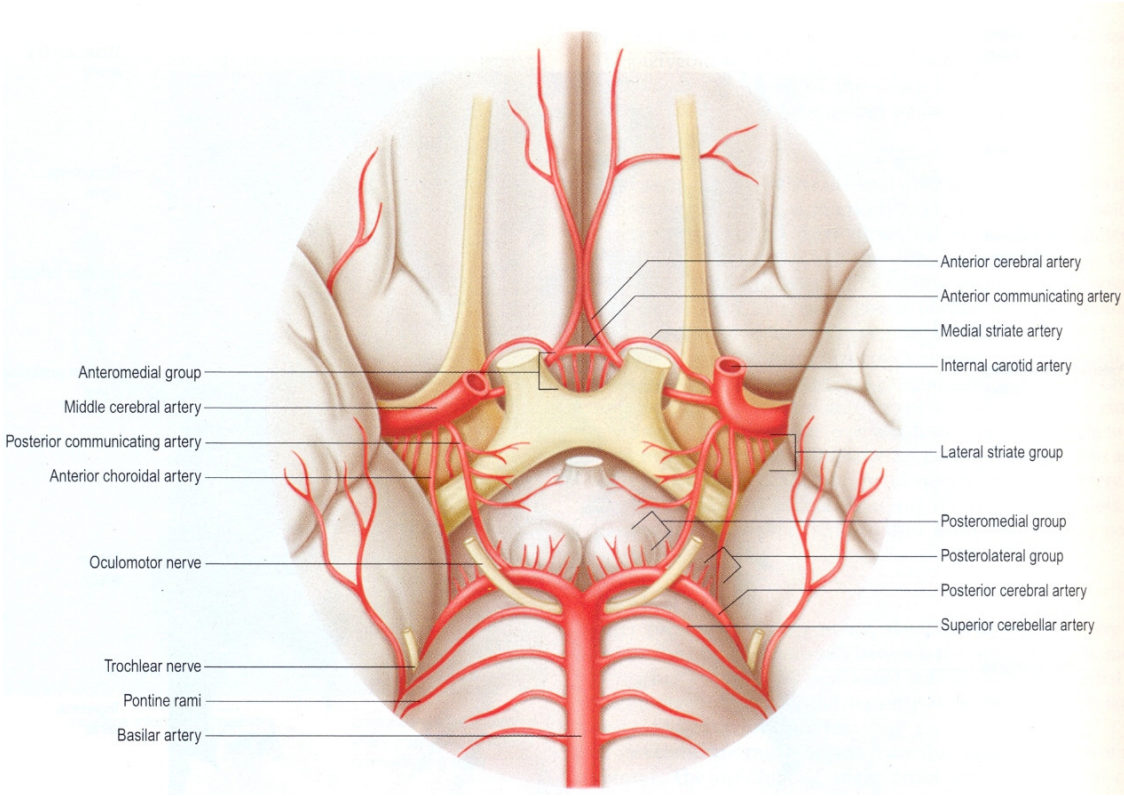

Figure 1: Anatomy of the circle of Willis (used with permission from Gray et al, 2005[55]).

In humans, each of the carotid arteries contributes 40% of the total perfusion of the brain[26]. Each internal carotid artery enters the cranial cavity through the foramen lacerum and divides into four further branches: the anterior cerebral, the middle cerebral, the anterior choroidal and the posterior communicating arteries. The anterior and middle cerebral arteries form the anterior circulation and supply the forebrain. Branches from these arteries supply the cortex and the deep structures in the brain such as the basal ganglia, thalamus and internal capsule.

The two vertebral arteries enter the cranial cavity through the foramen magnum where they fuse to form the basilar artery at the level of the pontomedullary junction. The basilar artery divides into the two posterior cerebral arteries, which then join the posterior communicating arteries to form the circle of Willis. Branches from all of these arteries supply the posterior cortex, the midbrain and the brain stem[54].

Dorsa-lateral arteries, such as the posterior inferior cerebellar artery (PICA) and the anterior inferior cerebellar artery (AICA), which supply the medulla and pons, and other branches of the basilar artery (the paramedian and short circumferential arteries) can be common sites of occlusion in the brain and result in specific deficits of brain function[26]. Arterial boundary zones are areas of the brain where ischaemic brain damage is most often observed following rapid, severe hypotension, such as that following cardiac arrest. They are localised at the territorial limits of the major arteries. These regions are shown in the figure below:

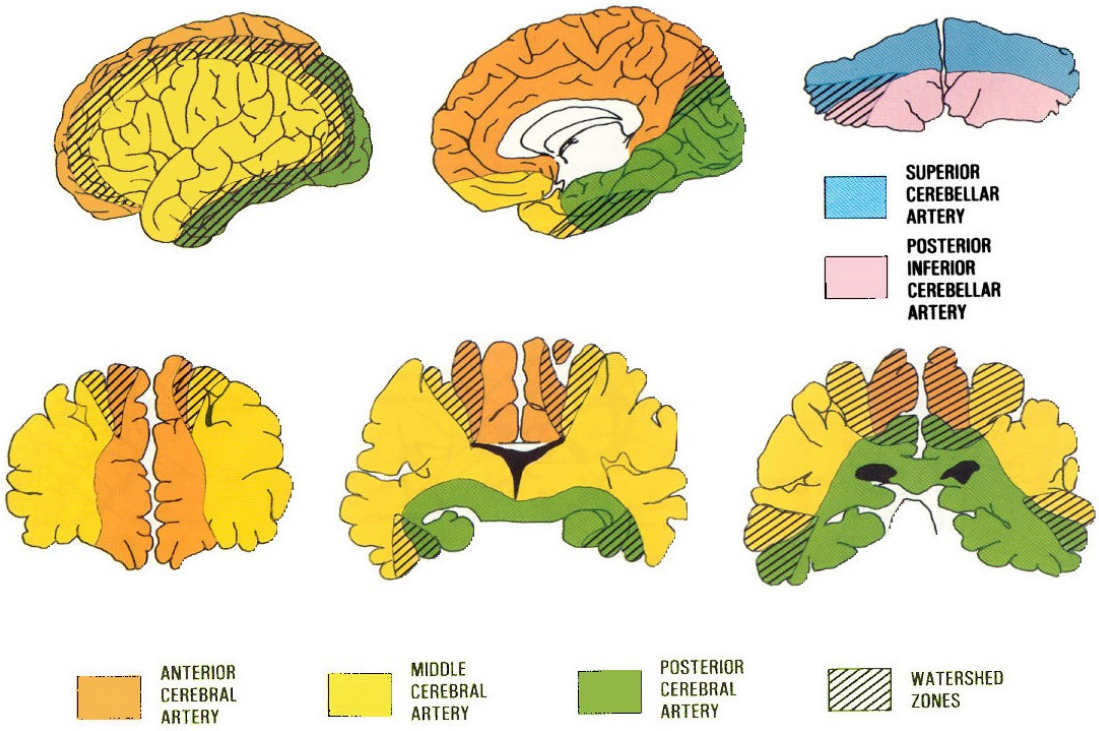

Figure 2: The cerebral and cerebellar arterial boundary zones (used with permission from Edvinsson et al, 1993[26]).

Pial arteries pass through the pia mater to supply cortical tissue. These are small vessels with a diameter of approximately 100 µm, they are known as resistance vessels. It is the vasoconstriction and vasodilation of these vessels that is a primary component of the autoregulation mechanism.

Arterioles penetrate the brain cortex perpendicular to the surface and give rise to capillaries at all laminae. Pre-capillary sphincters seem to be absent in the cerebral circulation, so regulation of resistance (or blood flow) is due to the arterial and arteriolar structures[56]. The distribution of capillaries within the central nervous system is heterogeneous and this is related to the number of synapses in the region. There is thought to be a proportional relationship between aerobic metabolism and microvascular density in the brain, i.e. between blood flow and capillary density[26].

Blood that drains from the capillaries collects in the large venous sinuses located in the folds of the dura mater. This blood then empties in to the internal jugular veins either side of the neck, and then into the brachiocephalic veins. These drain into the superior vena cava, which return the deoxygenated blood to the right atrium of the heart[26].

The structure of the vessels in the brain is fairly similar for both arteries and vein of all sizes. There are, however, some differences. The arteries have much thicker walls than the venous system. Both types of vessel have three distinct layers. In arteries, the outermost layer is the tunica adventitia, which comprises 31% of the total wall thickness. This is made up of elastic and collagen fibres tissue, which provide strength and protection to this elastic vessel. The middle layer is the tunica media, which is the thickest component of the vessel wall (52% in arteries) and it consists of a large proportion of vascular smooth muscle. This smooth muscle is arranged concentrically and controls vasoconstriction and vasodilation of the vessels, and is innervated by the sympathetic nerves of the autonomic nervous system. The innermost layer, the tunica intima, is the thinnest layer and actually consists of two layers; a layer of flat endothelium and a layer of elastic fibres (which separate it from the tunica media) called the internal elastic membrane. The next figure shows a cross section of a cerebral artery:

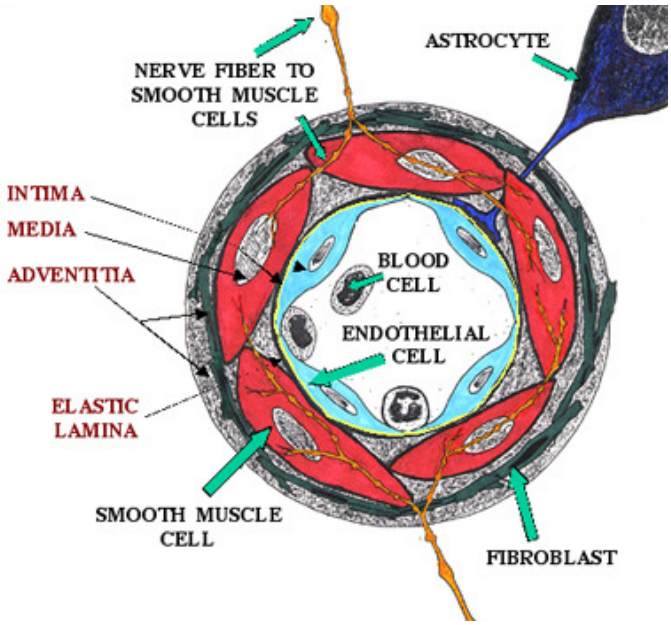

Figure 3: Cross section of the cerebral artery wall (Illustration courtesy of Dr Vini G Khurana, www.brain-aneurysm.com)[57].

The proportion of elastic tissue in the arterial vessels will vary according to the type of arterial vessel, and this relates to their specific function. The largest vessels are elastic arteries and these contain more elastic tissue, which allow them to stretch to accommodate the volume of blood pumped out during each cardiac cycle. In the brain, major cerebral arteries are much thinner than equivalent arteries elsewhere in the body. This may be because the arterial pressure pulse (during systole) is damped by the CSF that surrounds the vessels within the cranial cavity[26]. Muscular arteries contain more smooth muscle and less elastic tissue, which makes them less distensible. Finally, the arterioles are predominantly made up of smooth muscle fibre. However, the more distal arterioles have a tunica intima surrounded by only a few smooth muscle cells. As mentioned previously, arterioles are the primary vessels that regulate blood pressure and flow in the brain. Innervation of the tunica media in these vessels enables the smooth muscle to contract or relax causing vasoconstriction or vasodilation as

appropriate. This is the neurogenic mechanism of autoregulation, but there are mechanisms that allow contraction and relaxation without the need of a nerve input, namely myogenic, metabolic and endothelial mechanism; these are described later.

Capillaries are the smallest blood vessels in the body, often only the diameter of a red blood cell (10 µm). They join the arterial system to the venous system and they enable the exchange of nutrients, water, oxygen, carbon dioxide and other waste products. The capillaries are comprised of a one cell thick layer of endothelium; this is semi-permeable which allows plasma and small solutes to pass through. There is said to be an absence of pre-capillary sphincters in the brain, which is why the arterioles alone are involved in blood flow regulation[56]. Continuous capillaries are found in the brain. These have endothelial linings that form tight connections with neighbouring cells, the absence of pores in these capillaries in the brain mean that there is a very effective blood brain barrier.

Capillaries drain into venules, which in turn combine and drain into small veins. Venules have a tunica intima, and a very thin tunica adventitia, and the more distal venules have a thin tunica media consisting of scattered smooth muscle fibres. The venous vessels also comprise of three layers, but they are much thinner and collapsible; they have much less smooth muscle in their tunica media. The tunica adventitia is the thickest layer of the venous vessel wall, and is mainly comprised of collagen and elastic fibres[54].

2.3 Brain vascular physiology

Blood pressure, blood flow and blood volume

Blood pressure is defined as the force per unit area exerted by the blood on the walls of the vessel in which it is contained. Factors that affect blood pressure include cardiac output, blood volume, viscosity, resistance and the

elasticity of arteries. Resistance (R) varies with blood vessel diameter, d, ($R \propto 1/d^4$), blood viscosity and total blood vessel length[58].

Arterial blood pressure (ABP) is very quickly regulated by the nervous system. To cause a rapid increase in ABP it is thought that three major changes may occur simultaneously. Firstly, arterioles supplying less critical parts of the body vasoconstrict increasing peripheral resistance; secondly, the veins constrict, increasing resistance but more importantly, reducing volume thus displacing blood towards the heart. Lastly the heart is stimulated by the autonomic nervous system, which encourages greater cardiac pumping. The converse of these actions can occur to achieve a drop in blood pressure[58].

These reflex mechanisms maintain normal ABP via three types of sensors in the vasculature, baroreceptors, chemoreceptors and shear sensors. Baroreceptors are stretch receptors found in large arterial vessel walls and the vena cava. A rise in arterial pressure stimulates these sensors and a signal is sent back via the autonomic nervous system to reduce arterial blood pressure. This is achieved by a decrease in peripheral resistance and a decrease in cardiac output. Baroreceptors work most efficiently in the range of blood pressures where they are most needed and they respond to a changing pressure rather than to a changing flow[58].

Chemoreceptors have a similar role as baroreceptors except that it is the response of chemosensitive cells that trigger a reflex. These cells are sensitive to a decrease in oxygen, an increase in carbon dioxide and increase in hydrogen ions. They are found in the carotid artery bifurcations and in the aorta. Their primary purpose is to detect a change in blood chemistry and initiate a vasomotor response[58].

Shear sensors detect shear stress on the artery wall, which increases when blood flow increases. These sensors release a vasodilator into the blood stream and this is thought to be nitric oxide[58]. The chemical composition of nitric oxide is changed before it is re-circulated to the rest of the body, hence vasodilation only occurs locally downstream of the increase in blood flow[59].

Blood flow is directly proportional to a pressure difference of the blood between the two ends of a vessel (a pressure gradient) and inversely proportional to resistance. This relationship is based on Poiseuille's Law[60], which was one of the first descriptions of the relationship between flow and pressure difference along a tube[53]. This relationship was based on experimental work, but it was backed up by the theoretical application of the Navier-Stokes equations, which describe the general properties of flow of viscous fluids[61]. This relationship can be described by an analogy of Ohm's Law (voltage = current x resistance)[58]:

$$\Delta P = Q \times R \qquad (1)$$

Where ΔP is the pressure difference, Q is blood flow and R is resistance.

Resistance is given by[58]:

$$R = \frac{8 \times \upsilon \times l}{\pi \times r^4} \qquad (2)$$

Where υ is viscosity, l is length of the tube, and r is radius of the tube.

Cerebral blood flow (CBF) is the rate of delivery of arterial blood to the capillary beds of a particular mass of tissue; this is typically 60 ml/100 g min. Cerebral blood volume (CBV) is the fraction of the brain volume occupied by blood vessels, and this is typically 4%. This can be divided into arterial, capillary and venous volumes, and of this typically 5% (of the total CBV) is attributed to the arteries and the rest divided equally between capillaries and veins[5]. CBV can change on both the arterial side and the venous side, but absolute arterial blood volume is a much smaller component, as the blood volume on this side is much smaller. The venous side may expand in response to pressure changes. Changes in capillary volume may also occur through capillary recruitment, where previously collapsed capillaries are opened, but this is thought to be a small effect[62]. Another electrical analogue equation (Q = C x V, charge = capacitance x voltage) can be used to describe blood volume:

$$V = C \times P \qquad (3)$$

Where V is blood volume, C is compliance of the blood vessels and P is blood pressure. This equation describes the Windkessel model of volume changes within a blood vessel. This states that as the volume of blood in the arteries stretches the walls of the vessels (which are highly elastic), then the pressure within the vessel increases proportionally. Windkessel is the German name for a fire engine's compression chamber which delivers a steady stream of water and was first proposed by Frank in 1905.

Blood flow velocity is inversely related to the total cross-sectional area of blood vessels, i.e. blood flow velocity is slowest where the cross sectional area is the greatest (assuming blood flow is the same in all vessels). Velocity generally decreases from the aorta to arteries to capillaries and then increases again in the venules and veins. Blood velocity ranges from tens of centimetres per second in the arteries to as little as 1 mm/s in the capillaries[5]. Cerebral blood flow could be derived from cerebral blood velocity measurements by multiplying cerebral blood flow velocity (actually the average spatial velocity across the vessel of interest) by the cross sectional area of the vessel at the point where the velocity is being measured. In practice, for example in transcranial Doppler measurements, cerebral blood flow velocity values are used in place of absolute flow measurements, assuming a constant cross sectional area during the time of measurement.

CBF does not explicitly depend on either CBV or velocity. A quantity called the capillary transit time can relate blood volume and blood flow (rather than blood velocity) and this relationship is known as the central volume principle[63]:

$$\tau = CBV/CBF \qquad (4)$$

Where τ is the mean transit time through the volume defined by CBV.

Changes in CBV are also linked to changes in CBF. It is thought that they are related in the following relationship[64]:

$$\frac{V}{V_0} = \left(\frac{F}{F_0}\right)^{\alpha} \qquad (5)$$

Where V_0 is the resting blood volume, F_0 is the resting blood flow and α is a numerical exponent. Grubb[64] *et al* found that this relationship was described with α = 0.38 (in monkeys). As the veins are highly distensible vessels, changes in CBF may be accompanied by changes in CBV mainly on the venous side. A change in resistance on the arteriolar side, for example as a result of blood pressure changes or the action of the autoregulation mechanism, could result in increased blood flow and as a consequence, an increase in pressure in successive sections of the vascular tree. This may result in a passive dilation of the veins and thus an increase in blood volume. This hypothesis will be important when looking at the results from the BOLD-MRI experiments, as venous volume changes will affect the BOLD signal. It has also been suggested that volume changes follow flow changes, which would fit with this hypothesis[5,65].

2.4 Brain metabolism

The brain requires a large amount of energy to generate electrical activity for neuronal signalling. This energy is gained from the oxidative catabolism of glucose. To maintain this source of energy it needs a rich and constant supply of blood, which it obtains from an extensive network of vessels. There is usually only approximately a two-second supply of glucose (stored as glycogen) stored in neurons at any given point in time; hence the requirement for a constant blood supply. As stated previously, the brain, which accounts for 2% of the body's mass, consumes 20% of its glucose and oxygen and receives 20% of its blood supply. At normal levels of global blood flow in the brain (60 ml/100 g/ min), 50% of arterial oxygen is extracted and about 10% of arterial glucose. Oxygen is delivered to the brain tissue by diffusion whereas glucose is able to cross the blood-brain barrier by using a saturable carrier mechanism.

Ions must be pumped through neuronal membranes, namely to transport sodium and calcium outside and potassium and chloride inside. In addition, during neuronal activity these ions move in the opposite direction and a compensatory increase in membrane transport is required to restore the balance of ionic concentrations. During this process, neuronal metabolism can increase by 100 to 150%. The re-establishment of these chemical gradients is carried out by the conversion of adenosine triphospate (ATP) to adenosine diphosphate (ADP). The majority of the ATP used to fuel these cellular processes is derived from the metabolism of glucose and oxygen. This metabolism occurs in two stages; glycolysis and the trans-carboxylic acid (TCA) cycle. Glycolysis does not require any oxygen but does not produce as much ATP as the TCA cycle (which does require oxygen). The TCA cycle produces 18 times more ATP than glycolysis alone. Carbon dioxide, which is the waste product produced at the end of the glucose metabolism cycle, diffuses out of the cell into the blood and is transported back to the lungs to be expired. The consumption of glucose in the brain is heterogeneously distributed. The metabolic rate is three times higher in grey matter as compared to white matter[5].

Metabolism and blood flow both change during neuronal activation (as mentioned previously) and their relationship is an interesting if slightly surprising one. The metabolic rate increases much less than cerebral blood flow. This imbalance results in a drop in oxygen extraction (as fractionally less oxygen is being removed from the blood) and deoxyhaemoglobin content of venous blood also decreases (and oxyhaemoglobin content increases). There are many questions regarding the $CMRO_2$ – CBF relationship (as a result of neuronal activation) which are still to be answered; however an empirical relationship can be described. This can be summarised as follows: as a results of neuronal activation, CBF increases substantially, CBV increases moderately, the O_2 metabolic rate increases slightly, the oxygen extraction fraction drops considerably, and the local blood velocity in the arterioles, capillaries and venules increases with a corresponding drop in the

blood transit time. The capillary density most probably stays the same, but may increase due to capillary recruitment. All these phenomena will have an effect on the BOLD MRI signal, which is the MRI method being used and investigated in this project[5].

It is important to note however, that it is assumed that during the experiments carried out during this project that neuronal activation will not be induced during the course of the MRI measurements. Nevertheless, it is extremely valuable to understand how the MRI signal during activation does change and which physiological parameters affect it, as the signal changes that are observed in these experiments will be able to be explained much more rigorously. This is explored in more detail in Section 3.7 (BOLD MRI).

2.5 Cerebral autoregulation mechanisms

Autoregulation is the mechanism that protects the brain against the risks of hypoxia at low perfusion pressures (which can be described as the difference between arterial pressure and intracranial pressure) and the risks of brain oedema or haemorrhage at high arterial pressures. This mechanism is performed by blood vessels altering their cerebrovascular resistance to maintain constant cerebral blood flow (CBF) despite changes in blood pressure (cerebral perfusion pressure, CPP). Cerebral autoregulation may become impaired in a wide range of conditions, for example head injury[27,28], stroke[30], dementia[43,44], liver disease[42], anaemia[35], hypertension[36,37], diabetes[24,25] and epilepsy[31] or during therapeutic interventions such as surgery[66] or anaesthesia[67,68].

Autoregulation can maintain constant CBF over the range of blood pressures between approximately 50 and 170 mm Hg[1].

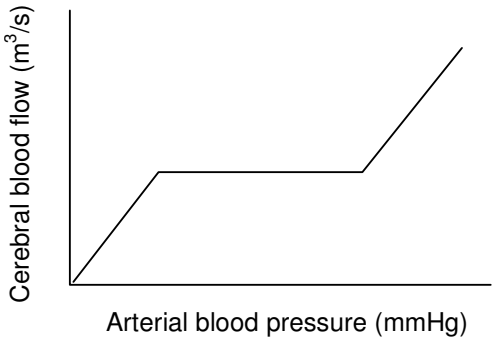

Figure 4: Schematic showing the relationship between arterial blood pressure and cerebral blood flow in normal autoregulation.

In healthy individuals, the autoregulation mechanism will act over a 5 – 15 second time interval after a large change in blood pressure, as seen in experiments using transcranial Doppler[69].

Cerebral autoregulation can be attributed to several mechanisms: myogenic, endothelial, metabolic and neurogenic. The degree to which each of these act on blood vessels is still not entirely clear. Certain mechanisms may have a greater effect on blood vessels in different parts of the body, or on vessels of varying sizes[70].

The Myogenic Hypothesis

The myogenic hypothesis for autoregulation suggests that the smooth muscle cells of the arteries and arterioles respond to changes in transmural pressure, i.e. they constrict or dilate accordingly. The autoregulation response takes place over a fairly short timescale (5 – 15 s) and this fast alteration in blood pressure changes the state of actin and myosin filaments in smooth muscle cells, which results in this quick autoregulation response[71]. This response was considered by Bayliss[72] in 1902 and has since been demonstrated in experiments, i.e. when an arterial tissue is stretched it automatically elicits a contraction response[26]. However, this hypothesis is open to question. When

central venous pressure is increased moderately (which would result in a rise in arterial pressure) it has been seen in animal experiments that blood flow is not altered[73].

The Endothelial Hypothesis

It has more recently been hypothesised that in response to decreases in flow, cerebrovascular endothelial cells release an endothelium-derived relaxing factor (EDRF). This is thought to be nitric oxide (NO), which initiates the relaxation of the vascular smooth muscle. This is a response to shear stresses induced as blood flow is altered. There may also be a similar factor which prompts vasoconstriction, the endothelium-derived constricting factor (ECRF) and one substance that has been investigated in relation to this is endothelin[74].

The Metabolic Hypothesis

The metabolic hypothesis states that changes in local blood flow result in the release of a metabolic factor, which initiates vasodilation or vasoconstriction. Changes in blood pressure will alter blood flow transiently and thus alter the metabolite concentration, which stimulates vasodilation or vasoconstriction. Various molecules have been put forward as mediators of this mechanism and there is some debate over which substance does act as a metabolic factor specifically for the cerebral autoregulation mechanism[26]. Adenosine is one likely factor as the concentration of adenosine has been found to increase with even moderate reductions in arterial blood pressure[26]. There are, however, studies that refute this claim, as administration of adenosine antagonists do not alter the autoregulation response when ABP is reduced below the lower limit of autoregulation. It may be that a combination of mediators act to initiate the autoregulation response and the metabolic component of the response may be oxygen sensitive[26]. This response is

distinct from the intrinsic coupling between neuronal activity and blood flow, which also results from a metabolic mechanism. It is unknown whether this metabolic mechanism is mediated by the same factors as those postulated for the cerebral autoregulation metabolic hypothesis.

The Neurogenic Hypothesis

All blood vessels are innervated (both extraparenchymal and intraparenchymal) and the neurogenic hypothesis states that it is these nerves that regulate vessel tone. The density of innervation is greatest in larger cerebral vessels at the base of the brain and less dense in more distal and intraparenchymal arteries[26]. Sympathetic nerves have a marked effect on cerebral blood volume[75] (i.e. cerebral capacitance). Electrical stimulation of sympathetic nerves causes constriction of larger cerebral arteries and this is compensated by the autoregulatory dilation of smaller vessels, which produces no resulting change in blood flow. At high pressures, sympathetic vasoconstriction as well as autoregulatory constriction occurs and there is a shift in the upper limit of autoregulation to higher pressures. At low pressures, the lower limit of autoregulation is also shifted towards higher pressures, as autoregulatory compensation is insufficient[70]. It is not entirely clear how the parasympathetic system affects autoregulation[26].

Autoregulation works on large pial arteries through a pressure dependent mechanism, activated by changes in perfusion pressure (the myogenic or neurogenic hypothesis) whereas small pial arteries are sensitive to small CBF changes (due to metabolic or endothelium-dependent mechanisms)[71,76]. The myogenic mechanism is a faster effect that occurs in the more proximal arteries and acts in response to a change in blood pressure rather than flow. In this way, the mechanism can regulate blood pressure and protect the more delicate vessels further down the arterial system. The neurogenic mechanism probably regulates shear forces (due to pressure changes) in the

endothelium and uses an EDRF (endothelium-derived relaxing factor) such as nitric oxide (NO). This is released into the blood stream to alter vessel diameter and flow[77].

There are other physiological and pharmacological modulators of autoregulation. As stated above activation of the sympathetic nervous system shifts the lower and upper limits of autoregulation to higher blood pressures. Blocking of the renin-angiotensin system shifts these limits towards lower pressures. Other physiological mechanisms change the limits of autoregulation, for example the states of hypercapnia and hypocapnia induce vasodilation and vasoconstriction respectively. The autoregulation plateau is narrowed at high rates of cerebral blood flow and increased at low rates[26,70].

2.6 Measurement of cerebral autoregulation

Although autoregulation is not explicitly measured in this project, it is informative to have an awareness of the techniques that have previously been used to do this. The methods and results from these experiments are useful in both formulating the methods for the experiments performed in this project and for interpreting the results. Measuring autoregulation involves looking at the signal changes induced as a result of blood pressure changes, which is also the aim of this work, albeit using a different modality to that which has been used previously. The two quantities that require measurement in order to assess cerebral autoregulation are cerebral blood flow (CBF) and cerebral perfusion pressure (CPP).

2.6.1 Measuring cerebral blood flow

The estimation of cerebral blood flow (CBF) is most accurately carried out by the injection of a tracer, which can then be detected, and its kinetics can then be investigated. This tracer may be radioactive or non-radioactive depending

on the method of detection used. Kety and Schmidt[78] were the first to propose an accurate non-invasive method of assessing blood flow. Tracer wash-out is used as a technique to provide quantitative information about regional cerebral blood flow, using a variety of methods. Xenon-133, a gamma emitter, has been used extensively as a tracer[79], but there are also agents that can be used in conjunction with PET, CT and MRI imaging. However, not all of these approaches are fully quantitative. A confounding issue in the measurement of CBF is that it is not desirable to measure the blood flow *within* the capillary bed (which may include an artery that is not delivering blood to the volume of interest but just passes through the volume of interest) but delivery of blood *to* the capillary bed within the volume of interest.

The main techniques used to measure CBF are transcranial Doppler ultrasound[69] (more recently) and Xe-133 clearance or other indicator-dilution methods[1]. Other methods used to measure CBF include arterio-venous O_2 difference (A-VDO_2), electromagnetic flowmeters, near-infrared spectroscopy and laser Doppler flowmetry[2]. However, none of these methods (with the exception of Xe-133) is a direct measurement of CBF; it is derived from these measurements after having made assumptions regarding the measurements.

2.6.2 Measuring blood pressure

Cerebral perfusion pressure (CPP) can also be measured using a variety of techniques when assessing static (or dynamic) autoregulation, the most accurate of which is the intravascular catheter. CPP is defined as the difference between systemic mean arterial blood pressure (ABP) and intracranial pressure (ICP) and in the majority of cases, ICP is considered to be low, so CPP can be assumed to equal ABP. However, in certain pathologies, such as severe head injury, high values of ICP can be observed and it is important to take this into account when measuring ABP. The assessment of autoregulation should be carried out with care in these cases.

The Finapres is another device that has been used to measure blood pressure changes in various types of autoregulation assessments[2,80]. This uses a finger cuff and can measure continuous arterial blood pressure (ABP) based on the arterial volume clamping principle. This is described in greater detail in Section 4.3.3 (The measurement of arterial blood pressure). Although the Finapres is less accurate than intravascular catheter measurements, it has the advantage of being non-invasive.

2.6.3 Measuring autoregulation

Measuring autoregulation is a special case of CBF measurement, one that looks at flow changes (or responses) rather than absolute flow. Different methods for the measurements of the autoregulation mechanism can be divided into two main categories; static and dynamic measurements. Dynamic measurements can be subdivided into experiments involving step, spontaneous and periodic changes in blood pressure.

Static measurements

The measurement of static autoregulation involves changing the blood pressure in discrete steps and measuring the blood flow after each change[68,81]. This was the predominant method for investigating CBF regulation for many years until high temporal resolution techniques for measuring CBF changes were established. The classic autoregulation curve (figure 4) by Lassen[1] is based on static autoregulation measurements and shows a plateau that is perfectly flat i.e. changes in blood pressure between the limits of autoregulation do not induce any change in CBF. This is not always the case and in the assessment of static autoregulation a plateau with a gradient does not always imply impaired autoregulation[68]. There are a variety of methods that can be used to assess static autoregulation, both using other physiological measurement modalities and TCD.

Static autoregulation experiments using Xe-133 are somewhat limited in their accuracy due to the restriction in the number of measurements of blood flow that are made (as these take a relatively long time to undertake, of the order of 15 minutes), as a response to a change in blood pressure[2]. CBF is only measured before and after a change in ABP is triggered. Doppler ultrasound measures blood flow velocity continuously and assumes that the cross-sectional of the vessel being investigated is constant throughout the measurement[82]. It is possible that cross-sectional area varies between measurements leading to inaccuracies.

The autoregulation mechanism has been stimulated by various pharmacological agents that cause a change in mean ABP. This is a non-transient change to a new ABP level that lasts for several minutes and is thus called a static autoregulation as measurements are made under stable conditions after a change in CBF is seen. Dynamic autoregulation measurements measure the change in signal during the CBF changes. There are several ways of classifying the state of autoregulation based on static autoregulation measurements. A simple method is to use linear regression and look at the regression slope of the autoregulation curve[2]. The correlation coefficient between CBF and CPP or mean ABP can also be used as an index[83]. Neither of these methods seems to give reliable results for assessing the presence or absence of autoregulation[2]. An index of static autoregulation has been defined by Tiecks[68] and this is defined as the percentage change in estimated cerebrovascular resistance relative to the change in ABP during infusion of phenylephrine (which increases mean ABP by approximately 20 mmHg). A threshold can be set between 0 and 1 to discriminate between normal and impaired (or absent) autoregulation; this has been reported to be between 0.5 and 0.85[2,68].

Dynamic measurements

One established approach used to assess autoregulation is transcranial Doppler ultrasound, which was first introduced by Aaslid[82] in the early 1980s. This produces a continuous measurement with excellent time resolution, which allows rapid velocity changes to be monitored thus enabling a dynamic autoregulation measurement. Dynamic measurements of autoregulation are valuable as they can characterise the transients in the autoregulation response to ABP (or CPP) changes.

Any autoregulation mechanism will take time to act and this is one of the parameters that could be used to assess the effectiveness of the autoregulation response. The response normally starts within 2 seconds of the blood pressure change and is usually completed after 10-15 seconds. This fast response can only be measured dynamically by a technique with an adequate temporal resolution, and TCD has an excellent temporal resolution of the order of 10 ms [2]. In this technique the middle cerebral artery (MCA) is insonated through the temporal bone window and a Doppler signal is received. This signal gives an indication of blood flow velocity in this artery.

Arterial blood pressure also needs to be measured continuously to enable the study of autoregulatory dynamics. A step change in blood pressure (actually cerebral perfusion pressure, CPP) may be used to study the autoregulatory mechanism. This can be achieved by inflating thigh cuffs for a period of approximately 120 seconds to produce leg ischaemia. The cuffs are then deflated rapidly (<200 ms), which re-perfuses the legs and produces a step change in arterial blood pressure (ABP) and hence cerebral perfusion pressure (CPP).

By comparing time course recordings of cerebral blood velocity and cerebral perfusion pressure it is possible to obtain measures of autoregulation for an individual[68,69]. A second order differential equation can be used to predict the CBF velocity response to a drop in ABP. The model parameters that best fit the data can then provide an index of autoregulation. Tiecks[68] et al proposed

nine sets of model parameters reflecting a range from good (fast) to absent autoregulation. The ABP input to the model is used to derive each of the nine responses to the pressure drop, and the predicted response that best fits the CBF velocity data is deemed to be the autoregulation index (ARI) from 0-9[68]. The following graph (modified from Birch[80] *et al*, with permission) shows the response of blood flow velocity measured using transcranial Doppler (green) to a step drop in blood pressure (red). It can be seen that blood flow recovers ahead of blood pressure and this is due to the action of the autoregulation mechanism. It is this type of blood flow recovery curve that can be used to generate an autoregulation index.

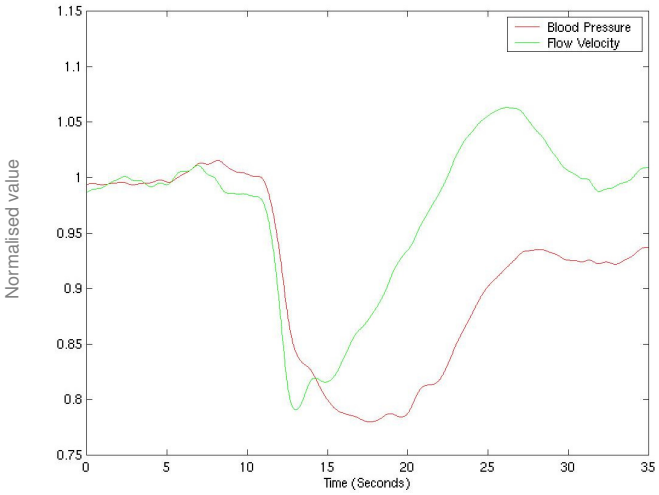

Figure 5: TCD measurement of blood flow velocity in response to a step drop in blood pressure (used with permission from A A Birch and adapted from Birch et al, 2003[80]).

There are many other ways of introducing transients to CBF in order to stimulate the autoregulation mechanism. These include occlusion of the carotid artery[84], the Valsalva manoeuvre[85] (forced expiration against a closed glottis) and lower-body negative pressure oscillations[86].

Spontaneous dynamic autoregulation measurements observe the changes in blood flow in response to natural changes in blood pressure in the body[87].

Finally, periodic measurements of autoregulation impose a regularly repeating variation of blood pressure on the body and measure blood flow in response to this. This variation can be achieved using a lower body negative pressure chamber[86] or controlled respiration.

Near-infra red spectroscopy (NIRS)

Another modality that may be used to assess dynamic cerebral autoregulation is near-infra red spectroscopy (NIRS). This is another non-invasive, non-ionising radiation technique. NIRS can continuously monitor both total cerebral haemoglobin saturation and changes in cerebral haemoglobin, as well as cerebral blood flow (using an oximeter to provide beat to beat S_{pO2} measurements). Many of the papers published on the topic of cerebral autoregulation measurement using NIRS have been made on neonates or premature infants[88,89]. This may be due to the fact that a neonate's skull is somewhat thinner than an adult's and may allow improved detection of the near infra-red signal. The spatial resolution of the NIRS technique is not comparable to BOLD MRI, but the temporal resolution is excellent (0.2 Hz). Light is transmitted via a fibre optic cable over a certain part of the brain (for example the temporo-parietal region). The signal is collected using a receiving optode positioned approximately 4 cm away to detect the signal. Sophisticated signal analysis is carried out to correlate CBF or haemoglobin changes to changes in mean arterial pressure (MAP). The haemoglobin changes that are measured are the changes in cerebral intra-vascular oxygenation (HbD), without contamination of the signal by extracerebral haemoglobin. This is described as the difference between the concentration changes of oxygenated haemoglobin (HbO_2) and deoxygenated haemoglobin (Hb)[90]. HbD is considered to be a measure of CBF if arterial oxygen saturation does not change. It has been found in premature infants that large spontaneous fluctuations in MAP are associated with changes in HbD (with a constant SaO_2). This is assumed to be evidence

of impaired cerebral autoregulation[90]. In adults, significant correlations between the NIRS signal (HbD) and intracranial pressure (ICP) have been observed. Varying patterns of response were seen depending on the state of the autoregulation mechanism. There was no correlation observed between total haemoglobin and ICP[91]. There are a number of issues with this type of measurement. It is assumed that signal is solely from intracranial vasculature, but this may not be the case; there may be contamination from the scalp. In addition, there is poor spatial specificity in these measurements, and this depends on positioning of the receiving optode, which may not be in the area of interest in the brain.

Chapter 3 Overview of Magnetic Resonance Imaging

3.1 Basic theory of MRI

Nuclear Magnetic Resonance (NMR) was first discovered independently in 1946 by Bloch[92] and Purcell[93]. It is the physical phenomenon that Magnetic Resonance Imaging (MRI) is based upon, although it was some years later that it was employed for medical applications[94,95,96,97,98]. It concerns the interaction between radio waves and nuclei in a magnetic field. The property associated with a nucleus that causes it to interact with a magnetic field is known as its 'intrinsic spin'. This quantity can only take integer or half integer values, depending on the number of nucleons present. This property results in a nucleus possessing angular momentum, **p**, which is related to the spin, **I,** by:

$$\mathbf{p} = \hbar\, \mathbf{I} \qquad (6)$$

where $\hbar$ = h/2π and h is Planck's constant. The magnetic dipole moment $\boldsymbol{\mu}$, is related to the angular momentum, **p**, by:

$$\boldsymbol{\mu} = \gamma\, \mathbf{p} \qquad (7)$$

γ is the gyromagnetic ratio, the ratio of the orbital angular momentum to the magnetic moment. In the case of the hydrogen nucleus, which is comprised of a single proton, and is the nuclei of interest, γ = e/2m, where e is the charge and m is the mass of the proton. A proton has **I** = ± ½.

Interaction of Protons with a Magnetic Field: A Classical Model

An external magnetic field $\mathbf{B_0}$ will exert a torque on the magnetic moment $\boldsymbol{\mu}$, resulting in the angular momentum changing at a rate equal to the torque. The torque, **L**, can be given by:

$$\mathbf{L} = \boldsymbol{\mu} \times \mathbf{B_0} \qquad (8)$$

$$= d\mathbf{p}/dt \qquad (9)$$

But $\mathbf{p} = \boldsymbol{\mu}/\gamma$ (7), so:

$$d\boldsymbol{\mu}/dt = \boldsymbol{\mu} \times \gamma \mathbf{B_0} \quad (10)$$

or

$$d\boldsymbol{\mu}/dt = \omega_0 \times \boldsymbol{\mu} \quad (11)$$

where $\omega_0 = -\gamma \mathbf{B_0}$. (12)

Equation (12) is the Larmor equation, and equation (11) describes the precession of $\boldsymbol{\mu}$ about $\mathbf{B_0}$ with angular velocity ω_0[99].

Interaction of Protons with a Magnetic Field: A Quantum Model

A classical model is useful when considering the net effect of a magnetic field on an assembly of spins but for an individual nucleus a quantum mechanical model is needed. In this model the nuclear magnetic dipole moment can only have 2I + 1 possible orientations of angular momentum. This magnetic dipole moment results in the nucleus interacting with a magnetic field, $\mathbf{B_0}$, and either aligning with or against the applied field, i.e. it has two possible orientations. These orientations correspond to spin up or spin down states, with the associated spins occupying low and high energy states. The energy difference between these two states is proportional to the applied magnetic field $\mathbf{B_0}$ and is given by:

$$\Delta E = \mu \mathbf{B_0} \quad (13)$$

$$= \gamma \hbar \mathbf{B_0} \quad (14)$$

A diagram of the two states is shown below:

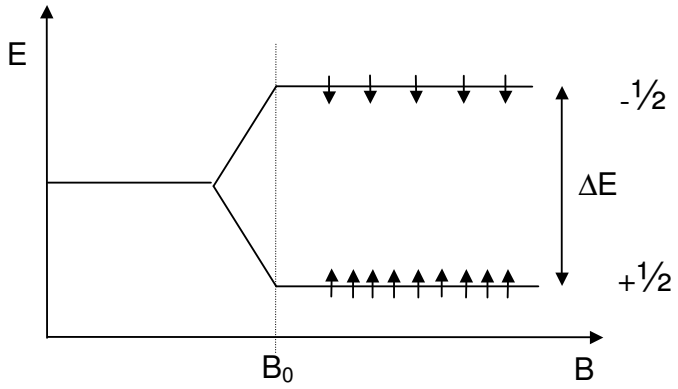

Figure 6: The splitting of an energy level and the distribution of spins within it.

Transitions between the two states can take place if energy is applied at the correct frequency ω_0, where:

$$\omega_0 = \gamma \mathbf{B_0} \qquad (15)$$

This is the Larmor frequency and this is when resonance occurs. If a system of such spins is considered and a magnetic field with a flux density, $\mathbf{B_0}$, is applied, the spins will be distributed between the two states and after a certain period of time the population of the two levels will reach equilibrium. The Boltzmann Distribution describes the population difference between the two states:

$$\frac{n(\text{spin up},+\tfrac{1}{2})}{n(\text{spin down},-\tfrac{1}{2})} = \exp -\left(\frac{\hbar\omega_L}{kT}\right) \qquad (16)$$

where k is the Boltzmann constant, T is the absolute temperature of the spin system and n is the number of spins in a given state (spin up is aligned with $\mathbf{B_0}$, this is the low energy state). The fractional excess of spins in the lower energy state is:

$$\frac{(n_L - n_U)}{n_U} \approx \frac{\hbar\omega_L}{kT} = \frac{\hbar\gamma\mathbf{B_0}}{kT} \qquad (17)$$

where n_L and n_U are the populations of the upper and lower energy levels respectively. These are the spins that are observed in the NMR experiment[99].

Bulk Magnetisation

In practice, in the presence of an applied magnetic field, it is not just one nucleus that is observed, but the total effect of all the nuclei that are being excited. This is known as the bulk magnetisation **M**:

$$\mathbf{M} = \Sigma\boldsymbol{\mu} \qquad (18)$$

In an applied magnetic field, the individual magnetic moments, $\boldsymbol{\mu}$, are precessing around $\mathbf{B_0}$, as described by the classical mechanical model. The net magnetic moment, **M**, is the sum of $\boldsymbol{\mu}$ and is directed along $\mathbf{B_0}$. **M** has no component perpendicular to $\mathbf{B_0}$ in this unperturbed state. The magnitude of **M** is equal to the excess of spins shown by the quantum mechanical model, equation (17).

An analogy can be made between **M** and $\boldsymbol{\mu}$ as the behaviour of **M** is comparable to a large magnetic dipole, so from equations (10) and (11)

$$d\mathbf{M}/dt = \mathbf{M} \times \gamma\mathbf{B_0} \qquad (19)$$

or

$$d\mathbf{M}/dt = \omega_0 \times \mathbf{M} \qquad (20)$$

To understand the concepts that will be described, it would be useful to explain the ideas of laboratory and rotating frames of reference at this point. As will be explained in the next section, NMR experiments involve the application of a sequence of radiofrequency magnetic field pulses and it is the behaviour of the magnetisation during these pulses that is examined. The motion of the magnetisation can be difficult to interpret in the static, laboratory frame of reference. To overcome this, the motion is considered from the point of view of an observer rotating about an axis parallel with $\mathbf{B_0}$, in synchronism with the precessing nuclear magnetic moments. This frame is known as the

rotating frame of reference and its axes are x′, y′ and z′, with z′ being parallel to z (and $\mathbf{B_0}$), as opposed to x, y, and z in the laboratory frame of reference.

To detect the precessing bulk magnetisation (which is what is detected in the NMR experiment) the system must be perturbed from its equilibrium state. This is achieved by the application of a second magnetic field $\mathbf{B_1}$ that is perpendicular to $\mathbf{B_0}$ and rotates about it at ω_0, in synchronism with the precessing magnetic moments.

The application of $\mathbf{B_1}$ causes **M** to be tipped away from $\mathbf{B_0}$ where it now traces out a spiral path:

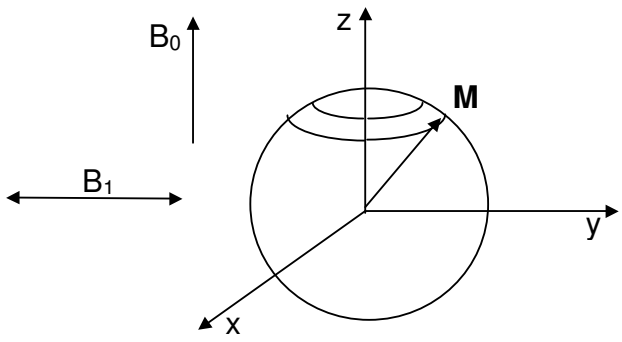

*Figure 7: Motion of **M** (in laboratory frame) in presence of $\mathbf{B_1}$.*

Once $\mathbf{B_1}$ is switched off, **M** carries on precessing at a constant angle α (the angle between the z-axis and **M**), called the flip angle. α is given by:

$$\alpha = \gamma \mathbf{B_1} t_p \qquad (21)$$

where t_p is the length of time the $\mathbf{B_1}$ field pulse is applied for. A 90° pulse is one where $\mathbf{B_1}$ has been applied for the appropriate amount of time to tip **M** through 90°, i.e. into the xy plane. A 180° pulse tips **M** onto the -z axis, and is twice the duration or magnitude of a 90° pulse. These pulses are referred to as the radiofrequency or RF pulses[99].

T_1 Relaxation

T_1 relaxation or spin-lattice relaxation as it is often known, describes the transfer of energy between the spins and the thermal motion of the molecules of which the spins are part, the "lattice". These exchanges occur when an RF pulse is applied to the system, thus disturbing it from equilibrium. Energy is absorbed by the system resulting in the population of the two energy levels becoming closer. T_1 is related to the time it takes for the spins to return to equilibrium, the state expressed in equation (13). It determines the rate of recovery of the bulk magnetisation vector, **M**, along the z-axis. This recovery cannot occur spontaneously, the magnetic field generated by the dipole moments of say, water molecules, will have components in the xy plane. Some of these will vibrate at a frequency of ω_0 and are able to stimulate emission of energy, which is transferred between the spin system and the lattice. This allows the spin system to relax with M_z, the longitudinal component of **M**, returning exponentially to its equilibrium value M_0, with a time constant T_1:

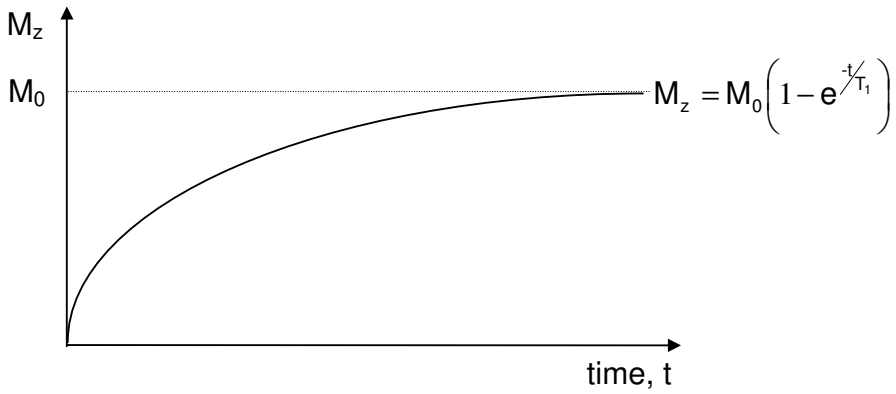

Figure 8: Exponential recovery of M_z due to T_1 relaxation.

T_1 is defined by the equation:

$$dM_z/dt = (M_0 - M_z)/T_1 \qquad (22)$$

or, solving:

$$M_z = M_0(1 - e^{-t/T_1}) \qquad (23)$$

The variable t can be replaced by TR, which is the repetition time of the sequence. This is the time between each consecutive RF pulse in the MRI pulse sequence.

If TR is shorter than T_1, saturation of the system results. This is because there is not enough time between RF pulses for complete T_1 relaxation to take place. This results in a reduced amount of longitudinal magnetisation along the z-axis, which means that there is less magnetisation to tip into the xy plane when the next RF pulse is applied, resulting in a smaller signal being detected in the xy plane. If this process continues for several RF pulses, the signal becomes progressively more saturated and a reduced signal is detected.[99]

T_2 Relaxation

T_2 relaxation, also known as spin-spin relaxation, concerns the dephasing of spins in the xy plane, i.e. a loss of magnetisation in the xy plane. This occurs because local magnetic fields from any other nucleus nearby, give rise to a z component as well the xy component when **M** is tipped into the xy plane. This slightly alters the external magnetic field, $\mathbf{B_0}$ that is experienced by the nucleus, which causes the precessional frequency of the nucleus to vary slightly, depending on the relationship between it and the local magnetic field. This, in turn, results in a loss of phase and xy magnetisation. An exchange of the spin state between two nuclei with no net loss of energy from the system also causes a loss of phase information. This decay of M_{xy} is exponential with a time constant T_2:

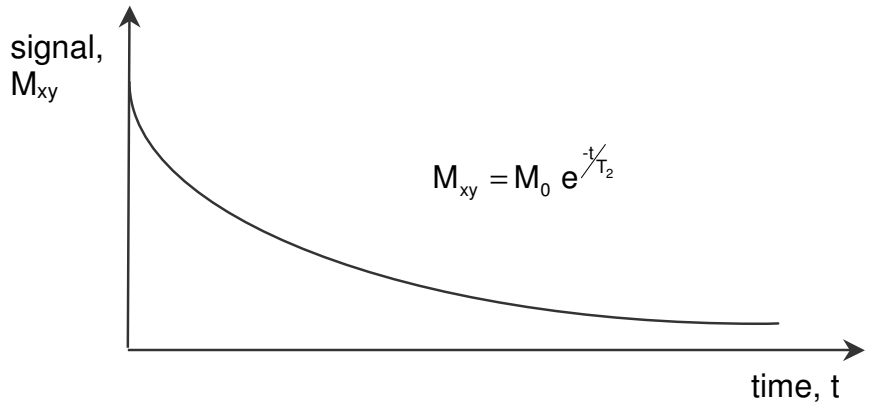

Figure 9: Exponential decay of signal due to T_2 relaxation.

T2 is defined by the equation:

$$dM_{xy}/dt = - M_{xy}/T_2 \quad (24)$$

or, solving:

$$M_{xy} = M_0 e^{-t/T_2} \quad (25)$$

The variable t can be replaced by TE, which is the echo time of the pulse sequence. This is the time between the initial RF pulse of the sequence and the echo that is produced[99].

3.2 Spatial encoding in MRI

The basis of MR imaging relies on the fact that magnetic field strength along a magnetic field gradient is linearly related to one spatial coordinate (x, y or z), i.e. it varies linearly along this gradient. This can be described by:

$$B_z(x) = B_0 + x\, G_x \quad (26)$$

where $B_z(x)$ is the resulting magnetic field, B_0 is the main magnetic field and G_x is the magnetic field gradient. Gradients can be generated along the x, y or z axes. These field gradients spatially encode the MR data, and there are

three methods to encode in the three orthogonal directions. These are selective excitation, frequency encoding and phase encoding.

Selective Excitation

This is the method used to select a tomographic slice through the object being examined, for two-dimensional imaging. An excitation radiofrequency (RF) pulse is applied simultaneously with a gradient that is perpendicular to the slice being imaged. The gradient allows the resonant frequency to be related to the position of the slice along the gradient. As the resonant frequency is proportional to the magnetic field strength, it is also proportional to position. This is given by:

$$\omega(x) = \gamma (B_0 + x\, G_x) \qquad (27)$$

The RF pulse is shaped so that it consists of a range of frequencies either side of the magnet resonant frequency. The only spins that will be excited by this pulse will be those whose resonant frequency (dependent on position) is within this range. Thus, a slice within the object will have been selected.

Frequency Encoding

As stated previously, the application of a magnetic field gradient results in the magnetic field becoming a linear function of position along the gradient. The NMR signal is observed with the gradient switched on. The amplitude of the signal is related to the number of spins in the region of interest and the frequency is related to the position along the gradient. To obtain spatial information from this signal, a Fourier Transform (FT) must be performed on it. The signal is digitised using an analogue-digital-converter (ADC) and the FT is calculated. The result is a histogram of the amount of signal present in a discrete frequency interval, which is equivalent to a one-dimensional projection of the object along the gradient. This technique enables spatial encoding along one axis.

Phase Encoding

This method spatially encodes along the third orthogonal axis to complete the MR image. It uses a magnetic field gradient to alter the resonant frequency of the spins along that gradient. When the gradient is switched of, the spins return to precessing at the same frequency, but there will be a phase difference between the spins along the third orthogonal axis, as they will have become dephased when they were precessing at different rates. The phase difference at a particular position will depend on the magnitude of the gradient at that position and thus the spins will be spatially encoded along the gradient. This gradient is applied many times, at different strengths, to spatially encode across the whole slice. This second gradient provides the information to produce a two-dimensional image of the object once a two-dimensional Fourier Transform has been performed on the signal.

These three steps are combined to form a pulse sequence. In a standard MR pulse sequence the slice selection is carried out first, then the phase encoding gradient and finally the frequency encoding is applied whilst the signal is collected. This whole process is repeated *n* number of times, where *n* is the number of phase encoding steps, which is equal to the number of lines in the image, or the number of lines in k-space. K-space is the domain in which the raw MR data (from the frequency and phase encoding steps) is saved as frequency and phase information. This data is then Fourier transformed to produce an image[99]. K-space is usually filled linearly, line by line, but it can be filled in a non-linear fashion; this is described in more detail in the Echo Planar Imaging section of this thesis.

3.3 Contrast in MRI

The contrast that is seen in MR images is due to varying T_1 and T_2 properties of different tissues within the body. The type of weighting that is achieved is determined by the TR (repetition time), which is the time between each

consecutive 90° RF pulse, and TE (echo time), which is the time between the 90° RF pulse and the signal echo.

As T_1 relaxation is due to relaxation of the spins back to the z-axis, TR controls the extent of this. So, for maximum T_1 contrast, TR should be short and TE should be short (to minimise T_2 contrast):

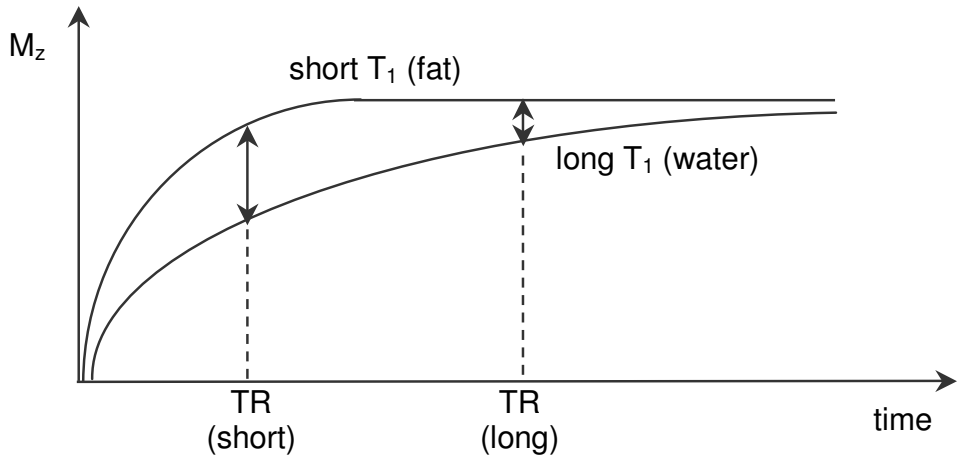

Figure 10: Weighting as a result of T_1 relaxation.

As T_2 relaxation is due to spins losing phase coherence with each other (dephasing), TE controls the extent of this. So, for maximum T_2 contrast, TE should be long and TR should be long (to minimise T_1 contrast):

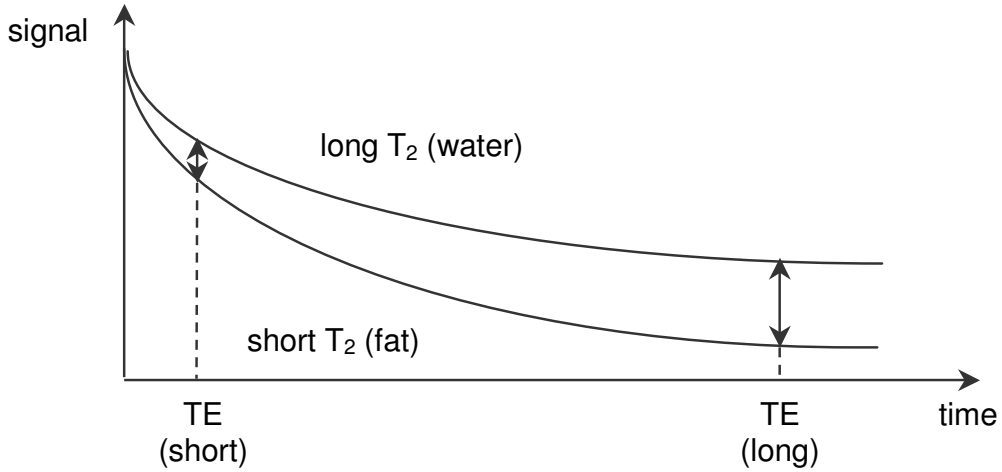

Figure 11: Weighting as a result of T_2 relaxation.

Two examples of T_1 weighted images are shown below:

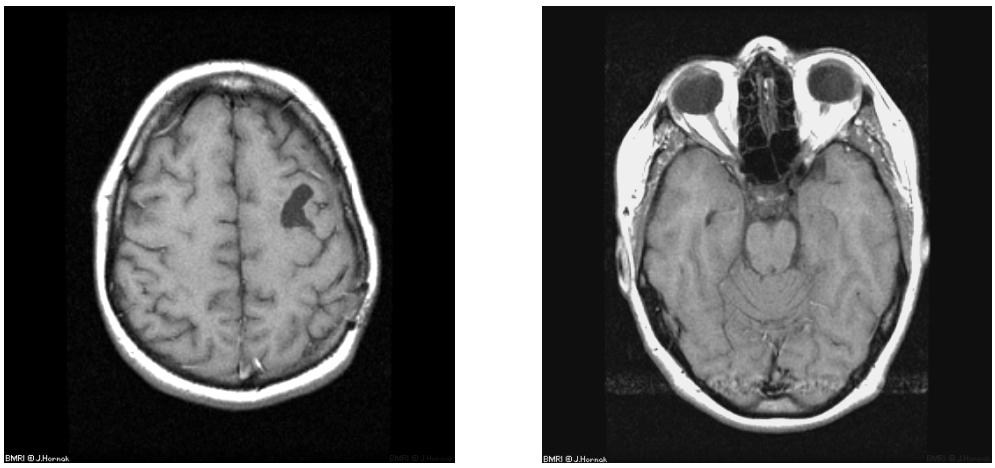

Figure 12: T_1 weighted MR images.

Two examples of T_2 weighted images are shown below:

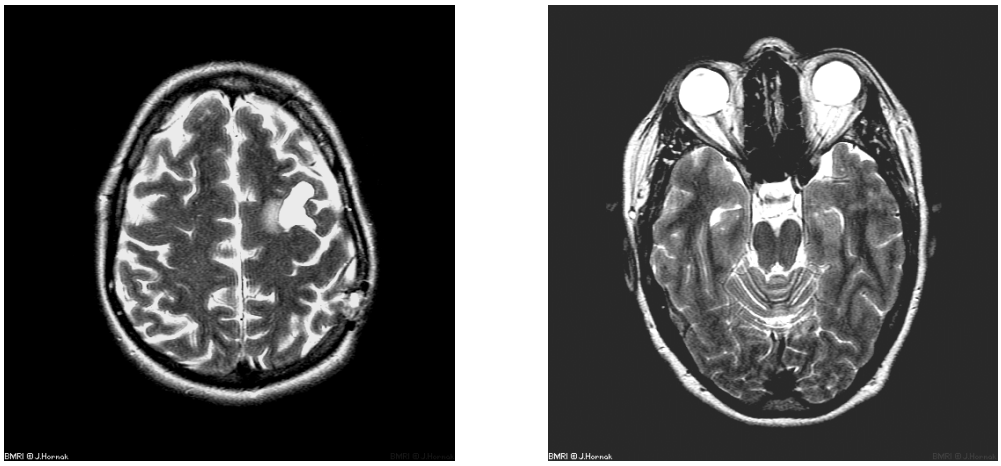

Figure 13: T_2 weighted MR images.

3.4 Spin echo and gradient echo imaging

Up to this point, the fundamentals of MR theory have been described. To actually produce an image, a pulse sequence must be applied and these commonly fall into two categories, spin echo sequences and gradient echo sequences. The difference comes from how the 'echo' (the signal that is actually detected) is produced. There are advantages and disadvantages to both techniques. In spin echo techniques spins are allowed to dephase due to T_2 relaxation and are refocused using a 180° RF pulse. In a gradient echo sequence spins are first dephased using a magnetic field gradient and then rephased using an equal and oppositely signed gradient to produce an echo. It is possible to use flip angles less than 90° in gradient echo sequences which means that these types of sequences are often used for rapid image acquisition. In gradient echo sequences, T_1 weighted images can be acquired as well as T_2* weighted images. T_2* weighting is achieved because a magnetic field gradient, rather than a 180° RF pulse (as in the case of spin echo imaging), is used to refocus spins. Consequently, relaxation effects due to inhomogeneities in the magnetic field are not corrected for when a magnetic field gradient is used to refocus spins, and as such T_2*, rather than pure T_2 weighting, results.

3.5 Some important MRI concepts

The following terms are all relevant to the observations noted in this project and it is important to understand them in order to appreciate how they relate to the signals that are being measured. This section is intended as a summary of them.

Saturation

This occurs when the T_1 of a substance is much more than the TR of the sequence that is being used to image it. If this is the case, then there will be incomplete recovery of longitudinal magnetisation back to the z-axis between each consecutive 90° RF pulse. This will result in there being less magnetisation to tip into the xy plane after the application of this 90° pulse, resulting in reduced signal intensity. This reduction in signal increases with each application of an RF pulse until a steady state is achieved, and the signal intensity remains constant. This effect can be reduced by using a smaller flip angle or a longer TR.

Dephasing

Spins dephase as they lose phase coherence with each other, i.e. when they start precessing at slightly varying frequencies. This occurs in inhomogeneous magnetic fields as neighbouring spins experience very slightly different magnetic fields and thus have slightly different precessional frequencies. The same effect can be seen if a magnetic field gradient is applied as spins along this gradient are subjected to linearly varying magnetic fields and thus their precessional frequencies vary linearly, leading to dephasing.

Magnetic susceptibility

This is a property of a material which describes how magnetised it becomes when it is placed in an external magnetic field. Substances can vary from being diamagnetic (extremely low susceptibility), to paramagnetic (moderate susceptibility) to ferromagnetic (high susceptibility). When materials or tissues of varying susceptibility are in close proximity to each other, magnetic field inhomogeneities are induced, leading to spin dephasing in these areas and a reduced signal.

Inflow effect

This is related to saturation and blood flow. It occurs when stationary tissue in the slice of interest becomes saturated, leading to low signal. However, unsaturated spins in blood can flow into the slice of interest resulting in a spuriously high signal from these spins compared to the stationary tissue surrounding the blood vessel. This happens when a short TR (compared to T_1) is used.

Diffusion

This is the random movement of water molecules due to Brownian motion and it can be detected using MRI. The amount of diffusion that takes place (i.e. the distance that a molecules moves) depends on the diffusion coefficient of the substance and the time interval over which the diffusion measurement is made. An equation can be used to describe this:

$$d = \sqrt{4.D.TE} \qquad (28)$$

where D is the diffusion coefficient and equals 1 $\mu m^2/ms$ and TE is the echo time of the MR pulse sequence[5]. The effect that diffusion has on the BOLD MRI signal is described more fully in the next section.

3.6 Echo planar imaging (EPI)

The MR imaging technique used to produce the images considered in this thesis was a fast imaging technique called Echo Planar Imaging (EPI)[100,101]. The acquisition time for such an image is in the order of 100 ms. In such a technique, the spins are rephased to form an echo using gradient rephasing. The frequency encoding gradient is switched from positive to negative to positive very rapidly and a series of echoes are produced. The phase encoding gradient can either be pulsed very rapidly to encode each echo that is re-phased or it can be applied continuously whilst the frequency encoding gradient is being switched (see figure 14). The signal must be fully encoded before the transverse magnetisation has decayed to zero. The whole image is then acquired within one repetition time of the sequence[99].

The majority of EPI sequences are 2D acquisitions, and this is what is used in this project to acquire a single, axial slice of the brain. In terms of gradients, the slice selection gradient is much the same as in conventional pulse sequences. However, the application of phase encoding and frequency encoding gradients result in k-space trajectories that are very different to conventional k-space sampling. This often results in EPI images being more susceptible to certain artefacts[102].

The frequency encoding (or read-out) gradient starts with a pre-phasing gradient and then continues with a series of alternating polarity gradient lobes. These gradient lobes can be trapezoidal, sinusoidal or a “catch-and-hold” shape (curved trapezoid). To achieve linear sampling of k-space throughout both the ramp-up and ramp down periods of the gradient application, as well as the plateau periods, temporal sampling must be non-linear on the ramps. This results in signals with a fixed dwell time (i.e. fixed bandwidth) that do not have to be re-sampled prior to fast Fourier transformation. To minimise the acquisition time of each signal (i.e. in order to maximise the echo train length during the decay of the transverse magnetisation) a wide receiver bandwidth should be used, and the number of

sampling points is limited to 64 or 128. There are confounding effects of increasing bandwidth; the SNR is decreased at higher bandwidths, however, it also reduces the effect of T_2^* - induced signal decay, which results in increased SNR. The frequency-encode gradient amplitude must be increased as a consequence of increased bandwidth, and this is limited by the hardware available on the scanner[102].

The phase encode gradient must also start with a pre-phasing gradient, which determines where the sampling in k-space starts (in the phase encoding direction). There are two methods of applying the phase encoding gradient in EPI. It can be applied continuously throughout the entire application of the frequency encoding gradients. This phase encode gradient produces a zigzag trajectory across k-space. As the k-space sampling points do not follow a grid pattern, there must be some regridding before the data can be Fourier transformed into an image. The other method involves applying the phase encode gradient as a series of blips, each with the same polarity and area. The timing of each is blip is just before each echo so that a rectilinear k-space trajectory is played out. The phase encoding gradient area is accumulated throughout the echo train. The shape of the blip gradient is generally a small triangular shaped lobe. The k-space samples in this case are evenly spaced along the phase encoding direction, which means that resampling is not required[102].

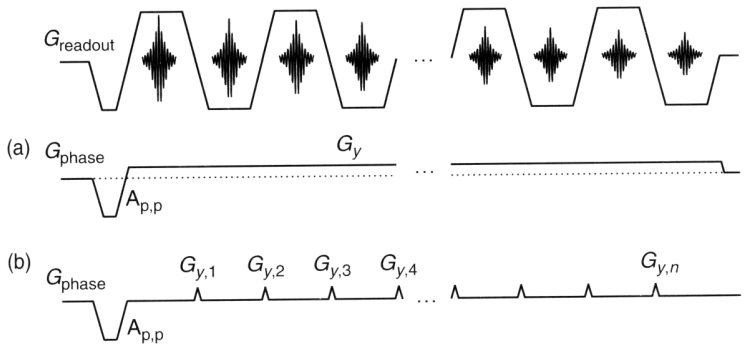

Figure 14: (a) A continuously applied phase encoding gradient and (b) a blipped phase encoding gradient (used with permission from Zhou et al, 2004)[102].

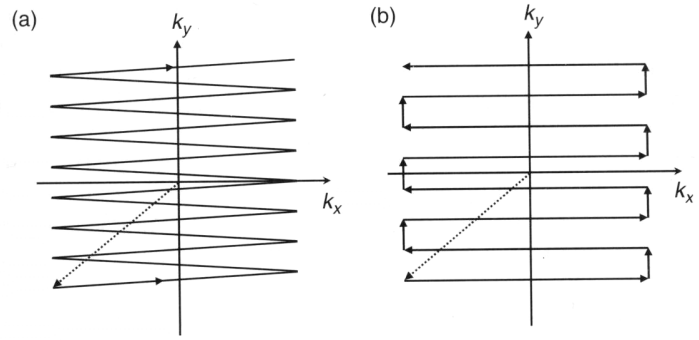

Figure 15: (a) A zigzag k-space trajectory corresponding to (a) above and a rectilinear k-space trajectory corresponding to (b) above (used with permission from Zhou et al, 2004)[102].

A typical gradient echo EPI sequence is shown below.

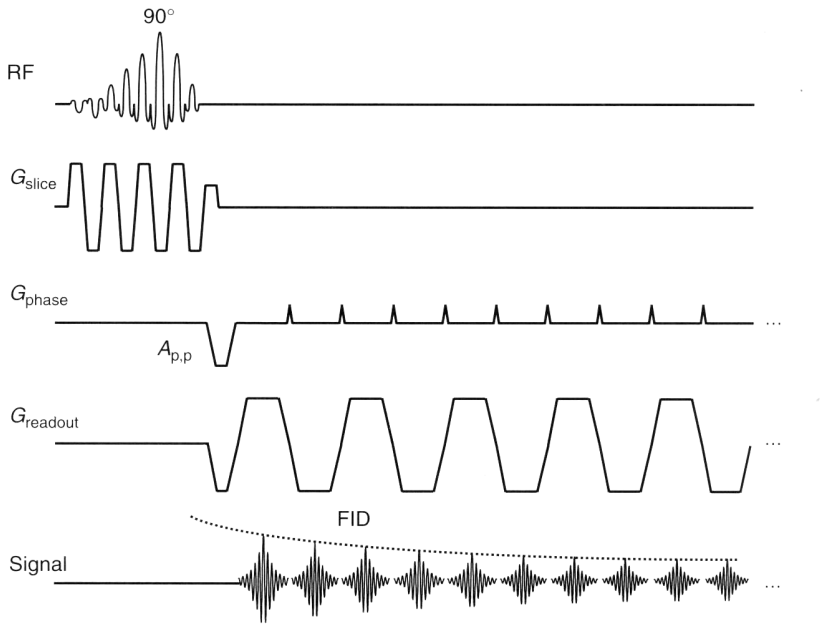

Figure 16: A typical gradient echo EPI pulse sequence (used with permission from Zhou et al, 2004)[102].

An initial selective excitation pulse produces a free induction decay (FID) signal. Whilst this FID is decaying, the previously described phase and frequency encode gradients are applied and the resulting signal are collected. The flip angle is usually set to less than 90° in order to optimise the SNR and this corresponds to the TR period that is used. A fat saturation pulse is often applied before the initial excitation pulse. At the end of the sequence a spoiler pulse is included to destroy the remaining transverse magnetisation so that it doesn't contribute to the next excitation. Each line in k-space in the phase encoding direction is obtained at a slightly different TE time, and as T_2* relaxation is taking place whilst the signals are being acquired, each line of k-space will correspond to a slightly different signal intensity. Contrast in the image is mainly determined by the data acquired that fills the centre of k-space, the contrast will be determined by the TE time of these central lines of k-space, and TE is defined as the TE when the central line of k-space is

acquired, the effective TE or TE_{eff}. Depending on the magnitude of the initial dephasing pulse, the sum of the succeeding blips will reach the same area as the dephasing pulse at a different time, i.e. the TE of central line of k-space will have a different value, thus changing the weighting of the sequence[102]. If TE is too short, T_2* contrast is poor, whereas if TE is too long, the MR signal will decay before it can be measured. The optimal TE value is approximately equal to the T_2* value in the brain and at 1.5 T, maximum BOLD contrast to noise ratio (CNR) is achieved with a TE of between 40 ms and 60 ms[5].

The technique used here is a single-shot technique, whereby all the data required for a single 2D image are acquired following one RF excitation. This provides the good temporal resolution that is required for the application in this project. However, the images that are produced can suffer from poor SNR, low spatial resolution and some artefacts. A wide receiver bandwidth is used (to allow fast data acquisition) and partial k-space acquisition can also be employed in the phase-encoding direction to reduce acquisition time. Various reconstruction methods have been devised to reconstruct partially sampled k-space.

In a spin-echo EPI sequence a 180° refocusing pulse is applied before the gradient echo train is played out. The centre of the gradient echo train is coincident with the timing of the centre of the spin echo, and hence spin echo weighting results. The contrast relating to this type of sequence is discussed in the next section.

With EPI data, k-space lines corresponding to even echoes follow one direction in k-space, whilst those corresponding to odd echoes follow the opposite directions. The consequence of this is that alternate lines of k-space data must be flipped about the frequency encoding direction, so that all lines of k-space space follow the same direction. There are often phase errors in the data following this process and this results in a lower intensity ‘ghost’ (known as a Nyquist ghost) appearing. This ghost is shifted by half the field

of view in the phase encoding direction. The phase errors must be corrected for to reduce these ghosts[102,103].

There are other image artefacts that arise in EPI; these include chemical shift artefacts, image distortion, T_2*-induced image blurring and intra-voxel dephasing. Chemical shift artefacts normally occur in the frequency encode direction but this is actually sampled very quickly in EPI. However, the phase encode direction is sampled only 64 or 128 times over the whole echo train, which results in a low bandwidth in this direction. The consequence of this is a large chemical shift artefact in the phase encoding direction. This can be diminished by the use of a fat suppression in EPI pulse sequences[102].

Another consequence of the low bandwidth in the phase encoding direction, is that considerable image distortions can be seen in areas of the image that are not exactly on resonance. These off-resonance effects can be caused by field inhomogeneities, magnetic susceptibility variations and eddy currents and they can be reduced by decreasing the inter echo spacing, but this can result in other acquisition problems. Magnetic field inhomogeneities can be characterised by acquiring a B_0 map and corrected for. T_2*-induced image blurring occurs because each line in EPI k-space possesses a different T_2* weighting (due to each being acquired with a different TE). Blurring is seen in the phase-encoding direction and increases as T_2* decreases as there will be a greater resulting difference in signal intensity as TE increases. The same off-resonance effect that results in image distortions can cause intra-voxel dephasing, which leads to a loss of signal. This artefact is most pronounced at tissue-air interfaces, i.e. near regions with high magnetic susceptibility differences[5,102,103].

3.7 Blood oxygenation level dependent (BOLD) MRI

The BOLD technique is normally used for functional MRI. This method can acquire images at high temporal resolution (less than 1 second) where the signal intensity reflects the concentration of deoxygenated blood within each

voxel. Signal intensity changes are interpreted as being due to changes in blood flow and metabolism as a result of activation in particular areas of the brain. When used to identify areas of functional activation it is assumed that blood pressure is constant, however this may not always be the case. This project will determine the impact of blood pressure changes on the BOLD signal.

BOLD MRI employs echo planar imaging techniques to produce images related to blood oxygenation levels in the brain[3]. This uses the fact that oxyhaemoglobin is diamagnetic, i.e. it has a low magnetic susceptibility, which is similar to that of the surrounding brain tissue. However deoxyhaemoglobin is paramagnetic and has a higher susceptibility relative to tissue.

Magnetic susceptibility can be defined as the extent a substance becomes magnetised when it is placed in an external magnetic field. It can be defined as the ratio between the induced magnetic field within the material and the externally applied magnetic field. This induced magnetic field results from orbital and delocalised electrons setting up currents in the presence of an external magnetic field. The induced magnetic field can be aligned with the applied field or it can oppose it, in the latter case the magnetic susceptibility is negative. Different materials can be categorised according to their magnetic susceptibility. These categories are[104]:

Diamagnetic – materials of very low negative magnetic susceptibility, e.g. water and most biological tissues.

Paramagnetic – materials of intermediate magnetic susceptibility, e.g. ions, simple salts and chelates of metals (including gadolinium) and molecular oxygen.

Superparamagnetic – materials of relatively high magnetic susceptibility, e.g. small Fe_3SO_4 particles.

Ferromagnetic – materials of very high magnetic susceptibility, e.g. larger Fe_3SO_4 particles and alloys (iron, nickel and cobalt).

When substances of differing magnetic susceptibilities are in close proximity, for example paramagnetic deoxyhaemoglobin and diamagnetic brain tissue, local magnetic field inhomogeneities or gradients are induced. Spins in these areas experience these varying magnetic fields; so start precessing at varying frequencies, which, by definition, results in dephasing. Blood with a higher concentration of deoxyhaemoglobin will have a shorter T_2^* than oxygenated blood (which contains a higher concentration of oxyhaemoglobin). This is due to the greater dephasing that spins undergo in the vicinity of paramagnetic deoxyhaemoglobin due to induced local magnetic field inhomogeneities, thus leading to a shorter T_2^*. A lower BOLD MRI signal from within and around deoxygenated blood results due to this dephasing and subsequent shorter T_2^*.

When the brain is at rest, there are higher levels of deoxyhaemoglobin within the blood volume than during brain activation. During activation, the increase in blood flow (over and above the increase in oxygen consumption), results in higher levels of oxyhaemoglobin, which produce a higher signal in areas of activation[3]. Activation and rest images are then statistically compared to produce parametric maps of activation. This is how the BOLD effect is used in functional MRI imaging to isolate motor, sensory and cognitive function. The echo planar imaging (EPI) pulse sequence (described in Section 3.6) is used to acquire the BOLD data. This is basically a very rapidly acquired T_2^* weighted sequence, which provides contrast between oxygenated and deoxygenated blood.

For this project, the same imaging technique is employed but with a different stimulus and method of analysis. There are questions concerning what changes are actually being measured using BOLD MRI; blood flow, blood volume or blood oxygenation changes. It is hypothesised that BOLD

measures oxygenation differences downstream from the activation region[6], i.e. signal is preferentially detected in the venous vasculature.

Signal originates from both the intravascular space and the extravascular space, and as an imaging voxel will contain both, the signal that is obtained will be a composite of the two. The relative contributions of the two spaces to the signal will depend on a number of factors, including the type of pulse sequence that is used. These various effects are described below.

Intravascular effects

Approximately 3-5% of water molecules are contained within the intravascular compartment, i.e. blood. However, the contribution of the intravascular component to the EPI signal is still significant compared to that of the extravascular component. Blood contains both plasma and erythrocytes and a water exchange process takes place between the intracellular (within the erythrocytes) and the extracellular (plasma) environments. The observed relaxation rate of magnetisation in blood is a weighted sum of the relaxation rates of the individual relaxation processes occurring in the different components of blood (erythrocytes, plasma and due to the exchange process)[105]. The orientation of blood vessels within each individual voxel will also have a bearing on the signal that is observed. This is due to the orientation of the water molecules in blood, in relation to the main magnetic field (B_0) (dependent on the orientation of the blood vessel), which will affect the intra-molecular dipole-dipole interactions. This results in the hydrogen nuclei within the water molecule experiencing a fluctuating magnetic field, which means that their individual rates of precession will vary very slightly. Because the direction of the capillaries and venules in a voxel can be randomly orientated, the protons within these vessels will resonate at very slightly different frequencies and this will result in a loss of phase coherence (dephasing) between these protons. This will produce a loss of signal in a gradient echo sequence. Signal changes will also occur if the oxygenation of

the blood changes, due to large field gradients existing around red blood cells carrying deoxyhaemoglobin (as a result of susceptibility differences) which do not exist around red blood cells carrying oxyhaemoglobin. Thus, it is important to consider this intravascular signal even though its fraction is small compared to the extravascular volume[8].

Extravascular effects

The extravascular signal will also contribute to the signal changes that are observed. The intravascular signal that has been discussed is the signal from blood within the vessel of interest, whether that is arterial, capillary or venous. The extravascular signal is signal from water outside the blood vessel, but in close proximity to the blood vessel of interest. This will be affected by both the size of the vessel and the oxygenation state of the blood within it. As oxyhaemoglobin is of a similar magnetic susceptibility to tissue (they are both diamagnetic), this results in little distortion around arterial blood vessels. Conversely, vessels that carry deoxygenated blood containing paramagnetic deoxyhaemoglobin (venules and veins) will cause distortions in the magnetic field surrounding them, due to greater susceptibility differences between intra and extravascular protons[5]. When a phrase such as 'capillary extravascular signal' is mentioned, this refers to extravascular signal in close proximity to capillary vessels. The type of vessel that it is in proximity to will influence this extravascular signal. The diagram below shows how the magnetic field around vessels of two different sizes varies and the random path of a water molecule through these fields:

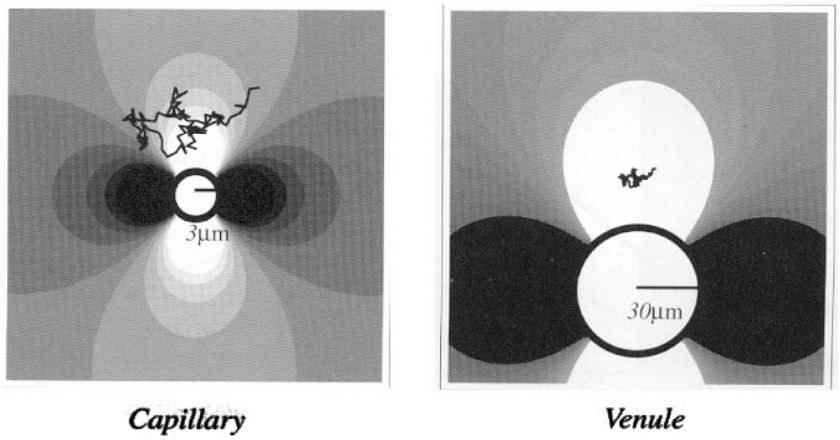

Figure 17: Diffusion paths through magnetic fields surrounding vessels of varying diameter (used freely from Buxton, 2002[5]).

As the magnetic field surrounding a large vessel varies over a much greater distance, the random path of water molecules (due to self diffusion processes, i.e. Brownian motion) in this extravascular space will be within a reasonably homogeneous area of magnetic field strength. During a typical echo time (TE) of 40 ms, the distance moved due to diffusion will be approximately 13 μm ($d = \sqrt{4.D.TE}$, in a cross-sectional plane, where D is the diffusion coefficient and equals 1 $\mu m^2/ms$)[5], which is smaller than the radius of a small vein and this diffusion will be within a homogenous area of magnetic field strength. During this process the molecules will experience greater dephasing as they are subjected to a magnetic field of constant strength. So the difference in signal between the brain at rest (more deoxyhaemoglobin) and its activated state (more oxyhaemoglobin) will be enhanced. However, the magnetic field around a smaller vessel such as a capillary will vary over a much smaller distance and as a result, when water molecules around the vessel diffuse, they will experience varying magnetic field strengths. This means that spins will undergo dephasing and re-phasing as they experience these varying magnetic fields. This results in a net loss of phase, which is less than what they would have lost if they had experienced a constant magnetic field over the same time period. This decreased dephasing will

result in an increased signal at rest, compared to that from spins found close to venous vasculature, and thus, less of a difference in signal between rest and activated states. So, the greatest signal change that is observed between rest and activated states will be seen around venous vasculature[5].

Although GE-EPI is the technique used in this project, it is interesting to note the differences between gradient echo and spin echo EPI techniques, as this may be useful in future developments of the project.

Gradient echo BOLD signal changes

As noted above, in gradient echo BOLD (GE-BOLD), the extravascular signal changes that are observed originate mainly from around the larger venous vasculature. This is due to the fact that at these larger vessel diameters, the typical distance travelled by a water molecule in the extravascular space is much less than the diameter of the vessel and the variations in magnetic field that it experiences (due to magnetic field inhomogeneities resulting from an increase in deoxyhaemoglobin) are much less. Thus, the signal becomes diminished as a greater degree of dephasing occurs. In the case of capillaries, diffusion processes result in the water molecule experiencing a wider range of magnetic field variations and averaging of these means that less dephasing takes place, resulting in less of a drop in signal. So in GE-BOLD, a greater difference in signal between the brain's rest and activated states takes place is seen around venules and veins.

The intravascular signal changes seen in the GE-BOLD experiment are due to the large magnetic field gradients found in the vicinity of red blood cells carrying deoxyhaemoglobin. As a result, venous blood BOLD signal can be reduced by up to 50% compared to the signal observed when blood is fully oxygenated[106]. So the absolute change in intravascular signal between rest

and activation can be comparable to the extravascular signal change, even though blood occupies a small volume in the brain.

Spin echo BOLD signal changes

In a spin echo BOLD (SE-BOLD) experiment, as extravascular molecules experience varying magnetic fields as they diffuse around the vicinity of a blood vessel, the resulting changes in phase may not be completely refocused, producing some reduction in signal. However, as a spin echo is being used rather than a gradient echo, partial refocusing does occur and the BOLD effect will always be weaker (i.e. less of a reduction in signal between activation and rest). In addition, the BOLD signal dependence on vessel size is quite different with SE-BOLD. For larger vessels, as extravascular protons experience a constant magnetic field, the spin echo efficiently refocuses these field offsets. However, for smaller vessels, as they experience varying magnetic fields due to diffusion, the spin echo cannot refocus these as effectively and a greater loss in signal is seen, which results in a greater difference in signal between rest and activation. This is optimally seen around vessels at a diameter of 7 μm. For even smaller vessels, averaging of the magnetic field that is experienced by spins, due to diffusion, reduces the dephasing that takes place and the signal difference between rest and activation. So, the extravascular signal changes in a SE-BOLD experiment are observed mainly in capillaries and venules[5].

There is also a large intravascular component, and it is argued that the SE-BOLD effect is dominated by intravascular signal changes in the veins at 1.5 T[105]. Because venous blood provides the largest signal changes, the largest intravascular signal changes in SE-EPI is in the veins. This is likely to dominate which would counteract the extravascular sensitivity to capillary and venular changes[5], which reduces the usefulness of the SE-EPI technique.

Inflow effects

At short TR intervals, signal originating from arterial inflow is seen. This is high, unsaturated signal from fast flowing arterial blood. This increase in signal is greater than expected because other (old) spins in slice of interest become saturated at these short TR times. So the large increase in signal is a false effect, which is not related to the oxygenation of the blood. This effect can be diminished by using RF saturation techniques, by reducing the flip angle (to enable complete T_1 recovery in the time period TR) or by using diffusion weighting (also known as velocity nulling) to dephase rapidly moving intravascular signal, but this last option also reduces the BOLD signal change[103].

The origins of the BOLD signal changes in functional MRI have been investigated in some depth by Haacke[107] *et al* by reviewing the theoretical basis of the signal changes. They concluded that there are six sources of signal change in fMRI, one from inflow and five from the BOLD effect. These five sources of signal change from the BOLD effect are:

1. Variations in T_2 values of blood due to diffusion through magnetic field gradients around deoxygenated blood cells, resulting from greater susceptibility differences around these cells.
2. Coherent intravascular phase changes and partial volume signal cancellations.
3. T_2^* shortening in the extravascular space due to gradient fields around vasculature (this is discussed in the previous section and the amount of shortening depends on the size of the blood vessel).
4. Diffusion of extravascular water, which is less restricted in its motion, which means that a greater range of magnetic field strengths is experienced.
5. Flow through external magnetic field gradients generated by blood itself.

It is these BOLD effects that should be maximised in these experiments and the inflow effect should be minimised, as this is an artefactual effect.

Taking the inflow effect into account, they found that for very fast flow, the difference in saturation of the BOLD signal between rest and activated blood is very low (as both blood at rest and at activation will have flowed out of the slice in one TR), so the blood signal is independent of flow. However, at very slow flow rates, blood will become saturated at any velocity (whether associated with the rest or activated state) and again the difference between the signal intensities of blood in the two different states will be zero. For slightly faster flow, the percentage signal intensity difference between rest and activated states increases with increasing flip angle. This is because the signal in blood at rest becomes more saturated at higher flip angles (due to its slower flow velocity), and when new unsaturated spins enter the slice at increased flow velocity during activation, higher signal intensity is seen. However at low flip angles, the slow flowing blood at rest does not become saturated, and therefore, the difference in signal between the unsaturated blood at activation and the blood at rest is minimised. The signal changes that are seen are not due to the inflow effect, but purely due to deoxyhaemoglobin concentration changes. So to minimise signal changes due to the inflow effect in fMRI a small flip angle should be used. This has all been investigated in the context of functional MRI. The experiments in this project do not have rest and activated states, but there are flow transients and inflow effects need to be minimised in these situations.

Other papers have also investigated the inflow effect, and in some cases utilised this phenomenon to explore signal changes during functional MRI experiments. Righini[108] found that inflow effects contribute to the signal changes seen during hypercapnia in dogs (this was used as an analogue for neural activation in humans, as it also results in increased blood flow). A GE-EPI sequence was used, with different repetition times from 0.5 s to 10 s, and the flip angle was set at 90°, but this was subsequently found to have varied

between 50° and 80° during the experiments. They found that signal increases during the hypercapnic state were dependent on TR, which leads to the conclusion that these signal changes are due to both T_2* effects and T_1 (inflow) effects, and these effects became significant at repetition times shorter than 1 second.

Work by Frahm[6] explored methods that can be used to reduce inflow effect in functional MRI images. Three methods were proposed: (i) flow dephasing using motion-encoding gradients (similar to those used in diffusion weighted images), (ii) spatial pre-saturation of spins flowing into the imaging slice and (iii) the use of a very low flip angle to remove T_1 saturation effects. These methods were tested using a high-resolution, long echo time FLASH sequence (and thus very short repetition times of less than 100 ms), which produced activation maps in response to photic stimulation and a motor task. The use of a very low flip angle (less than 10° in this case) was found to be most effective at removing effects due to flow (T_1 effects) in these images but retaining deoxyhaemoglobin-induced susceptibility changes (T_2* effects).

An associated problem that can arise when measuring the MRI signal at a high frequency is due to what are termed 'saturation effects'. These effects occur when there is not enough time between RF pulses for the bulk magnetisation to relax fully back (due to T_1 processes) to the equilibrium state (along M_z, see Section 3.1), so by the time of the next RF pulse only a partial component of M_z is available to tip back into the xy plane. This results in a reduced signal being detected as the sequence progresses, resulting in 'saturation' of the system. This can be overcome by using a reduced flip angle in gradient echo sequences, this is known as the Ernst angle[102]. This will also reduce the inflow effects that have been described above. This is considered further in the methods chapter.

Chapter 4 Background information

4.1 The BOLD technique and blood flow and pressure variations

4.1.1 Introduction

In this project, the main aim is to characterise the changes in the BOLD-MRI response to changes in arterial blood pressure due to two different stimuli, thigh cuff deflation and the Valsalva manoeuvre. This section aims to describe some of the previous work relating to this area of investigation. This includes work concerned with BOLD-MRI and blood pressure changes (due to both physiological and pharmacological stimuli) which is the main focus of this piece of work. In addition, the discussion of the following areas is thought to be relevant to the questions posed in this project: the use of BOLD-MRI in the assessment of cerebrovascular reactivity using a variety of stimuli including CO_2, acetazolamide, breath holding and respiration effects, BOLD variations during the Valsalva manoeuvre, and finally resting state functional MRI and spontaneous fluctuation in the BOLD signal due to a variety of factors, but mainly blood pressure variations and respiration.

This chapter begins by describing how slow static blood pressure variations affect the BOLD signal in the brain; this is the followed by a discussion of the effect of pharmacological agents on cerebral blood flow and the resulting changes in cerebrovascular reactivity. Finally this section examines the current work that has been carried out investigating the BOLD signal changes observed whilst carrying out the Valsalva manoeuvre.

Many studies concerning the effect of blood pressure changes on the BOLD signal are based on static changes in blood pressure or alterations of blood pressure over long timescales, rather than investigating faster, dynamic changes, which is the aim of this project. In addition, these studies are often carried out at much higher field strengths (greater than 4 T) than those available clinically (1.5 T in this project), which will increase the signal-to-noise ratio of BOLD signals and resulting changes that are observed.

However, these experiments form the starting point for this project and are introduced here. Imposed blood flow changes are also investigated, rather than explicit blood pressure changes. The next section of this chapter examines these imposed changes in blood flow. It is informative to discuss this area of work, as the end outcome of a change in arterial blood pressure in the brain is a corresponding change in blood flow, even though the mechanism causing these blood flow changes may be different. These changes are usually in response to CO_2 inhalation (or sometimes hypoxia). This technique can be used to assess cerebrovascular reactivity (CVR) in the brain, which is the cerebral blood flow response to vasodilation caused by a chemical or pharmacological agent, usually CO_2, and this is increasingly being investigated using BOLD-MRI techniques. Hence, these kinds of studies are also discussed in this section, as they may provide information about the BOLD signal changes seen when blood pressure is altered. There is also a growing body of literature that discusses pharmacological provocations and the BOLD effect; some of these effects are due to blood pressure induced changes (these are discussed), but most prompt blood flow alterations (as a measure of CVR), as it is thought that vasodilatory agents such as acetazolamide do not affect blood pressure or metabolism[109] or vascular tone[110,111,112].

The BOLD signal has also been investigated in relation to breath hold induced changes in blood flow, often as a measure of CVR, and this area of work is related to the effects of respiration on the BOLD signal and functional MRI; both these areas are considered. Previous work examining the effect of the Valsalva manoeuvre on the BOLD signal is also discussed; this can be thought of as an extension to the breath hold studies and this is one of the blood pressure stimuli used in this study. These studies are almost always only considered in terms of blood flow changes in the brain, rather than blood pressure induced changes. In this study, the Valsalva manoeuvre has been used as a potent modulator of arterial and venous blood pressure. Resting state functional MRI is an emergent area of work and recent studies have

been looking into physiological variations that influence this resting state BOLD data. Vasomotor action and spontaneous changes in blood pressure are particularly pertinent effects to this study and investigations into these will be introduced.

This section will provide background information as to why the experiments carried out in this study are important and give an indication of current thinking in this field of work. In summary, blood pressure changes on the functional MRI signal are poorly understood, especially during fast, transient changes of blood pressure, such as those induced by thigh cuff deflation. Although autoregulation should maintain blood flow during small blood pressure provocations, this may not be immediate or always effective and during fast changes in blood pressure there may be a delay in the blood flow response. In has been found that mean arterial pressure does vary during some activation tasks, by up to 40 mmHg, although this change has been measured over longer periods of time (of the order of minutes)[9,10]. So, changes in blood pressure may induce blood flow changes in functional MRI, which are not purely induced by neuronal activity, particularly if the autoregulation mechanism is not effective. It is for this partly for this reason that the BOLD response to dynamic blood pressure variations is being examined in this project. It is also hoped that such a study of the effect of dynamic changes in blood pressure on the BOLD signal may also provide information about the vascular regulation (i.e. autoregulation) in response to such changes.

4.1.2 BOLD and blood pressure changes

This is a poorly explored area of work and in particular over the short timescale blood pressure (BP) challenges that this study is investigating. There have, however, been some investigations into these effects, although these are often due to static or long time-scale changes in blood pressure (BP), and other studies have purely examined the functional MRI regional

response across the brain to BP changes, rather than looking into the precise vascular dynamics causing these changes. Many of these studies are in animal models (rats or cats) and hence in the anesthetised state. This may be another issue when considering the conclusions gained from these experiments.

Zaharchuk[81] *et al* carried out one of the first investigations in this area. They examined changes in cerebral blood flow, cerebral blood volume (both total and microvascular) and BOLD-MRI contrast during autoregulation and hypotension in rats (at 9.4T). However, changes in blood pressure were induced over a long timescale using arterial blood withdrawal (at a rate of approximately 1mmHg/min), which limits this to an investigation of static autoregulation rather than dynamic autoregulation. No significant changes in signal intensity were seen in the BOLD experiments, with changing arterial blood pressure, as long as BP remains within the range of autoregulation. It was concluded that BOLD-MRI can be used to infer neuronal activity even in the presence of systemic blood pressure changes, for example, in studies using pharmacological agents.

Kalisch[113] examined the effect of arterial blood withdrawal in rats and its implication for pharmacological MRI studies (at 7T), but at a faster rate than that used by Zaharchuk, of the order of 8 mmHg/min, to replicate blood pressure changes in pharmacological MRI experiments. The justification for this is because they have observed similarities between the BOLD signal and blood pressure time courses and after pharmacological stimulation. Once again the time period of the BOLD measurements was much lower than in the experiments in this project (of the order of minutes), but the study did find that systemic arterial blood pressure decreases did result in regionally varying BOLD signal decreases (and some recovery of the signal). These decreases in signal are hypothesised to be as a result of increased CBV, due to the dilation of cerebral resistance vessels in response to a decrease in cerebral perfusion pressure. An abrupt blood pressure challenge that leads to venous

(as reported by Auer[114]), as well as arterial/arteriolar dilation will lead to a decrease in grey matter T_2, and a corresponding decrease in BOLD signal. Since the venous compartment of a cortical voxel is greater than 40% of the total blood volume[115], even a small venous dilation will lead to an increase in CBV and a decrease in signal due to the resulting greater concentration of deoxyhaemoglobin.

In work by Tuor[116] tonic pain or the administration of a vasopressor agent (that does not cross the blood-brain barrier) norepinephrine, was used to increase BP in rats and blood pressure was monitored simultaneously to functional MRI data acquisition (at 9.4T). This meant that functional MRI data could be cross-correlated with BP data to produce regional activation maps relating to BP changes. However, the time resolution of the functional MRI scans was 10 s, hence higher frequency dynamic changes in BP could not be investigated. The injection of formalin (to induce tonic pain) resulted in a 15–55 mmHg increase in mean arterial blood pressure lasting about 146-124 s whereas infusion of norepinephrine produced a transient increase in BP of 15–90 mmHg at an average rate of 7.3 ± 3.4 mmHg/s, with the elevations in pressure returning to baseline within 2–4 minutes. Formalin injection produced activation correlated with the resulting BP increase. Activation detected with the administration of the norepinephrine, was correlated to both the amount and rate of increase in BP. The response ranged from being sparse, localized within cortex or widespread during modest, moderate or severe elevations in BP, respectively. They concluded that small changes in blood pressure are unlikely to cause major changes in cerebral blood flow and blood oxygenation, however their influence will be unpredictable in individuals with an impaired autoregulation of cerebral blood flow. Hence, it is suggested that during the acquisition of fMRI data blood pressure (or even just heart rate) monitoring should be undertaken to establish whether cardiovascular changes are occurring and that changes in BOLD signal may not be solely due to altered neural activity.

A study by Luo[117] used different agents to alter BP in rats; they examined the effect of two cocaine analogues, one that crosses the blood brain barrier (cocaine) and one that doesn't (cocaine methiodide), on the BOLD signal. Administration of the drugs produced a 30-80% increase in MABP within 2 minutes. Once again, these BP changes were monitored over a long time scale (30 minutes) with time resolution of 2 s. Regional maps of brain activation (correlations to BP changes) were produced and very sparse activation was seen after administration of cocaine methiodide, the agent that does not cross the BBB, but does induce arterial BP changes. However, activation was seen in the corresponding cocaine induced maps, which they conclude is purely due to neuronal activation. They concluded that autoregulation compensates for any changes in blood pressure that are induced during the administration of such drugs, and hence the BOLD signal is not affected by these changes. They proposed that BOLD-MRI can be used to map drug-induced neuronal activity, despite associated changes in blood pressure. This is discussed further on in this section with regard to more recent work by Liu[118] and Gozzi[119].

Henderson[17] proposed an interesting link between blood pressure and metabolism in areas of the brain involved in autonomic control. This involved examining regional functional MRI activation in response to pressors (phenylephrine) or depressors (sodium nitroprusside) of BP, in anaesthetised cats at 4.7 T. The objective was to identify the areas of the brain recruited in response to blood pressure challenges and describe the temporal sequence of the recruitment, rather than investigating the vascular haemodynamics of the effects. Short latency (within 2-5 s) decreases in arterial BP of 45% ± 3% (nadir of 45 s) were seen with the administration of the depressor agent, and similar latency increases of 24% ± 3% (nadir of 20 s) were observed with the pressor agent. Two analysis methods were used. Fixed effects analysis used a voxel-by-voxel procedure to search for regions in which BOLD signal intensity changes matched the changes in BP after depressor and pressor administration. A voxel of interest analysis used anatomically defined regions

to explore changes in signal intensity irrespective of the pattern of change. Both approaches highlighted signal intensity changes in response to BP changes. Some pertinent conclusions from this study were that:

1) transient depressor and pressor challenges evoke signal changes over a variety of neural sites, ranging from hypothalamic, insular, and amygdale areas to the cerebellum;

2) signal intensity changes in response to depressor challenges are much larger in magnitude than those induced by hypertensive challenges; and

3) these signal intensity changes do not result from global influences on the MRI signal due to BP alterations and instead represent regional neural responses mediating the challenge, as shown by barodenervation. Animals were tested with barodenervation and without; mean arterial pressure changes remained the same but the BOLD signal intensity changes differed, indicating that that the regional signal intensity responses did not derive from global perfusion effects but from baroreceptor mediation of central mechanisms.

The widespread distribution of areas responsive to AP elevation or lowering includes extramedullary regions not traditionally considered to be components of central cardiovascular reflex networks (e.g., cerebellar-related structures), and many of these components show both short- and long-term response patterns; some of these responses may represent “compensatory” actions.

This is a most informative piece of work but there is no discussion regarding the vascular mechanism affecting the observed changes, other than the effect of baroreceptors, and the discussion is much more concerned with regional neural responses.

Another related study was carried out by Kimmerley[18] but this time using a different BP provocation in healthy human volunteers at 4T; that of lower body negative pressure (LBNP). This study investigated specific areas of the

brain that affect autonomic cardiovascular function and was very much concerned with localisation of neuronal activity in response to baroreceptor control during LBNP. Once again, there is no exploration of the haemodynamics associated with LBNP BP changes and BOLD and during these experiments, it was found that arterial pressure did not change; however, venous pressure did decrease with varying levels of LBNP.

Along the same lines as Henderson, Wang[19] examined how the activation detected with functional MRI (in response to forepaw stimulation) is affected by either BP increases by bolus injection of norepinephrine (NE) or BP decreases by injection of arfonad (maximum change ± 60 mmHg), in rats at 9.4T. These agents were chosen, as they do not cross the blood-brain barrier, and as such act peripherally on BP and do not have a direct influence on intracerebral haemodynamics. In addition, the administration of bolus injections of these agents precipitated a transient change in blood pressure, but this was still over a timescale of 10 seconds, which is longer than the BP changes evoked in this study. BOLD signal changes in voxels that correlated to either purely BP time courses or activation due to forepaw stimulation were identified. Hypertension resulted in increased BOLD signal (without fore-paw stimulation) and an increase in activated voxels (with fore-paw stimulation). The increase in BOLD signal without fore-paw stimulation is thought to be related to perfusion changes in response to BP increases rather than a neuronal response to these BP changes. Hypotension (without forepaw stimulation) resulted in decreased BOLD signal and the number of voxels corresponding to this BP change increased as BP decreased. However there was no decrease in the extent of activation (with forepaw stimulation), just a decrease in the BOLD signal increase during stimulation with the detection of neuronal activation being unaffected. This decrease could result in BOLD signal changes being interpreted as 'deactivation'. They also conclude that transient hypertension could affect functional MRI data in healthy tissue if BP changes follow the time course of the fMRI paradigm that is employed, or in

brains with impaired autoregulation, cerebral blood flow would be much more sensitive to increases in BP.

The use of functional MRI in neuropharmacological studies necessitates the investigation of the effect of BP changes on the BOLD signal, as these changes could confound drug induced neuronal activation. In a study by Liu[118] dobutamine was infused to increase mean arterial BP (by approximately 150%) in cocaine-dependent participants. This was chosen as it increases peripheral BP without affecting brain activity. Subjects were scanned over a period of 25 minutes. They found that there was no global change in BOLD signal with increasing BP, but localised activation (i.e. correlation between BP and BOLD signal changes) was found in the anterior cingulate, but they argue that this observation could be due to functional control of BP. Generally, they dispute that there is any effect of dobutamine induced BP changes on the BOLD signal due to the action of autoregulatory mechanisms. This contradicts other findings, such as those presented in studies by Tuor[116] and Kalisch[113], and Liu argues that cerebral blood flow (CBF) and cerebral blood volume (CBV) changes were also induced in these studies, thus confounding the effect of BP changes in isolation. This may be the case, but in reality, blood pressure changes do affect CBF and CBV, and these all contribute to BOLD signal alterations. Their results agree with those demonstrated by Luo[117] and Zaharchuk[81], who also attribute the lack of BOLD signal changes in response to BP alterations, as being due to the autoregulation mechanism. These studies all examine signal changes over fairly long timescales, and as such, the autoregulatory response will have enough time to respond, and due to the slow time resolution of these experiments, transients in BOLD signal changes (before the autoregulation mechanism has time to respond) may be missed.

In work associated with that carried out by Henderson and Wang, Qiao[120] examined transient hypertension imposed (using norepinephrine) at the same time as forepaw stimulations in rats. They found that BOLD responses are

enhanced by concurrent hypertension in rats, despite the action of the autoregulatory mechanism, and they suggest that this could be due to transient decreases in oxygen consumption, or a redistribution of flow through more non-exchange vessels. In previous similar experiments by the same group, flow was measured using laser Doppler flowmetry, and oxyhaemoglobin and deoxyhaemoglobin was measured using near infrared spectroscopy (NIRS). Similar increases in CBF and oxyhaemoglobin were seen as well as a decrease in deoxyhaemoglobin.

Gozzi[119] *et al* investigated at the effects of a pharmacological agent on CBV and CBF in order to elucidate the effect of arterial BP changes on the BOLD signal. Independent measurements of CBV and CBF were made in response to injection of norepinephrine (as used in Tuor's approach). A contrast-enhanced MR technique was used to evaluate CBV changes whereas laser Doppler flowmetry (LDF) was used to investigate the CBF response to varying doses of norepinephrine; and mean arterial BP was also measured. No changes in CBF or CBV were found in the 60-130 mmHg mean arterial BP range, but at BP levels above this, both LDF and microvascular regional CBV (rCBV) showed transient but significant increases. An interesting point to note is that significant microvascular CBV changes were not detected, within the autoregulatory range for MABP. However, a spin-echo technique was used to measure rCBV changes, and this is primarily sensitive to changes in capillaries and the contribution from large vessels is reduced. As vascular resistance (and hence blood volume change) is thought to be controlled by arterioles, it may be that this technique did not detect the volume changes associated with these larger vessels. However, it is noted by the authors that during pharmacologically induced hypertension, arteries and arterioles do not change diameter below 170-190 mmHg, after which point they do dilate with increasing MABP. This study quotes Zaharchuk's[81] work, which also reported small microvascular CBV changes when MABP was decreased from 140 mmHg to 50 mmHg, and hence postulated that CBV changes only occur in the arterioles, which only comprise 5% of overall cerebral blood volume.

This, however, disagrees with results from Kalisch[113], who saw decreases in the BOLD signal with arterial blood withdrawal and suggested these changes are due to venous volume changes as an autoregulatory response.

A recent paper by Kamba (2007) tries to explain the disparity observed between visual stimulation and resulting negative BOLD responses in particular areas of the brain. These regions were found bilaterally on the lateral surface of the occipital lobe just anterior to the occipital pole and were situated in the border zone between the territories of the middle and posterior cerebral arteries They concluded that insufficient perfusion pressure in these parts of the brain may diminish the BOLD and perfusion responses to stimulation of a large portion of the visual field. Alternatively, it may be that a condition in which a large extent of the visual areas was activated in the proximal regions of the territories perfused by the middle and posterior cerebral arteries (i.e. areas with insufficient perfusion pressure) was the cause of these findings. This is a different approach to the question of the effect of BP changes on BOLD, as BP changes were not explicitly imposed, but it is thought that negative responses that are seen are due to inadequacies in blood pressure in these regions. Their final conclusion was that regional differences in circulatory condition might result in alterations of the relationship between neuronal activation and BOLD signal changes in physiologically normal conditions.

So, in conclusion, although the effect of BP changes on the BOLD signal has been studied, these results can sometimes be contradictory, which may be due to the type of BP challenge imposed, or due to the timescale of the challenge. None of these studies is looking at blood pressure changes with the fast timescales involved with thigh-cuff deflation (the Valsalva manoeuvre will be discussed later), or from the perspective of the cerebrovascular haemodynamics that may be causing the BOLD changes that have been observed. Rather, most papers have concentrated on the end result of the BOLD signal changes in response to a BP change, that is, the regional

specificity of the variations that are seen. However, some useful information has been provided in terms of the time courses of the BOLD signal changes, the effect of differing degrees of BP change and the resulting effect on activation studies.

4.1.3 BOLD and cerebrovascular reactivity

In the previous section, BOLD signal changes were discussed with regard to blood pressure challenges. Although it is advantageous to isolate BOLD signal changes purely due to BP alterations, these challenges do also affect cerebral blood flow. Vasodilation and hence changes to blood flow (but not necessarily blood pressure) in the brain can be induced in a vast number of ways, and it is the response of the vasculature to these changes that can be examined to assess cerebrovascular reactivity, which is a slightly different approach for examining vascular function in the brain. In this section, measurements of cerebrovascular reactivity (CVR) using BOLD will be discussed, as this is also relevant to the effect of BP changes on the same signal. The main mediators that are used to induce vasodilation in these types of studies are carbon dioxide, acetazolamide, carotid compression (which is also a blood pressure stimulus), breath holding and hypoxia, and the effect of these will be discussed.

In an early piece of work by Bruhn[121] acetazolamide, a vasodilatory agent was administered. This increases blood flow without a corresponding change in oxygen consumption and their approach introduces a method of monitoring autoregulation in the human brain under vasodilatory stress. The signal intensities of deoxyhaemoglobin-sensitive images (similar to BOLD images) increased in cortical and subcortical gray matter and to a lesser extent in white matter. It is thought that this signal increase is due to increased venous oxygenation, which comes from an increase in cerebral perfusion with oxygen consumption remaining constant. They concluded that by observing cerebral blood oxygenation changes using MRI will elucidate the mechanisms of

modulation of vasomotor tone and cerebral perfusion, which is also a secondary aim of this project.

Kleinschmidt[122] *et al* continued previous work by Bruhn. They used a BOLD technique to examine regional blood oxygenation changes under acetazolamide (a vasodilator) in patients with carotid occlusive disease. The temporal resolution for this study was 6 seconds, much slower than in these experiments. However there are some pertinent points to be taken from this study. A gradient echo sequence (FLASH) was used with a low flip angle (10°) to emphasise changes in signal due to blood oxygenation rather than blood flow velocity. MR signal increases (due to administration of acetazolamide) were attenuated in the vascular territories of occluded arteries. This corresponded to decreased haemodynamic reserve capacity (as measured by TCD) and demonstrated exhaustion of autoregulatory reserve capacity, which could be a measure of cerebral autoregulation. After administration of acetazolamide, signal intensity increased in normally perfused hemispheres. Regional changes (using a region of interest analysis approach) were seen in macroscopic pial vessels and underlying grey matter (none were seen in white matter). The slow time resolution of Bruhn's technique was not a problem, as the response to acetazolamide is a fairly slow one. However, in this project a fast response mechanism is being examined and a slow time resolution would be a concern. They have also mentioned that absolute quantification of oxygenation is not possible with MRI; however, this study will be looking at regional changes, so this should not be a problem.

More recent work by Mukherjee[112] (2003) examined the regional response of the BOLD (using SE-EPI) signal in rats to acetazolamide administration to assess cerebrovascular reactivity solely by examining vasodilatory CBF effects, separate to metabolic or systemic blood pressure effects on the BOLD signal. As expected, signal intensity increased in all areas across the brain, and the time courses of these increases were approximately the same.

However, there were variations in the magnitude of the response, particularly in the hippocampus (which is known to be susceptible to ischaemic damage); this may indicate limited regulation of perfusion in this region and a paucity of either flow-regulatory arteriolar vessels or volume-regulatory venular vessels. Similar differences were seen within white matter regions, which would be consistent with lower vascularity in these regions. These regional differences are thought to be important for the investigation of stroke, particularly in relation to neuroimaging studies.

There are other methods of testing this response and several have been employed whilst measuring the BOLD-MRI signal in the brain. Righini[123] (1998) used compression of the common carotid artery to test cerebrovascular reactivity, i.e. the use of cessation of blood flow to the brain to induce changes in the BOLD signal. They saw a decrease in signal intensity during common carotid compression, which could be due to three factors: (a) increased deoxyhaemoglobin within the microcirculation, (b) the inflow effect, and (c) reduced brain pulsation. The inflow effect was eliminated as a reason for the signal changes seen, as when the experiments were repeated with a long repetition time (TR), the same effect was seen. Righini concluded that (a) is the most likely explanation, which is a similar effect to the one that is attempting to be observed in this study. One subject did show a signal overshoot, which could be explained by an over-compensatory hyperaemia washing out accumulated deoxyhaemoglobin. However, the fact that they only saw this in one subject could be due to the low time resolution of their technique (5 seconds).

Work carried out by Lythgoe[124] mapped cerebrovascular reactivity using BOLD MR imaging, this time using the vasodilatory cerebrovascular response to CO_2 breathing, rather than a stimulus such as carotid compression. This study examined patients with unilateral carotid artery stenosis greater than 70% or internal carotid artery occlusion. A time resolution of 3 seconds was achieved and two sets of 10 images were acquired with the subject breathing air and then breathing a 6% CO_2/air mixture. From these data, BOLD

reactivity maps were produced on a voxel-by-voxel basis. These depicted the fractional increase in image intensity due to CO_2 inhalation, normalised to the increase in end tidal CO_2. Regions of interest were determined for left and right middle carotid artery (MCA) territories, and weighted mean reactivities were calculated. Similar measurements were made using transcranial Doppler, where blood velocity changes were measured rather than signal intensity changes. A good correlation was found between inter-hemispheric MCA reactivity differences measured with transcranial Doppler and BOLD MRI. There was also a decrease in BOLD reactivity in areas of established infarction. The signal intensity changes appeared to be greatest in the vicinity of the major blood vessels and the signal change appears to be global and hence associated with the microvasculature. The authors concluded that BOLD imaging provides semi-quantitative information regarding CO_2-reactivity, at high spatial resolution. However, they assume that the signal changes that are seen in the BOLD imaging are purely due to flow and they relate this directly to TCD measures of flow, which may not be valid without making certain assumptions.

A method for the quantitative assessment of cerebrovascular reactivity has been proposed by Vesely[125], whereby changes in MRI signal intensity are related to square wave forced alterations in P_{ETCO2} (end tidal CO_2 level). This method has an advantage over both inhalation of gas mixtures containing CO_2 or breath-holding as neither of these provides known or steady levels of CO_2, which means fully quantitative CVR assessment is limited.

The effect of end tidal CO_2 levels on the functional MRI response has been investigated by Cohen[126]; this was achieved by varying basal CO_2 levels to produce states of hypocapnia, normocapnia and hypercapnia. An increase in baseline functional MRI signal was seen as levels of CO_2 increased from hypocapnia through to hypercapnia, due to a vasodilatory effect of increased CO_2, which increased the BOLD signal as oxygen saturation of the venous circulation increases (as $CMRO_2$, oxygen consumption, is assumed constant).

At the same time, the magnitude of the BOLD response to visual stimulation decreased linearly; whilst various measures of the dynamics of the BOLD response to visual activation increased with end tidal CO_2. This is thought to be due to the vasodilatory mechanism of the arterial circulation counteracting blood velocity effects during stimulation.

Van der Zande[48] also attempted to map CVR induced by hypercapnia (using Vesely's methodology) and using BOLD, in healthy volunteers. Their main findings were that there was a strong relationship between end-tidal P_{CO2} and MR signal intensity, with a higher percentage of signal change (three times larger) in grey matter than in white matter. They concluded from this that hypercapnia-induced cerebrovascular reactivity can be assessed by BOLD MRI and this could enable the detection of exhausted cerebrovascular autoregulation in patients with a compromised cerebral vasculature. More recently Mandell[49] (2008) has built on this study by extending this assessment to patients with arterial steno-occlusive disease and compared BOLD with arterial spin labelling (ASL), which solely measures blood flow. They found that there is a strong correlation between CVR measured using BOLD and ASL, which indicates that the BOLD signal response to hypercapnia is predominantly due to flow changes, even in diseased patients. Previous studies did not enable this conclusion to be made.

Breath-holding is also a powerful vasodilatory stimulus. Early work in this area by Kastrup[127] (1998) used breath holding as a vasodilative stimulus (which results from an increase in arterial P_{CO2}) and examined the resulting blood oxygenation changes. The authors emphasised the advantages of using this easy to implement, non-invasive technique compared to other more invasive techniques such as CO_2 inhalation or administration of acetazolamide. This technique results in an increase in CO_2 and cerebral blood flow (due to vasomotor reactivity), which increases oxyhaemoglobin and results in an increase in signal intensity. However, the reduction of arterial oxygen saturation during breath holding will have the opposite effect. The resulting signal change will depend on the relative contributions of these

two competing factors. In general, an increase in BOLD signal was seen, but this did vary with the type of breath-hold technique employed. The BOLD signal intensity changes were again greatest in grey matter but insignificant in white matter. Once again the time resolution of measurements was much slower than that used in this project, of the order of 3 seconds and a gradient echo sequence was used. Kastrup[128] also looked at regional changes in cerebral blood oxygenation. They found that the response to hypercapnia varied across the brain and the highest signal changes were found in the cerebellum and visual cortex.

Other breath hold experiments have been carried out in last decade in various groups. Li[129] *et al* compared the results of breath holding on both BOLD and FAIR (flow alternating inversion recovery, a perfusion technique) MR images. Although the time resolutions of these images were 3 and 6 seconds respectively, interesting transients were noted. With periodic breath holding, global changes in grey matter were seen in both BOLD and FAIR images, although fewer activated pixels were detected in the FAIR images. In the case of prolonged breath holding, the time courses of signal intensity changes depended on the particular breathing techniques used. Breath holding after expiration produced immediate signal intensity increases in both BOLD and FAIR images, and breath holding after deep inspiration showed a biphasic change in BOLD and FAIR, which was manifest as a transient decrease followed by a rise above the baseline level. The results from this deep inspiration challenge are thought to be related to the effects of an incomplete Valsalva manoeuvre after the deep inspiration. They state that during this manoeuvre a large increase in intra-thoracic pressure will produce a transient rise in cerebral venous pressure, intracranial pressure and venous pressure in the great veins, thus decreasing arterial blood pressure (actually cerebral perfusion pressure) and cerebral blood flow. Pa_{CO2} (partial pressure of arterial CO_2) also decreases initially as a result of the deep inspiration. An initial decrease of jugular P_{O2} will result in a decrease in the BOLD signal, and a decrease in Pa_{CO2} will result in reduced blood flow, which is demonstrated

by the FAIR signal. After prolonged breath holding, Pa_{CO2} increases, thus increasing blood flow and the resulting BOLD and FAIR signals.

An investigation into varying durations of breath holding has been made by Liu[130], to evaluate the feasibility of detecting BOLD changes with short breath hold durations in clinical practice. Volunteers were asked to hold their breath for time periods of 3 s, 5 s, 10 s, 15 s, 20 s and 30 s. Significant changes in the BOLD response could be detected with durations greater than 10 s. Maximum signal changes were found in deep grey matter. Other activation related parameters increased with breath hold duration, namely the activated brain volume, the full-width half-maximum (FWHM) of the BOLD response and the onset time of the BOLD response. No quantitative parameters related to CVR were extracted from this data, as CO_2 levels were not measured. However they concluded that 20 s breath holding is the optimal choice for clinical breath hold studies.

More recently, Shiino[131] (2003) has also attempted to estimate cerebral perfusion reserve using BOLD and breath holding in patients with carotid artery occlusion, and results from this have been compared to SPECT (single photon emission computed tomography). Some interesting transients were noted, although the time resolution of the BOLD acquisition was 3 seconds, so some features of the time courses may be missed. They also found that BOLD signal increased in a biphasic manner. They postulated that this was due to the following sequence of events: during breath holding, there was an initial decrease in signal but then accumulation of CO_2 leads to an increase in CBF, which was proportionally greater than the increase in deoxyhaemoglobin levels (i.e. volume effects) due to the breath hold, resulting in an increase in signal. There was then a rapid increase in the BOLD signal after resumption of breathing, as highly oxygenated blood flows through already dilated blood vessels. Other results from this study found that BOLD signal changes correlated with SPECT data (as a result of acetazolamide challenge), however BOLD imaging failed to distinguish between moderately and severely impaired patient groups.

Hamzei[16] *et al* investigated the effect of extra and intracranial artery stenosis on the BOLD signal. This was tested using a carbogen breathing regime with BOLD imaging to enable the calculation of CO_2 reactivity maps. These maps were compared to BOLD functional maps obtained from a motor activation paradigm. Patients with normal cerebrovascular reserve capacity (CVRC), as determined from the CO_2 reactivity maps showed no BOLD activation differences between affected and unaffected hemispheres. However, patients with impaired CVRC showed a decrease in BOLD signal in the sensori motor cortex on the affected side of the brain. Similar findings were reported by Krainik *et al* in patients with stroke[132].

Another paper that looks at BOLD changes in a patient group is by Hsu[12], where a breath hold paradigm was employed in patients with gliomas. Periods of breath holding for 15 seconds were employed and the BOLD signal change within normal grey matter and glioma were observed during the experiment. It was concluded that there was a lack of BOLD signal enhancement in areas of tumour, which may be due to inadequacy or lack of responsiveness of the vasculature, severe tumour hypo-oxygenation or a combination of these effects. However, breath hold regulated decreases in the BOLD signal were only seen in high-grade gliomas and this is attributed to a 'steal' effect. This is thought to occur when blood flow from tumour regions with poorly responding neovasculature is redistributed to surrounding normal tissue. The BOLD signal was found to increase in normal tissue during the breath hold paradigm. This was a study with a small cohort of patients, and as such, it is thought a larger study would strengthen these findings. In addition, no calibration of arterial CO_2 or O_2 tension was carried out during these studies.

A slightly different approach to characterise cerebrovascular reserve was carried out by Carusone[14] in 2002. In this work, abnormalities in the BOLD response to a motor task in patients with cerebro-occlusive disease were linked to measurements of cerebrovascular reserve using transcranial

Doppler. Areas of impaired cerebrovascular reserve (as detected by TCD) were found to have an impact on the BOLD signal changes. In the event related BOLD experiments, a decrease in the amplitude and a delay in the peak BOLD signal was seen ipsilaterally to the occlusion. This was not seen in the block design experiments, which had a much longer stimulus period (30 seconds compared to 2.5 seconds in the event related experiments). The repetition time (TR) for the block design experiments was much longer than that employed in the event related trials (3000 ms and 500 ms respectively). Transient haemodynamic responses may be missed when a long TR is used. It is thought that the short stimulus duration in event-related functional MRI measurements may provide the potential haemodynamic variations in which to examine autoregulatory mechanisms. It is possible that decreased vascular reserve capacity would result in the impaired ability of the vasculature to respond to neuronal activity in this case (or alterations in blood pressure), as a result of exhaustion of vasodilatory function in these vessels at rest. This decreased vascular reserve was found to be distal to severely diseased vessels in this study. This was an interesting clinical study linking the impairment of autoregulation of blood flow to BOLD signal changes, although neuronal activation was used as a blood flow stimulus rather than blood pressure changes.

Up to this point, all these investigations look at the BOLD signal and correlate this with changing CO_2 levels rather than BP changes which is the aim of this project. A valuable study that does relate arterial pressure changes to CBF and BOLD signal, in apnea, under different anaesthetic regimes has been published by Kannurpatti[133]. They postulated that two anaesthetic agents, pentobarbital and urethane would have different effects on the mean arterial blood pressure (MABP) dynamics induced by apnea which can be used to understand the relationship between MABP, CBF and the BOLD signal. This is due to the differing physiological actions of these agents; urethane anaesthesia does not influence GABAergic mechanisms involved in the control of cardiovascular functions unlike pentobarbital, which does. CBF

was studied in rats (at 3 T) using laser Doppler flowmetry, whereas oxygenation was investigated using the BOLD-MRI technique. They found that the decrease in BOLD signal was greater in grey matter than white, which agrees with previous studies. When comparing flow and mean arterial blood pressure, it was found that flow increases with apnea and the administration of both anaesthetic agents; however, MABP decreases with pentobarbital whereas MABP followed flow changes with urethane. In addition, MABP did not change significantly in response to apnea during hyperoxic or hypercapnic baseline conditions with both anaesthetics. The changes in BOLD signal were similar with the administration of both anaesthetics, which suggest that these changes were dominated by an alteration in arterial blood oxygenation and independent of changes in MABP. This suggests that the $CMRO_2$ (oxygen metabolism) was relatively higher with urethane anaesthesia than that with pentobarbital anaesthesia, so even though MABP varies between the two agents, the fact that $CMRO_2$ also varies, results in similar BOLD signal changes, due to uncoupling of CBF and oxygen consumption.

Another use of the breath-holding task could be to remove variability in neuronal activation data, by assessing the component of this, which is due vascular variability, and removing it. Handwerker[134] has carried out work to do this, particularly in the case of ageing populations, where vascular variability may become significant. The method they propose is to divide the magnitude of the fMRI response to a neural task (a visual saccade task) by the magnitude of the hypercapnia task, as there is a strong correlation (by voxel) between the two tasks.

A very recent paper by Thomason[135] (2008) explores how the variability in breath holding induced BOLD signal changes can be reduced. Visual cues were employed to prompt breath holding and feedback was given regarding the depth of inspiration. Variance in the BOLD signal change was reduced when feedback was provided and greater activation was also demonstrated in these scans. They discussed the increased reduction in BOLD signal with

increased inspiration being due to blood kinetics resulting from changes in the peripheral nervous system and also interactions with the pulmonary system. They describe three phases of BOLD signal change during the breath hold period following inspiration:

(1) chest expansion → decreased intrathoracic pressure → reduced vascular resistance → increased blood flow to the heart,

(2) autonomic regulation by baroreceptors → reduced HR → decreased blood flow to brain → increased paramagnetic Hb (deoxyhaemoglobin)→ reduced signal intensity (SI),

(3) Increase in CO_2 → increased CBF in brain → drop in paramagnetic Hb → rise in oxyhaemoglobin and signal intensity.

This produces a bi-phasic response, similar to that described by Li[129]. In this study, when subjects inspired more deeply during phases 1 and 2, a greater reduction in BOLD signal results, and a greater difference between the trough and peak in this bi-phasic response was seen. They conclude that the results of this study will be important if this type of technique is used to assess neurovascular responsitivity, i.e. cerebral reactivity.

A recent paper by Bright[136] *et al* characterises the magnitude and dynamics of the vascular response to a hypocapnia task, using BOLD fMRI. The hypocapnic task consisted of a cycles of cued deep breaths to produce a BOLD signal decrease. A breath hold hypercapnic paradigm was also imposed. Reactivity maps (defined as the percentage change in BOLD signal relative to the change in end tidal CO_2) were derived from data obtained from both hypo and hypercapnic challenges and there was found to be reasonable qualitative agreement between the two. Similar regional heterogeneity was found in the timings of the BOLD response to both paradigms. Bright's study concludes that this type of hypocapnic task (cued deep breath) may be more applicable in a clinical setting for assessing cerebrovascular reactivity rather than breath holding or administration of CO_2.

The use of breath holding studies are becoming more commonplace as a means of assessing CVR, and improvements are being made in order to provide a more quantitative result from these types of studies.

In conclusion, it is informative to examine previous work relating to the assessment of cerebrovascular reactivity, as it is a parameter closely related to autoregulation, which is the mechanism invoked when BP changes are applied to the brain. There are many different techniques that can be employed to assess CVR, and a few of these are discussed. Recent developments have explored the possibility of mapping CVR across the brain. Perhaps the most relevant technique to this project is the use of breath holding and BOLD as this is somewhat similar to the Valsalva manoeuvre employed here. However, the majority of these studies have examined the response to breath holding in terms of flow and CO_2 changes and very few have made any attempt to explain the effects of blood pressure changes during breath holding on the resulting BOLD signal.

4.1.4 BOLD and the Valsalva manoeuvre

As an extension to the work that has been carried out examining BOLD signal changes during breath hold, is to examine the changes seen with the Valsalva manoeuvre (VM), which can be thought of as a more extreme form of breath holding. It is often described as forced expiration against a closed glottis and is known to be a powerful modulator of both arterial and venous blood pressure.

Some BOLD signal intensity changes due to inspiration have already been discussed by Li[129], and they postulated that this kind of deep inspiration is similar to an incomplete Valsalva manoeuvre. The resulting biphasic signal change has also been described by Thomason[135]. This is informative, however no quantitative measures of blood pressure have been made during these challenged, and hence, these explanations are of limited use.

King[20] has examined regional changes in BOLD signal with the Valsalva manoeuvre and the manoeuvre is primarily used as a visceral stimulus. Other heart rate (HR) and blood pressure (BP) altering stimuli are also employed, namely maximal inspiration and isometric hand grip; this is the first functional MRI study to investigate such stimuli. Although time courses of heart rate and BP are shown, the study is really just looking at the extent and distribution of activation in relation to these stimuli, and no BOLD time course information is provided. They found that the neural activity in response to VM is bimodal in nature. Initial increases in activity were observed in the insular cortex, and posterior ventrobasal thalamus at times corresponding to the initial increases in BP in the first 12 seconds. Subsequent increases in activity, occurring between 18 and 30 seconds after the start command, were seen in the insular cortex, and medial prefrontal cortex; these changes correspond with the secondary increases in BP and the change in HR. During time periods when BP and/or HR were elevated, and especially during the initial periods of change, activity levels in the insular cortex, posterior thalamus, and medial prefrontal cortex were significantly elevated above baseline. The authors conclude that this activity most likely reflects cardiopulmonary inputs and a role in the regulation of HR and BP for these forebrain regions.

In a similar vein to King, Harper[137] looked at activation due to transient blood pressure increases in healthy volunteers, and three different pressor challenges were used, one of which was the Valsalva manoeuvre, the other two being cold application to the hand or forehead. It was noted that no change in oxygen saturation was observed during the Valsalva manoeuvre and a minimal change in CO_2 saturation was seen in one subject out of eleven in the study. Blood pressure elevations of over 50% were seen, and thus this was considered to be the main physiological effect. A time resolution of 3.5 seconds was achieved, and although this enabled volume coverage of the regional changes in activation due to the challenges, it is mentioned that a faster time resolution would allow better elucidation of

dynamic neural responses and better define the sequence of activation in different regions of the brain (this approach has been used by Henderson[17] using pharmacological agents to alter BP). Pressor challenges resulted in activation in a wide range of areas in the brain, including orbitomedial prefrontal cortex, temporal cortex, amygdala, hippocampal formation, thalamus, and hypothalamus. Cerebellar, midbrain, and pontine areas were also demonstrated signal changes and signal changes were often highly lateralized (especially at forebrain sites), although this varied between subjects. The time course of signal changes also varied from region to region, although, as stated above, the time resolution of these measurements was relatively low.

The same group extended this work to investigate the dynamics of neural activation to just the Valsalva manoeuvre[21] (Henderson *et al*, 2002). This time the VM was repeated three times during a 90 second scanning sequence, with the time resolution of 6 seconds, and each VM lasting 18 seconds. The time course of signal intensity changes was examined in different regions of interest across the brain. A peak in signal intensity was first seen in the hippocampus and amygdala, next within the dorsal medulla, pons and midbrain, and deep cerebellar nuclei, and lastly within the lentiform nuclei and the lateral prefrontal cortex. Signal intensity changes were correlated with heart rate alterations during the Valsalva manoeuvre but arterial BP changes were not measured or considered in Henderson's study, which makes the interpretation of the paper difficult and lessens the relevance of these findings to this project.

In a more comparable approach to that used in this project, Gareffa[22] (2003) investigated negative BOLD signal changes resulting from a stimulus similar to the Valsalva manoeuvre (breath holding after inspiration). Two approaches were used, a rest-activity experiment, with inspirational apnea used as the stimulus and normal respiration the rest activity. A single-phase task was also used, where only one period of inspirational apnea was

performed. A diffuse negative BOLD response (i.e. a drop in BOLD signal) was observed in all subjects, across the whole brain, and this bore no relation to spatial neural activity. A strong negative BOLD response was also seen near the venous sinuses. Oxygen saturation was measured in all subjects and this did not change during apnea for any of them. They suggest that a slowing of venous flow during inspirational apnea induces a venous dilation with a corresponding increase in deoxyhaemoglobin volume, resulting in the negative BOLD effect. They also asked subjects to perform a jugular bilateral compression test, to mimic the reduction of venous flow during the VM, and similar behaviour was demonstrated. This study has been extended to include a hierarchical cluster analysis[138]. Volunteers performed the same single-phase task as that described above. Various clusters were defined including a mean value at baseline, root mean square of the time course during inspirational apnea (IA), the greatest negative BOLD difference value between the baseline and the minimum value of the time course during IA, the maximum positive difference between the baseline and maximum value of the time course during recovery post IA, and finally the time delay between onset of IA and minimum BOLD signal. They found that the areas of interest during IA and during the recovery phase were identified as venous vasculature. This concurs with the hypothesis that a slowing down or pooling of venous blood flow during IA (due to increased thoracic and hence venous pressure) induces an increase of the diameter of the small and medium venous network located close to cortical sulci. This is an interesting observation especially as negative BOLD signals associated with visual activation have been explained by either a neural deactivation-inhibition mechanism[139], or blood flow redistribution, characterised as blood stealing by the active constriction of vessels under neural control and the decrease of local pressure in vessels that share the same blood supply[140]. This paper concludes with the opinion that the use of such a stimulus such as IA or VM, for the estimation of cerebral vasodilatory capacity and vascular resistance in

functional MRI seems to be a promising research tool for the understanding of cerebral functional architecture.

In conclusion, some investigation into the BOLD response to the Valsalva manoeuvre have been carried out, both in terms of neuronal responses, and the temporal patterns of these, and the basic BOLD signal changes due to the VM. The signal changes have been described in a qualitative manner, but not in any great detail and not in respect to dynamic BP changes in the brain, which is the aim of this project.

4.1.5 Resting state functional MRI

A brief description of work involving resting state functional MRI is presented here. Resting state functional MRI has been used to examine spontaneous fluctuation in the BOLD signal, especially low frequency fluctuations (LFF) of less than 0.1 Hz, and these fluctuations are thought to contribute to noise in the fMRI signal. These fluctuations may be due to a variety of physiological phenomena and one such confound could be small changes in blood pressure. Other contributions to physiological noise in fMRI are cardiac[141] and respiratory[142,143] related rhythms. An interesting paper by Windischberger[144] looked at the origin of respiratory artefacts in the brain. They found differing spatial distributions of respiratory artefacts and those induced by cardiac function, and postulated that different vessel systems are affected by respiratory and cardiac fluctuations. Artefacts occurring at cardiac frequencies mainly occur in the arterial vascular system (due to inflow effects), whereas they hypothesis that breathing related artefacts arise from cerebral veins (due to combined BOLD and inflow effects). During breathing, variations in intra-thoracic pressure lead to changes in central venous pressure, and it is these variations that may be transpire in the BOLD signal as noise. This information is pertinent to this study as a more extreme venous (and arterial) pressure stimulus is being applied in the form of the

Valsalva manoeuvre, and the effect of this on the BOLD may act in a similar manner.

Spontaneous low frequency fluctuations in arterial CO_2 levels have also been found to contribute to this noise[145]. Slow oscillations in the BOLD signal may be related to autoregulatory, metabolic or myogenic oscillations. Of particular interest is the action of vasomotion, which describes the slow cycling of arterial vessel diameters, which has an immediate haemodynamic effect on the BOLD signal. Further justification for considering this mechanism is that the frequency of this phenomenon matches that of the oscillatory frequencies detected in resting state fMRI. These oscillations can be seen in most vascular territories including those in the brain, and are thought to be a myogenic response that takes place at the lower limit of autoregulation[146]. Kannurpatti[147] examined the changes in amplitude of these vasomotor oscillations and found that after exsanguination in rats, i.e. a decrease in mean arterial blood pressure, resulted in an increase in the amplitude of these low frequency fluctuations. As the behaviour of the BOLD signal fluctuations was similar to those seen in CBF under exsanguination, this suggests a myogenic dependence for this mechanism.

Razavi[148] looked into the source of these oscillations and suggested that they are primarily attributed to small CBF variations, and it is initially hypothesised that these variations are due to fluctuations in vascular resistance or blood pressure. However, this is dismissed, as fluctuations in blood pressure are thought to be of a frequency of 0.1 Hz (Mayer's waves) whereas these fluctuations correspond to frequencies of 0.01 Hz, which match the frequency of spontaneous oscillations of cerebrovascular resistance. These vasomotion effects occur in the arterial compartment and these effects are transmitted downstream to the vascular system, thus inducing an effect on the BOLD signal. In addition to accounting for these low frequency fluctuations, higher frequency fluctuation due to changes in cerebrovascular resistance and cerebral perfusion should also be considered as possible confounds in

functional MRI and this should be investigated to increase quality and consistency in functional MRI studies. These fluctuations are considered in studies using transcranial Doppler[2], and provide valuable information regarding the autoregulatory processes occurring in the brain.

4.1.6 Conclusions

This section has provided a comprehensive description of the current state of investigation of blood pressure variations on the BOLD signal, as well as discussing other relevant subjects. The discussion started with changes in the BOLD signal induced by BP changes using a variety of stimuli, both physiological and pharmacological. These studies are often on animals and higher magnetic field strengths than used clinically, and none of the studies examine fast dynamic changes in blood pressure as in this project. However, useful information has been gathered from reviewing these studies regarding the time courses of signal changes and the effect of varying BP challenges. The section on the measurement of cerebrovascular resistance was useful in describing the effect of flow changes on the BOLD signal as the blood pressure changes that are imposed in this project, will ultimately affect blood flow. The assessment of CVR using breath holding also provided useful information about the dynamics of this perturbation and this was extended in the discussion on the BOLD signal and the Valsalva manoeuvre. However, there is a paucity of information regarding the blood pressure changes that occur during such challenges, and how these affect the resulting BOLD signal. Most studies have used these challenges to investigate the regional distribution of autonomic function within the brain, which, although valuable in its own right, is a slightly different endeavour to this study. Finally a brief discussion about resting state functional MRI has provided some information about spontaneous fluctuations in blood pressure and the BOLD response to these, although most studies seem to consider the low frequency fluctuations

due to vasomotion rather than higher frequency fluctuations in cerebrovascular resistance.

4.2 Mathematical modelling

4.2.1 Introduction

Mathematically modelling any process provides a method for testing the theories underlying the physical principles of that process, without the need for real experimentation. It also enables the parameters that control the process to be adjusted in a consistent and reliable manner. This is particularly important in human biological systems, where invasive measurements of physical parameters are not always possible and these parameters cannot always be controlled in a systematic manner. In this project, two existing models have been amalgamated to investigate the effect of arterial blood pressure changes on the BOLD MRI signal. The purpose of this will be to investigate the processes involved in both the blood flow regulation (i.e. cerebral autoregulation) in response to blood pressure changes and then how these affect the measured BOLD MRI signal.

In any type of modelling, there exists the compromise between the simplicity of the model and its accuracy in depicting real processes. In this project, widely used basic models have been employed to give an approximation of the resulting signal changes; further development of these models may be carried out in future work. An outcome of the modelling process is to enable quantification of a process, and greatly aid our understanding of the human body and the factors that influence measured signals and the subsequent derived images.

4.2.2 Modelling the cerebral circulation and its vascular response

Background

There are many approaches to modelling cerebrovascular circulation, from simple linear lumped parameter models, to those with complex non-linear components and distributed parameter systems. Compartmental or lumped parameter models of cerebrovascular haemodynamics can be represented by an electrical circuit analogy where flow is equivalent to current (I), pressure is equivalent to voltage (V), vascular resistance is equivalent to electrical resistance (R) and compliance is equivalent to capacitance (C). Vascular compartments are comprised of resistors and capacitors, referenced to earth.

Compartmental or lumped parameter models of the cerebrovascular system have been around for a long time. Monro and Kellie[149,150] were most probably the first exponents of such modelling techniques and they proposed a three-compartment model consisting of arteries, veins and brain tissue.

A relatively recent model was proposed by Fincham and Tehrani[151] in 1983, which attempted to describe cerebral autoregulation in terms of oxygen and carbon dioxide and the metabolic rate ratio. However, this was a steady state model and as such, this type of model cannot replicate the dynamics of the cerebral autoregulation system; it is these dynamics that the cerebrovascular modelling aspect of this work is concerned with, i.e. the response of blood flow to blood pressure changes in the brain and the effect of this on the BOLD MRI signal.

Other early models only considered the regulation of blood flow in certain components of the cerebrovascular network, for example the carotid arteries[152] (Hillen *et al* in 1986) or the Circle of Willis[153] (Perktold *et al* in 1995). This approach is a reasonably good approximation of the processes occurring during autoregulation. However, these models do not provide any information about the haemodynamics in the venous compartment, and as BOLD MRI signal changes are dominated by blood in the venous compartment, these models are not complete enough for the purposes of this project.

Another valuable early contribution to the modelling literature was from Zagzoule[154] *et al* (1986). This model included the mechanisms regulating blood flow in the brain, and blood flow was considered across the whole cerebrovascular network, not just within the Circle of Willis. The number of compartments in this lumped parameter approach were also increased. The model was based on non-linear equations of pulsatile blood flow in distensible conduits, and described the whole cerebrovascular network from the arteries to the sinuses and jugular veins. The model was applied to the study of autoregulation during arterial hypotension and despite some simplifications; the maintenance of blood flow over a range of pressures was demonstrated. Some interesting findings regarding the precise location of vasomotor changes (i.e. within which vascular compartment of the brain) during the BP challenge were also noted. However, an important detail to note is that the regulatory mechanisms incorporated within this model were derived in an empirical manner rather than looking at the associated feedback mechanisms and modelling each of these in turn, depending on their origins.

The addition of more compartments to the lumped parameter modelling approach, improved the accuracy of such models. In 1996, Bekker[155] *et al* proposed a seven-compartment model and this was used to investigate the effects of vasodilatory and vasoconstrictive drugs on intracranial pressure. The effects of these drugs on blood flow were modelled by means of a variable arteriolar-capillary resistance, whilst in this model autoregulation was explicitly modelled by transmural pressure-dependent, arterial-arteriolar resistance.

Ursino devised an excellent model around this period[156,157,158]. This has been developed and extended over the years and has been employed to examine cerebral haemodynamics, autoregulation, CO_2 reactivity and ICP variations[50,159,160,161,162]. This model will be discussed in more details at the end of this section.

A large contribution to the field of cerebrovascular modelling and another detailed, lumped parameter model (similar to Ursino's) has been suggested by Czosnyka's group[163,164]. This model uses a set of non-linear differential equations to model time-dependent interactions between pressure, flow, cerebral blood volume and cerebrospinal fluid. As well as examining arterial inflow and storage, arteriolar and capillary blood flow controlled by cerebral autoregulation, venous blood storage and outflow modulated by ICP changes, cerebrospinal fluid storage and re-absorption was also included in the simulation. The inclusion of CSF circulation in this model adds greater clinical relevance to this type of model when considering slower dynamics of the order of minutes-to-hours rather than seconds-to-minutes.

A very simple lumped parameter model that attempts to explain cerebral blood flow regulation was devised by Olufsen[165]. The model was kept simple, as the main aim of the work was to demonstrate a new method of data analysis, rather than devising a detailed model to capture every detail of the process. However, this kind of model still managed to reproduce blood flow changes, but just in the middle cerebral artery, in response to arterial blood pressure changes. Blood flow velocity was measured in the MCA during posture change (sitting to standing) using transcranial Doppler and arterial blood pressure was measured in the finger using a Finapres device (the same device is used in this project). Blood flow in the MCA was calculated by multiplying the measured blood flow velocity by the area of the MCA (which was assumed to be constant throughout the experiment). A Windkessel model was proposed, with two resistors and a capacitor to reproduce beat-to-beat changes in middle cerebral artery (MCA) blood flow velocity as a response to ABP changes. The capacitor and one of the resistors were one lumped parameter, representing the vessels leading to and including the MCA. The other resistor represented the peripheral vascular bed. Effects due to venous and intracranial pressure changes were not considered in this model. A windowed Fourier transform was used to extract time-dependent spectra from a finite length time series. This method was used to extract

transient variations of the peripheral and systemic resistances on a beat-to-beat basis. Although this is a simple model and only includes very basic mechanisms, it improves on previous models as it includes both autoregulation and pulsatility. The study found good agreement between the model output and the measured blood flow velocity data. However, this model is really too simple for the needs of this project, as variations in blood pressure need to be derived across the whole vascular tree, as well as variations in intracranial pressure.

The most complex model to date has been described by Banaji[166]. This is a comprehensive model that combines models of the biophysics of the circulatory system, brain metabolic biochemistry and the functioning of the vascular smooth muscle (VSM). Whilst this model is potentially the best theoretical representation of the cerebral circulation, it is has been proposed relatively recently and is therefore not as well validated as other, older models (particularly Ursino's). Validation is a particularly difficult challenge for larger models, which contain a large number of parameters.

Distributed models (rather than the previously described lumped parameter models) have been proposed[167,168,169,170] that model pulsatile flow and pressure phenomena; these are based on transmission line equations. These differ from lumped parameter models by the fact that one spatial dimension is included and thus enabling flow and pressure to be determined at any location along a vessel at any particular time. These can be considered to be more continuous descriptions of the vasculature rather than describing each component as a discrete entity (as is the case in lumped parameter models). However, the models that have been proposed do not take the dynamics of regulation into account and only examine changes in flow and pressure as a pulsatile pulse wave propagates along the arterial tree (and usually not within the venous system). These models are able to provide information at a particular point in space, which is more representative of the measurements made with a transducer (which is the case with transcranial Doppler measurements in the middle cerebral artery).

As precise spatial information is not required in this project, a lumped parameter model is considered appropriate. In addition, the difference between pressure derived from a distributed model and that from an individual compartment in a lumped parameter model, is only significant over very short timescales, i.e. one R-R interval.

The model that has been implemented in this study is the one proposed and developed by Ursino[50] (and Lodi) over a number of years (particularly the model published in 1998). The biomechanical aspects of the model by Banaji[166] and that proposed by Czonyka[163] are similar to this Ursino model. This model has been chosen due to the comprehensiveness of this model and also its availability for relatively simple implementation in this project. It is possible to input measured data into the model, such as arterial blood pressure and venous blood pressure, and predict pressures throughout the vascular tree (and blood flow) as well as intracranial pressure and venous volume changes. Outputs from this model can be entered into a model of BOLD MRI signal changes to predict the resulting BOLD signals that are measured in the experimental work. The model has been used and quoted in a number of other studies (for example Jung *et al*[171]) and is thus thought to be reasonably well tested and validated.

This model considers the behaviour of the intracranial arterial and venous vascular bed, as well as CSF production and absorption. This is another lumped parameter model, with each component of the model being represented by a capacitor and a resistor. Both passive and active resistors have been used and it is the active resistors that are used to replicate the autoregulation mechanism. The entities that have been characterised in the model are the middle cerebral artery (MCA), large and small pial arteries, the venous bed, the intracranial pressure, and the CSF circulation.

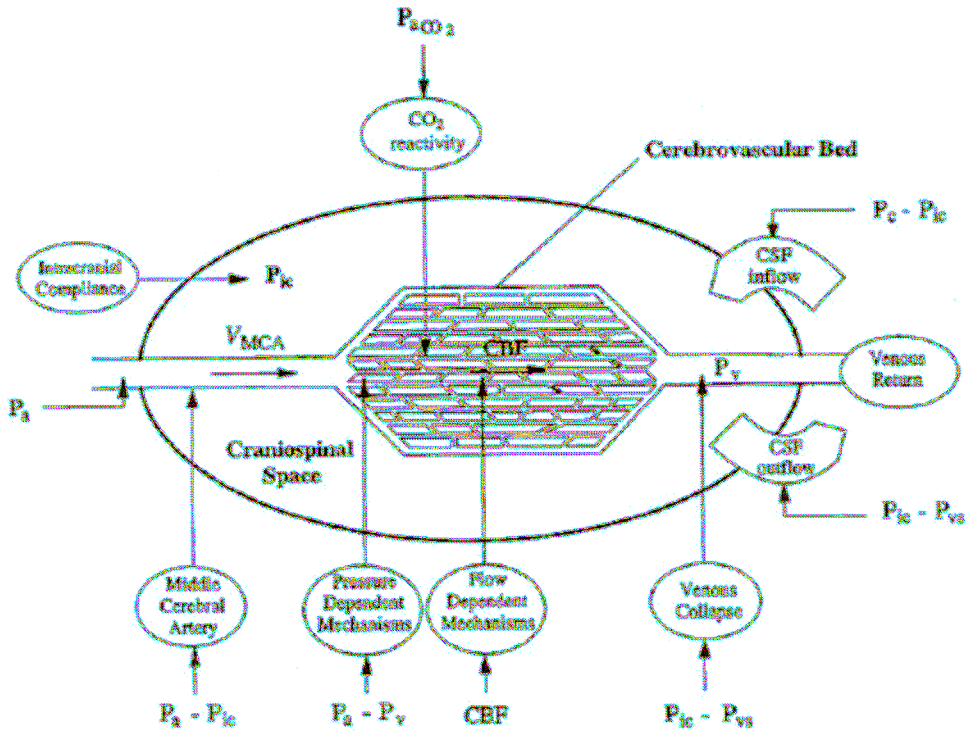

Figure 18: Diagram illustrating the main physiological factors included in Ursino's model (used with permission from Lodi et al[160], 1998).

In the model, intracranial compliance is inversely related to intracranial pressure (ICP). It is assumed that the middle cerebral artery (MCA) behaves passively, and as such its radius depends on the difference in pressure between the arterial pressure and intracranial pressure (P_a-P_{ic}). Two different mechanisms initiate autoregulation in the large and small pial arteries, one sensitive to perfusion pressure changes (which is arterial pressure minus cerebral venous pressure (P_a-P_v)) and another to cerebral blood flow (CBF) changes. However, both large and small pial arteries are sensitive to CO_2 levels in arterial blood (Pa_{CO2}). The terminal portion of the cerebral venous vascular bed collapses according to the difference between ICP and sinus venous pressure (P_{ic} - P_{vs}) (i.e. it behaves as a Starling resistor – this is described below). Cerebrospinal fluid (CSF) production at cerebral capillaries

depends on the difference between capillary pressure and ICP (P_c - P_{ic}) whereas CSF outflow depends on the difference between ICP and sinus venous pressure (P_{ic} - $P_{vs)}$. V_{MCA} is the blood flow velocity in the middle cerebral artery.

The model incorporates active control of the arterial resistance in response to changing pressure and CO_2 levels (although CO_2 is assumed to be constant in this application of the model). The dynamic response of these two mechanisms has been modelled by incorporating a gain factor and a first order low-pass filter with a time constant, and these parameters can be varied. The model incorporates the Laplace Law, i.e. the arterial resistance terms are derived from the inner radius of the vessel, which is determined from local pressure and wall characteristics and modulated by the action of cerebrovascular regulatory mechanisms, which modify smooth muscle tension. The action of a Starling resistor is incorporated into the venous outflow resistance, i.e. during intracranial hypertension the venous cerebrovascular bed collapses at the junction of the dural sinuses depending on the difference in pressure between cerebral venous pressure and ICP (P_{cv} – P_{ic}) and sinus venous pressure (P_{cv} – P_{vs}). As a result of this, changes in cerebral venous pressure closely follow ICP changes, and cerebral venous pressure is always slightly higher than ICP[50].

The cranium can be thought of as a rigid box as described in the Monro-Kellie doctrine[149,150]. This doctrine states that as the volume inside the cranium is of a fixed volume, the total volume of the various components (i.e. brain tissue, blood, CSF) within the cranium must be constant. So, if the volume of one component decreases, the volume of the other components will increase to compensate. Hence, storage capacity of the craniospinal system determines intracranial pressure (ICP), and this can be described as a mono-exponential pressure volume relationship:

$$C_{ic} = 1/k_e \, P_{ic} \qquad (29)$$

Where C_{ic} and P_{ic} refer to the intracranial compliance and ICP respectively and k_e is the intracranial elastance coefficient[172]. This coefficient is inversely related to the pressure-volume index (PVI). Dynamic ICP changes are dependent on both CSF dynamics and cerebral haemodynamics, and both these transients are built into the Ursino model. The compliance of the large cerebral veins is inversely proportional to local transmural pressure, which suggests a mono-exponential pressure-volume relationship[50].

The model that Ursino has proposed can be represented by an electrical circuit diagram shown below:

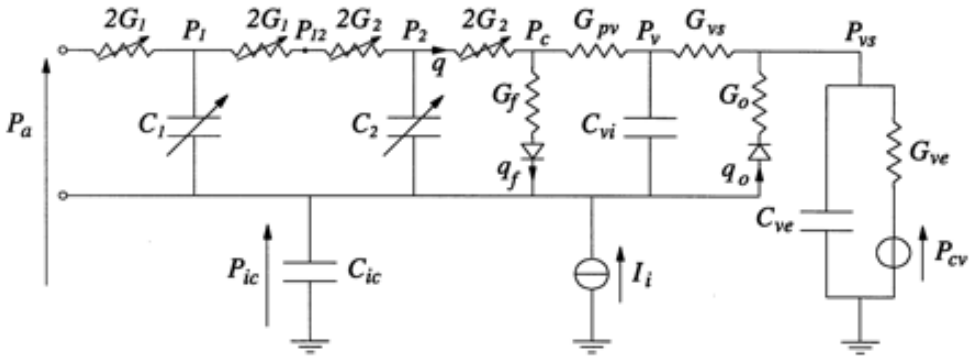

Figure 19: Electrical analogue of the intracranial dynamics (used with permission from Ursino et al[50], 1998).

In this circuit diagram the following parameters have been included:

G_1 and G_2: hydraulic conductance of proximal and distal arterial vessels;

C_1 and C_2: hydraulic compliance of proximal and distal arterial vessels;

P_a: arterial pressure;

P_1 and P_2: intravascular pressure at the level of large pial arteries and pial arterioles, respectively;

P_c, P_v: capillary and cerebral venous pressures;

P_{vs}: venous sinus pressure;

P_{cv}: central venous pressure;

P_{ic}: intracranial pressure;

C_{ic}: intracranial compliance;

G_{pv}, C_{vi}: hydraulic conductance and compliance of large cerebral veins;

G_{vs}: hydraulic conductance of terminal intracranial veins;

G_{ve}, C_{ve}: hydraulic conductance and compliance of the extracranial venous pathways;

G_f, G_o: conductances to CSF formation and CSF outflow.

In Ursino's model intracranial pressure (ICP) is compared to zero, i.e. earth. The model also considers the formation and bulk flow of cerebrospinal fluid (CSF), but this is a very slow process and can effectively be ignored over the timescale of the experiments in this study (one minute). Venous drainage into the jugular vein is also taken into account, with the draining veins varying their resistance to maintain a pressure gradient from inside the skull to outside the skull regardless of flow. As stated above, the action of the autoregulation mechanism is another aspect of this model, where vessel wall tension is altered to enable a change of resistance, which in turn regulates flow. This mechanism is initiated by pressure and CO_2 changes in the small arterioles, and by flow and CO_2 changes in larger arterioles. In this project it is assumed that CO_2 levels are constant, so it is only flow mediated mechanisms that are being considered.

The objective of using this model is to derive blood flow and venous volume signals to input into the Buxton model of the BOLD MRI signal (which is described in the next section), and this will enable an explanation of the BOLD changes that are being observed, as well as a comparison of this output to the arterial changes that are being imposed. Other outputs obtained from the Ursino model can also be compared to experimental measurements in this project. For example, time series of ICP changes derived from the

model can be compared to tympanic membrane displacement (TMD) measurements.

The aim of this model will be to add a degree of quantification to the experimental aspects of the study. The blood flow (and by inference, deoxyhaemoglobin level) and venous volume changes predicted in this part of the model will link in to the model of the BOLD signal to produce an overall picture of the signal changes seen in the experiments. The model should add weight to the arguments proposed in the conclusion as to the origin of the signal changes that are observed as well as being able to predict the response to any input.

4.2.3 Modelling the BOLD MRI signal

The origins of the BOLD signal can be elucidated by both experimental and mathematical means. There is a considerable body of work that describes models of blood flow and oxygenation changes during the BOLD experiment based on mathematical representations. The first model was introduced by Ogawa et al in 1993[173], which was a biophysical model, i.e. the physiological contributions to the signal change were not considered. This model was developed to quantify the fundamental changes seen in the BOLD signal during neural activation, such as the signal amplitude and the dependence of this on the magnetic field strength. The end result provides an expression for the apparent in-plane relaxation constant (R_2*) in terms of magnetic field strength, the degree of oxygenation of the venous blood, and venous blood volume fraction in tissue, and the size of the blood vessel, whether larger venules and veins, or smaller capillaries. The dilation of the blood vessel was modelled to see what change this would have on the blood volume of the compartment that was being imaged and the resultant effect on the BOLD signal. It was found that the dependence of R_2* (relaxation rate equal to $1/T_2$*) on blood volume fraction is approximately linear for small vessels. There also seems to be a linear dependence on the number of capillaries containing

deoxygenated blood (i.e. the active capillaries) and BOLD signal. Hence, a change in blood volume will result in a proportional change in BOLD signal. The results from this modelling form the basis of other models in many subsequent publications, including the model used in this project.

Intra-voxel phase dispersion give rise to the BOLD effect, due to magnetic field inhomogeneities produced by nearby deoxyhaemoglobin containing blood vessels. The emphasis of the model is to examine the dependence of water molecule diffusion on the attenuation of the resulting signal. To produce a model reflecting this, the signal attenuation due to such phase dispersions for a voxel containing a collection of blood vessels, was numerically calculated. Equations expressing the induced local magnetic field variations, due to vessel orientation in relation to the main magnetic field, and the volume susceptibility difference between blood in the vessel and the surrounding tissue, were proposed, for both inside and outside the vessel. A random walk approach (to mimic diffusion processes) was used to estimate an accumulated phase and corresponding phase factor for each voxel from these equations (by integration over echo time, TE), and an attenuated signal (S_{voxel}) was calculated. This attenuation could be represented by an exponential decay:

$$S_{voxel} = S^{0}_{voxel} e^{-R_2^*.TE} \qquad (30)$$

The full decay curve was not calculated, instead, S_{voxel} was calculated for two echo times, and R_2^* was determined from the line connecting them. This model was used to derive relations between R_2^* and the susceptibility induced frequency shift and the blood volume for large vessels (venules and veins) and small vessels (capillaries).

The susceptibility induced frequency shift at the vessel surface is defined as:

$$\nu = \Delta\chi(1 - Y)\omega_0 \qquad (31)$$

Where ν is the frequency shift, $\Delta\chi$ is the susceptibility difference between blood in the vessel and the surrounding tissue, (1 – Y) is the degree of

deoxygenation of the blood, and ω_0 is the Larmor frequency corresponding to the main magnetic field strength. It was found from simulations, that at larger vessel diameters, this frequency was proportional to R_2^*, when diffusion in the brain is taken into account and for small vessel, this relationship was found to be quadratic. When blood volume is considered, in larger vessels, R_2^* can also be implied to be a linear function of b (blood volume). Two models of blood volume changes have been described in this paper. The first is capillary recruitment model, where capillaries are thought to have two states, active and inactive, and an increase in CBV is thought to increase the fraction of active capillaries (p), i.e. the state in which blood cells can pass; however, in this model, there is no change in blood vessel geometry within a voxel, and R_2^* is thought to be proportional to p. In the alternative model, vessel dilation occurs to produce a change in blood volume, b, which is also proportional to R_2^*. Numerical simulations also found that the change in R_2^* produced by a change in b can be described as:

$$\Delta R_2^* / \Delta b^{\gamma} \approx \text{constant} \qquad (32)$$

With the condition of free diffusion, γ was 0.5, however, with constrained diffusion (i.e. within the voxel) this became 1. From all these simulations, for large vessel and small vessels, the following relationships for R_2^* can be implied:

$$R_2^* = \alpha \nu b_l \qquad \text{large vessels} \qquad (33)$$

$$R_2^* = \beta \nu^2 (b_s)^{\gamma} p \qquad \text{small vessels} \qquad (34)$$

where b_l and b_s are the blood volume fractions corresponding to large vessels (venules and veins) and small vessels (capillaries) respectively. The α term in the equation for large vessels was found to be 4.3 ± 0.3 from simulation data. In the equation for small vessels, $\gamma = 1.0$ and $\beta = 0.04 \pm 0.01$, for both the recruitment model and the dilation model. In the equation for large vessel, the proportion of active vessels can be taken as equalling 1, i.e. all vessels are recruited and active. It is the relation for large vessels that is of

interest for the modelling aspects of this project, as it is just the contribution of these vessels that is considered. It is also important to note that the signal contribution from the small volume of blood water is neglected here, only tissue water (extravascular signal) is considered. The intravascular contribution to the signal changes seen in the BOLD experiment will be discussed later on in this section.

This model was extended by Davis[174] in 1998 taking into account some approximations and the results of numerical studies. This is a simple model, which is purely based on the origin of the BOLD effect and relates the corresponding signal changes to underlying physiological variables and some parameters that describe the tissue being investigated[175]. Once again, the question that this modelling approach tries to answer is how does the change in R_2* (i.e. $1/T_2$*) change with respect to blood oxygenation and volume? It is this model that has provided the fundamental relationships that have been developed in the Buxton model, which is used in this project. For a standard gradient echo acquisition there is an exponential dependence on echo time (TE) and the change in R_2* is one of the exponents when considering the signal change in the BOLD signal. The BOLD signal change (S) with activation is:

$$\frac{\Delta S}{S_0} = e^{-\Delta R_2^* . TE} - 1 \approx -\Delta R_2^* . TE \qquad (35)$$

where

$$\Delta S = S_{act} - S_0 \qquad (36)$$

$$\Delta R_2^* = R_{act} - R_0 \qquad (37)$$

where TE is the echo time of the pulse sequence and the subscript ‘act’ refers to the activated state whilst the ‘0’ subscript refers to the resting, baseline value.

This difference in magnetic susceptibility (ΔR_2*) has a linear dependence on the local deoxygenation concentration which in turn is related to a change in

oxygen extraction fraction (E), but this is modulated by an exponent when diffusion effects around small vessels are considered, E^{β}. For a typical variety of vessel sizes, β=1.5 at a field strength of 1.5 T[174,106,176]. The other factor that must be considered is blood volume and it is thought that R, magnetic susceptibility, is proportional to V, the venous blood volume. So these two factors combine to give the following relationship:

$$R \propto V\, E^{\beta} \tag{38}$$

Using equation this equation, the BOLD signal change can be expressed in terms of V and E[174]:

$$\frac{\Delta S}{S_0} \approx A \cdot \left[1 - \frac{V_{act}}{V_0} \left(\frac{E_{act}}{E_0} \right)^{\beta} \right] \tag{39}$$

The parameter A combines both the unknown proportionality constant from equation (38) above and echo time, TE, and has been estimated as 0.079. This form of the BOLD signal change represents a biophysical model. Changes in blood oxygenation relating to changes in $CMRO_2$ and CBF are described by a physiological model. Considering that the normalised concentration of deoxyhaemoglobin is equal to the normalised $CMRO_2$ divided by normalised CBF, this leads to such a model:

$$\frac{\Delta S}{S_0} = A \cdot \left(1 - f^{\alpha - \beta}\, m^{\beta} \right) \tag{40}$$

where f and m are normalised values of blood flow and $CMRO_2$ respectively and assuming that $v = f^{\alpha}$ (Grubb's relationship[64]). One issue with this expression is that factors that affect the MR signal, that are independent of the BOLD effect, such as inflow effects or arterial volume changes, will also have an impact on the resultant overall MR signal, and these are not considered in this version. However, both these effects are due to arterial blood changes, which are in addition to the BOLD effect (as deoxyhaemoglobin is negligible in this compartment), but these effects are thought to be small compared to the BOLD effect. This is also a less useful

form of the BOLD signal change for this project as metabolism changes ($CMRO_2$) are explicitly included, whereas metabolism is considered to be constant in the experiments carried out for this project.

Buxton[51] described the Balloon Model, which proposes an alternative form of the BOLD signal change equation, as blood volume changes are considered to be significant. Nevertheless, this equation and equation (40) are approximately equivalent expression for BOLD signal changes[175]. The derivation of this model considers the contribution of intravascular and extravascular signal changes, and frames the expression for the signal change in terms of deoxyhaemoglobin (q) and blood volume (v). Dynamic changes in deoxyhaemoglobin are derived from the venous flow changes resulting from the blood pressure challenges imposed (obtained from Ursino's model); volume dynamics are also obtained from Ursino's model. This will be discussed further in the section describing implementation of the models.

Improvements were made to the original Buxton balloon model, by Obata[52] in 2004. This corrects an error in the original work, makes fewer approximations and incorporates more recent experimental data to estimate the constant parameters. As stated previously, the derivation for the BOLD signal change is based intra and extravascular signal changes during activation. The BOLD signal at rest can be expressed as a weighted average of these contributions:

$$S_0 = (1-V_0)S_E + V_0S_I \qquad (41)$$

where V_0 is the resting blood volume fraction, S_E is the extravascular signal and S_I is the intravascular signal. As proposed in Ogawa[3,173] the two vascular signals can be modelled as:

$$S_E = S_{E0}e^{-TE/T_{2E}^*} \qquad (42)$$

$$S_I = S_{I0}e^{-TE/T_{2I}^*} \qquad (43)$$

$$\varepsilon = S_E / S_I \qquad (44)$$

where T_{2E}^* is the extravascular apparent transverse relaxation time at rest, T_{2I}^* is the equivalent intravascular relaxation time, S_{E0} and S_{I0} are the respective effective spin densities (i.e. MR signal from these compartments at rest) and ε is the intrinsic ratio of blood (intravascular) to tissue (extravascular) signals at rest.

With activation, or indeed any change in blood volume or deoxyhaemoglobin, the two transverse relaxation rates ($1/T_2^*$) are changed by the quantities ΔR_{2E}^* and ΔR_{2I}^*, and the blood volume will also change to a new value V. Hence, the new signal, S becomes:

$$S_E = (1 - V)S_E e^{-TE \times \Delta R_{2E}^*} + VS_I e^{-TE \times \Delta R_{2I}^*} \qquad (45)$$

The fractional signal change can be expressed as:

$$\frac{\Delta S}{S_0} = \frac{1}{(1 - V_0 + \varepsilon V_0)} \left[(1 - V) e^{-TE \times \Delta R_{2E}^*} + \varepsilon V e^{-TE \times \Delta R_{2I}^*} - (1 - V_0) - \varepsilon V_0 \right] \qquad (46)$$

In the case of small changes in the relaxation rate, the exponential in the extravascular term can be expanded to form a linear approximation. In addition, for small volumes (i.e. voxels excluding large draining veins) the factor at the beginning approximately equals one, and thus, by eliminating products of small quantities, the signal change becomes:

$$\frac{\Delta S}{S_0} = (-TE \times \Delta R_{2E}^*) - \varepsilon V TE \times \Delta R_{2I}^* + (V_0 - V)(1 - \varepsilon) \qquad (47)$$

So, to enable the expression to be calculated, the terms ε, ΔR_{2E}^* and ΔR_{2I}^* need to be approximated.

Extravascular signal changes

As shown at the beginning of this section (equation 33), $\Delta R_{2E}^{*} = 4.3\,\nu V$ where $\nu = \nu_0(1\text{-}Y)$ is the frequency difference (in Hz) between blood and tissue at the surface of the vessel, and the offset between oxygenated and fully deoxygenated blood ν_0 = 40.3 s^{-1} at 1.5 T, and Y is the fractional oxygen saturation of haemoglobin. The resulting relaxation rate (from a rest state) due to changes in both blood volume and blood oxygenation is:

$$\Delta R_{2E}^{*} = 4.3\nu_0\left[V(1-Y) - V_0(1-Y_0)\right] \qquad (48)$$

where Y is the average saturation of the venous pool in the activated (or changed) state. The total deoxyhaemoglobin content, Q, is Q=V(1-Y)[Hb], where [Hb] is the effective total haemoglobin concentration in blood. This means that the activated deoxyhaemoglobin content normalised to rest (q), can be written as:

$$q = \frac{Q}{Q_0} = \frac{V(1-Y)}{V_0(1-Y_0)} \qquad (49)$$

If E_0=1-Y, and using this equation, the change in relaxation rate can be written as:

$$\Delta R_{2E}^{*} = 4.3\nu_0 V_0 E_0 (q-1) \qquad (50)$$

Intravascular signal changes

A linear relationship can describe intravascular relaxation rate changes, as described by Li[177], where $\Delta R_{2I}^{*} = r_0\left[(1-Y) - (1-Y_0)\right]$, where r_0 is the empirically determined slope of the relation between R_{2I}^{*} and the oxygen extraction fraction E (=(1-Y)) and this equals 25 s^{-1}. So, this can be expressed as:

$$\Delta R_{2I}^{*} \approx r_0(1-Y_0)\left[\frac{(1-Y)}{(1-Y_0)} - 1\right] \qquad (51)$$

And if the normalised volume $v=V/V_0$:

$$\frac{q}{v} = \frac{Q/V}{Q_0 / V_0} = \frac{1 - Y}{1 - Y_0} \tag{52}$$

So, by substituting this, ΔR_{2I}^* becomes:

$$\Delta R_{2I}^* = r_0 E_0 \left(\frac{q}{v} - 1 \right) \tag{53}$$

Total signal change

By combining these terms for intra and extravascular signal changes, and by employing the normalised blood volume term, $v=V/V_0$, the overall BOLD signal change can be written as:

$$\begin{aligned} \frac{\Delta S}{S_0} &\approx -4.3 \nu_0 V_0 E_0 TE(q - 1) - \varepsilon V r_0 E_0 TE\left(\frac{q}{v} - 1 \right) + (1 - \varepsilon)(V - V_0) \\ &= V_0 \left[k_1 (1 - q) + k_2 v \left(\frac{q}{v} - 1 \right) - k_3 (1 - v) \right] \\ &= V_0 \left[(k_1 + k_2)(1 - q) - (k_2 + k_3)(1 - v) \right] \end{aligned} \tag{54}$$

where:

$k_1 = 4.3\nu_0 E_0 TE$

$k_2 = \varepsilon r_0 E_0 TE$

$k_3 = \varepsilon - 1$

The parameter ε, was calculated from values for $T_{2E}^* = 50\,\text{ms}$ and $T_{2I}^* = 90\,\text{ms}$ [177](with equal spin densities).

In Buxton's paper, dynamic expressions for dq/dt and dv/dt are developed for the Balloon model, i.e. driving functions for the model. These have been numerically integrated and combined with the above equation to predict curves of the BOLD MRI signal in response to various flow inputs. In the

Buxton model, the venous compartment is thought to 'inflate' as cerebral blood flow increases. This 'balloon' compartment is expanded when there is a difference in normalised arterial inflow and normalised venous outflow. It is also noted that time constants for flow and blood volume changes are not the same; blood volume alterations occur on a much slower timescale than blood flow changes. The initial increase seen in deoxyhaemoglobin component of the signal (in response to an increase in flow during brain activation) is due to a blood volume increase rather than a change in deoxyhaemoglobin concentration in the blood. They concluded that measurements of deoxyhaemoglobin content are not reliable indicators of flow and oxygen metabolism changes without taking into account changes in blood volume. In this project, these volume changes are derived from parameters within Ursino's model, which is thought to be a much more sophisticated model of the biomechanical changes occurring within different vascular compartments during blood pressure challenges. This is discussed further in the implementation of the modelling section.

Buxton notes that an interesting case to illustrate the contribution of volume and deoxyhaemoglobin changes could be that if there is an increase in blood volume, but a decrease in oxygen extraction fraction (E) which results in no change in total deoxyhaemoglobin, i.e. $q = 1$ but $v > 1$. So, as there is no change in overall deoxyhaemoglobin, the field distortions around the blood vessels (which affect the extravascular signal) will stay fairly constant, but as E has decreased, the concentration of deoxyhaemoglobin in the blood must have also decreased. As the intravascular signal is strongly dependent on this, this component of the signal will increase, resulting in an increase in BOLD signal, despite a constant level of deoxyhaemoglobin. The consequence of this is that volume (i.e. intravascular) effects must be taken into account when considering BOLD signal changes and there is not direct relationship between the BOLD signal and total deoxyhaemoglobin.

In the wider context, Friston[178] postulates that modelling the BOLD reponse to neuronal activation can be considered to comprise of five stages, linking:

1. neural activity to flow changes,
2. flow changes to oxygen delivery to tissue,
3. flow changes to changes in blood volume and venous outflow,
4. changes in flow, volume, and oxygen extraction fraction to deoxyhaemoglobin changes and,
5. volume and deoxyhaemoglobin changes to the BOLD response.

In this project, stage one is not considered, but in most other BOLD modelling papers, this is explored in some detail. This can be thought of as the physiological aspect of the model, i.e. the driving equations for volume and deoxyhaemoglobin changes due to neuronal activation, as opposed to the biophysical aspect. Obata and Buxton's description of the biophysical aspects of the BOLD response are considered a good description for the signal changes taking place. The driving equations have developed over time from a Windkessel model[65] (similar to a balloon model) to more sophisticated two or three compartment models[179,180]. However, we are using Ursino's model as a driving function, which is a far more complex model than those described in the BOLD literature, as it comprises multiple compartments and includes CSF flow and drainage. This approach has also been used by Payne[23], in which a model has been developed to predict the response of the cerebral vasculature to changes in arterial blood pressure, arterial CO_2 concentration and neuronal activation. Payne's paper has used Ursino's model to predict haemodynamic changes, and has extended this to include feedback mechanisms for the adjustment of arterial compliance relating to neural stimulation, as well as CBF and CO_2. A model of haemoglobin transport is also included which is derived from Buxton's balloon model and in addition includes a term relating to neural activation. This study found that there is significant interaction between autoregulation and activation processes, and that the degree of autoregulation determines both CBF and deoxyhaemoglobin responses to neural activation, which is correspondingly also affected by changes in arterial blood pressure.

Other authors have described modelling the BOLD response to neuronal activation. One of the first papers to describe this, shortly after Buxton, was by Mandeville *et al*[65], who proposed a Windkessel model. This described the cerebral blood volume response to neuronal activation, as a rapid elastic response of capillaries and veins followed by a slow venous relaxation of stress, i.e. venous delayed compliance. This used a much-simplified electrical circuit analogue of the balloon, or Windkessel, which just represented resistance and compliance downstream of the arterioles as one compartment. This model has been extended by Kong[181] by using an additional state variable to model the delayed compliance.

Friston[178] (2000) added components to replicate the haemodynamics of perfusion change, including a time constant for autoregulatory feedback from blood flow, as well as parameters that represent the efficacy with which neuronal activity increases signal and the time constant for signal decay. Zheng[182] expands on the Friston model by modifying the Buxton and Frank[183] model of oxygen transport to take into account the modulatory effect of changes in tissue concentration and the dynamics of oxygen delivery to tissue (in particular the capillaries), which allows the estimation of transient changes in $CMRO_2$. Behzadi[184] also expands on Friston's model by modelling the link between neuronal activity and alterations in arteriolar compliance, as there is a non-linear dependence of vessel radius on muscular compliance. Zheng[179] extended their one compartment model (the venous compartment) to consider three compartments (arterial, capillary and venous) to take into account haemodynamics changes taking place in all three compartments and they conclude that this improves on the one compartment model. More recently, Huppert[180] (2007) *et al* have proposed a multi-compartment model of cerebral vascular and oxygen transport dynamics, to enable the estimation of dynamic dilation of the arterioles and the transient metabolic processes associated with neuronal response to stimuli. In addition, information regarding the structural and baseline properties of the vascular anatomy, such as baseline oxygen consumption,

blood flow, and resting haemoglobin concentrations could be obtained. This has been achieved by including such terms as capillary compliance and oxygen extraction form arteriole and venule compartments, not just capillaries. One of the main uses of these multi-compartment models is in their use in examining the results from optical imaging and laser Doppler flowmetry experiments, where signals do not solely originate from the venous compartment (as in the BOLD response). These types of studies have been employed as validation of BOLD-MRI measurements, and this provides some of the motivation for these extensions to the modelling literature.

The Buxton balloon model approach has been used in others papers as an appropriate method to model the changes seen in the BOLD signal response[185,186,23,187,188,189,190]. The fact that the Buxton model is well established and widely used is one of the reasons for implementing this model in this project. The model also incorporates parameters that can be derived and entered from the Ursino model. Because this project uses different stimuli to alter blood flow than those used in the Buxton model, and indeed most other BOLD modelling approaches, i.e. challenges to arterial blood pressure rather than neuronal stimulation (with constant $CMRO_2$), different haemodynamic mechanisms may be initiated, leading to possible inaccuracies in the modelling.

4.3 Altering and measuring blood pressure and ICP

4.3.1 Thigh cuff deflation

Thigh cuff deflation has been used for many years as a non-invasive stimulus for testing cerebral autoregulation. This type of blood pressure challenge can induce a near step drop in arterial blood pressure. It was first implemented by Aaslid[69] in 1989. This work measured the cerebral blood flow response using the transcranial Doppler ultrasound technique. The basic principal of thigh cuff deflation involves applying thigh blood pressure cuffs to both thighs and inflating these to a supra-systolic pressure, i.e. above 170 mmHg. This occludes blood flow to the lower limbs; the pressure is applied for two or three minutes. When the thigh cuffs are deflated rapidly, blood flows into the dilated blood vessels of the lower limbs, and this causes a steep drop in central arterial blood pressure and hence cerebral perfusion pressure. Pooling of blood in the lower limbs reduced venous return to the heart, which further reduces arterial blood pressure. Recovery of arterial blood pressure to baseline levels is expected after 10 – 15 seconds[69]. The main use of this kind of blood pressure challenge has been to assess dynamic cerebral autoregulation, by examining the restoration of blood flow once the drop in blood pressure has been imposed. A typical blood pressure time series and corresponding blood flow velocity time series are shown below:

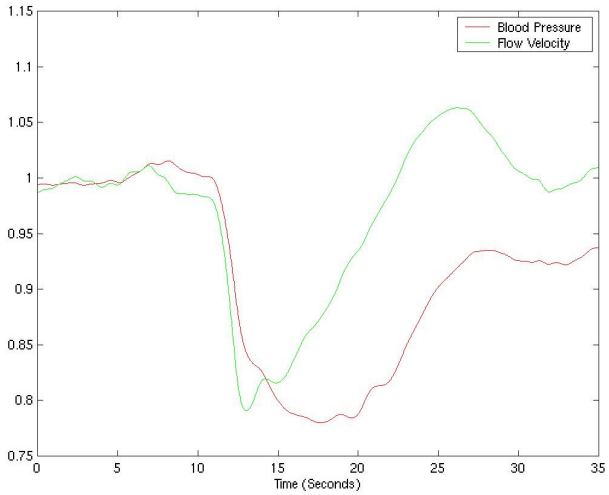

Figure 20: Blood pressure and blood flow velocity during thigh cuff deflation (as figure 5).

In this measurement, blood pressure in measured continuously throughout the procedure, and blood flow velocity is measured using transcranial Doppler, and is assumed to be proportional to blood flow.

Although this is a relatively simple and non-invasive method for altering arterial blood pressure (and something that can be implemented in an MRI scanner), there are some disadvantages to the technique. It is known to be painful to have the thigh blood pressure cuffs inflated for an extended period of time at such a high pressure; this is not tolerated by everyone, and potential volunteers have withdrawn from this study due to this reason. Another problem is the consistency in the drop of blood pressure. This can vary between individuals, in terms of the magnitude of the drop, the time period over which this takes place, and how quickly it occurs. A blood pressure decrease of 15% is typically achieved, but this can be as large as 40%, or in other extreme cases, either no drop is seen, or an increase can be observed if other challenges occur simultaneously, such as breath holding or the Valsalva manoeuvre. Despite these limitations, this blood pressure challenge suits the needs of this project, as it is easy to implement within the restrictions of the MRI scanner environment, and is non-invasive.

4.3.2 The Valsalva manoeuvre

This is a self-imposed airway or thoracic pressure challenge, i.e. the subject uses their chest muscles to alter their thoracic pressure. The Valsalva manoeuvre (VM) is carried out frequently in everyday life; it can be thought of as a straining action. It is described as 'forced expiration against a closed glottis'. Thoracic pressure changes induce changes in the vascular system, both arterial and venous, that are transmitted beyond the thorax. This is another blood pressure challenge that has been used to assess autonomic function and cerebral autoregulation. A good description of the blood pressure changes that occur during the VM is provided by Tiecks[85]. At the start of the manoeuvre a transient increase in arterial blood pressure takes place, which is due to transmission of increased intrathoracic pressure to the arterial tree (phase I, see figure 21). The next stage results in a fall in ABP due to impaired atrial filling in the heart (phase IIa). However, this is counteracted by a sympathetic response to this fall, originating from the baroreceptors in the carotid sinus. This response involves an increase in heart rate and peripheral vasoconstriction, leading to a rise in ABP and heart rate (phase IIb). When the VM is stopped, a sudden decrease in intrathoracic pressure occurs, and this again is transmitted to the arterial system (phase III). This results in a transient decrease in ABP. As sympathetic tone and systemic vascular resistance are still elevated from before, there is an overshoot in ABP above baseline (phase IV), but then the action of the baroreceptors restores the ABP to normal.

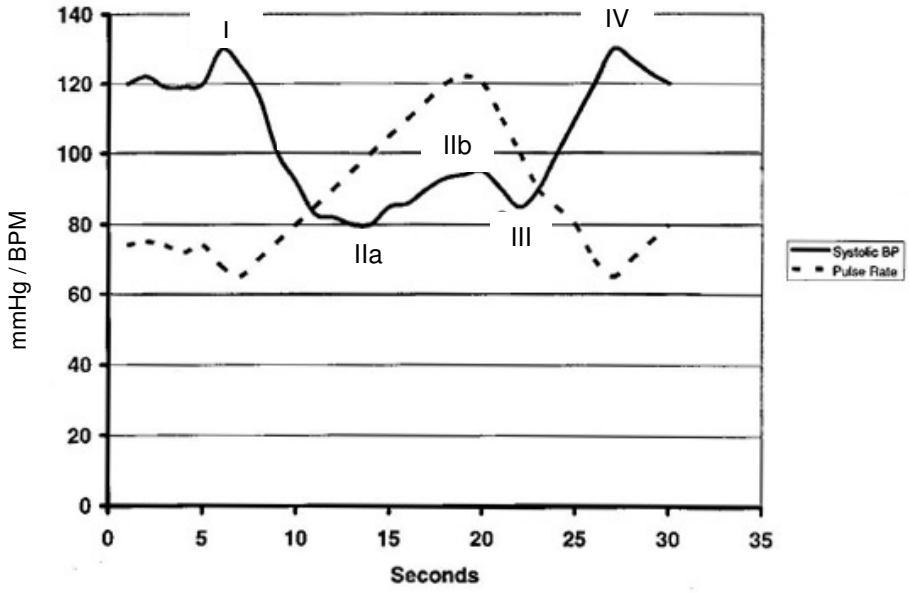

Figure 21: Blood pressure and heart rate changes during the Valsalva manoeuvre[191] (used freely from http://en.wikipedia.org/wiki/Valsalva_maneuver).

A complex interaction between systemic and cerebral pressures occurs during the VM. It has been found that during the transient increases in ABP, venous and cerebrospinal fluid pressure (and therefore ICP) increases by a similar magnitude to the intrathoracic pressure. This rise in ICP counteracts the rise in ABP during phase I, which results in little change in CPP, and hence CBF. By phase IIa, raised ICP amplifies the effect of decreased ABP (due to impaired atrial filling) resulting in a significantly greater decrease in CBF. In phase IIb, ICP remains raised whilst ABP is restored and then decreases during phases III and IV[85].

In conclusion, the Valsalva manoeuvre is a useful method of imposing blood pressure changes on the body, and in particular the brain, due to its non-invasiveness, and ease of implementation within the MRI scanner environment. One disadvantage of the manoeuvre is the variability in executing the task, and the lack of feedback regarding how well this was achieved. This can be obtained by breathing against a resistance valve with

an open glottis, and monitoring the resulting airway pressure using a pressure transducer recording pressure in the mouthpiece.

4.3.3 The measurement of arterial blood pressure

The measurement of arterial blood pressure can be achieved using a great many different methods, with each having its own advantages and disadvantages. The simplest methods of measuring blood pressure involve the use of a blood pressure cuff and sphygmomanometer. The cuff is inflated to above systolic pressure to occlude arterial flow, and pressure is slowly decreased, whilst listening for the resumption of blood flow, the Korotkoff sounds. However, this is only a measure of systolic and diastolic blood pressure averaged over several heartbeats with a relatively slow maximum measurement frequency. Invasive means of determining blood pressure allow more rapid, dynamic measurements of blood pressure to be made. For example, a pressure transducer can sample blood pressure changes at high temporal frequencies (40 Hz) via an arterial line. The approach used in this project lies is a non-invasive, but dynamic method of measuring arterial blood pressure. The method that has been used employs the volume clamp technique[192] in a digit. The use of a device called a Finapres™ (Finapres Medical Systems, Arnhem, The Netherlands) allows measurement of beat-to-beat mean arterial pressure, using this technique.

This device uses a small blood pressure cuff that fits round a finger, and incorporates an infrared transmitter on one side and a receiver on the other (i.e. on opposite sides of the finger). Transmission of the infrared light through the finger can be detected at the receiver and this is found to oscillate with the cardiac cycle. The cuff is inflated through a range of normal blood pressures and the cuff pressure that produces the largest amplitude oscillations corresponds to the mean finger arterial pressure. The mean amount of light that is transmitted is recorded as a calibration value. After this calibration process, rapid and continuous inflation and deflation of the cuff

takes place (through servo control feedback) to maintain the mean value of light transmission. The arterial pressure waveform is represented by the variations in finger cuff pressure required to maintain this volume clamp. Under normal operating conditions, the Finapres re-calibrates every 70 heartbeats, although this can be switched off. Inaccurate calibration and a difference in pulsatility between finger pressure and arterial, especially when hands are cold, can lead to further errors in this technique. Peripheral vasoaction, where arterial volume in the finger is reduced and light transmission is increased, can also lead to alterations in the cuff pressure, which are not due to changes in arterial blood pressure. However, studies have found that there is good agreement between Finapres data and that obtained from invasive arterial pressure measurements[193]. Hence, this method of measuring arterial blood pressure, which can be carried out both continuously and non-invasively, is thought to be an appropriate technique to employ in this study.

4.3.4 The measurement of venous blood pressure

There have been far fewer studies into properties of the venous vascular system than the arterial, particularly the pressure dynamics of the system. One of the reasons for this is the lack of a simple, non-invasive measurement technique. In rats and other animal studies, invasive pressure transducers have been employed for this purpose. Central venous pressure is monitored in patients via indwelling internal jugular catheters but this is not a method that can be used in healthy volunteers, and this technique does not enable the measurement of *cerebral* venous pressure. In this project changes in venous blood pressure were derived from measurements of jugular vein cross-sectional areas, obtained from angiographic MRI scans (this is described in the methods chapter). Jugular vein cross-sections have been studied using ultrasound[194,195] but not, as far as this group are aware, specifically using angiographic MRI techniques. Veins have a highly elliptical

cross section at low transmural pressures, but become more circular as pressure increases, resulting from a high distensibility within a wide pressure range. Berczi[194] investigated this in healthy volunteers using ultrasound measurements, in different positions and during the Valsalva manoeuvre. Capacity of the jugular vein increased as the pressure applied during the Valsalva manoeuvre increased, which was assumed to equal the venous pressure. Distensibility was found to decrease with applied Valsalva pressure, which would influence the proportional relationship between venous cross sectional area and pressure that is assumed in this study. However, in Berczi's study, the venous pressure change (which is used to calculate distensibility) is assumed to equal the applied Valsalva pressure. This has found to be the case for large veins located not too far away from the affected body cavities[196], but this may not always be the case.

4.3.5 The measurement of intracranial pressure

Measuring intracranial pressure (ICP) is a challenging but very important undertaking. Intracranial pressure changes are an important measure of intracranial compliance and the ability of the brain to tolerate volume increases. Central to this is the Monro-Kelllie[149,150] doctrine, which states that, as the cranium is a closed system, the sum volume of the components within the cranium (blood, tissue, CSF) remains constant.

Although ICP can be measured invasively, by measuring pressure within the cerebrospinal fluid compartment in the spine for example, this is a painful and hazardous procedure and not a viable option in healthy volunteers. A non-invasive approach has been proposed by Marchbanks[197,198]. This involves determining ICP changes via the trans-aural route using a device that measures tympanic membrane displacement in response to ICP changes. This is called the tympanic membrane displacement (TMD) technique, as it measures tympanic membrane (TM) movement in terms of volume displacement. The device consists of a headset onto which an airflow sensor

is mounted. Basically, this can measure the volume of air expelled from the ear canal, or drawn into the ear canal when the tympanic membrane moves, i.e. when ICP changes. Volume changes as small as a nano-litre can be detected using this method. TMD measurement assesses the resting position of the stapes within the ear by stimulating the acoustic reflex of the stapes footplate[199]. This produces a movement in the tympanic membrane, and intracranial pressure changes are transferred to the cochlear via the cerebral aqueduct.

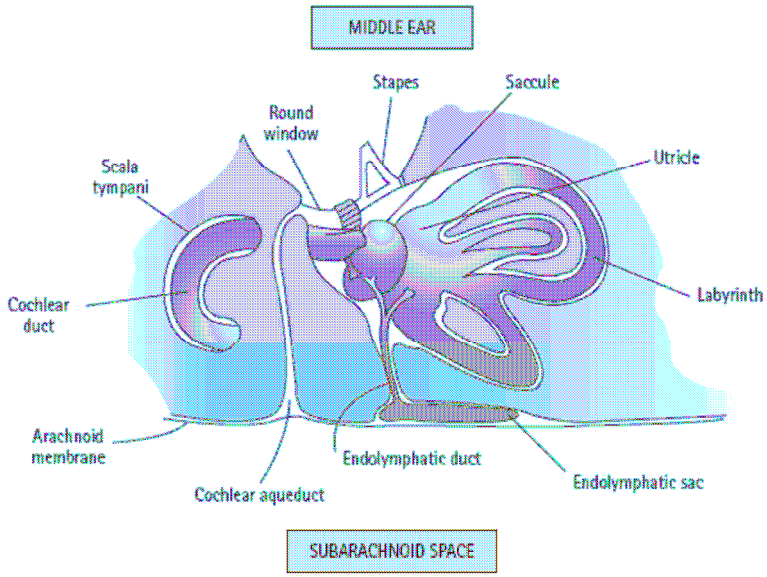

Figure 22: Schematic of the cochlear showing the pressure transmission routes between the intracranial fluid and inner ear (used with permission and adapted from Marchbanks, 2003[199]).

This cochlear aqueduct acts as a conduit between the subarachnoid space and the perilymphatic spaces and pressure changes within the cranium are transmitted through here, to the stapes and eventually to the tympanic membrane. If the outer ear is sealed, movements in the tympanic membrane result in air-pressure variations that can be recorded[200]. It has been demonstrated[198] that in cases of low or normal pressure, there is outward

movement of the tympanic membrane; in normal pressure there is either outward or bi-directional movement, followed by outwards; and in instances of high pressure there is an inward motion of the tympanic membrane[199]. This stapedial-reflex approach is a different approach of the use of TMD measurements, than the one that is being used in this project. The alternative approach can be thought of as a spontaneous measure of tympanic membrane displacement, due to physiological events, rather than an evoked response, which is the case in the stapedial-reflex approach. In the methodology used in this project, intra-aural pressure wave changes in response to blood pressure challenges are being investigated and these waves are thought to have a direct correspondence to intracranial pressure waves[198,201,200]. The amplitude of these pressure waves has been found to vary with intracranial pressure, and this is used to assess the degree of ICP elevation. In this project, it is the absolute intra-aural pressure wave changes that occur when a blood pressure challenge is imposed that are under investigation, rather than the amplitude of the individual pressure waves. This kind of measurement has been demonstrated in one patient[202], when she underwent mechanical ventilation under general anaesthetic, which allowed CSF pressures to be measured at the same time as TMD measures of trans-aural air volume changes (see figure 23). A close relationship was found between the time courses intracranial pressure changes and TMD signal changes and it is this type of non-invasive measure of ICP that is required in this project.

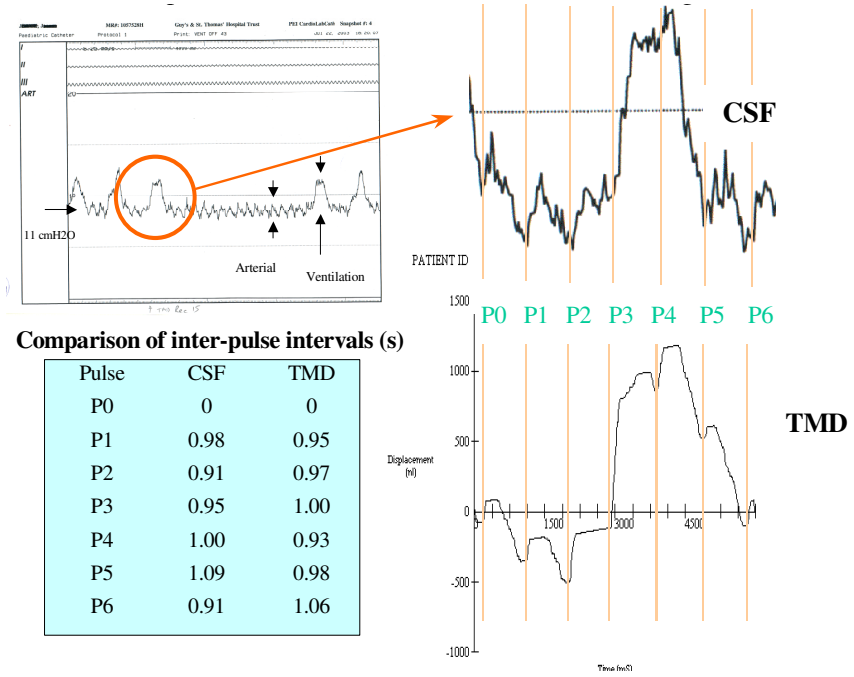

Comparison of inter-pulse intervals (s)

Pulse	CSF	TMD
P0	0	0
P1	0.98	0.95
P2	0.91	0.97
P3	0.95	1.00
P4	1.00	0.93
P5	1.09	0.98
P6	0.91	1.06

Figure 23: Intracranial pressure and intra-aural (TMD) air volume changes (used with permission from Lin J-P et al, 2005[202]).

Chapter 5 Methods

5.1 Experimental study design

Ethical approval for the study was obtained from the Southampton and South West Hampshire Research Ethics Committee (B). Healthy volunteers were recruited; subjects were aged between 18 and 65, not currently on any medication, and with no history of cardiovascular disease or respiratory problems, including asthma. Other exclusion criteria included pregnancy and any contra-indications for MRI. Ten subjects were recruited; 3 other volunteers refused to consent for the study after thigh inflation was attempted and found to be too painful.

Experiments were carried out in two separate visits for each volunteer. The first visit consisted of the MRI experiments and the second visit comprised the arterial blood pressure (ABP) and tympanic membrane displacement (TMD) measurements. The induced blood pressure changes were assumed to be the same for the two sets of experiments.

The first MRI experiment was the BOLD data acquisition. Each blood pressure stimulus (thigh cuff deflation and the Valsalva manoeuvre) was applied during separate 60 second long BOLD MRI acquisitions. Each of these experiments was carried out three times (i.e. three thigh cuff deflation experiments and three Valsalva manoeuvre experiments). The MR angiography experiments, data from which is used to derive venous pressure, were carried out immediately after the BOLD-MRI experiments, using the same blood pressure stimuli, again repeated three times for each stimulus.

The TMD and arterial blood pressure experiments were carried out in the Department of Medical Physics and Bioengineering, i.e. remote to the MRI scanner, and on a different occasion for each volunteer. Prior to the TMD measurements being carried out, the inner ear pressure of each subject was tested, to ensure that this was normal. Once this had been verified, the TMD and simultaneous blood pressure measurements were carried out. The subject was in a supine position on a bed (to mimic the set up in the MRI

scanner) and the Finapres blood pressure monitor was attached to the subject's left middle finger. The TMD probe was inserted into the right ear of the subject to enable the TMD measurements to be carried out. Thigh cuff pressure was also monitored so that the point of cuff deflation could be recorded and aligned with the TMD and ABP data. Three sets of data were sampled and recorded on a laptop pc, namely the TMD data, the blood pressure measurements and the thigh cuff pressure (each sampled at 100 Hz). Timings of the Valsalva manoeuvres were also recorded manually.

Timings between all these experiments were synchronised to the start of each of the blood pressure stimuli. To enable this, thigh cuff pressure was measured outside the scanner at a frequency of 100 Hz. The start of the step-drop in thigh cuff pressure was taken as the moment of thigh cuff deflation. The start of the Valsalva manoeuvre was inferred from the TMD data, as the timing of the start had been noted in relation to these measurements, and this could be matched up to the simultaneously acquired blood pressure data. These time points were synchronised with MRI measurements, as the start of each stimulus had been noted during each MRI acquisition.

Each of these measurements is described in greater detail in the following sections.

5.2 Application of blood pressure stimuli

5.2.1 Thigh cuff deflation

Thigh blood pressure cuffs were placed around the right and left thigh, mid way between the knee and top of the thigh. The thigh cuffs were 18 cm wide and attached to a manual inflation bulb and a quick release manual shutter valve. The thigh cuffs were manually inflated using a normal pressure cuff bulb to 180 mmHg (which was assumed to be supra-systolic). A stopwatch was used for timing the experiment and this was started once thigh cuff

pressure reached 180 mmHg. After 3 minutes the cuffs were deflated through 2cm bore tubing, by pulling a handle on the quick release manual shutter valve. Data was collected for 20 seconds before and 40 seconds after the release of the valve in the MRI experiments. In the experiments conducted outside the MRI scanner, data was acquired over a longer timescale. A rest of at least 2 minutes was allowed between successive inflations.

5.2.2 The Valsalva manoeuvre

Subjects were instructed and trained to carry out the Valsalva manoeuvre before entering the MRI scanner. They were instructed to tighten their chest muscles to produce a strain and to maintain this strain at a constant level for 15 seconds. They were also told to keep their head and body as static as possible during this manoeuvre to minimise movement artefacts in both the MRI and TMD experiments. They were prompted to start the manoeuvre by the investigator telling them to 'start Valsalva' and told to stop by the instruction 'release'. The time points when the manoeuvre commenced and finished was noted. In the MRI experiments, this was 20 and 35 seconds into the measurements respectively, whilst in the ABP experiments this was 5 seconds and 20 seconds into the 4^{th} epoch of the TMD measurements. A time period of at least 2 minutes was allowed between each repeat of the Valsalva manoeuvre experiment.

5.3 Measurements of blood pressure and ICP

5.3.1 The measurement of arterial blood pressure

Blood pressure (BP) was measured outside the scanner environment in this project, at the same time as the tympanic membrane displacement measurements. The finger cuff for the Finapres was attached to a finger on the left hand following the manufacturer's recommendations. Data was

recorded via a digital recording system on a laptop, sampled at a frequency of 100 Hz. Before any blood pressure challenges were applied, the Finapres went through a calibration procedure. Once this had been completed and a stable, realistic waveform was evident, the auto re-calibration was disabled to avoid loss of data at critical times during the experiments. The blood pressure measurement was allowed to run continuously throughout three thigh cuff deflations, and three Valsalva manoeuvres. Calibrations were performed between these procedures if resting pressure waveforms appeared to have changed.

The data was exported from the data collection system and manipulated within Matlab™ (The MathWorks Inc, Natick, Massachusetts, USA). A low-pass Butterworth filter (order 5 and cut-off frequency 0.5 Hz) was applied to smooth the data. Data epochs were selected that covered 20 seconds preceding thigh cuff deflation or the start of the Valsalva manoeuvre, and 80 seconds afterwards. Point by point averaging of data from the three runs of each blood pressure stimulus was carried out to obtain a mean BP trend. The data is presented in Chapter 6 and used as an input to the Ursino model as arterial pressure or P_{in}.

5.3.2 The measurement of venous blood pressure

The MRI technique used here is an ultra fast MRI technique, called trueFISP. This is a Siemens pulse sequence, which stands for fast imaging with steady state precession or more generically it is a fully rewound gradient echo sequence. In this type of sequence, the residual magnetisation left after the data acquisition period is rewound, i.e. set to back to zero by reversing the polarity of the gradient pulse, and in the case of a trueFISP sequence, this is in all three directions (not just in the phase encoding direction). This technique provides good contrast between blood and soft tissue, and images can be acquired at a very high temporal resolution. The pulse sequence parameters for the sequence used in this study are: TR = 4.6 ms, TE = 2.3

ms, flip angle = 69°, pixel size = 0.51 mm × 0.51 mm, slice thickness = 8mm. This technique enabled the acquisition of good spatial resolution cross-sectional images of the internal jugular vein, at a good temporal resolution of 0.6 s.

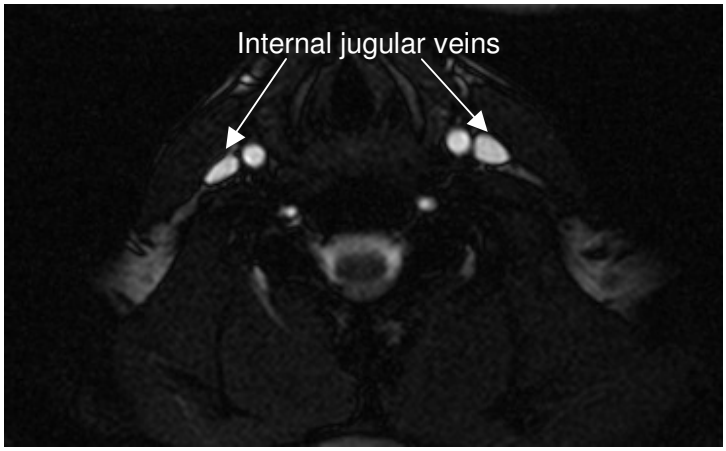

Figure 24: Example trueFISP image of jugular veins.

The blood pressure stimuli used for this data acquisition were the same as that used for the BOLD image acquisition. Images were acquired every 0.6 seconds for one minute, at the level of vertebra C6 (planned on a sagittal cross sectional image of the head and neck). During this time, at approximately 20 seconds into the scanning sequence, either thigh cuffs were deflated (which has been inflated for 3 minutes previous to this) or the subject was instructed to start the Valsalva manoeuvre and hold this for 15 seconds. This enabled the acquisition of a set of 100 images, acquired every 0.6 seconds, with the jugular veins clearly visible. The pulse sequence was run during three repeats of the thigh cuff deflation and three repeats of the Valsalva manoeuvre.

Regions of interest were drawn manually around each jugular vein, in each of the 100 images in each dataset, a total of 1200 regions of interest per subject. The region of interest function within the Osiris software package (developed by the Digital Imaging Unit of the Service for Medical Computing of the University Hospitals of Geneva, Switzerland[203]) was used. The order of

the images in each dataset was randomised, so that assumed cross-sectional area changes during each type of blood pressure challenge would not influence the drawing of these regions of interest. After this data had been obtained, the randomisation was reversed and the data re-ordered into the correct time sequence. The regions of interest were drawn by several trained volunteers, and not by the principal investigator to minimise bias in the results. One volunteer analysed two datasets (volunteers 1 and 2), another analysed one dataset (volunteer 3), another analysed a further two datasets (volunteers 4 and 6) and the final volunteer analysed 4 datasets (volunteers 7, 8, 9 and 10). One single image dataset (relating to thigh cuff deflation) was analysed by both a volunteer and the principal investigator to examine the repeatability of this method. The two resulting time series were correlated and the correlation coefficient was found to be 0.79, which shows good repeatability. A Bland-Altman plot[204] was also generated and this is shown below:

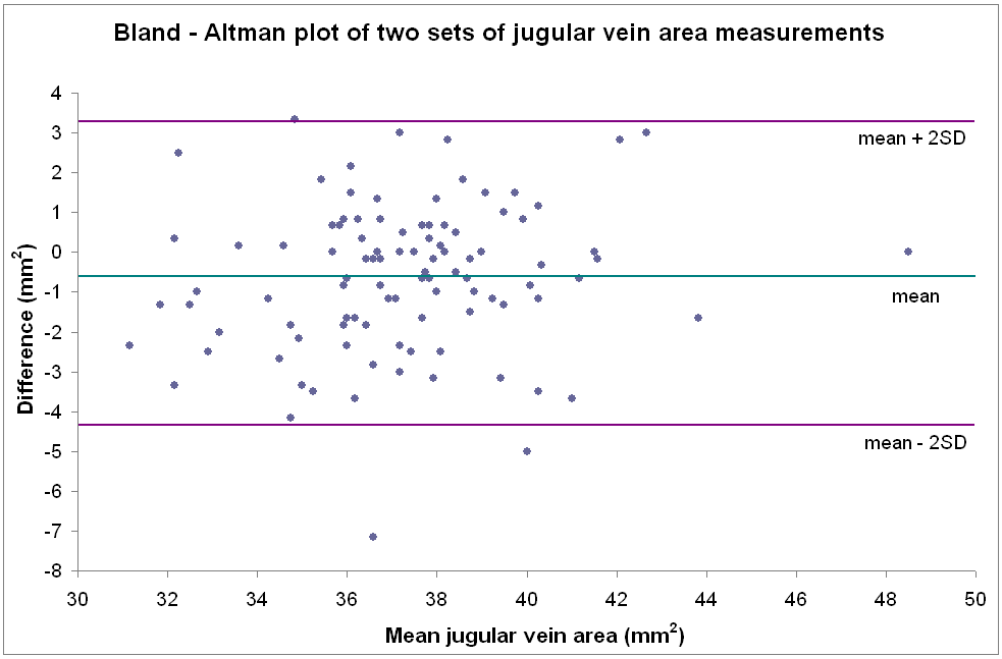

Figure 25: Bland-Altman plot of two sets of jugular vein area measurements.

This also demonstrates reasonable agreement between the two sets of measurements.

The cross sectional areas of the right and left vein were averaged for each time point and then normalised to a mean cross-sectional area obtained from images 6-18, i.e. against a baseline value for cross-sectional area. A mean baseline venous pressure of 8 mmHg was assumed, and the normalised time-series multiplied by this factor to produce a time-series of pressure changes throughout the blood pressure challenges. The data was smoothed using a Butterworth filter of order 5 and a cut-off frequency of 0.4 Hz. The validity of this method is considered in the results and discussion chapters. The data is presented in Chapter 6, and used as an input to the Ursino model, as a time series of venous sinus pressure changes or P_{vs}.

5.3.3 The measurement of intracranial pressure

The non-invasive intracranial pressure (ICP) measurements for this project were undertaken simultaneously with blood pressure measurements, outside the scanner environment. The Marchbanks MMS-11 Cerebral and Cochlear Fluid Pressure Analyser (CCFP) was used to measure the time course of tympanic membrane displacement (TMD). Subjects were investigated in the fully supine position to replicate the conditions under which they underwent MRI scanning. Prior to the TMD measurements, the function of the middle ear was assessed, to verify that this was normal. The TMD earpiece (which was mounted on a headset) was inserted into the outer ear of the subject. The seal was checked for leakage before measurements commenced. The earpiece was adjusted until a good seal was achieved. Due to low frequency drift, the longest continuous TMD measurement that can be consistently made is 30 seconds. A pause of approximately 1 second is then required for re-zeroing before the measurement can continue. The TMD device was set up so that 8 measurements (epochs) were made in total, each of a 30 second duration, resulting in 4 minutes' recording of TMD data with calibration and a

temporary loss of data at 30 second intervals throughout this. Thigh cuffs were inflated prior to the measurements taking place, and kept inflated for 3 minutes. After one minute of this inflation period, the TMD measurements were started and after a further 2 minutes, the thigh cuffs were deflated; this occurred 5 seconds after the start of epoch 5. A recording was also made of the thigh cuff pressure so that the exact point of cuff deflation could be correlated with TMD and BP measurements. A similar procedure was carried out for the Valsalva manoeuvre measurements, except that the subject was instructed to start the manoeuvre 5 seconds into epoch 4 (the time of this was noted), and asked to hold the VM for 15 seconds. The thigh cuff and Valsalva manoeuvre challenges were repeated three times each on each subject. The data was digitally recorded (along with BP data and thigh cuff pressure data) and exported to Matlab for analysis.

The TMD data was divided into 8 individual 30 second epochs for each run of the experiment. Any epochs with movement artefacts contaminating the data were rejected. The data was filtered in the same manner as the BP data. The focus of the analysis was the data epoch in which the blood pressure stimulus occurred. The remaining epochs were used to generate a detrending template. This is required as there is a non-linear downward trend in the TMD trace throughout each epoch, thought to be machine related, which obscures the real signal changes taking place. This detrending was achieved by taking the data from each epoch, excluding epoch 5 or 4 (the one when the thigh cuff deflation or VM took place, respectively). These epochs were then averaged, thus reducing noise in this data, and used as the detrend template, assuming that the variations in these epochs are purely due to the drift in the device, and not physiologically derived. This template was then subtracted from the stimulus-containing epoch, thus revealing the true physiologically evoked signal change. To confirm that this detrending technique was appropriate, an assessment of the other epochs was made by subtracting a template (which excluded the epoch under investigation as well as the stimulus-containing epoch) from each epoch and examining the

results. This was carried out by taking an average of all the other detrended epochs and verifying that there was no trend present in this average. The TMD data relating to the three thigh cuff deflations and three Valsalva manoeuvres was averaged over the three repeats, to provide a mean TMD response for each subject.

5.4 BOLD MRI experiments

The aim of these experiments is to examine the effect of two blood pressure stimuli (thigh cuff deflation and the Valsalva manoeuvre) on the BOLD-MRI signal in the brain.

Images were acquired on a 1.5 T Siemens Symphony MR system (Siemens Medical Systems, Erlangen, Germany). The first experiments were carried out using thigh cuff deflation as the stimulus. The subject was placed in the scanner, with their head firmly secured in the head coil (CP head array coil), with the cuffs around their thighs. The cuffs were inflated and then kept inflated for a further three minutes. The MR measurement was then started. After 20 seconds the cuffs were deflated rapidly by means of releasing a valve. The measurement was then allowed to continue for another 40 seconds. This procedure was carried out three times on each subject.

The next blood pressure challenge involved the subject carrying out the Valsalva manoeuvre. The scan was started and after approximately 20 seconds into the measurement the subject was instructed (over the intercom) to start the Valsalva manoeuvre. After a further 15 seconds had elapsed, they were instructed to stop the manoeuvre. The total duration of the scan was 60 seconds. Subjects had been coached beforehand to carry out the manoeuvre in a consistent manner, and were encouraged to keep head motion minimal. Again, this experiment was carried out three times within the scanner. Data was only acquired from one slice of the brain (to keep measurement time to a minimum). This slice was a medial, oblique axial slice over the ventricles.

Figure 26: Slice position of BOLD image acquisition.

A gradient echo, echo planar imaging (GE-EPI) BOLD sequence was used; this was the default BOLD sequence available on the scanner. The sequence had a repetition time (TR) of 1000 ms, an echo time (TE) of 60 ms and a flip angle (α) of 50°, a 64 x 64 matrix, a 210 mm x 210 mm field of view, a 3 mm slice thickness, one signal average, 0.62 ms echo spacing and a bandwidth of 1860 Hz/pixel. A relatively short TR was employed in this study, to ensure that signal transients in response to the blood pressure challenges were not missed. This was considered to be the shortest TR that could be employed to sample the signal transients adequately without degrading signal-to-noise ratio (SNR) too much. The other parameter that influences SNR is the flip angle (α). The TR determines the amount of longitudinal magnetisation available to tip back into the xy plane after each RF pulse, as a result of the T_1 relaxation that has occurred in this time. If the flip angle is reduced then less time is required for complete (or near complete) relaxation of the magnetisation back to the z-axis, and SNR is maximised. If a large flip angle is used in a short TR sequence, incomplete relaxation takes place; there is less magnetisation available to tip back into the xy plane and saturation of the MR signal results, i.e. a reduction in SNR.

The use of the Ernst angle maximises signal-to-noise ratio of the BOLD signal and also reduces inflow effects. Minimising inflow effects ensures that the

signal that is being observed is a true signal of deoxygenated blood and is not confounded by alterations in longitudinal magnetisation of the blood signal (i.e. T_1 effects) due to the bulk flow of unsaturated arterial blood into the imaging plane.

The repetition time (TR) is 1000 ms in these experiments and the Ernst equation can be used to calculate the optimum flip angle for this TR and particular T_1 time of the tissue of interest. This is obtained by maximising the steady state equation for signal intensity in a spoiled GE-EPI sequence[102]:

$$S = \frac{M_0(1 - e^{-TR/T_1})}{1 - \cos\alpha\, e^{-TR/T_1}} \times \sin\alpha\, e^{-TE/T_2^*} \qquad (55)$$

Where S is signal intensity and M_0 is the longitudinal magnetisation at the start of the experiment. The flip angle α that maximises S is known as the Ernst angle and this is given by:

$$\alpha = \cos^{-1}[\exp(-TR/T_1)] \qquad (56)$$

For a TR = 1000 ms, and $T_{1deoxyHb}$ = 1350 ms[8], $\alpha = 62°$.

The relationship between signal intensity and flip angle was investigated in one volunteer, by plotting the signal intensity of brain parenchyma (using the GE-EPI sequence) against flip angle for a TR of 1000 ms, and this curve peaked at a flip angle of 50°. This value is less than the value of the Ernst angle corresponding to deoxygenated blood calculated above, as there may be contamination of CSF signal within the large region of interest that was used to measure signal intensity. The longer relaxation time of CSF (3 – 5 seconds) when combined with that of deoxygenated blood would result in a smaller optimal flip angle. The use of the Ernst angle in such experiments is a common approach and is used routinely[5,205,144,206]. A flip angle of 50° was thus used in these experiments. The reduction of the flip angle also decreases the inflow effect; using a much smaller flip angle (for example 20°) would minimise this effect, but this would also reduce the SNR of the BOLD signal. As the signal changes in this experiment are expected to be small,

this was not considered to be an optimal solution; hence the flip angle was kept at 50°.

The EPI sequence that was employed used blipped phase encoding with ramp-sampled trapezoidal readout gradients and gradient spoiling at the end of each acquisition. Three-echo Nyquist ghost phase correction was also used. The series of 60 images were motion corrected on the Siemens scanner. Images were aligned with the first image in the dataset by means of in-plane translations and rotations using a six-parameter rigid-body realignment method[207]. This data was used for image analysis. No smoothing was applied to the BOLD MRI images as this may average out and reduce the signal changes that were being measured (this may be investigated in further work).

The analysis of the BOLD images was carried out by drawing freehand regions of interest relating to grey matter and white matter on the first of the motion corrected set of 60 images, and propagating these regions of interest throughout the data set, to produce a time series of BOLD signal intensity throughout the experiment. This data was re-sampled at a higher frequency to allow comparison with the BOLD model output, which resulted in slightly smoothed time series. Similar regions of interest have been used in other publications[208]. This was carried out using the ImageJ software package[209]. Typical regions of interest are shown on an example BOLD image and a high resolution T_1 weighted image, which has been acquired at a similar oblique angle and level in the brain. However, the T_1 image is not from the same subject, as T_1 images were not acquired in these experiments:

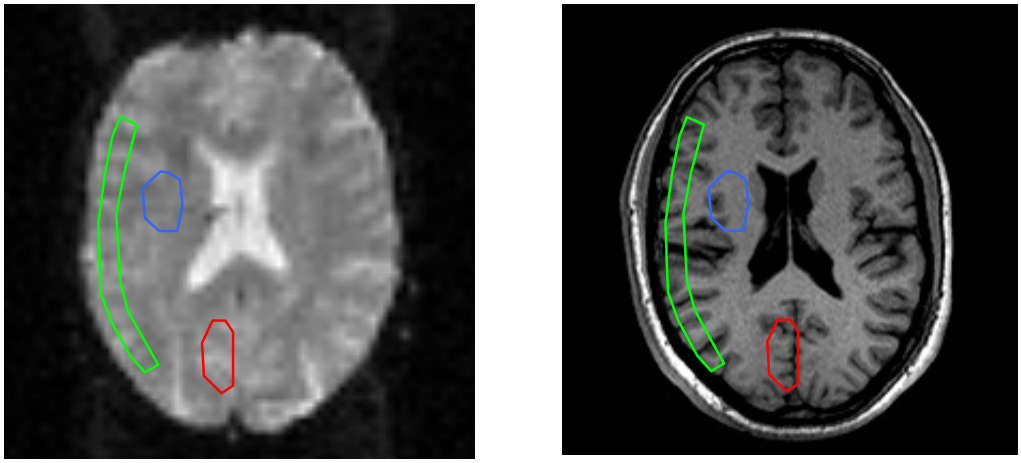

Figure 27: Regions of interest, red – grey matter (back), green – grey matter (cortex), blue – white matter, shown on a typical BOLD image (left) and high resolution T_1 weighted image (right).

It can be seen that in the white matter (blue) region of interest, a small part of the insular cortex may be included, and there may be some inclusion of the basal ganglia. However, in the majority of subjects, this region was predominantly white matter and this is referred to as the white matter region of interest in the rest of the thesis. The consequence of the partial volume effect, i.e. that each region of interest may contain signal from other tissue types, is included in the discussion of the results. The data from the grey matter at the back of the brain was used as a comparison to the modelling results.

5.5 Implementation of models

5.5.1 Ursino's model

The purpose of implementing Ursino's model is to predict changes throughout the cerebral vasculature in response to imposed blood pressure alterations. Various output parameters can be derived from this model; the two of interest to this project are venous flow and venous volume, which are used as inputs to the Buxton model for BOLD signal changes. Many other models of the

cerebral vasculature have been developed[154,155,163,164,166,171], but this one has been chosen for this study due to its comprehensiveness and ease of implementation. The fact that the model has been implemented using SIMULINK within Matlab, means that it can easily be integrated with the Buxton model, which has been developed in using the same software. The version of Ursino's model that has been used was published in 1998[50,210]. I am grateful to Yi Liu for permission to use a copy of the model that he has complied in SIMULINK within Matlab[211].

The Model

This model comprises a large number of differential equations (over 20) that are amenable to computational simulation (using numerical algorithms) using a software package such as SIMULINK. These equations comprise numerous constants to describe the compliances and resistances of the various vascular compartments in the brain. Although these values are of importance to the functioning of the model, they have not been optimised in this project; they are considered to be set at appropriate values for a normal healthy brain. Venous conductance (the reciprocal of venous resistance) is set at 2.77 $mmHg^{-1}$ s^{-1} ml[50] when $P_{ic}=P_{vs}$, otherwise this varies. A circuit diagram of the model can be seen in figure 19 and this model is described in Section 4.2.2. The components of the model can be seen in the figure below:

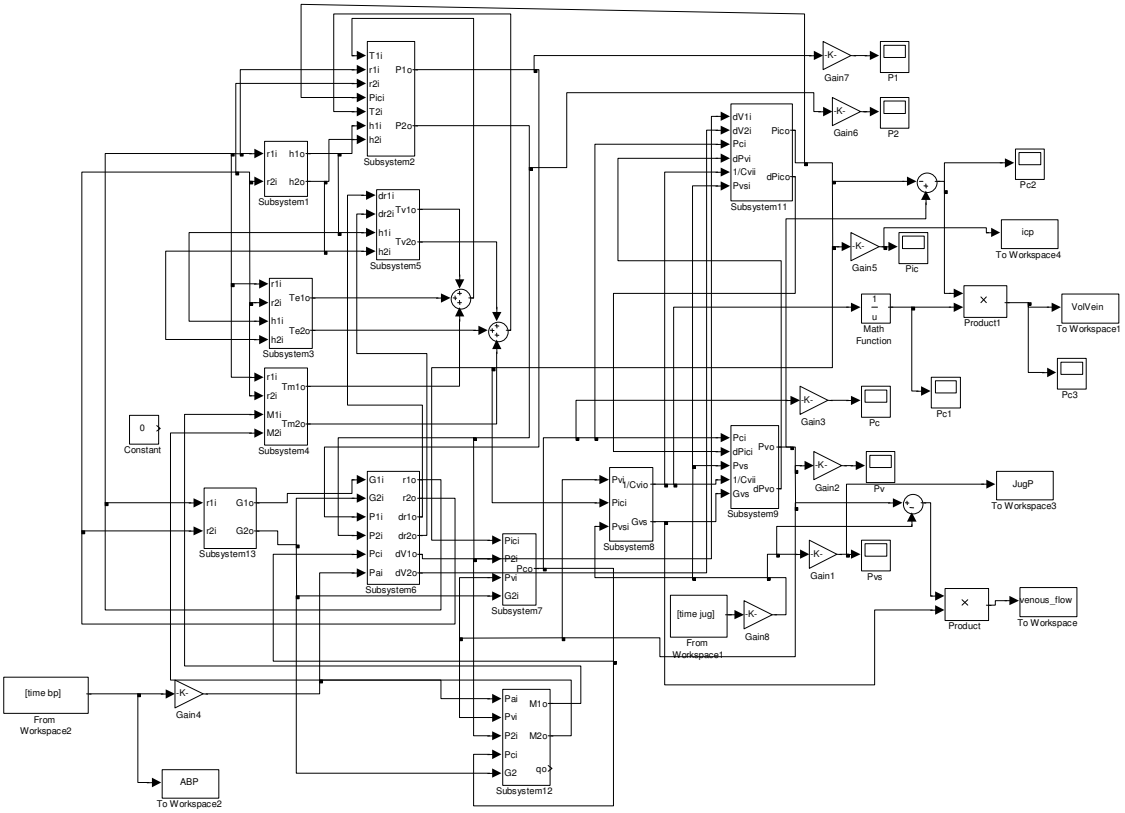

Figure 28: Diagram of Ursino's model implemented in SIMULINK.

The model was run in SIMULINK with an automatically determined step size, a tolerance of 1 x 10^{-7} and using the ode23t (moderate stiffness/trapezoidal), variable step size solver. A delay was added to the input function before the change in blood pressure occurred, to allow stabilisation of the model parameters.

Model inputs

Two measured inputs were used in this model, P_a, arterial blood pressure and P_{vs}, venous sinus pressure. Arterial blood pressure data was obtained from continuous Finapres measurements of blood pressure in the middle finger, during blood pressure alterations (thigh cuff deflations and Valsalva manoeuvres). These measurements are described more fully in Section 5.3.1, in this chapter. Venous sinus pressure variations during these experiments were derived from measurements of jugular vein diameters (taken from MRI images). Again, this process is described in more detail in Section 5.3.2.

Model outputs

In this model, a cerebral venous blood volume time series was derived by multiplying model data pertaining to venous transmural pressure and compliance ($P_v - P_{ic}$ and C_{vi} respectively). Venous blood flow was also derived from this model, by multiplying the venous outflow pressure gradient by venous conductance ($P_v - P_{vs}$ and G_{vs} which is the reciprocal of venous resistance). These values were used as inputs to the Buxton model, which is described in the next section. Intracranial pressure changes were also derived from this model.

Autoregulation

The regulatory mechanisms built into this model are varied by two constants in this model; a gain (H) and a time constant (t) of the smooth muscle response to blood flow alterations. These are defined for two vascular compartments in the brain; the large pial arteries and small pial arteries. These were set equal to the following values[211]: $H_1 = 0$, $H_2 = 20$, $t_1 = 20$, $t_2 = 20$. The subscript 1 refers to large pial arteries and the subscript 2 to small pial arteries. It is thought that autoregulation works on large pial arteries through a pressure dependent mechanism, activated by changes in perfusion pressure (myogenic or neurogenic mechanisms) whereas small pial arteries are sensitive to small CBF changes (due to metabolic or endothelium-dependent mechanisms)[71,76]. As H_1 is set to zero, the large vessel pressure dependent mechanism is turned off, however, the distinction between large and small vessel autoregulation is only really relevant if pressure and flow distributions are required in the different components of arterial circulation, which is not the case here as signal is being detected downstream from the autoregulating compartments. In all of this work, a single flow dependent autoregulation mechanism has been implemented. This was in the small pial arteries with the corresponding gain and time constant set to represent a normal healthy response.

5.5.2 Buxton's model

The use of the Buxton model (modified by Obata) in this project allows BOLD signal changes in response to physiological stimuli to be predicted. As stated previously, this model has been widely used and validated. The part of the Buxton/Obata model that is used in this project is the expression for the signal change in the BOLD signal due to changes in venous blood volume and deoxyhaemoglobin levels. The derivation of this model has been described in Section 4.2.3. This model has also been implemented within SIMULINK to enable it to link in with the Ursino model. The model simulation

parameters were a tolerance of 1 x 10^{-8}, a maximum step-size of 1 x 10^{-1} and using the ode45 (Dormand-Price), variable step size solver.

The equation that has been implemented in this model is taken from Obata *et al* (2004)[52]:

$$\frac{\Delta S}{S_0} = V_0[(k_1 + k_2)(1 - q) - (k_2 + k_3)(1 - v)] \qquad (57)$$

where:

$$k_1 = 4.3\nu_0 E_0 TE$$

$$k_2 = \varepsilon r_0 E_0 TE$$

$$k_3 = \varepsilon - 1$$

and ν_0 = 40.3 s^{-1}, E_0 = 0.4, TE = 60 ms, ε = 1.43, r_0 = 25 s^{-1} (these are defined in Section 4.2.3). This leads to values for k_1+k_2 = 5.01696 and k_2+k_3 = 1.288. These constant are incorporated into the model. The other constant defined in the model is V_0, which is the actual venous blood volume fraction and is set at 0.02 (from Buxton *et al*[51]).

The implementation of this model in SIMULINK is shown in the figure below:

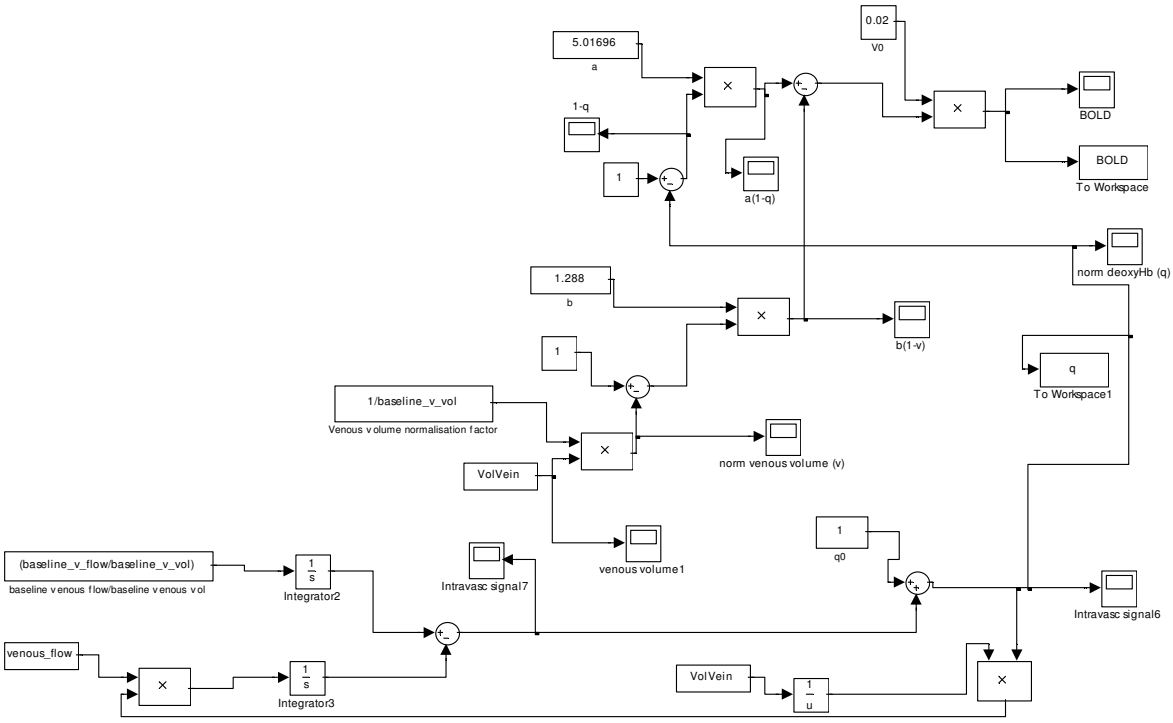

Figure 29: Diagram of Buxton's model implemented in SIMULINK.

The model takes time series of normalised venous blood volume (v) and normalised deoxyhaemoglobin (q) and outputs the BOLD signal time series. The venous blood volume changes can be derived directly from the Ursino model; however, the deoxyhaemoglobin changes must be derived from changes in venous blood flow, assuming that metabolism is constant. As metabolism is assumed to be constant, this implies that oxygen extraction fraction changes as blood flow changes. This results in alterations in deoxyhaemoglobin concentration.

A conservation of mass approach was employed to derive deoxyhaemoglobin changes in response to flow changes. This took into account the inflow and outflow of deoxyhaemoglobin in the venous compartment, and how this altered as venous blood flow changed.

At any point in time within the venous compartment, the absolute amount of deoxyhaemoglobin, Q_t, can be written as:

$$Q_t^v = Q_{t=0}^v + \int f_t^i \left[Q_t^i\right] dt - \int f_t^o \left[Q_t^o\right] dt \qquad (58)$$

where Q = amount of deoxyhaemoglobin

f = flow

v refers to the venous compartment

t refers to time

i refers to inflow

o refers to outflow

This can be normalised to values of Q at time t=0:

$$\frac{Q_t^v}{Q_{t=0}^v} = \frac{Q_{t=0}^v}{Q_{t=0}^v} + \int \frac{f_t^i \left[Q_t^i\right]}{Q_{t=0}^v} dt - \int \frac{f_t^o \left[Q_t^o\right]}{Q_{t=0}^v} dt$$

$$q_t^v = 1 + \int \frac{f_t^i \left[Q_t^i\right]}{Q_{t=0}^v} dt - \int \frac{f_t^o \left[Q_t^o\right]}{Q_{t=0}^v} dt \qquad (59)$$

where q_t^v is the normalised deoxyhaemoglobin content in the venous compartment.

Note that:

$$Q^v_{t=0} = \left[Q^v_{t=0}\right] \times V^v_{t=0} \qquad (60)$$

where V is the absolute volume of the venous compartment. This means that equation (59) becomes:

$$q^v_t = 1 + \int \frac{f^i_t \left[Q^i_t\right]}{\left[Q^v_{t=0}\right] \times V^v_{t=0}} dt - \int \frac{f^o_t \left[Q^o_t\right]}{Q^v_{t=0}} dt \qquad (61)$$

Assuming constant oxygen metabolism, $f^i_t \left[Q^i_t\right]$ = constant. Since $\left[Q^v_{t=0}\right]$ and $V^v_{t=0}$ are both constants, the whole second term in equation (61) is constant. Assuming a steady state at time t=0 (and thus defining all quantities in the second term at time t=0), $\left[Q^i_{t=0}\right] = \left[Q^v_{t=0}\right]$ and equation (61) becomes:

$$q^v_t = 1 + \int \frac{f^i_{t=0}}{V^v_{t=0}} dt - \int \frac{f^o_t \left[Q^o_t\right]}{Q^v_{t=0}} dt \qquad (62)$$

In addition $[Q_t^o] = Q_t^o / V_t^v$, which results in:

$$q_t = 1 + \int \frac{f^i_{t=0}}{V^v_{t=0}} dt - \int \frac{f^o_t \left(Q^o_t / V^v_t\right)}{Q^v_{t=0}} dt \qquad (63)$$

and $Q^o_t = q^o_t \; Q^v_{t=0}$:

$$q_t = 1 + \int \frac{f^i_{t=0}}{V^v_{t=0}} dt - \int \frac{f^o_t \left(q^o_t \; Q^v_{t=0} / V^v_t\right)}{Q^v_{t=0}} dt$$

$$q_t = 1 + \int \frac{f^i_{t=0}}{V^v_{t=0}} dt - \int \frac{f^o_t \; q^o_t}{V^v_t} dt \qquad (64)$$

This equation states that the amount of deoxyhaemoglobin within the venous compartment at any point in time is equal to the original amount of deoxyhaemoglobin plus the amount that flows into the compartment over the

time of measurement, minus the amount that flows out; this is an example of mass conservation. The variables $f^{i}_{t=0}$ and $V^{v}_{t=0}$ are these values at time t=0, i.e. baseline values of venous flow and venous volume. The values f^{o}_{t} and V^{v}_{t} can be derived from quantities in the Ursino model as described in the previous section. They can be thought of as functions of venous flow and volume that vary with time (i.e. f(t) and V(t)), which are derived from the Ursino model. The normalised amount of deoxyhaemoglobin flowing out of the venous compartment, q^{o}_{t} is assumed to be equal to the normalised amount of deoxyhaemoglobin at t = t – 1.

5.5.3 Using the models

Both models were implemented within SIMULINK in Matlab, but kept as two separate models rather than joining them together. Inputs to the model were arterial blood pressure and jugular vein pressure. Both inputs were resampled at a frequency of 100 Hz. Resting baseline values were determined from the mean measurement recorded from 6 seconds to 15 seconds into the acquisition. Both inputs were padded with this baseline value before the start of the measurement to allow a stable model response to develop, with any start up transients removed before the measured data with the blood pressure stimulus was introduced. For each subject, average arterial blood pressure and jugular vein pressure waveforms were derived from the three repeats of each experiment (thigh cuff deflation and Valsalva manoeuvre) and used as model inputs to the Ursino model. Venous volume and venous flow time series were derived from this model, and entered into the Buxton/Obata model, and used as described above. The resulting output was a normalised BOLD signal change, which was compared to the re-sampled experimental BOLD data, derived from the grey matter region of interest. As the BOLD modelling results are expressed as $S\text{-}S_0/S_0$ (where S is BOLD signal and S_0 is baseline BOLD signal), whereas the BOLD data is

expressed as S/S_0, to allow the results to be compared directly, a value of 1 was added to the BOLD model outputs, which renders this output equivalent to S/S_0.

Measured data and outputs derived from the modelling are described above and detailed in the results chapter. Two sets of results were produced, one comparing ABP, venous flow, venous volume, deoxyhaemoglobin, BOLD model output and BOLD grey matter data, and another comparing ABP, jugular vein pressure, intracranial pressure, and TMD data.

Chapter 6 Experimental results

6.1 Arterial blood pressure measurements

The following plots show the arterial blood pressure (ABP) data collected from each subject during both the thigh cuff deflation and the Valsalva manoeuvre. One subject (Volunteer 5) only attended the MRI scanning session; hence 9 subjects in total completed the whole study, and only results from these 9 volunteers are presented. The subject group consisted of 3 males and 6 females with a mean age of 39 (range 28 – 55). The plots show three repeats and a mean dataset of ABP measurements during the two types of blood pressure challenges and the data has been filtered to remove high frequency noise.

6.1.1 ABP response to thigh cuff deflation

In the following plots, the point of thigh cuff deflation takes place at 20 seconds into the acquisition. The blue, green and red lines represent each separate measurement (first, second and third respectively) and the black line is a point-by-point average of three runs of the experiment.

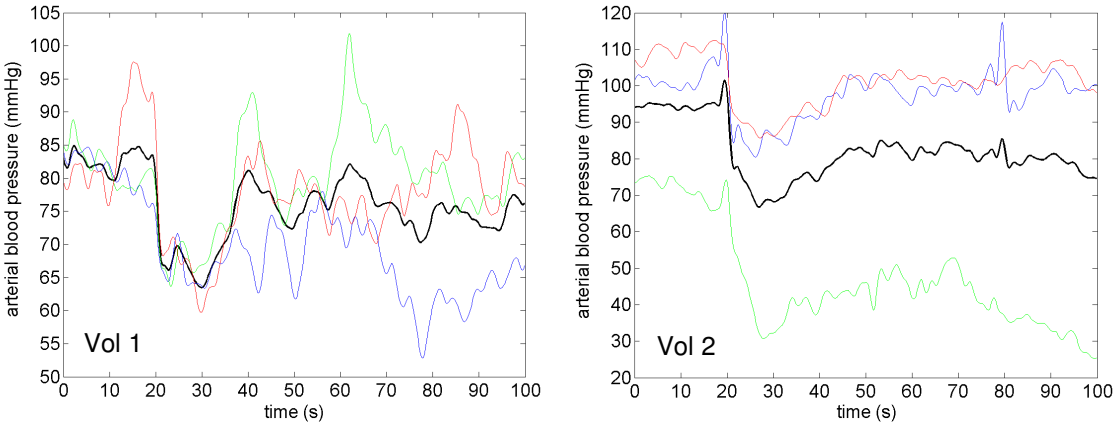

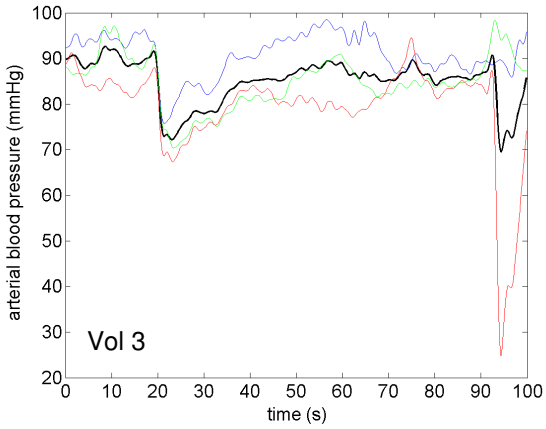
arterial blood pressure (mmHg)
time (s)
Vol 3

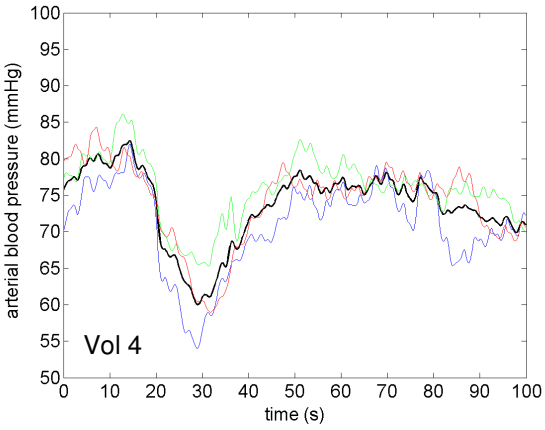
arterial blood pressure (mmHg)
time (s)
Vol 4

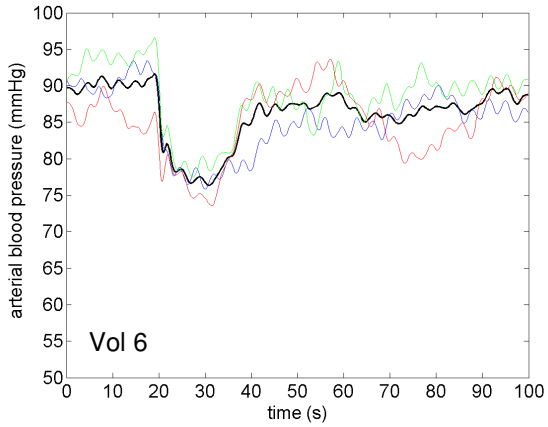
arterial blood pressure (mmHg)
time (s)
Vol 6

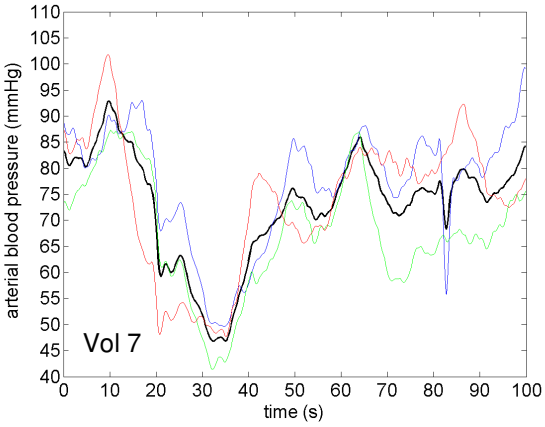
arterial blood pressure (mmHg)
time (s)
Vol 7

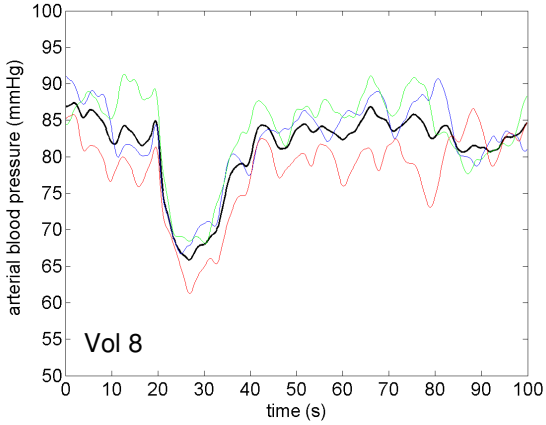
arterial blood pressure (mmHg)
time (s)
Vol 8

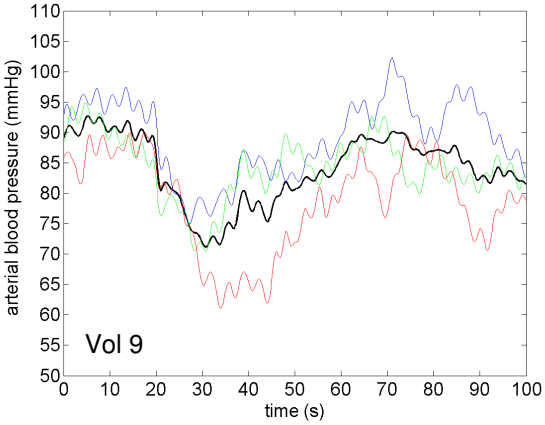
arterial blood pressure (mmHg)
time (s)
Vol 9

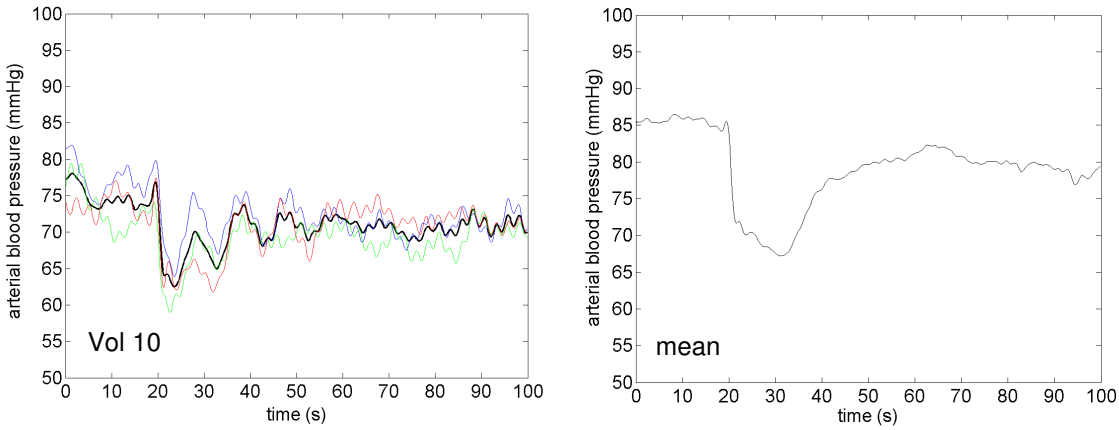

Figure 30: Arterial blood pressure response to thigh cuff deflation for Volunteers 1,2,3,4,6,7,8,9,10 and a mean dataset.

The variation in the three measurements of blood pressure differs between subjects. There is greatest consistency in volunteers 6 and 8, whereas a much greater variation is seen in volunteers 1 and 2. The shift in baseline blood pressure seen in volunteer 2 could be due a calibration error of the Finapres. The averaged results do show that in all nine subjects, a rapid drop in arterial blood pressure occurs after the point of cuff deflation. The magnitude of this drop however, varies between subjects. In addition, the time taken for the blood pressure to recover to its original baseline level also varies between subjects. This could be due to the variable action of blood pressure regulation in response to a sharp drop in blood pressure. A large drop in blood pressure is recorded at the end of the acquisition for volunteer 3; this is considered to be an artefact. The mean drop in blood pressure is 18.2 mmHg ± 6.3 mmHg, or 21.9 %± 7.6 % (± SD). This compares well with published data. For example Birch[80] *et al* reported a maximum blood pressure drop of 25.1 %± 7.1% using the same methodology and device. Aaslid[69] reported a drop of 24.1 %± 1.1% (± SEM in this case) in 10 subjects in a normocapnic state, after a similar blood pressure challenge. No statistically significant differences were found between the results from this study and Aaslid's figures, for maximum blood pressure drop, when this was

tested using a two-sample t-test at a significance level of $p<0.05$ (this criteria is used in all subsequent statistical analysis). The mean time for recovery of blood pressure back to a static (baseline) level is 28.6 s ± 8.6 s.

6.1.2 ABP response to the Valsalva manoeuvre

In the following plots, the start of the Valsalva manoeuvre (VM) takes place at 20 seconds into the acquisition (time point 820) and the subject was instructed to release the manoeuvre after 15 seconds. The blue, green and red lines represent each separate measurement (first, second and third respectively) and the black line is a point-by-point average of three runs of the experiment.

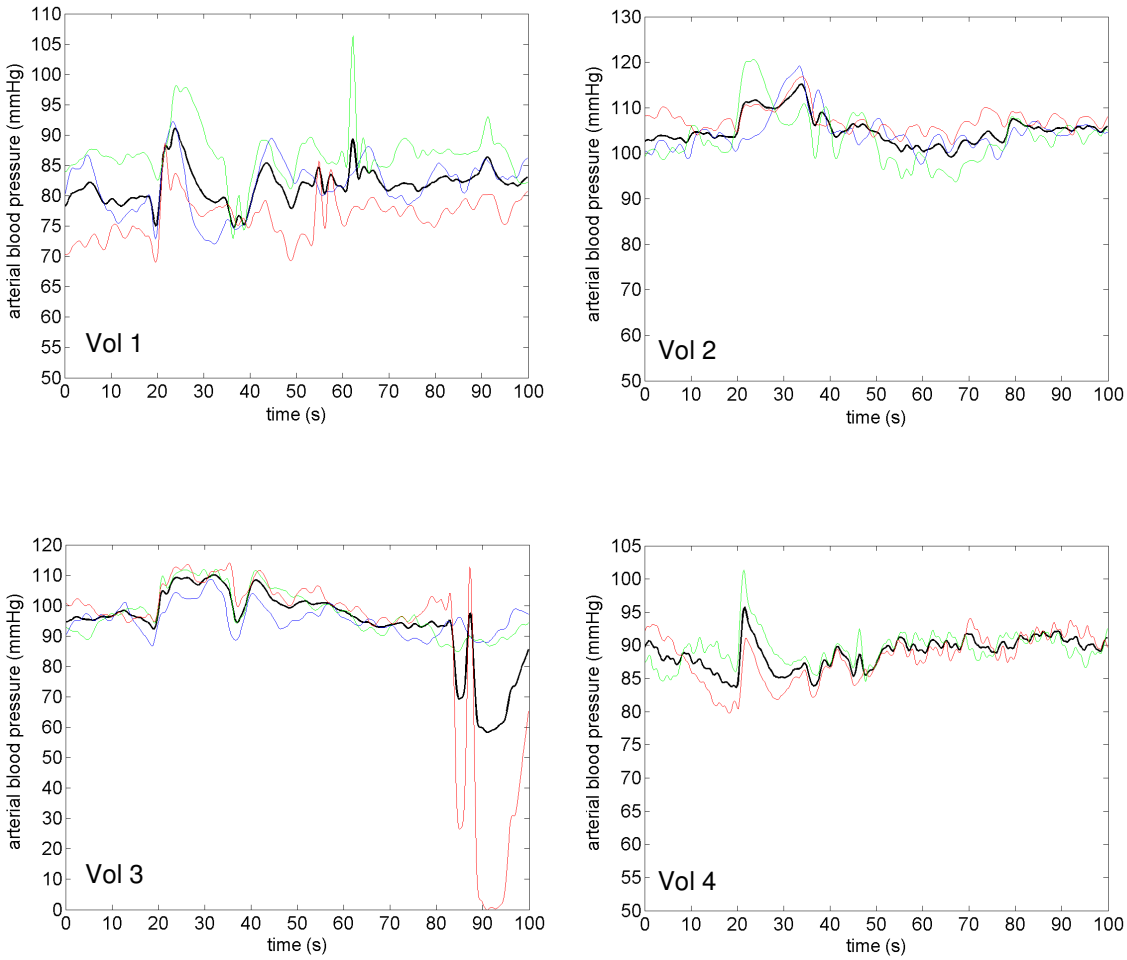

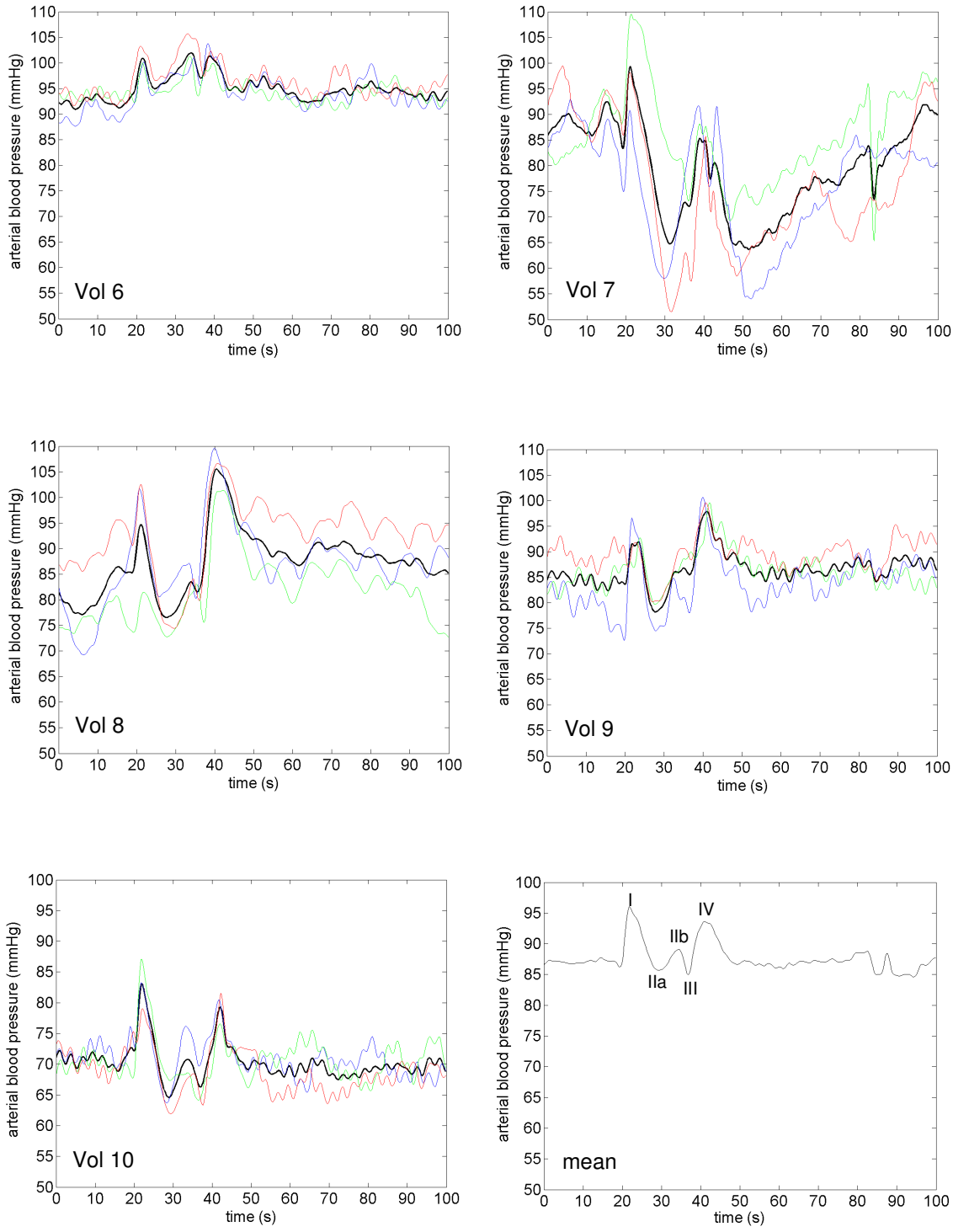

Figure 31: Arterial blood pressure response to the Valsalva manoeuvre for Volunteers 1,2,3,4,6,7,8,9,10 and a mean dataset.

It is perhaps surprising to see that there is reasonable similarity between each repeat of the Valsalva manoeuvre in most individual subjects, with volunteers 1 and 2 showing the greatest variation. There is however, considerable variation in the averaged arterial blood pressure during the Valsalva manoeuvre between subjects; however, the expected features of the curve can be picked out in most subjects. The first peak represents phase I of the Valsalva manoeuvre, with the decrease representing phases IIa, and the subsequent increase phase IIb. The next trough is phase III of the manoeuvre (which occurs at the end of the VM) and the following (usually large) peak coincides with phase IV. The shape of the arterial blood pressure curve during and after the Valsalva manoeuvre follows those reported in the literature[85]; however the magnitude of the changes is smaller than that reported by Tiecks. Two parameters were quantified by Tiecks, the drop in ABP from baseline during phase II (the difference between baseline and the trough labelled 'IIa' in the mean plot above) and the increase in ABP from baseline during phase IV. These were found to be 10.1% ± 9.7% and 26.7% ± 16.0% respectively (whilst maintaining an intrathoracic pressure of 20 mmHg for 15 seconds during the VM). Similar changes were seen when an intrathoracic pressure of 40 mmHg was maintained. In the experiments in this project, these values were 1.87% ± 10.81% and 7.23% ± 9.75% respectively. The values for these parameters were much smaller than those reported by Tiecks but only the change during phase IV was found to be a statistically significant difference (using a two-sample t-test at a significance level of $p<0.05$) to the change reported in this paper. This could be due to a number of reasons. The Valsalva manoeuvre was implemented in Tiecks' study using a slightly different method than the one used in this study. In Tiecks' study, subjects were asked to maintain an intrathoracic pressure of 20 mmHg or 40 mmHg, for 15 seconds, by first taking a large breath in and then exhaling forcefully against a closed valve that was connected to an aneroid pressure gauge. This was a much more controlled application of the Valsalva manoeuvre with subjects being given feedback on their performance of the

manoeuvre, which could result in these pressures being much larger than those applied in this study. There could be greater variation in the quality of the VM across all subjects in this study, as there was no monitoring of the intrathoracic pressure during the manoeuvre and subjects were asked to exhale against a closed rather than open glottis. Although subjects were instructed on how to carry out the manoeuvre, there was some variation as to how well, and to what extent this was carried out. Continuous arterial blood pressure monitoring was carried out using a tonometric blood pressure monitor (Nellcor, N-Cat N-500) in Tiecks' study, whereas the Finapres device was used in this project. Discrepancies in arterial blood pressure changes measured using a different blood pressure tonometer (Colin® CBM-700) and the Finapres have been seen in another study[80], although thigh cuff deflation was used as the blood pressure challenge in that study.

In this study, in some subjects there is a large increase at the start of the VM (phase I, transmission of increased intrathoracic pressure to the arterial tree), but not much of decrease during phase II (fall in ABP due to insufficient filling of the atria in the heart), as seen in volunteers 2 and 3. In other subjects, the peak during phase IV (overshoot of ABP as vascular tone and resistance remain elevated after the release of the VM and normalisation of atrial filling) is not as pronounced as the initial peak during phase I (volunteers 1 and 4). A dip in ABP during Phase III is consistently seen in all subjects at the end of the manoeuvre as arterial pressure is influenced by the sudden decrease in intra-thoracic pressure.

6.2 Jugular vein pressure measurements

In the following graphs, the venous blood pressure has been derived from measurements of the cross sectional area of the jugular veins in the neck. The raw data from all three repeats of the experiments are presented first. The data has then been averaged over three repeats of the thigh cuff deflation and Valsalva manoeuvre, and filtered, for inputting into the Ursino model. All measurements have been calibrated by assuming a mean resting jugular vein pressure of 8 mmHg, before the blood pressure stimulus is applied.

6.2.1 Jugular vein pressure response to thigh cuff deflation – all data

The following plots show the data from three repeats of the jugular vein pressure experiments in blue, green and red, with the mean of these repeats in black. These datasets have not been filtered; the filtered data is presented in the following section, and it is the filtered datasets that are used as inputs into the Ursino model.

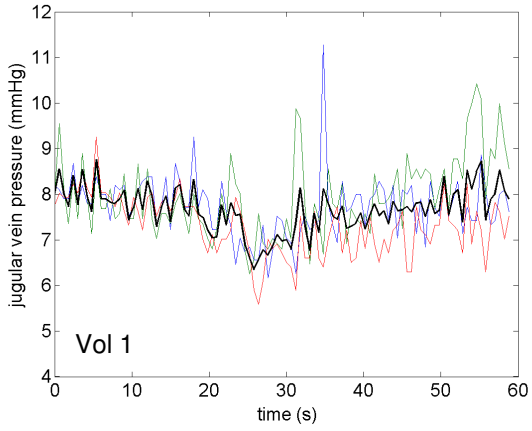

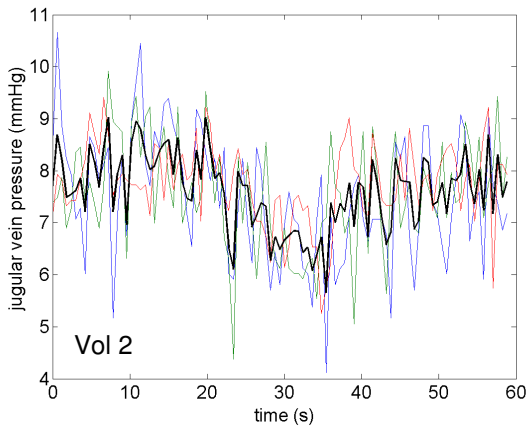

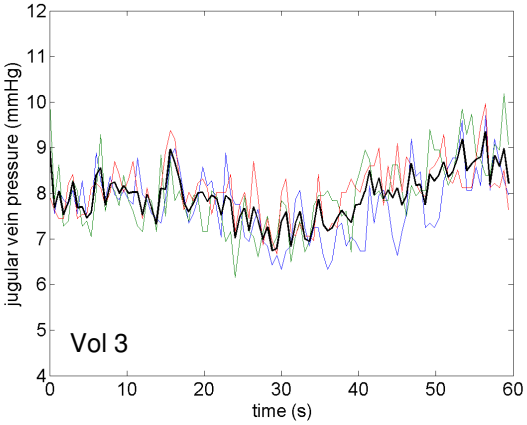
jugular vein pressure (mmHg)
time (s)
Vol 3

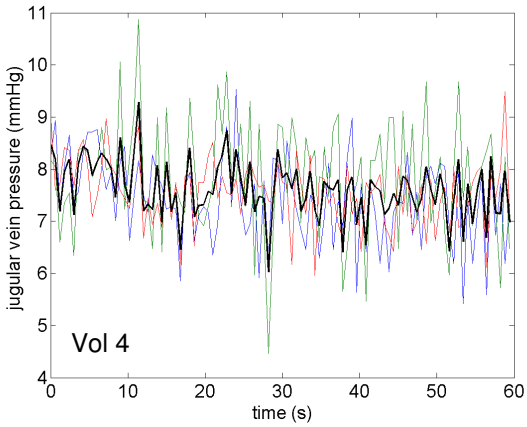
jugular vein pressure (mmHg)
time (s)
Vol 4

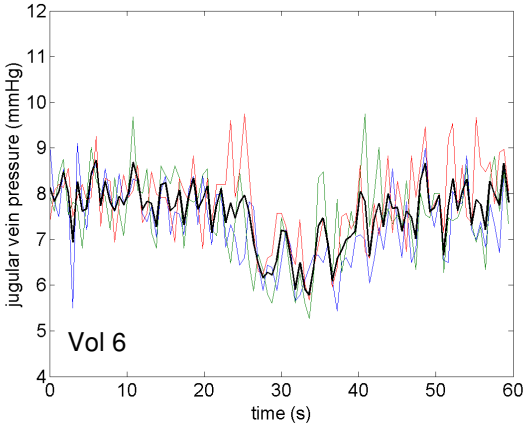
jugular vein pressure (mmHg)
time (s)
Vol 6

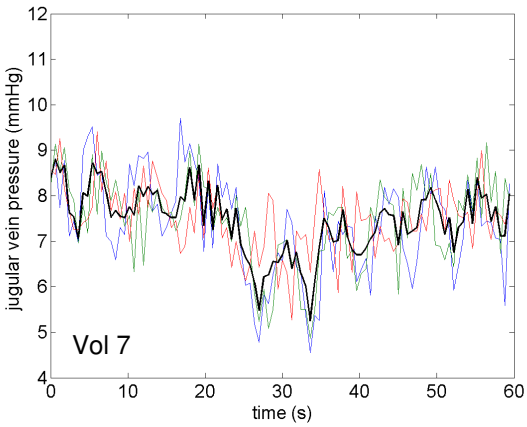
jugular vein pressure (mmHg)
time (s)
Vol 7

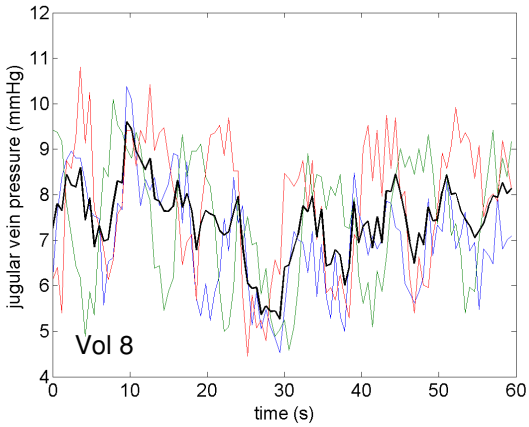
jugular vein pressure (mmHg)
time (s)
Vol 8

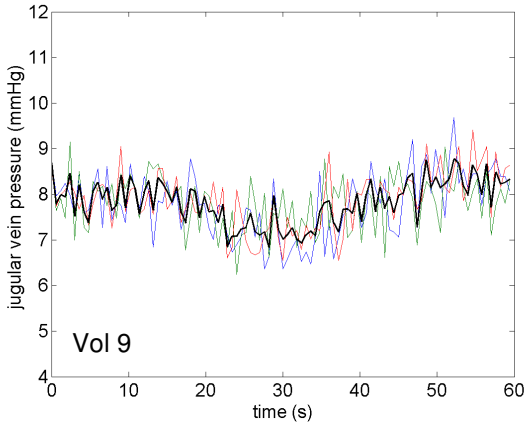
jugular vein pressure (mmHg)
time (s)
Vol 9

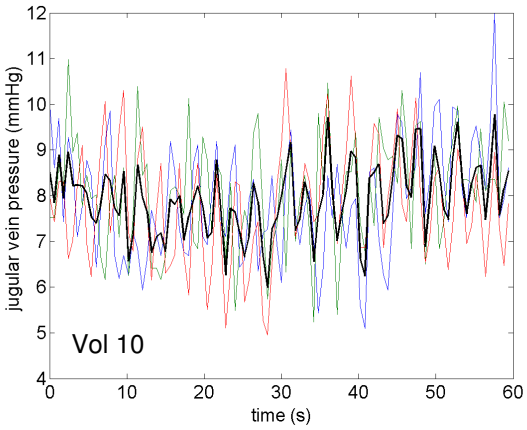

Figure 32: Jugular venous pressure measurements for three repeats of the experiment (blue, green and red lines respectively) and averaged data (black line), in response to thigh cuff deflation in Volunteers 1,2,3,4,6,7,8,9 and 10.

The raw data can be seen to be quite noisy, most probably due to cardiac pulsatility. This was the reason why the data was both averaged over the three datasets and filtered in order to reduce some of this variation. The greatest variation within each subject is seen in volunteers 4 and 10 and the decrease in pressure is less well demonstrated in these subjects.

6.2.2 Jugular vein pressure response to thigh cuff deflation – averaged and filtered data

In the following plots of the averaged and filtered data, the point of thigh cuff deflation takes place at 20 seconds into the acquisition (time point 820).

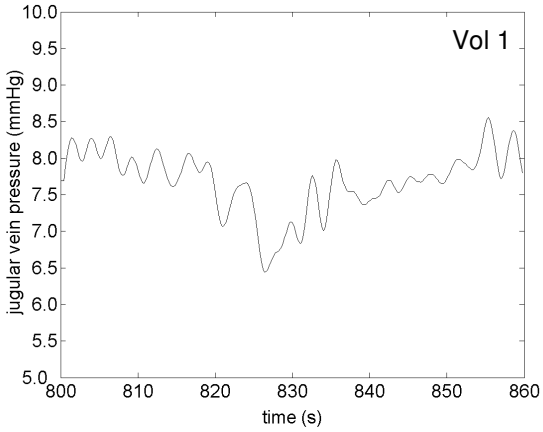
Vol 1
jugular vein pressure (mmHg)
time (s)

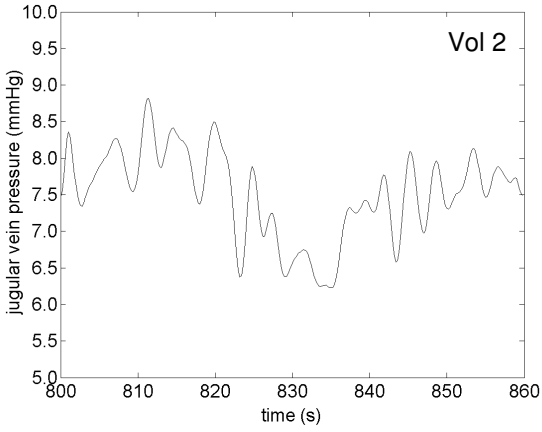
Vol 2
jugular vein pressure (mmHg)
time (s)

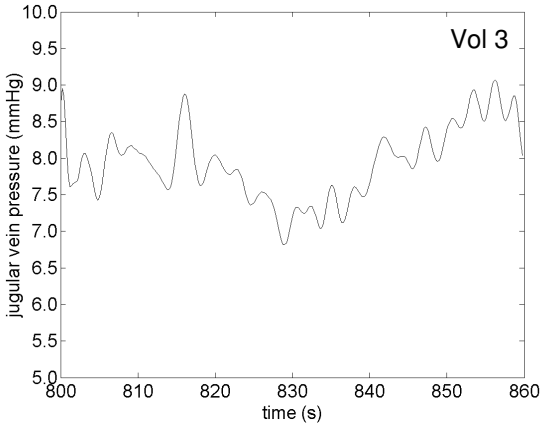
Vol 3
jugular vein pressure (mmHg)
time (s)

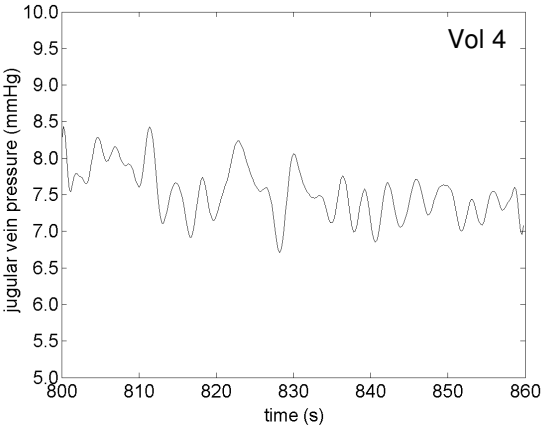
Vol 4
jugular vein pressure (mmHg)
time (s)

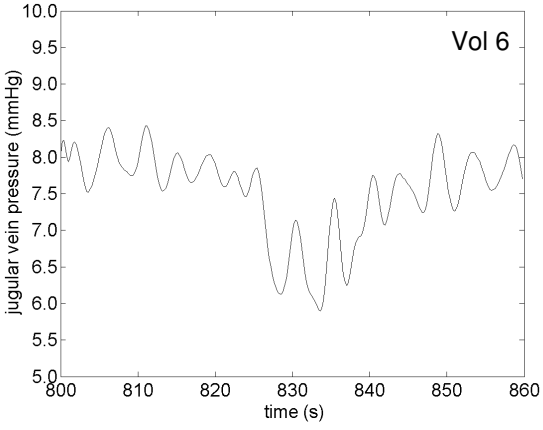
Vol 6
jugular vein pressure (mmHg)
time (s)

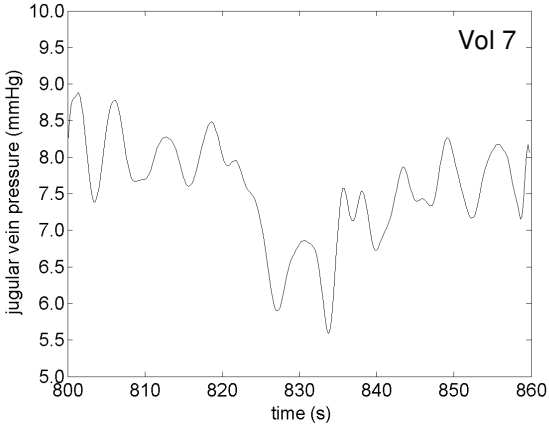
Vol 7
jugular vein pressure (mmHg)
time (s)

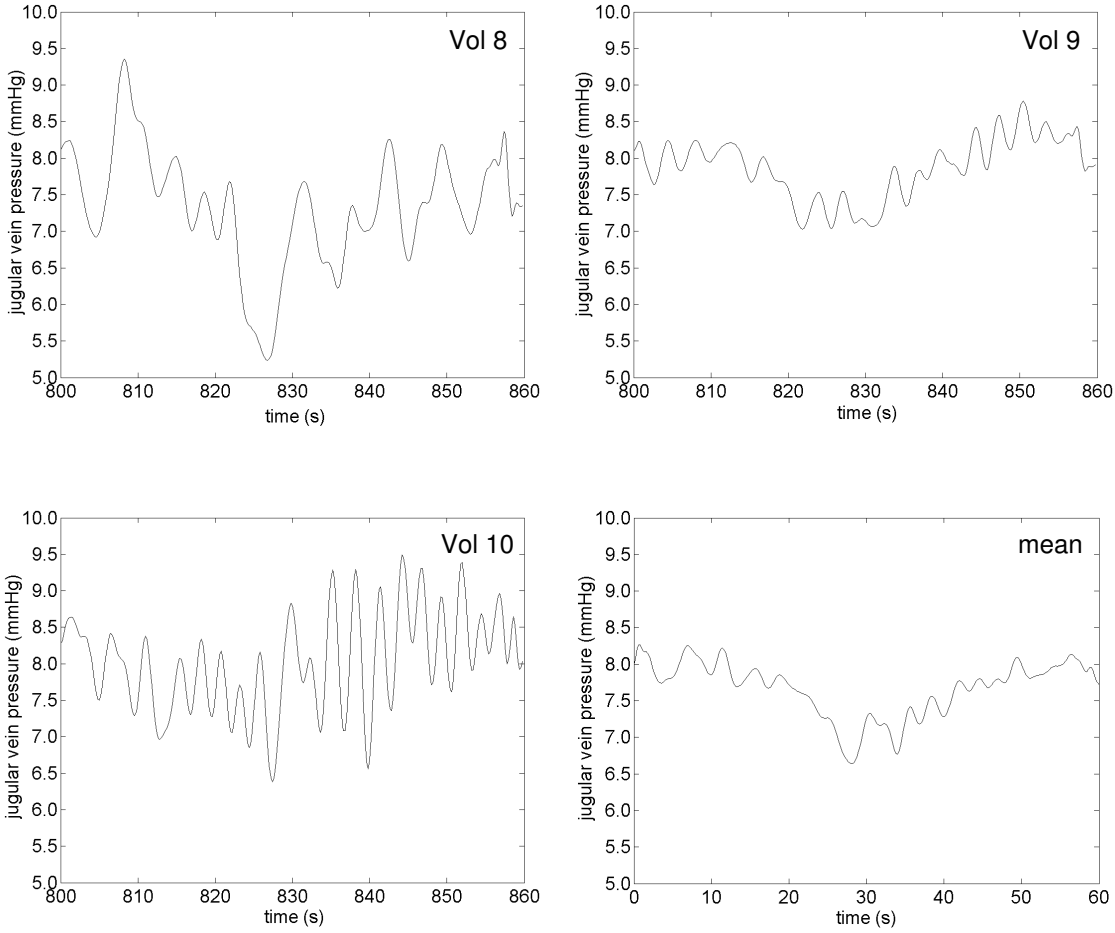

Figure 33: Averaged and filtered jugular vein pressure response to thigh cuff deflation for Volunteers 1,2,3,4,6,7,8,9,10 and a mean dataset.

The general trend that is seen in this data is that there is a decrease in jugular vein pressure after the point of cuff deflation, which then recovers back to baseline levels. This decrease is not as immediate as with arterial blood pressure; it takes place over a time period of 8.0 s ± 1.3 s. The mean maximum decrease in jugular vein pressure is 17.0% ± 6.6% and the time for recovery back to baseline levels is 21.6 s ± 3.3 s. This is not an area of measurement that has been explored in the literature, due to the invasive nature of most venous blood pressure measurements; hence there are no published values to compare these results with. The measurements made in

this study are approximations of venous blood pressure, assuming a linear relationship between jugular vein cross-sectional area and blood pressure. This assumption has been investigated by Berczi *et al*[194], where capacity (mm^3/mm) in the jugular vein was found to be linear with pressure. This provides an estimation of the venous blood pressure time course in the jugular veins. The percentage drop in jugular venous pressure after cuff deflation is similar in magnitude to that seen in the arterial blood pressure measurements, i.e. approximately 20%.

6.2.3 Jugular vein pressure response to the Valsalva manoeuvre – all data

Again, the following plots show the data from three repeats of the jugular vein pressure experiments in blue, green and red, with the average of these repeats in black.

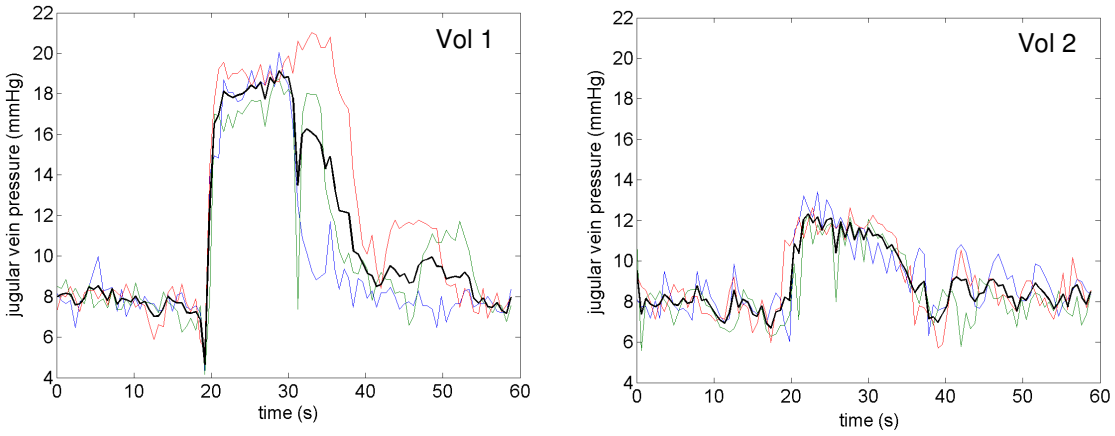

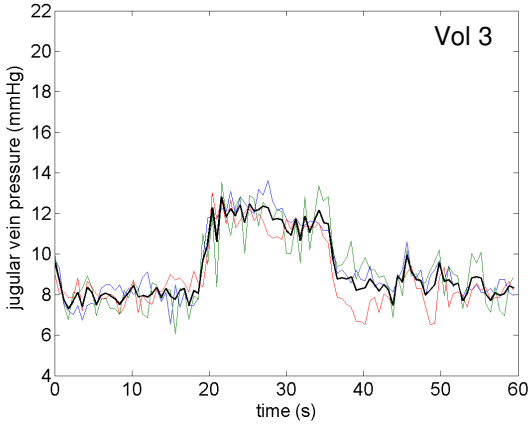
Vol 3
jugular vein pressure (mmHg)
time (s)

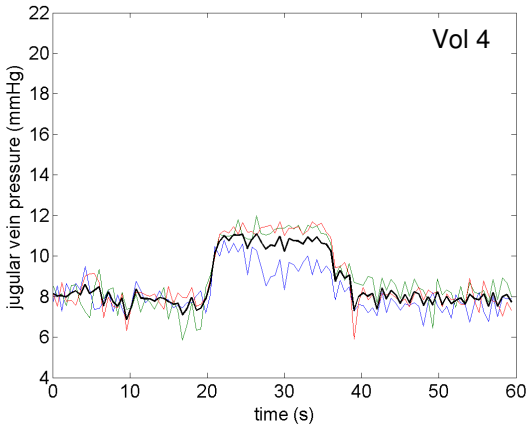
Vol 4
jugular vein pressure (mmHg)
time (s)

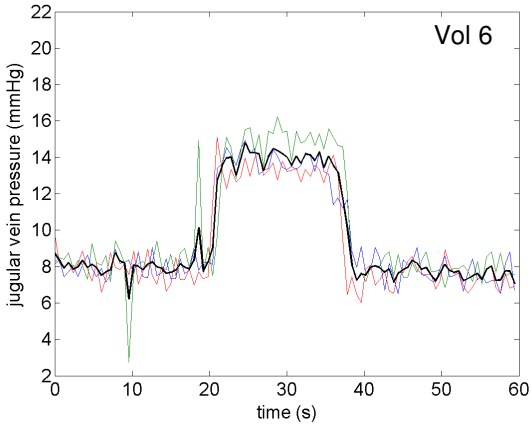
Vol 6
jugular vein pressure (mmHg)
time (s)

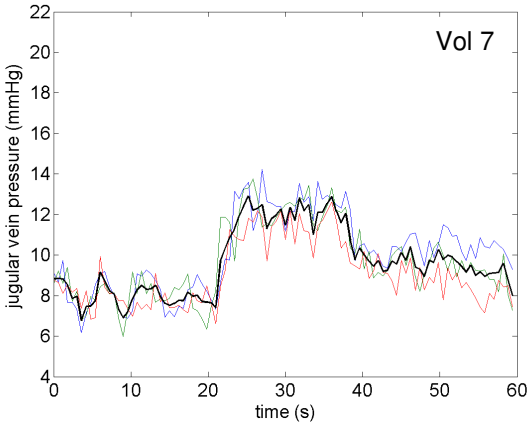
Vol 7
jugular vein pressure (mmHg)
time (s)

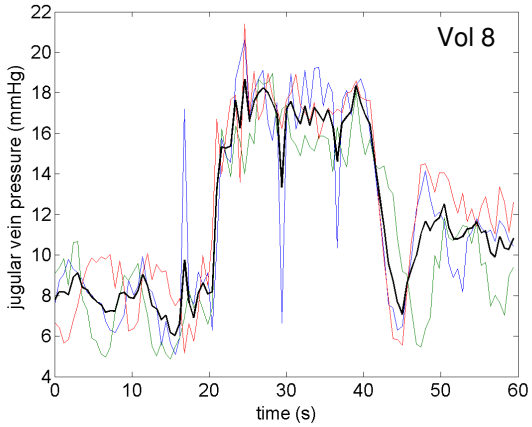
Vol 8
jugular vein pressure (mmHg)
time (s)

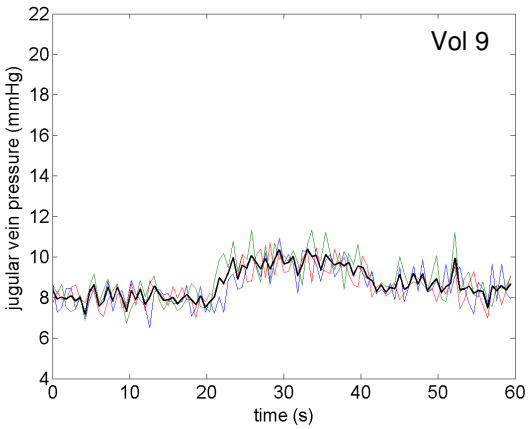
Vol 9
jugular vein pressure (mmHg)
time (s)

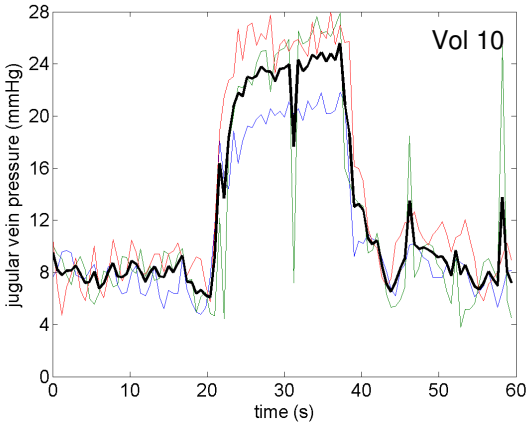

Figure 34: Jugular venous pressure measurements for three repeats of the experiment (blue, green and red lines respectively) and averaged data (black line), in response to the Valsalva manoeuvre in Volunteers 1,2,3,4,6,7,8,9 and 10.

A much clearer and consistent response is seen over the three repeats of the experiment in the case of the Valsalva manoeuvre, and averaging reduces some of the noise in the data. The greatest variation in response in seen in volunteers 1 and 10, and there is a similar magnitude and shaped response in other subjects. Further smoothing of the average data was deemed appropriate and these results are shown in the next section. It is these smoothed datasets that are used as inputs to the Ursino model.

6.2.4 Jugular vein pressure response to the Valsalva manoeuvre – averaged and filtered data

In the following plots (again datasets were averaged over three repeats of the experiment and filtered), the start of the Valsalva manoeuvre takes place at 20 seconds into the acquisition (time point 820) and the subject was instructed to release the manoeuvre after 15 seconds.

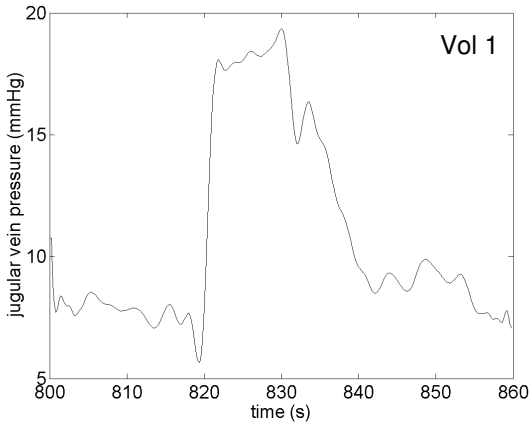
Vol 1
jugular vein pressure (mmHg)
time (s)
20
15
10
5
800
810
820
830
840
850
860

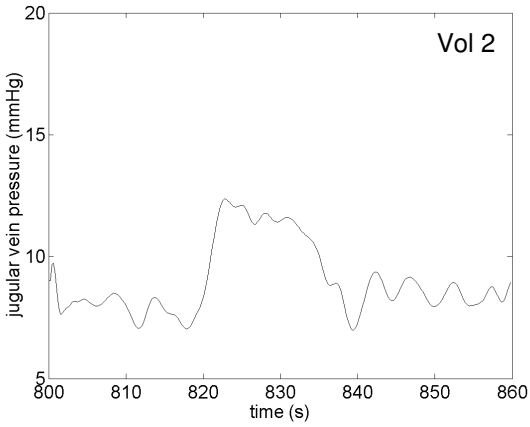
Vol 2
jugular vein pressure (mmHg)
time (s)
20
15
10
5
800
810
820
830
840
850
860

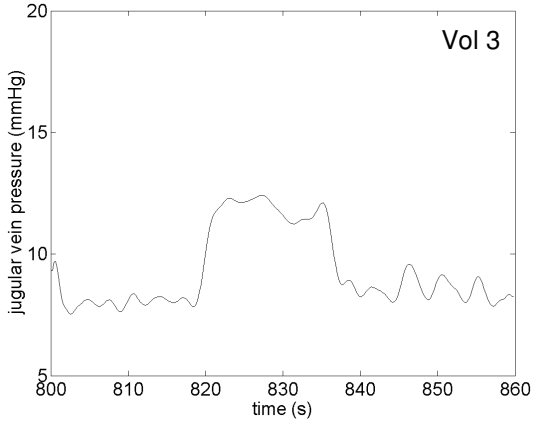
Vol 3
jugular vein pressure (mmHg)
time (s)
20
15
10
5
800
810
820
830
840
850
860

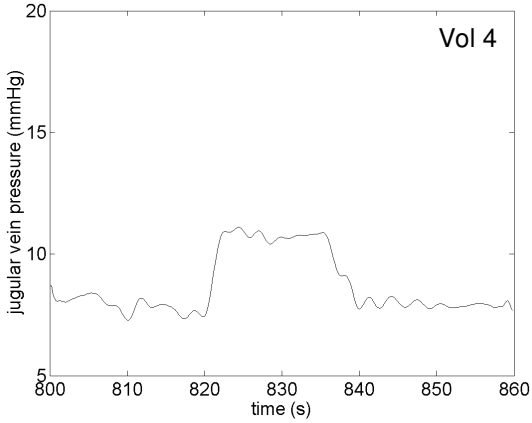
Vol 4
jugular vein pressure (mmHg)
time (s)
20
15
10
5
800
810
820
830
840
850
860

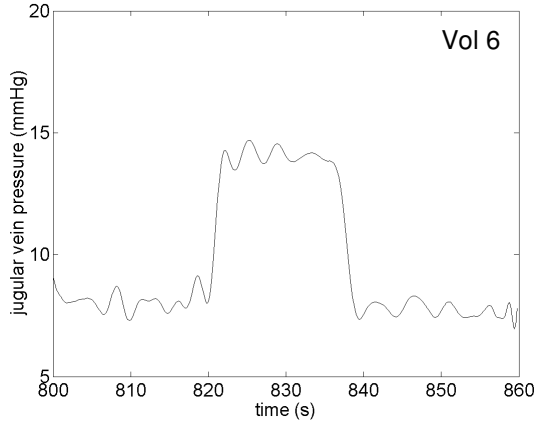
Vol 6
jugular vein pressure (mmHg)
time (s)
20
15
10
5
800
810
820
830
840
850
860

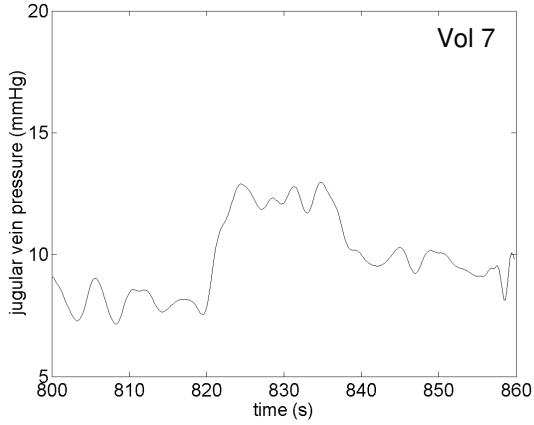
Vol 7
jugular vein pressure (mmHg)
time (s)
20
15
10
5
800
810
820
830
840
850
860

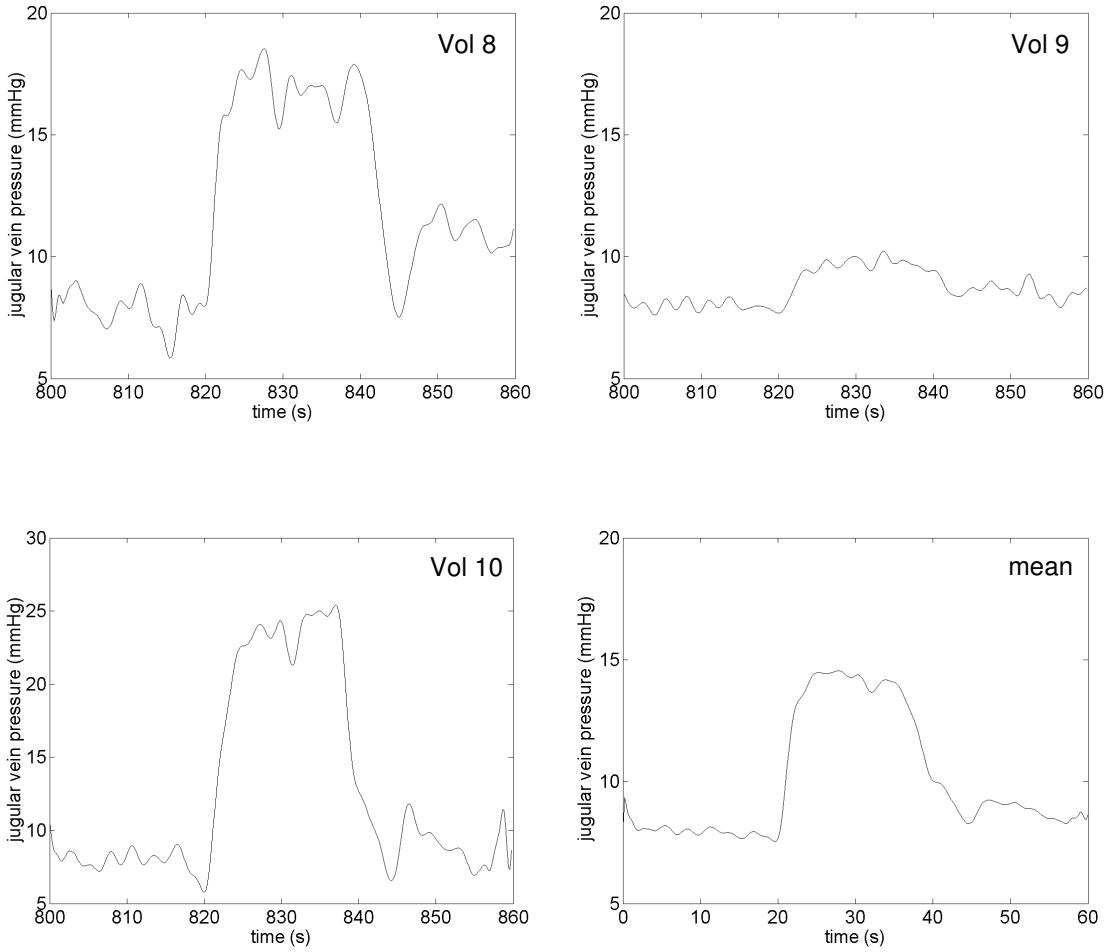

Figure 35: Averaged and filtered jugular vein pressure response to the Valsalva manoeuvre for Volunteers 1,2,3,4,6,7,8,9,10 and a mean dataset.

There is a marked trend in jugular vein pressure (JVP) changes during the Valsalva manoeuvre. This is characterised by a sharp increase (over 3-5 seconds) of JVP at the start of the VM until a plateau is reached. There is a subsequent, usually more gradual, decrease in jugular vein pressure after the release of the VM. In some cases this occurs as soon as the VM is released, in other cases, the plateau is maintained for approximately 5 seconds before JVP starts to decrease. A mean increase of jugular vein pressure of 86.5% ± 60.4% is observed with a return to baseline levels approximately or 9 s after the end of the VM. This type of dynamic measurement of jugular vein

pressure has not been found reported in the literature, so it is difficult to compare these values with published data. Berczi[194] measured the maximum cross-sectional areas of various veins, including the right jugular vein and has assumed full equilibration of venous pressure during the Valsalva manoeuvre. He assumed that the intrathoracic pressure applied during the manoeuvre results in the same pressure change in the venous system, and this pressure change was used to calculate capacity and distensibility in each vein that was studied. This is the reverse approach to that used in this study, where distensibility is assumed to be constant throughout the VM, and pressure changes are derived from cross-sectional area changes. Intrathoracic pressure was not monitored in these experiments, so no quantitative comparison between this pressure and derived jugular vein pressure measurements can be made in this study. As expected, the increased intrathoracic pressure throughout the manoeuvre maintains high jugular venous pressure. It is interesting to note that the shape of the jugular vein pressure curve is similar to the tympanic membrane displacement (TMD) response to the Valsalva manoeuvre; this is discussed further in the next section.

6.3 Intracranial pressure measurements

The following plots show the tympanic membrane displacement (TMD) data relating to the epoch within which the blood pressure challenge was performed. Each epoch lasts 30 seconds and the data has been re-aligned. The blood pressure challenge starts 5 seconds into the epoch, which corresponds to the 20 second time point in these plots. The data has been filtered and de-trended (this is explained in more detail in the methods chapter), and averaged over three repeats of each blood pressure challenge (data from these three repeats are also shown). To present the data, the first 15 seconds of these time courses were zero padded; there was then 5 seconds of TMD recording before the thigh cuffs were deflated at time point 20. The TMD recording continued for a further 25 seconds, and after this point (time point 45), the data was again zero padded.

6.3.1 TMD response to thigh cuff deflation

In the following plots, the three repeats of the experiment are shown as the blue, green and red lines, with the average of these datasets shown in black. The point of thigh cuff deflation takes place at the 20 seconds time point. In the actual experiment, the thigh cuffs were deflated approximately 5 seconds into the TMD epoch of 30 seconds.

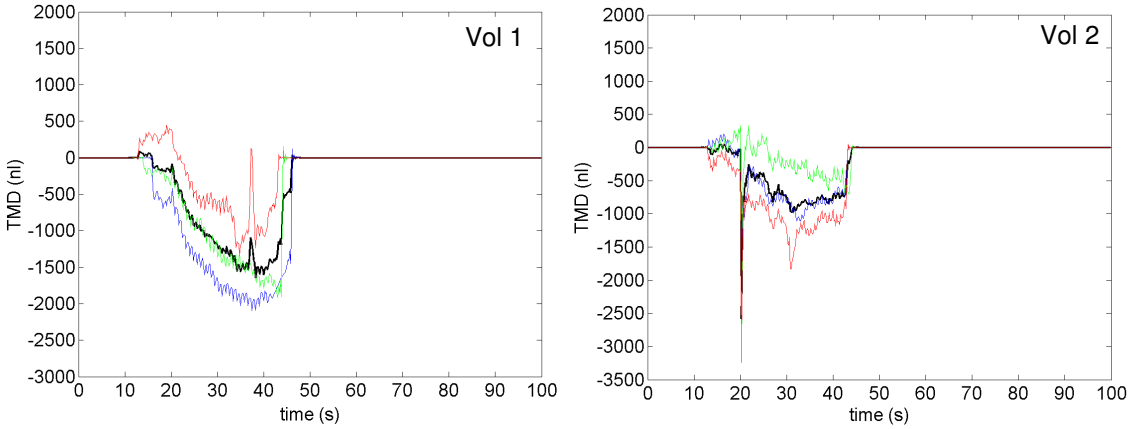

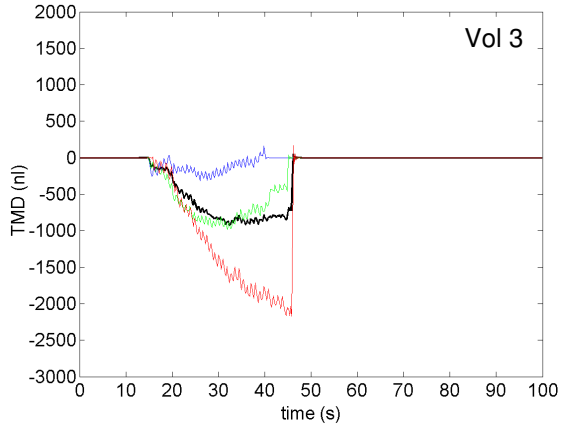
Vol 3
TMD (nl)
time (s)

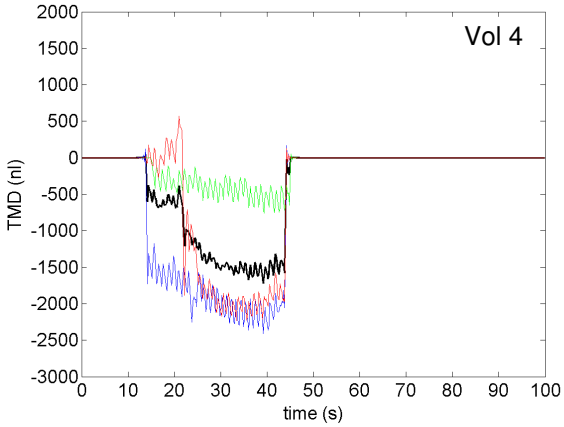
Vol 4
TMD (nl)
time (s)

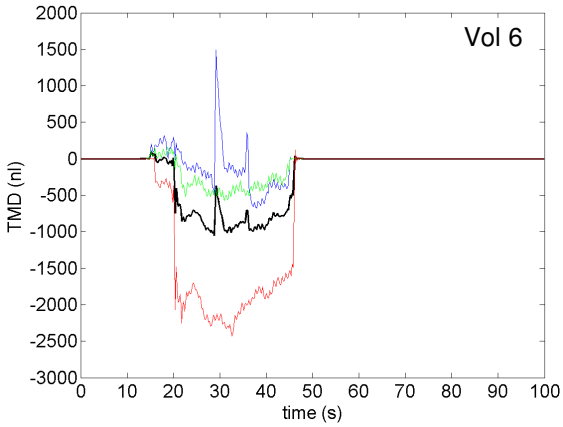
Vol 6
TMD (nl)
time (s)

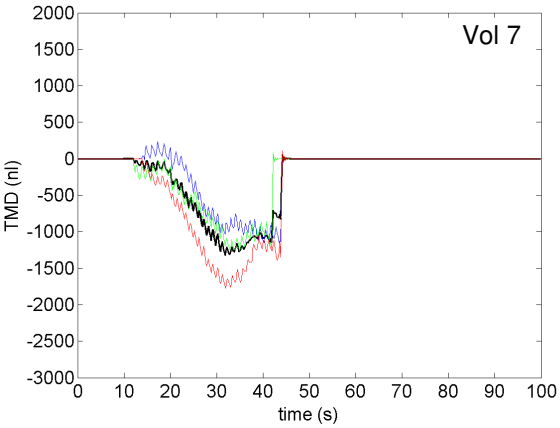
Vol 7
TMD (nl)
time (s)

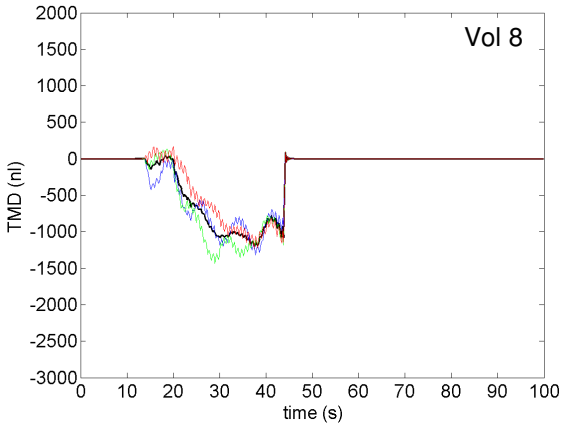
Vol 8
TMD (nl)
time (s)

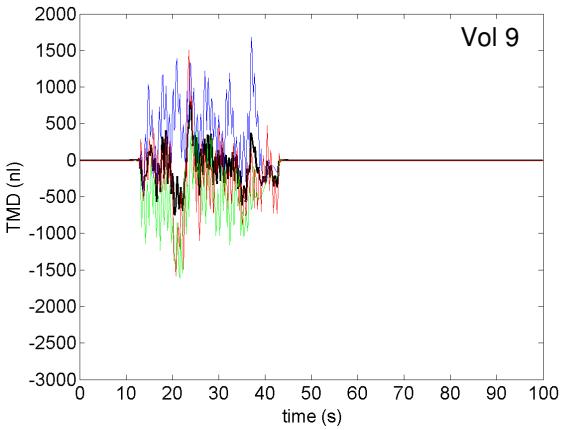
Vol 9
TMD (nl)
time (s)

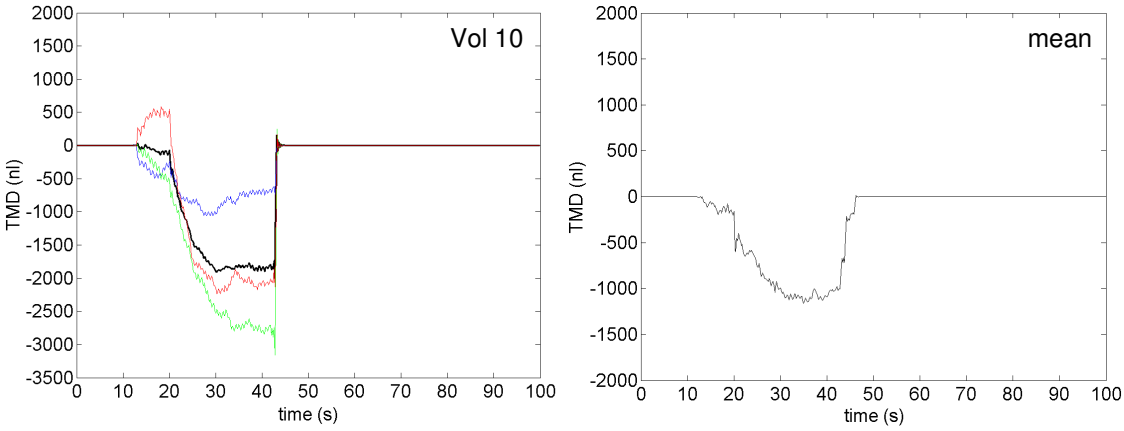

Figure 36: TMD response to thigh cuff deflation for Volunteers 1,2,3,4,6,7,8,9,10 and a mean dataset.

The degree of variation within the three repeats of the experiment varies for each subject, with volunteers 7 and 8 showing the most similar time series, and volunteers 3, 6, 9 and 10 showing a greater difference in each of their three TMD measurements. In examining the averaged data however, a decrease in tympanic membrane displacement is seen at the point of thigh cuff deflation, relating to a decrease in intracranial pressure. There seems to be a sharp decrease until time point 30, when the TMD reaches a plateau until the end of the measurements (time point 45), i.e. a two-stage response. This is particularly marked in volunteers 3, 4 and 10. Artefacts can be seen in volunteers 1, 2, 6, and 9 and these are manifested as large spikes in the data, usually due to movement of the subject's head. The technique is particularly sensitive to these types of artefact. This is once again a new area of investigation, and as such, there is scarcity of literature relating to the effect that thigh cuff deflation has on tympanic membrane displacement, and the assumed changes in intracranial pressure (ICP). In common with arterial blood pressure and jugular vein pressure measurements, a decrease in tympanic membrane displacement is observed. Unfortunately, due to limitations of the technique, data is only available for a 30 second time period, 5 seconds before thigh cuff deflation and 25 seconds after this. Data from the

next epoch could not be reliably appended to this data, as it was difficult to align the data and match the detrending. No quantitative measures are derived from this data; rather general trends are described. The relationship of this measurement to ICP is discussed in Chapter 8.

6.3.2 TMD response to the Valsalva manoeuvre

As in the previous section, the following plots show the three repeats of the experiment as the blue, green and red lines, with the average of these datasets shown in black. The Valsalva manoeuvre starts at a time point of 20 seconds and is released 15 seconds later. In the actual experiment, the subjects were instructed to start the manoeuvre approximately 5 seconds into the TMD epoch and asked to release it 15 seconds later.

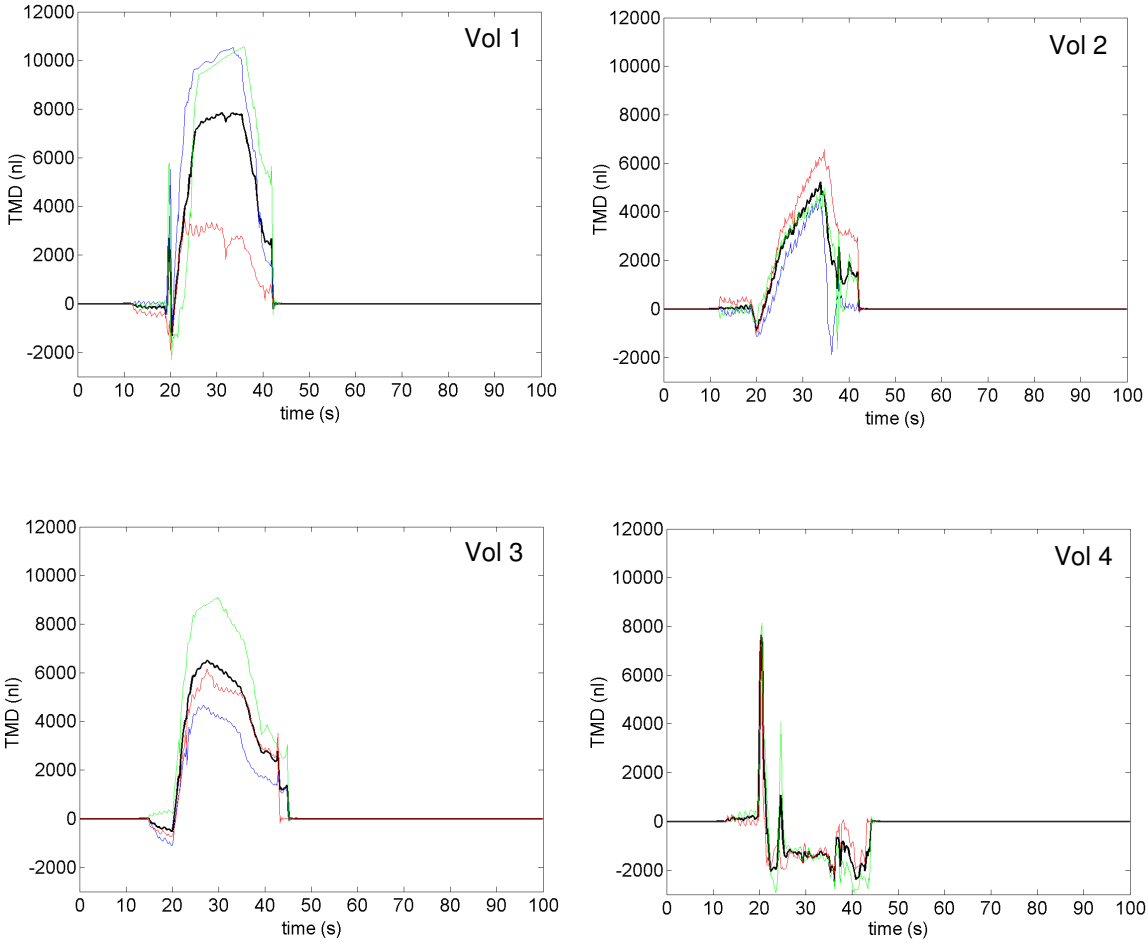

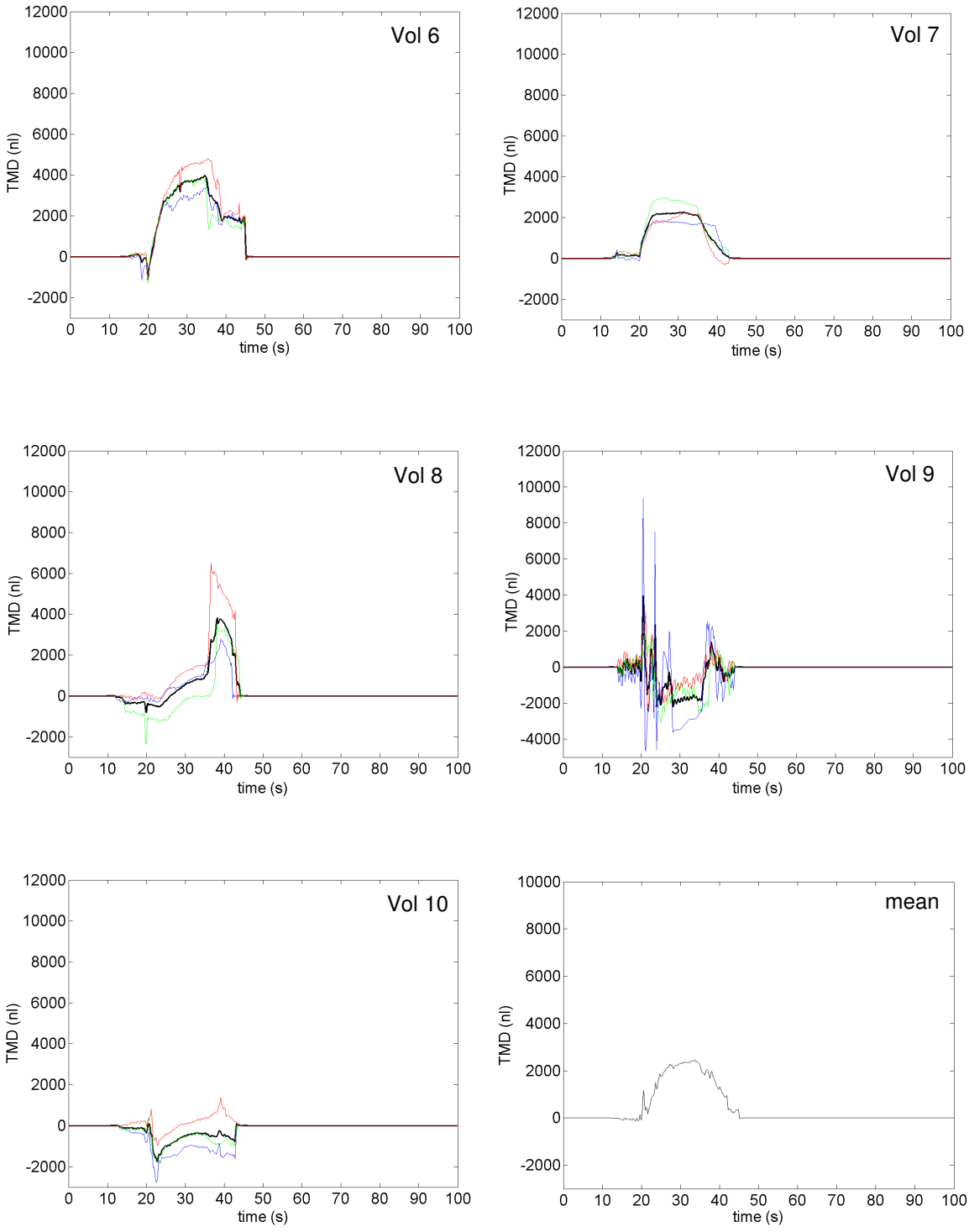

Figure 37: TMD response to the Valsalva manoeuvre for Volunteers 1,2,3,4,6,7,8,9,10 and a mean dataset.

There is surprising similarity in the shape of the TMD responses within each of the three readings from each subject, even in those where an unusual response is seen (volunteers 4, 8, 9 and 10). There is some variation between subjects; however a general trend can be observed which is somewhat similar to the trend seen in the jugular vein pressure data. A rapid increase in TMD is seen at the start of the Valsalva manoeuvre, this then reaches a plateau and decreases once the VM ends. TMD starts to decrease as soon as the VM is stopped. In most cases there is an increase in TMD reflecting an increase in intracranial pressure; however in three volunteers (4, 9 and 10) a decrease in amplitude is seen. It is thought that TMD changes reflect changes in intracranial pressure. However, the decrease in amplitude is not likely to be related to a decrease in ICP; it is more probably due to a shift in baseline following a movement artefact. It is also possible that in some individuals, raised ICP produces an outward deflection of the tympanic membrane, whereas in most subjects, an inward displacement is observed. Once again, movement artefacts are seen in some of the subjects (volunteers 4 and 9).

6.4 BOLD MRI data

The raw data from the BOLD MRI experiments are presented in the next three sections. These data correspond to normalised signal intensity values from each of the three repeats of the experiment, for three different regions of interest, the white matter, grey matter at the back of the brain and grey matter in the cortex, in one slice of the brain. The data is plotted against image number, and the time period between each image is one second. There is some truncation of the datasets at the beginning and end, as a result of the re-alignment of the individual time series to the start of the blood pressure challenge (thigh cuff deflation or Valsalva manoeuvre) at approximately 20 seconds into the acquisition (image number 21). The BOLD responses from each subject, averaged over the three measurements, for each region of interest, are shown after the raw data plots.

6.4.1 BOLD response to thigh cuff deflation – white matter

Results from three repeats of the experiment are shown in blue, green and red (first, second and third runs respectively), with the mean of these datasets overlaid in black. Region of interest data is plotted against image number, with a one second time interval between images.

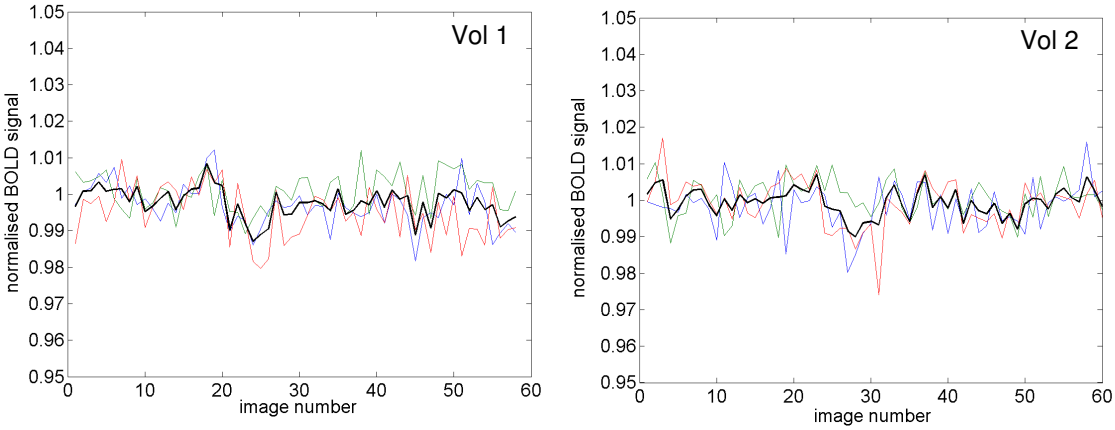

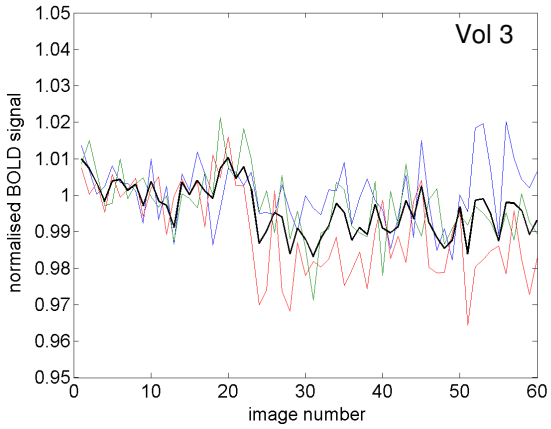
Vol 3
normalised BOLD signal
image number

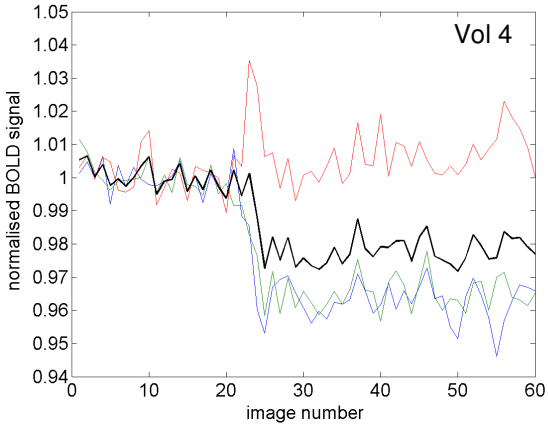
Vol 4
normalised BOLD signal
image number

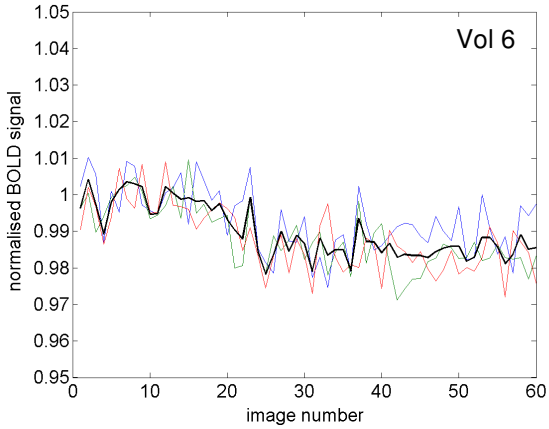
Vol 6
normalised BOLD signal
image number

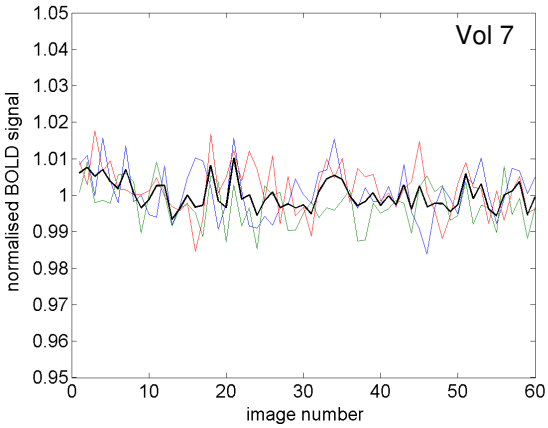
Vol 7
normalised BOLD signal
image number

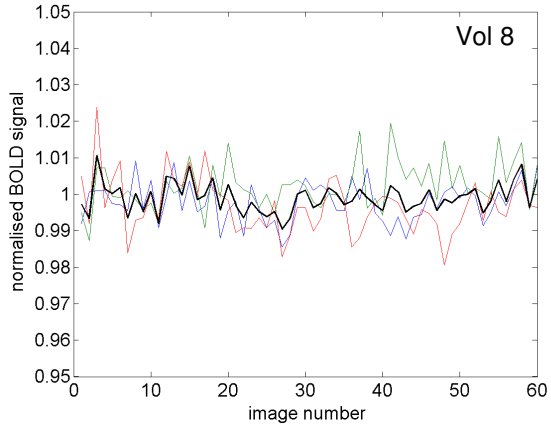
Vol 8
normalised BOLD signal
image number

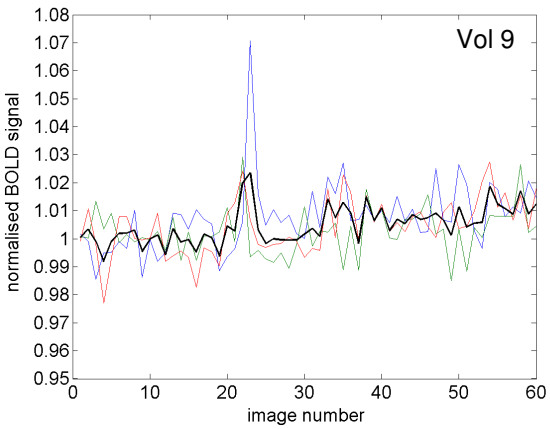
Vol 9
normalised BOLD signal
image number

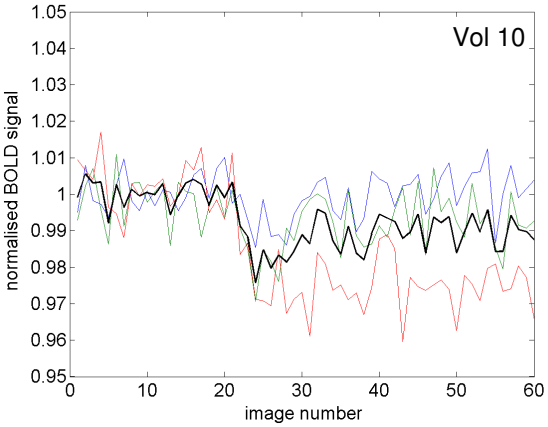

Figure 38: White matter BOLD MRI measurements for three repeats of the experiment (blue, green and red lines respectively) and averaged data (black line), in response to thigh cuff deflation in Volunteers 1,2,3,4,6,7,8,9 and 10.

It can be seen that within each subject, there is some variation in the BOLD time series. This is particularly apparent in volunteers 3 and 4. Averaging of the results enables a clearer response to be seen.

6.4.2 BOLD response to thigh cuff deflation – grey matter back

As above, results from three repeats of the experiment are shown in blue, green and red (first, second and third runs respectively), with the mean of these datasets overlaid in black. Region of interest data is plotted against image number, with a one second time interval between images.

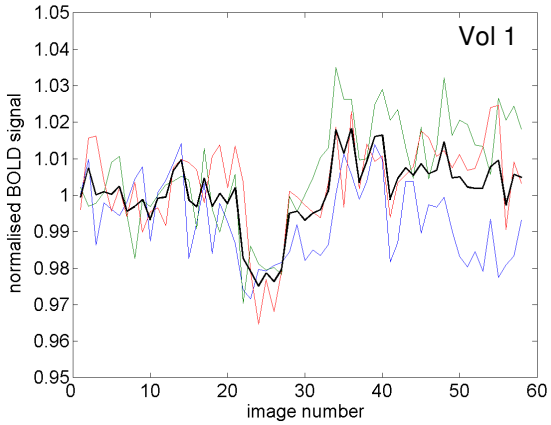
Vol 1
normalised BOLD signal
image number

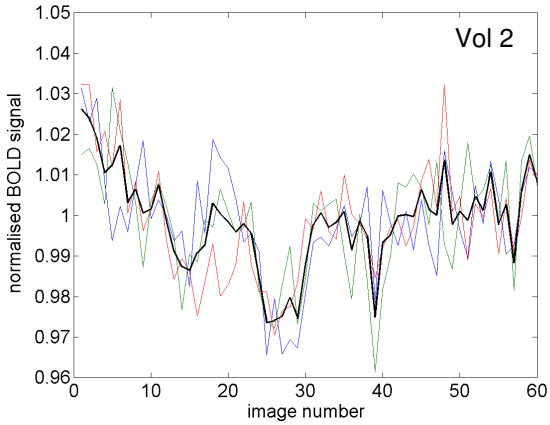
Vol 2
normalised BOLD signal
image number

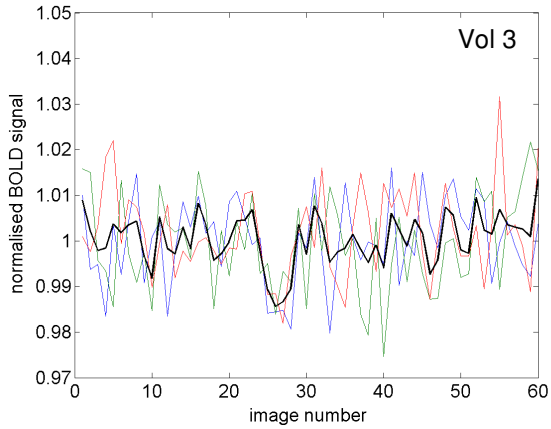
Vol 3
normalised BOLD signal
image number

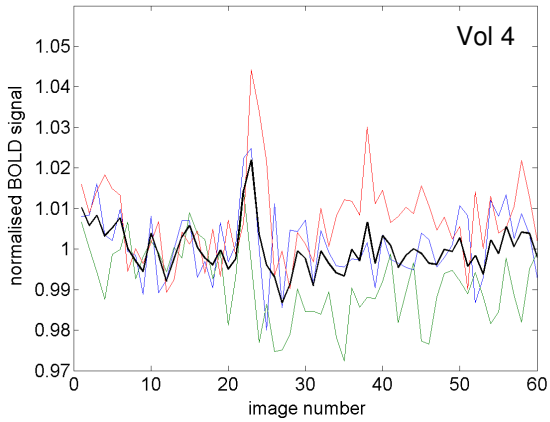
Vol 4
normalised BOLD signal
image number

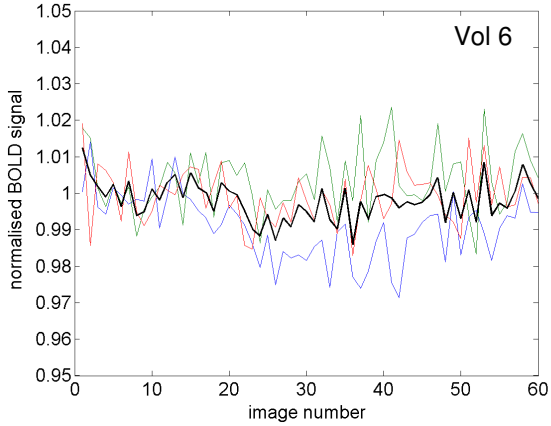
Vol 6
normalised BOLD signal
image number

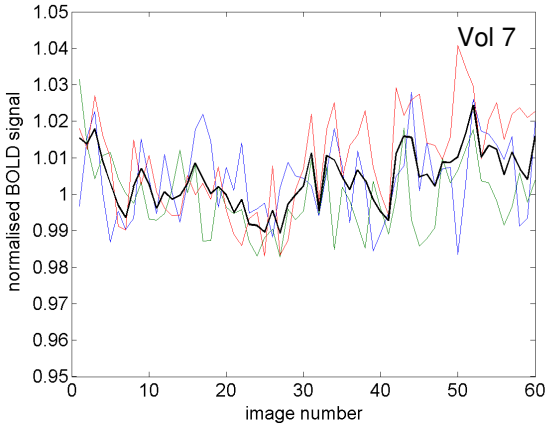
Vol 7
normalised BOLD signal
image number

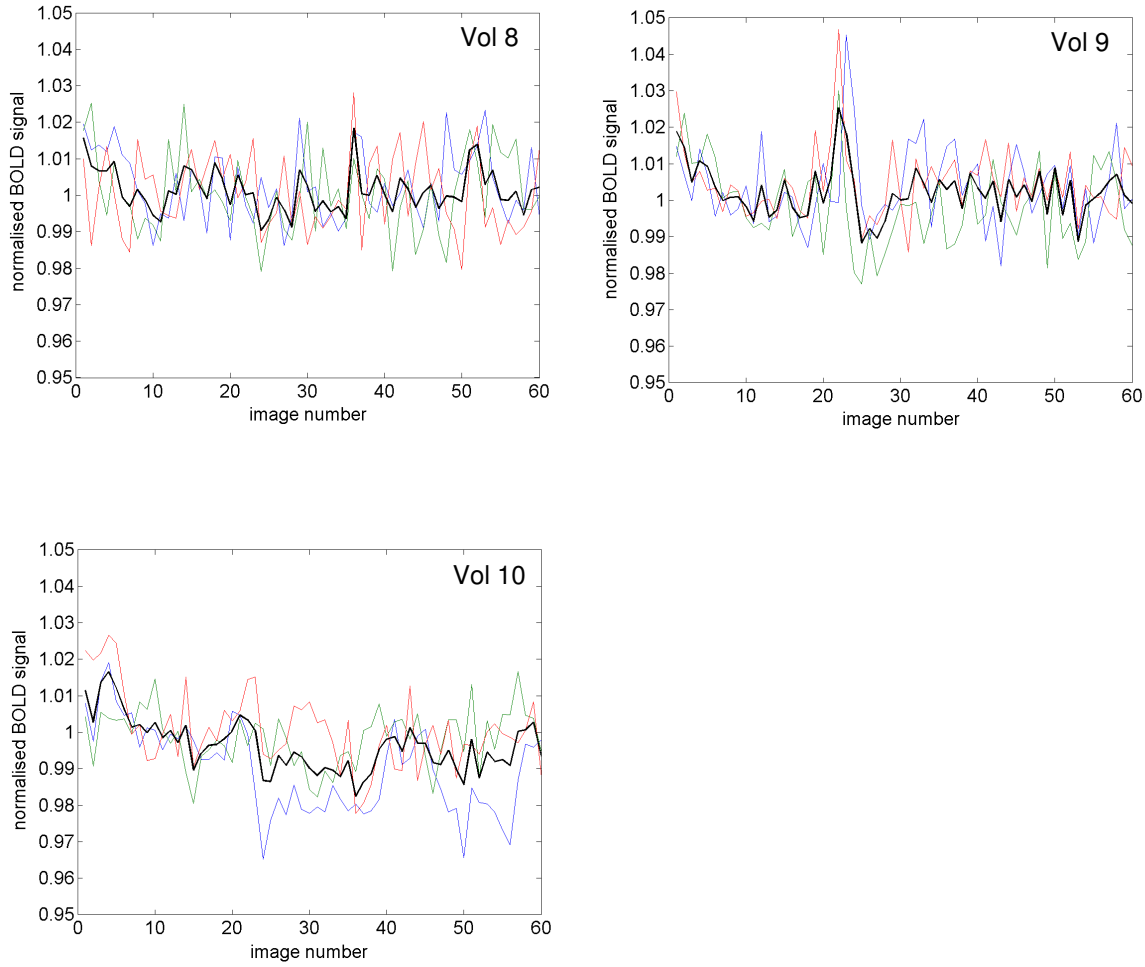

Figure 39: Posterior grey matter BOLD MRI measurements for three repeats of the experiment (blue, green and red lines respectively) and averaged data (black line), in response to thigh cuff deflation in Volunteers 1,2,3,4,6,7,8,9 and 10.

Again, a reasonable amount of intra-subject variation in signal intensity is seen, and this is most obvious in volunteers 4 and 10. A clearer drop in signal intensity is seen in this region of interest, and this is most apparent in the data from volunteers 1, 2 and 3. Spikes in signal intensity are seen in volunteers 4 and 9 at the point of cuff deflation.

6.4.3 BOLD response to thigh cuff deflation – grey matter cortex

Similar plots to those presented in the preceding two sections are shown below, corresponding to the cortical grey matter region of interest.

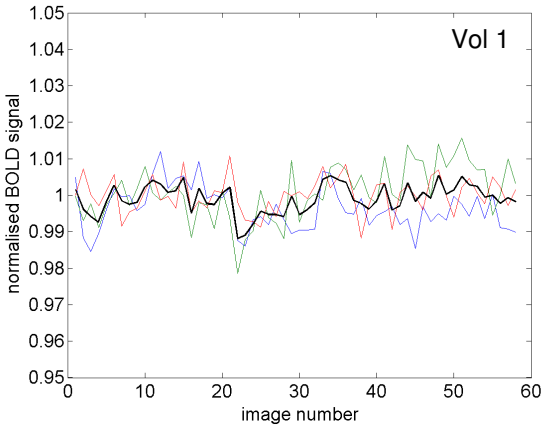

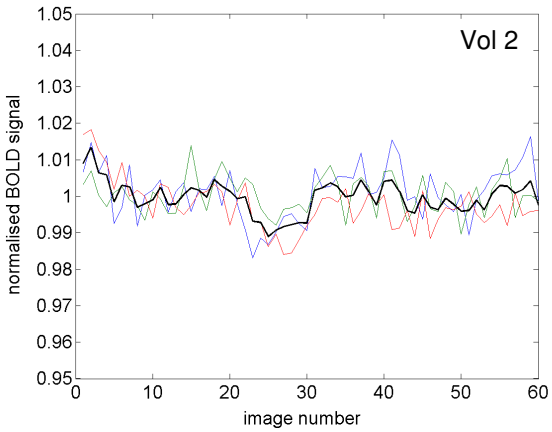

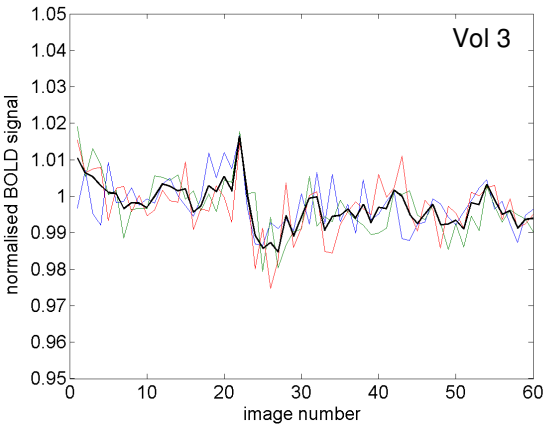

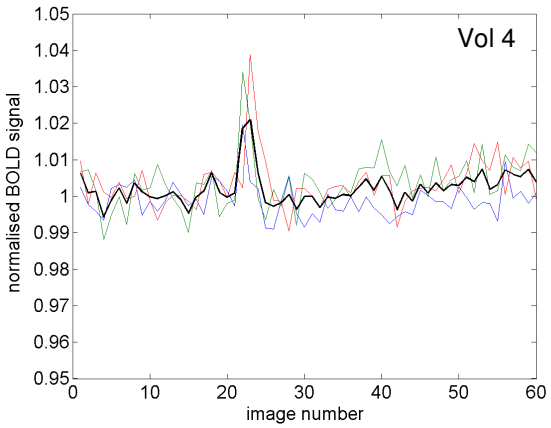

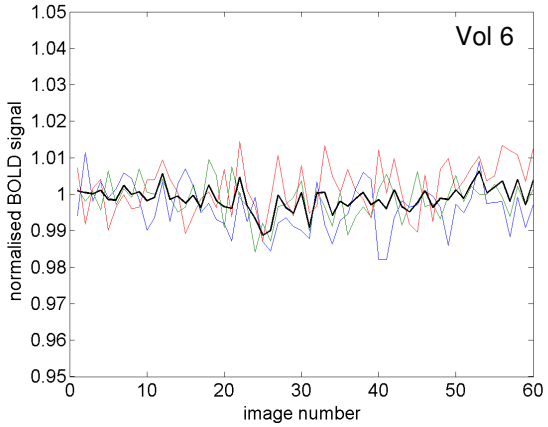

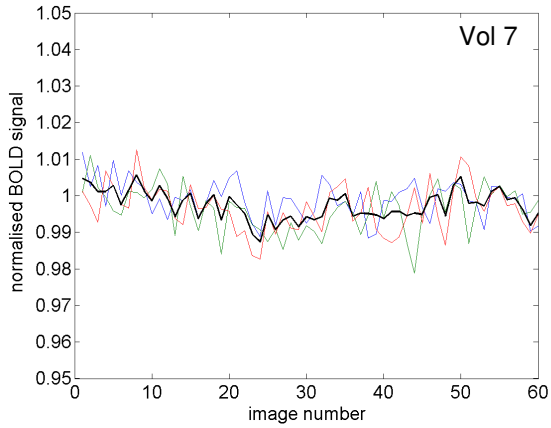

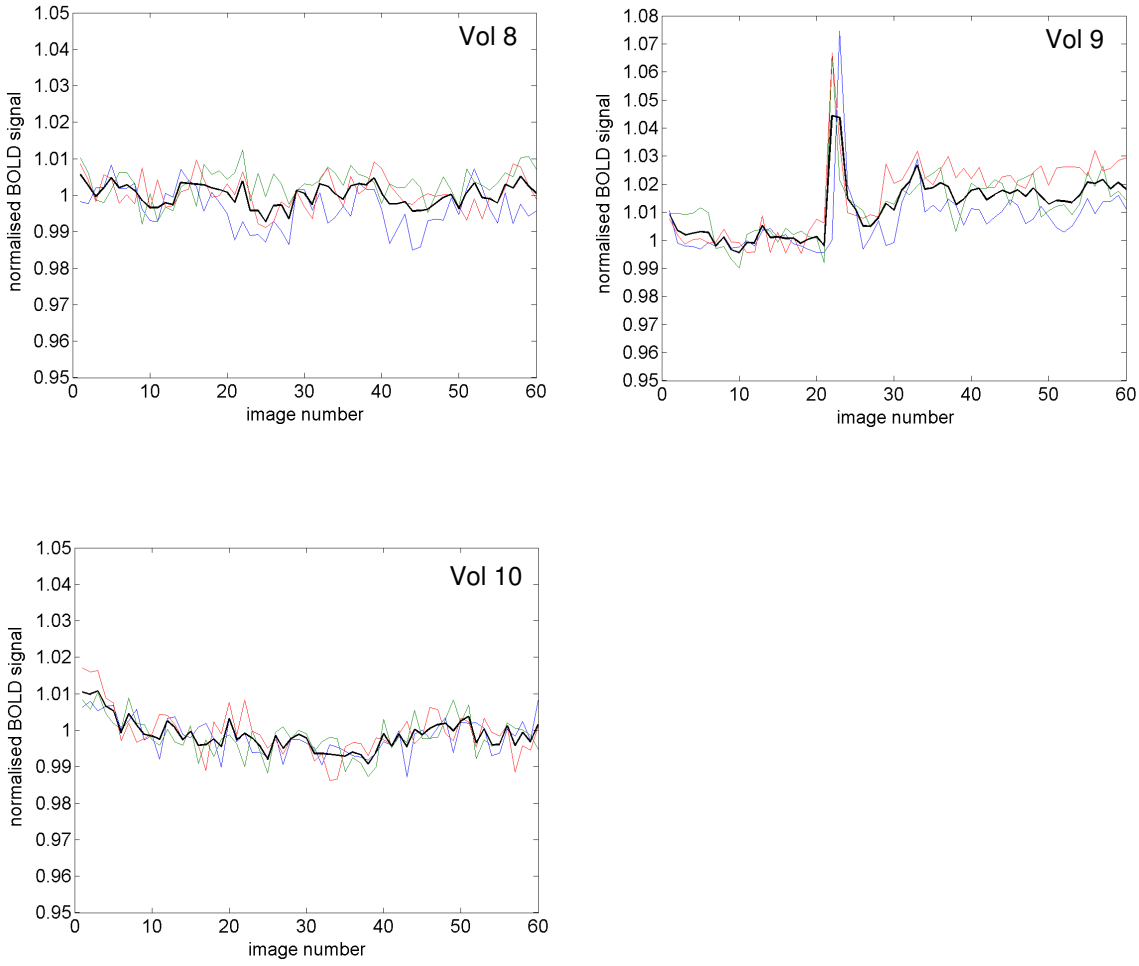

Figure 40: Cortical grey matter BOLD MRI measurements for three repeats of the experiment (blue, green and red lines respectively) and averaged data (black line), in response to thigh cuff deflation in Volunteers 1,2,3,4,6,7,8,9 and 10.

Spikes in the signal intensity data are seen in volunteers 3, 4 and 9 at the point of cuff deflation and these may be due to subject movement in the scanner. A less distinct signal intensity decrease is seen in this region of interest compared to the grey matter back region, but a clear drop (at thigh cuff deflation) is seen in volunteers 1 and 2.

6.4.4 Averaged BOLD response to thigh cuff deflation

The following plots show the BOLD data obtained from three regions of interest within one slice of the brain, the white matter (WM – blue), grey matter at the back of the brain (GM-back – red) and grey matter in the cortex (GM-cortex – green). This data is obtained from a 60 second MRI acquisition, with one image acquired per second. The point of thigh cuff deflation is at 20 seconds, and the datasets have been re-aligned to this point. The plots show the average normalised BOLD signal intensity changes over three repeats of the experiment and data has been re-sampled at a higher frequency (100 Hz), which has smoothed the data and introduced a few small transients in the data. This was carried out to enable a direct comparison to the modelled BOLD data, which was sampled at this frequency.

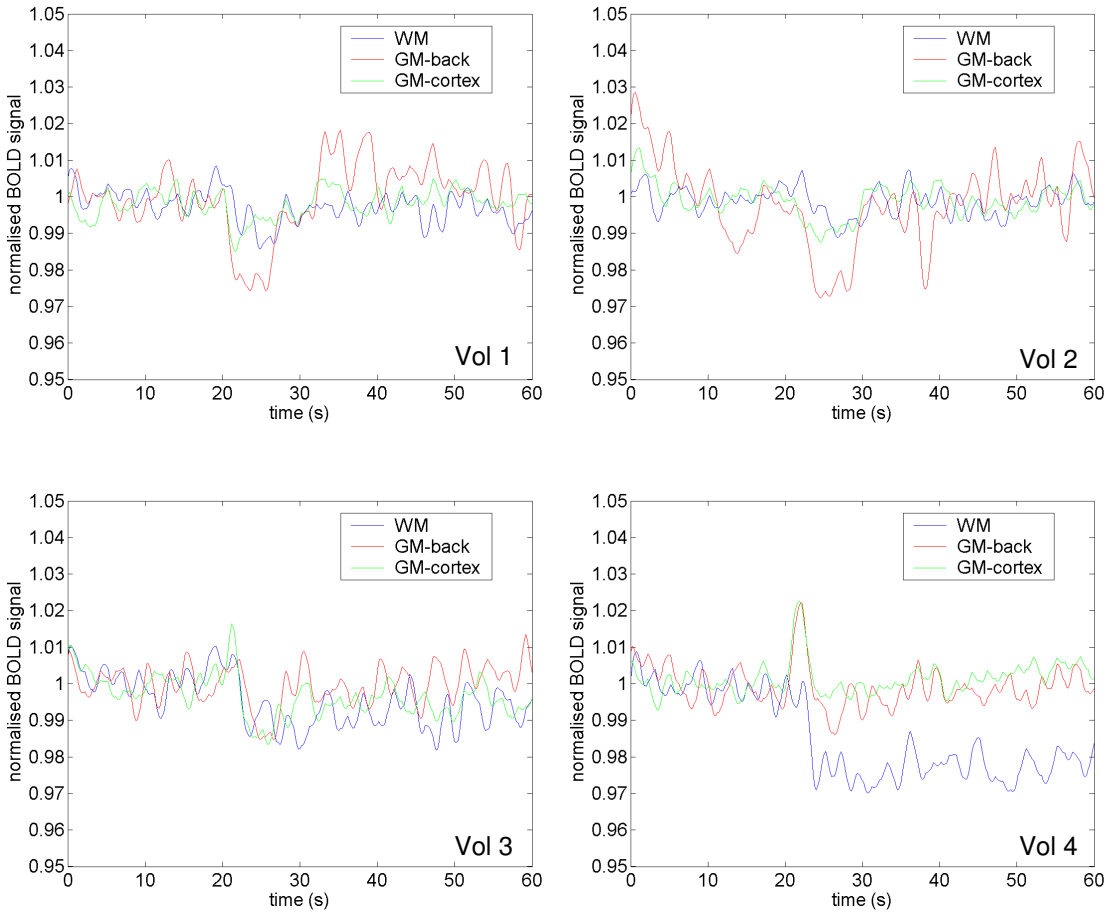

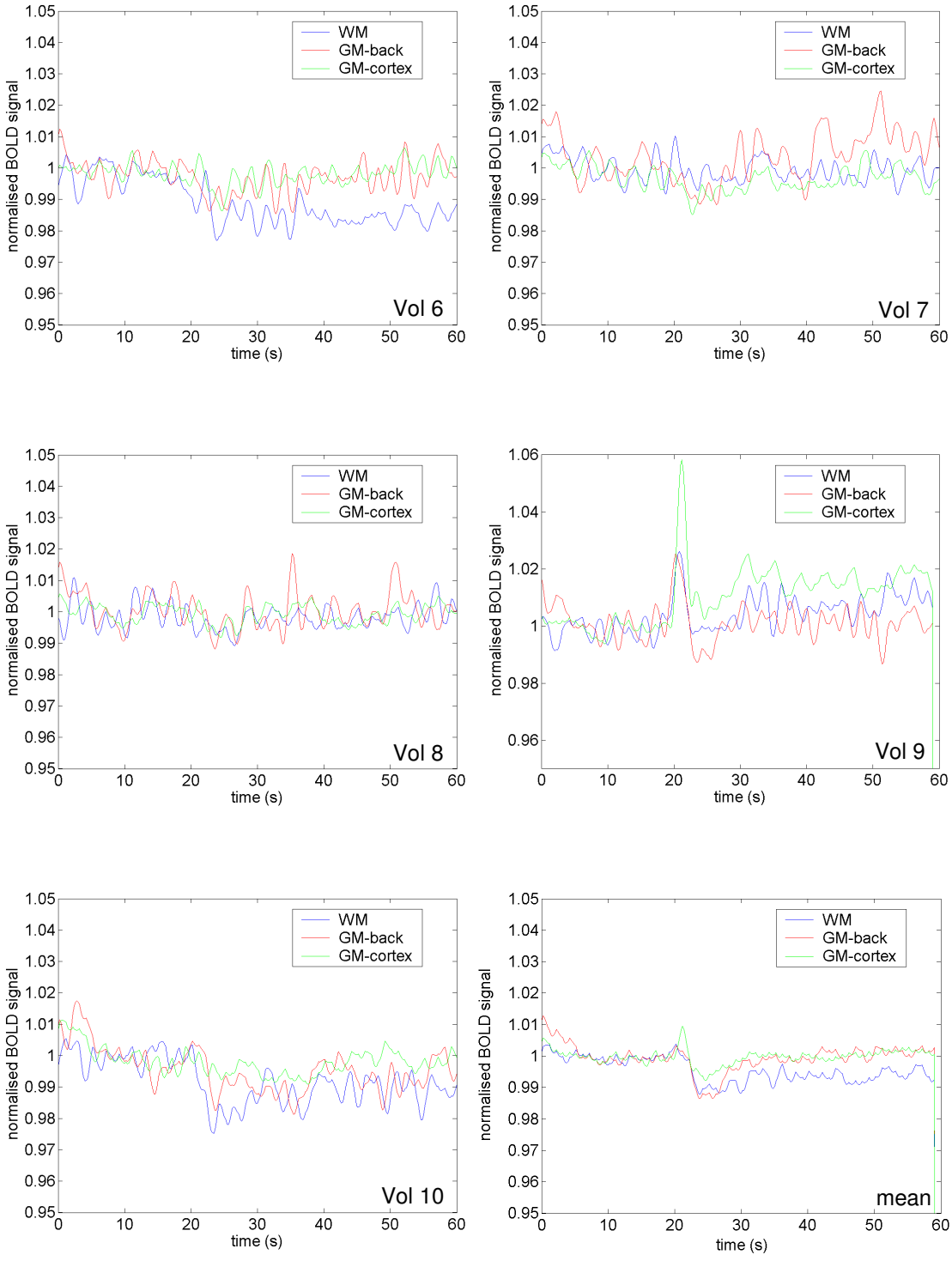

Figure 41: BOLD signal response to thigh cuff deflation for Volunteers 1,2,3,4,6,7,8,9,10 and a mean dataset.

In these datasets BOLD signal intensities from the three different regions of interest can be seen. In general, a decrease in signal intensity is observed after thigh cuff deflation. The data is quite noisy and this change is seen more clearly in some subjects than others. There are some unexpected variations in the data, most probably due to motion artefacts that haven't been corrected for by the motion correction, i.e. a shift of the head out of the plane of the slice at the time of cuff deflation. These are manifested as increases in signal intensity due to spin-history effects. This is markedly seen in volunteers 4 and 9 at the time of cuff deflation. The motion correction data obtained from the scanner provides some evidence for this, although this only provides an idea of in-slice movement. The largest motion correction parameters were seen in these subjects (up to 1 mm in one dimension) compared to all the other volunteers (up to 0.5 mm in one dimension).

Signal from the white matter region of interest does not seem to recover to the same extent as signal from the grey matter in some subjects, particularly in volunteer 4. CBF is much higher in grey matter than white matter, and it could be speculated that autoregulation is faster in grey matter than in white matter, thus leading to a slower recovery of the BOLD signal in white matter. The GM-back data is subjectively the best quality data. It seems to have the least artefact and the clearest signal change. This data has been selected for comparison with the model predictions. Quantitative comparisons will be considered in the modelling results section and the discussion chapter.

Again, in the following three sections, the region of interest BOLD MRI data in response to a Valsalva manoeuvre is shown, corresponding to white matter, grey matter at the back of the brain and grey matter in the cortex, as described at the start of this section.

6.4.5 BOLD response to the Valsalva manoeuvre – white matter

Similar plots to those presented in previous sections are shown below, corresponding to the normalised BOLD signal changes in the white matter region of interest, in response to the Valsalva manoeuvre. The three repeats of the experiment are shown as blue, green and red lines, with the black line representing the mean of these three measurements.

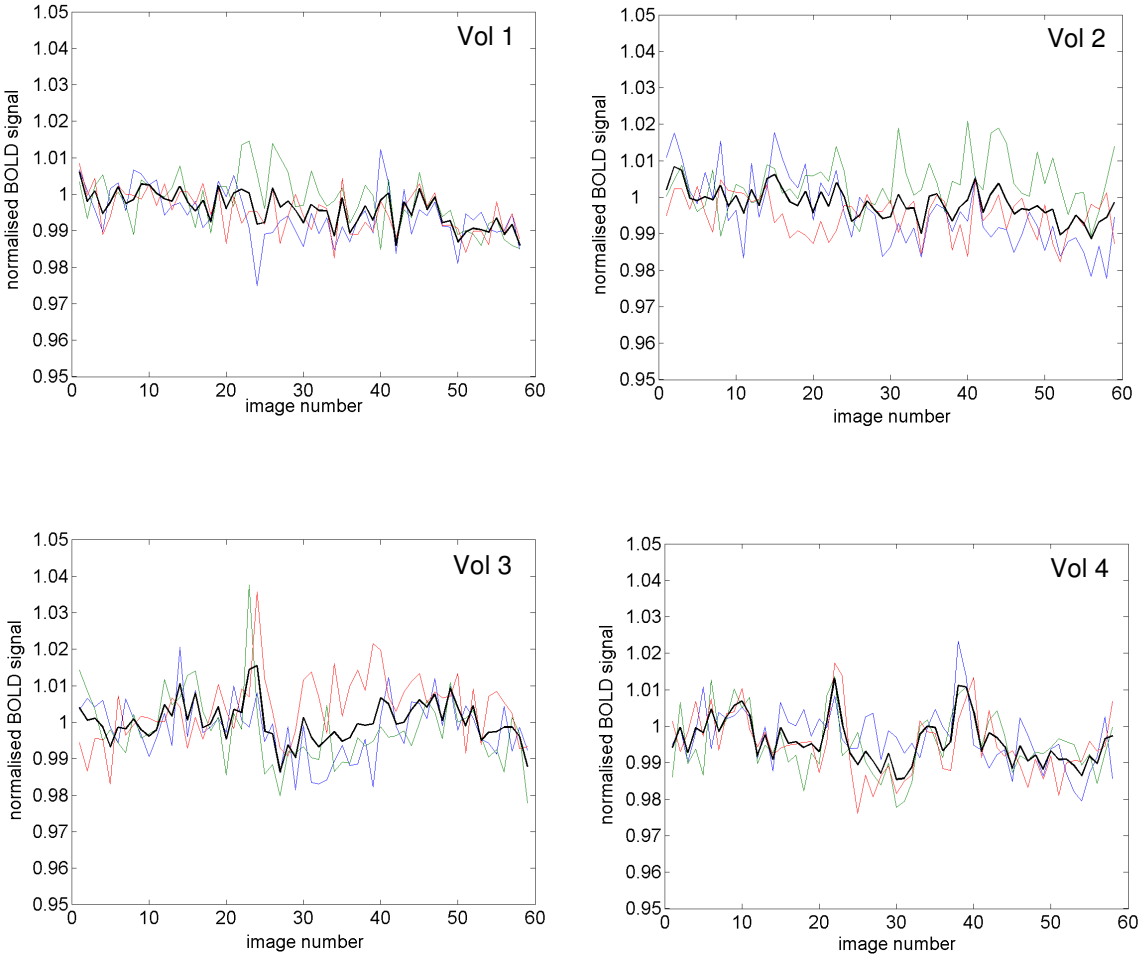

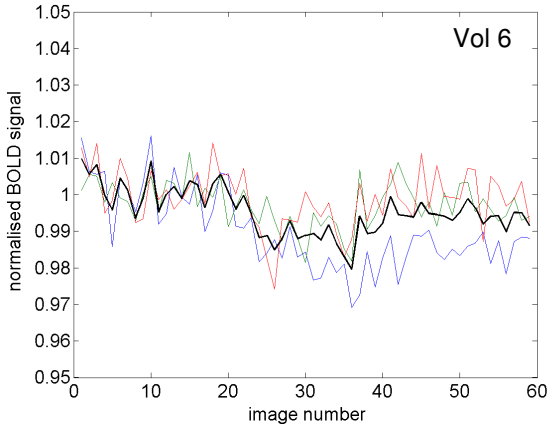
Vol 6
normalised BOLD signal
image number
1.05
1.04
1.03
1.02
1.01
1
0.99
0.98
0.97
0.96
0.95
0
10
20
30
40
50
60

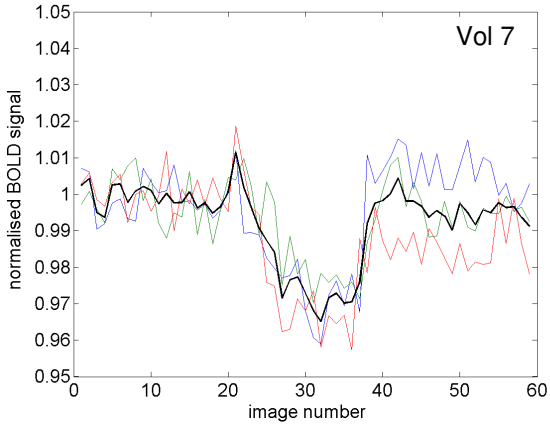
Vol 7
normalised BOLD signal
image number
1.05
1.04
1.03
1.02
1.01
1
0.99
0.98
0.97
0.96
0.95
0
10
20
30
40
50
60

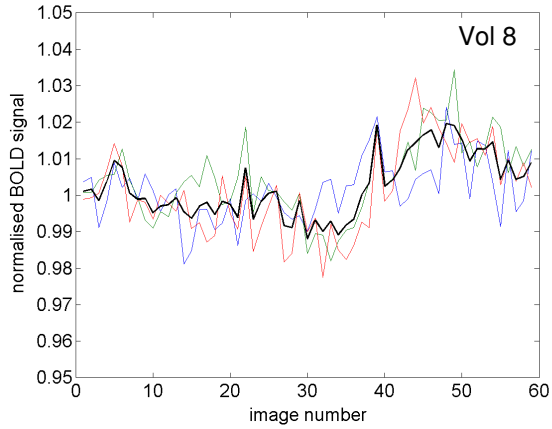
Vol 8
normalised BOLD signal
image number
1.05
1.04
1.03
1.02
1.01
1
0.99
0.98
0.97
0.96
0.95
0
10
20
30
40
50
60

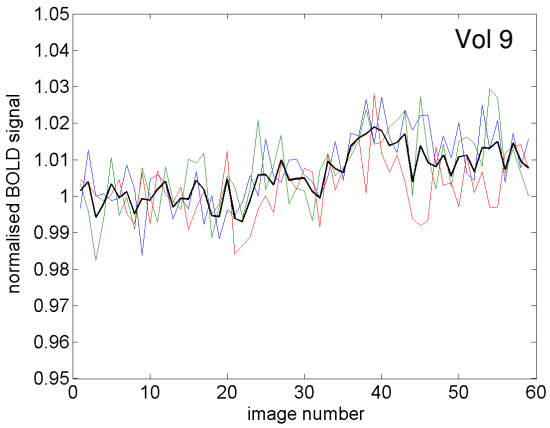
Vol 9
normalised BOLD signal
image number
1.05
1.04
1.03
1.02
1.01
1
0.99
0.98
0.97
0.96
0.95
0
10
20
30
40
50
60

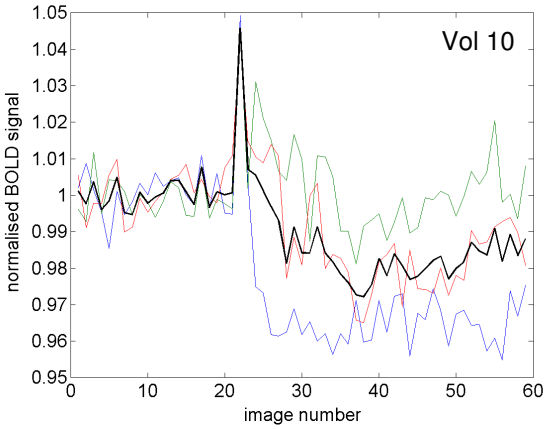

Figure 42: White matter BOLD MRI measurements for three repeats of the experiment (blue, green and red lines respectively) and averaged data (black line), in response to the Valsalva manoeuvre in Volunteers 1,2,3,4,6,7,8,9 and 10.

There is considerable intra-subject variability; nevertheless, some general trends can be seen. Peaks at the start and after the end of the Valsalva manoeuvre can be observed in volunteers 4 and 7. A general decrease during the manoeuvre is particularly apparent in all three repeats from volunteer 7.

6.4.6 BOLD response to the Valsalva manoeuvre – grey matter back

Plots showing the normalised BOLD signal changes, in response to a Valsalva manoeuvre, in a grey matter region of interest at the back of the brain, are presented below. Again, three repeats of the experiment are shown as coloured lines, and the black line is the average of these measurements.

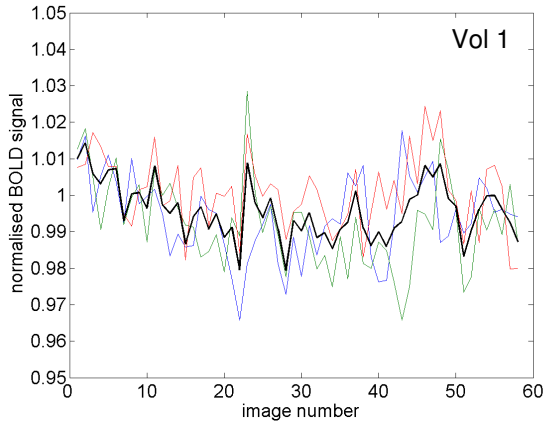
Vol 1
normalised BOLD signal
image number

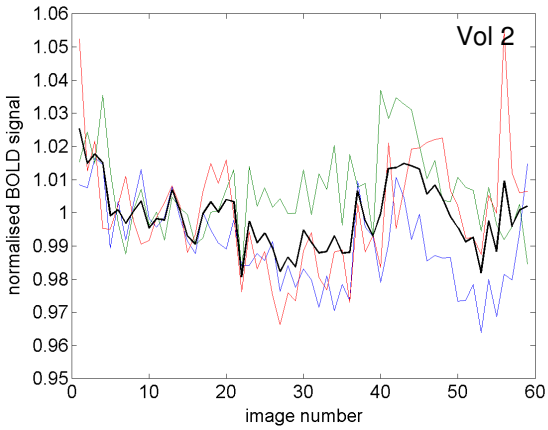
Vol 2
normalised BOLD signal
image number

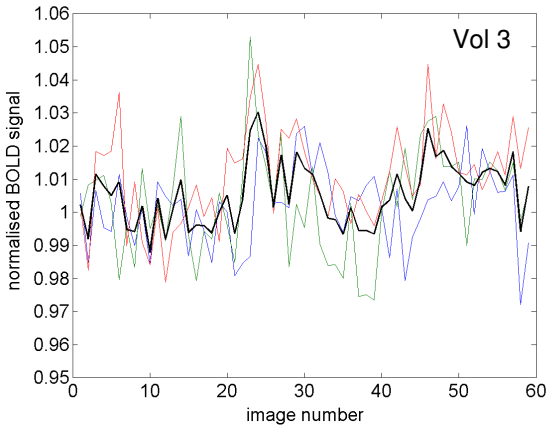
Vol 3
normalised BOLD signal
image number

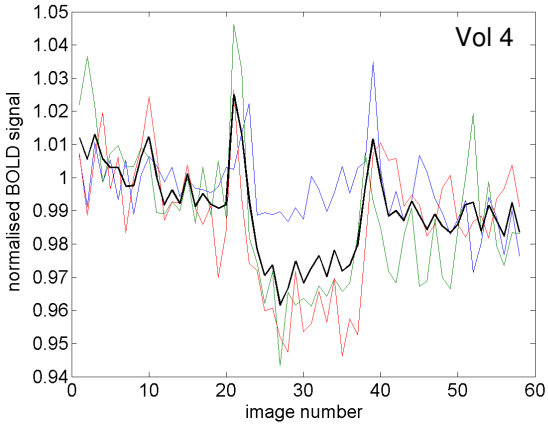
Vol 4
normalised BOLD signal
image number

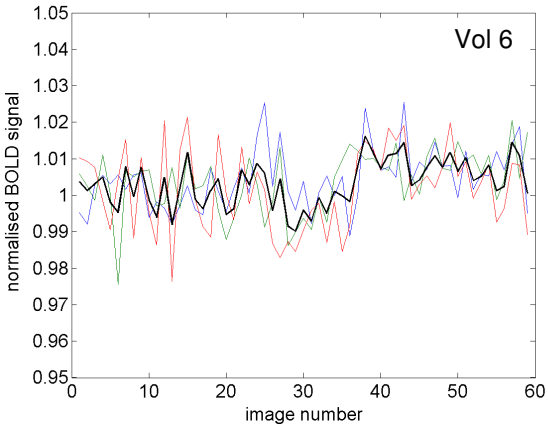
Vol 6
normalised BOLD signal
image number

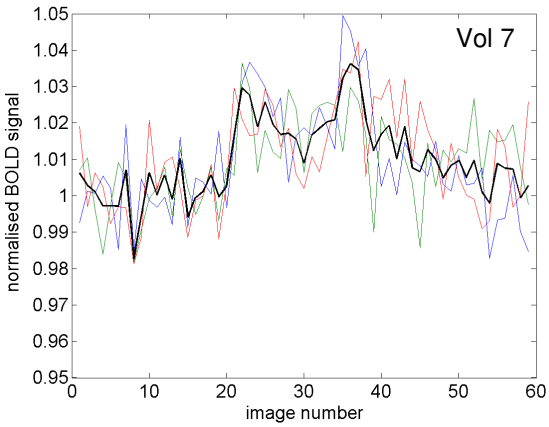
Vol 7
normalised BOLD signal
image number

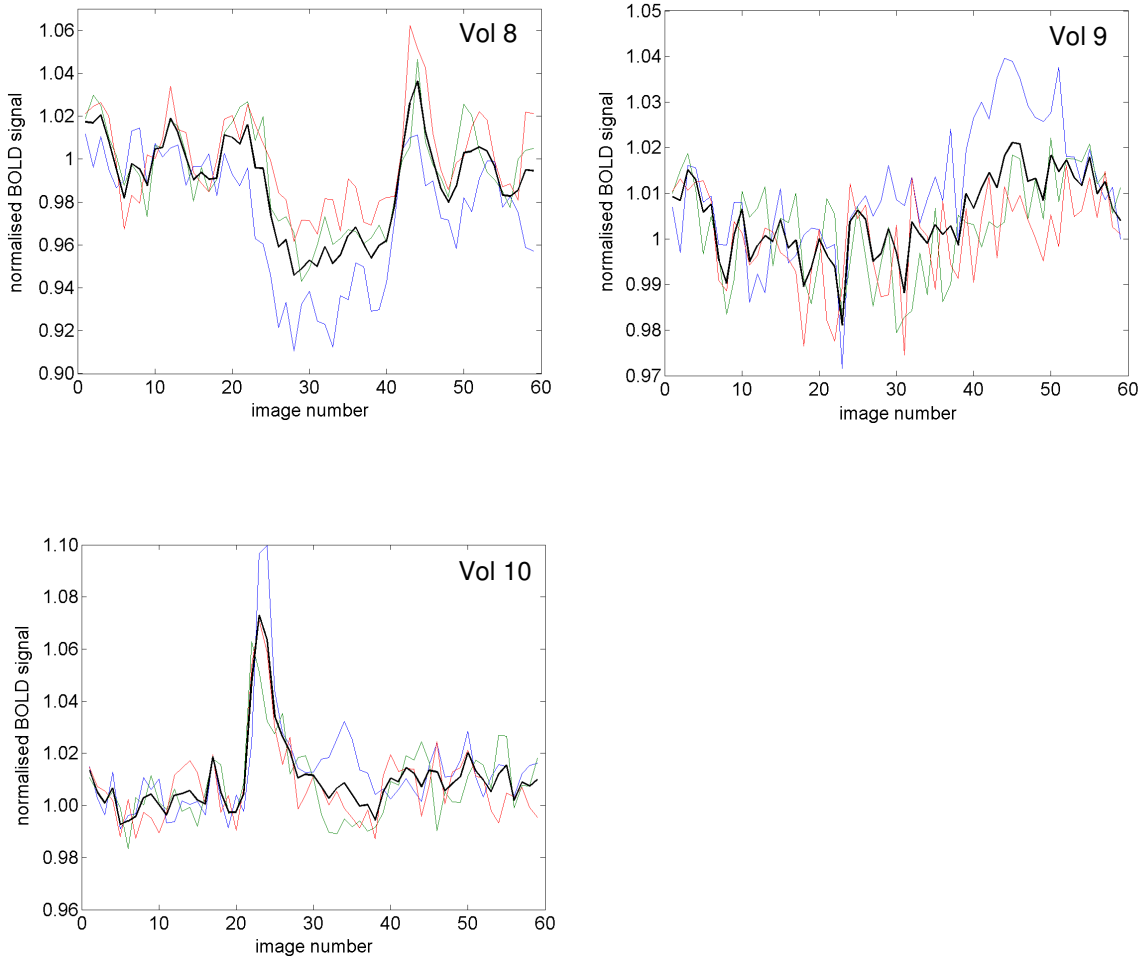

Figure 43: Posterior grey matter BOLD MRI measurements for three repeats of the experiment (blue, green and red lines respectively) and averaged data (black line), in response to the Valsalva manoeuvre in Volunteers 1,2,3,4,6,7,8,9 and 10.

More consistent changes can be seen in data from this region of interest compared to the white matter region. Volunteers 4, 8 and to a certain extent, 7, show the characteristic peaks at the beginning and after the end of the Valsalva manoeuvre, with a decrease in signal during the manoeuvre. Volunteer 10 shows a large signal increase at the start of the manoeuvre, which may be due to a movement artefact.

6.4.7 BOLD response to the Valsalva manoeuvre – grey matter cortex

The normalised BOLD signal changes in a cortical grey matter region of interest, in response to a Valsalva manoeuvre, are shown below. The three repeats of the experiment are shown as blue, green and red lines, and the average of these measurements is the black line.

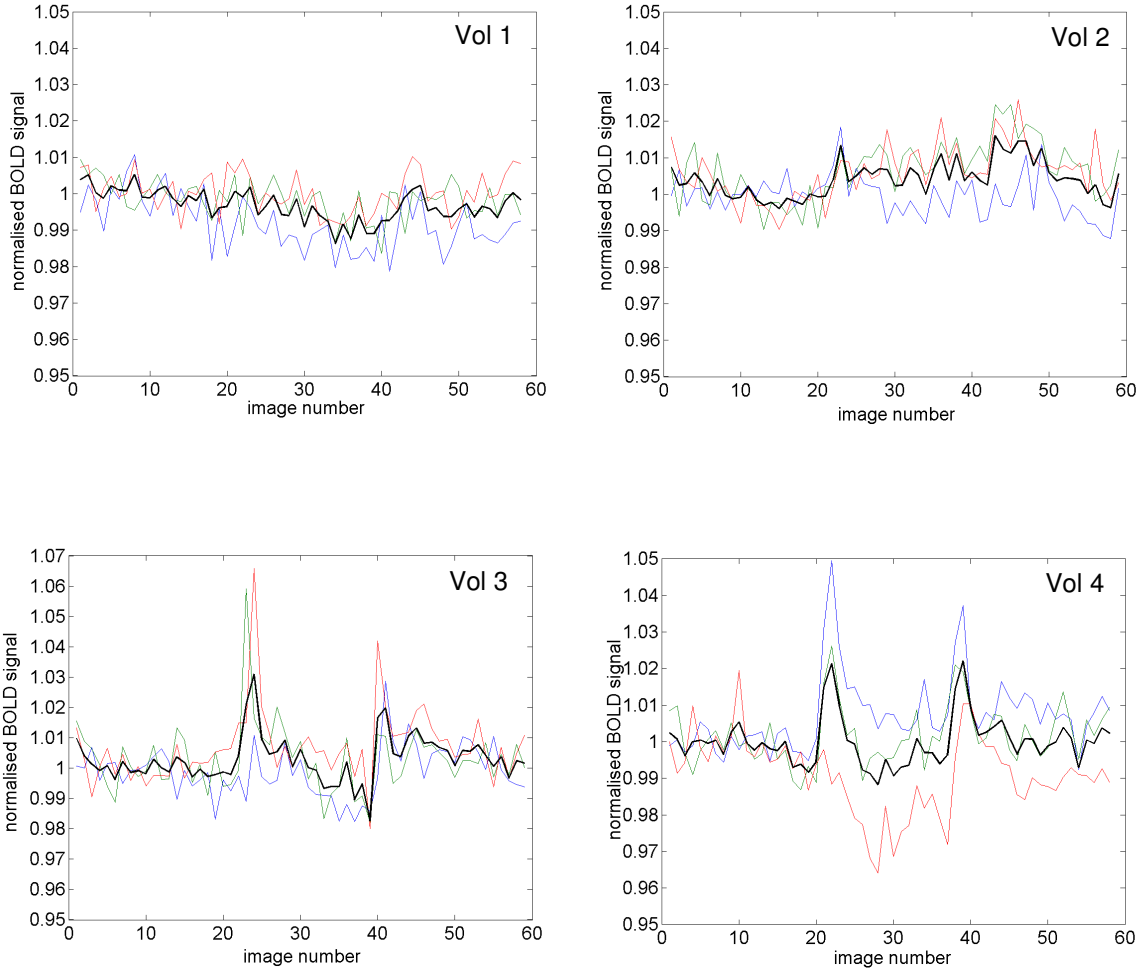

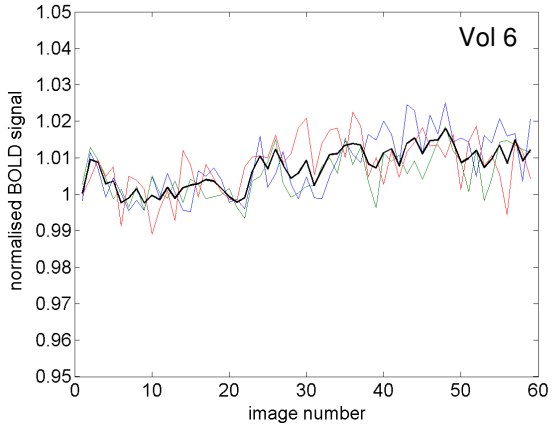
Vol 6
normalised BOLD signal
image number
1.05
1.04
1.03
1.02
1.01
1
0.99
0.98
0.97
0.96
0.95
0
10
20
30
40
50
60

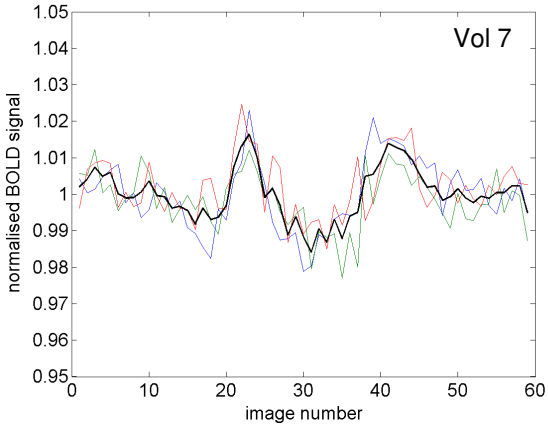
Vol 7
normalised BOLD signal
image number
1.05
1.04
1.03
1.02
1.01
1
0.99
0.98
0.97
0.96
0.95
0
10
20
30
40
50
60

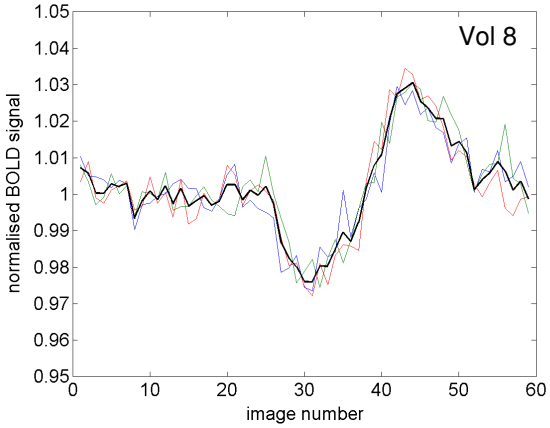
Vol 8
normalised BOLD signal
image number
1.05
1.04
1.03
1.02
1.01
1
0.99
0.98
0.97
0.96
0.95
0
10
20
30
40
50
60

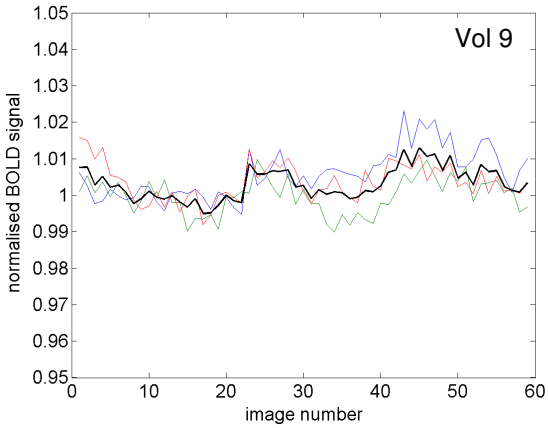
Vol 9
normalised BOLD signal
image number
1.05
1.04
1.03
1.02
1.01
1
0.99
0.98
0.97
0.96
0.95
0
10
20
30
40
50
60

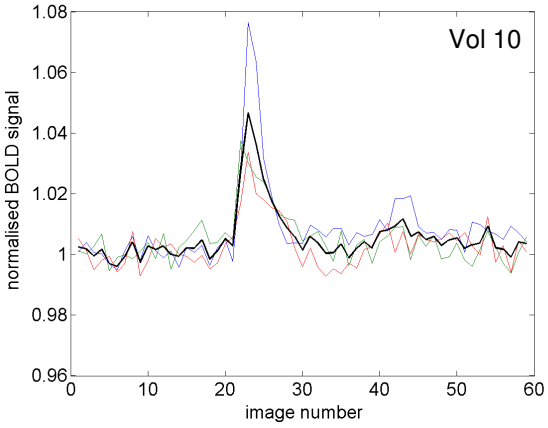

Figure 44: Cortical grey matter BOLD MRI measurements for three repeats of the experiment (blue, green and red lines respectively) and averaged data (black line), in response to the Valsalva manoeuvre in Volunteers 1,2,3,4,6,7,8,9 and 10.

This data shows perhaps the most consistent intra-subject signal intensity changes, compared to the other two regions, particularly in volunteers 7 and 8. Once again, a large peak is seen at the start of the manoeuvre in volunteer 10.

6.4.8 Averaged BOLD response to the Valsalva manoeuvre

Similar averaged plots as described for thigh cuff deflation (Section 6.4.4) are presented below. In the following plots, the Valsalva manoeuvre commences at 20 seconds and is released 15 seconds later.

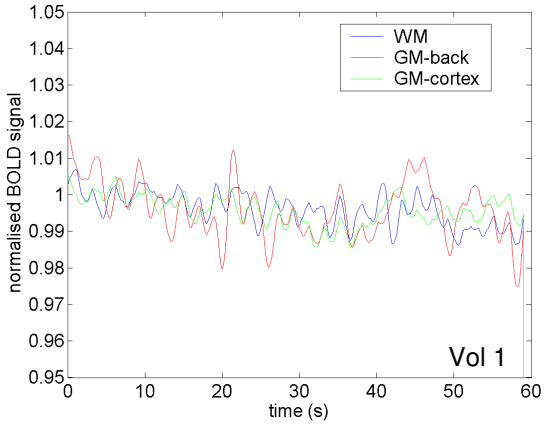
WM
GM-back
GM-cortex
Vol 1
normalised BOLD signal
time (s)

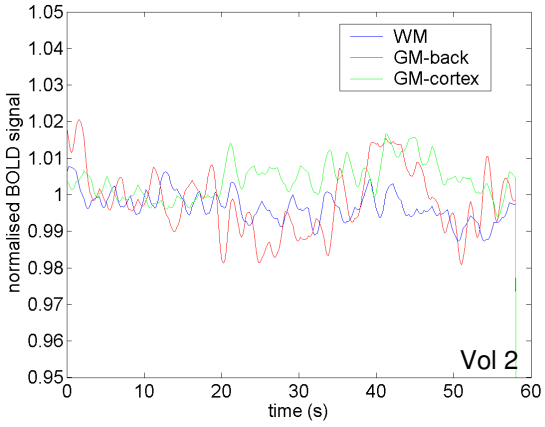
WM
GM-back
GM-cortex
Vol 2
normalised BOLD signal
time (s)

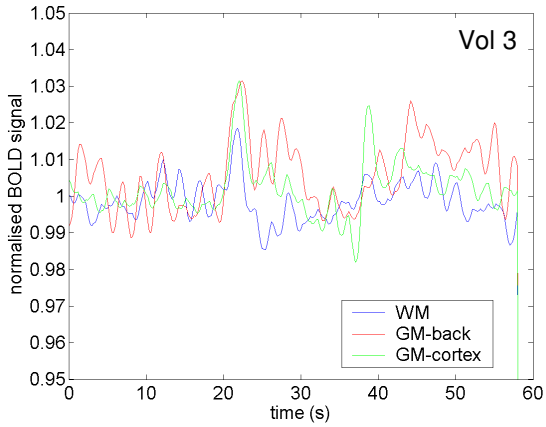
Vol 3
WM
GM-back
GM-cortex
normalised BOLD signal
time (s)

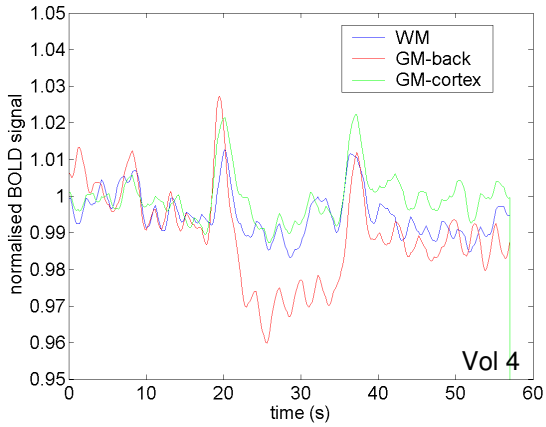
WM
GM-back
GM-cortex
Vol 4
normalised BOLD signal
time (s)

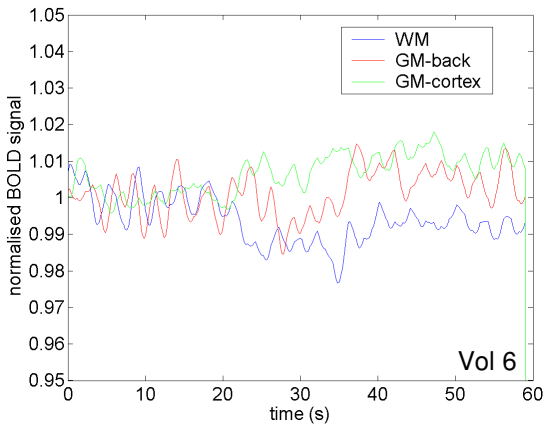
WM
GM-back
GM-cortex
Vol 6
normalised BOLD signal
time (s)

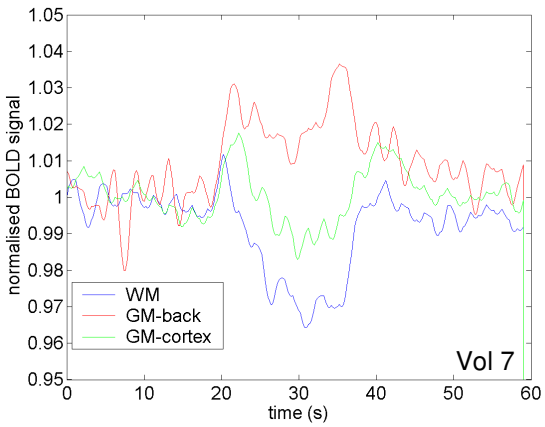
WM
GM-back
GM-cortex
Vol 7
normalised BOLD signal
time (s)

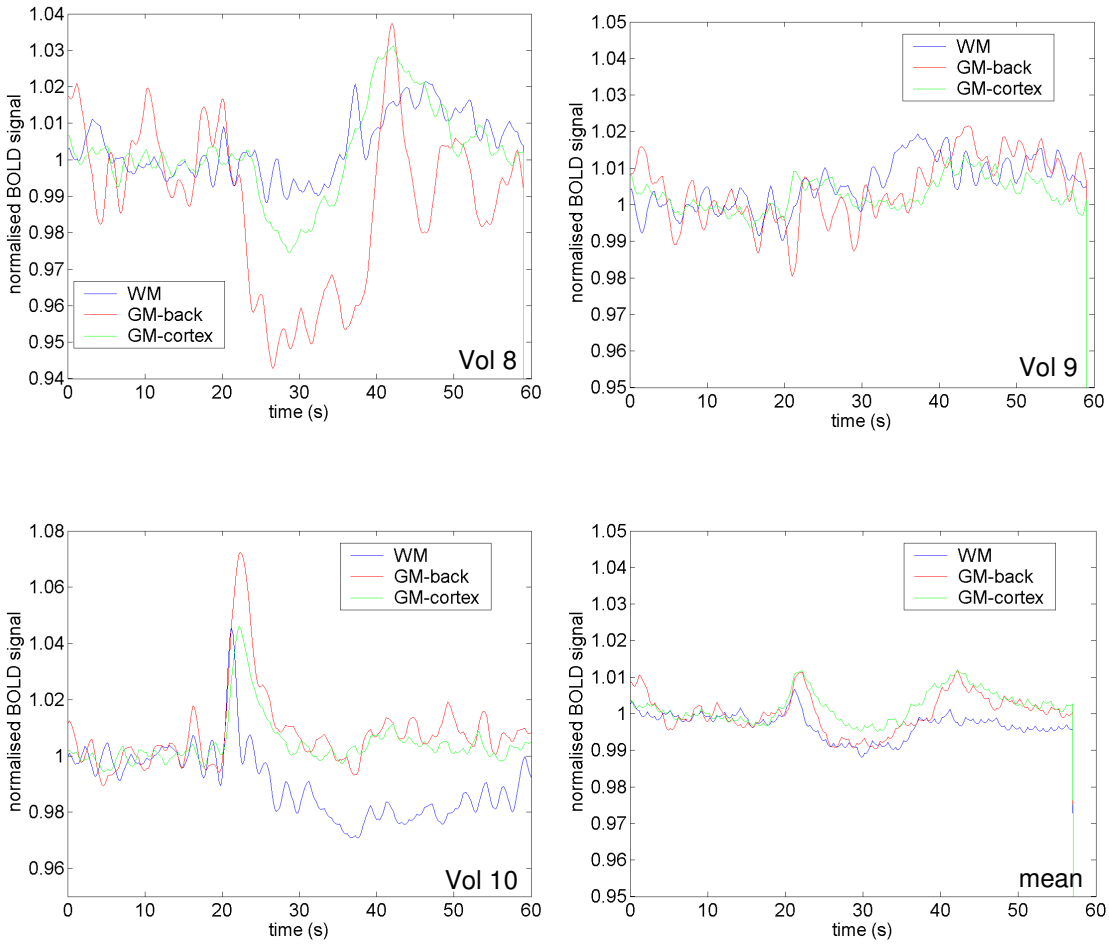

Figure 45: BOLD signal response to the Valsalva manoeuvre for Volunteers 1,2,3,4,6,7,8,9,10 and a mean dataset.

There is a large variation in the time series patterns derived from BOLD datasets collected during the Valsalva manoeuvre. There is a clear movement artefact at the start of the Valsalva manoeuvre in volunteer 10, which again may be due to movement of the head out of the plane of the slice at the start of the VM. No corresponding artefact is seen at the end of the manoeuvre. In volunteers 4, 7 and 8, increases in signal are seen at the start and end of the VM. There is evidence for this from motion correction data collected from the Siemens scanner but again this only provides in-slice movement information. Once again, there are no clear differences that can be seen between regions of interest. In the mean dataset an increase in

signal at the start of the VM is clearly seen, followed by a signal decrease below baseline levels, which then does not increase until after cessation of the VM. There is an overshoot above baseline after release of the manoeuvre, after which the signal returns to its baseline value.

Chapter 7 Modelling results

7.1 Thigh cuff deflation

7.1.1 BOLD modelling results

The following graphs show results from the modelling work and these are compared to experimental results. These plots (figure 46) show parameters relevant to the BOLD modelling aspects of the project. The parameters that are shown are arterial blood pressure (ABP), taken from Finapres measurements; venous flow and venous volume, derived from Ursino's model; deoxyhaemoglobin (dHb), derived from these flow and volume estimates; the resulting BOLD signal in response to the arterial pressure change, predicted by the Buxton model; and the BOLD signal change measured in the thigh cuff experiment. These plots show the average data from all nine subjects and all data is normalised apart from ABP, where absolute values are shown.

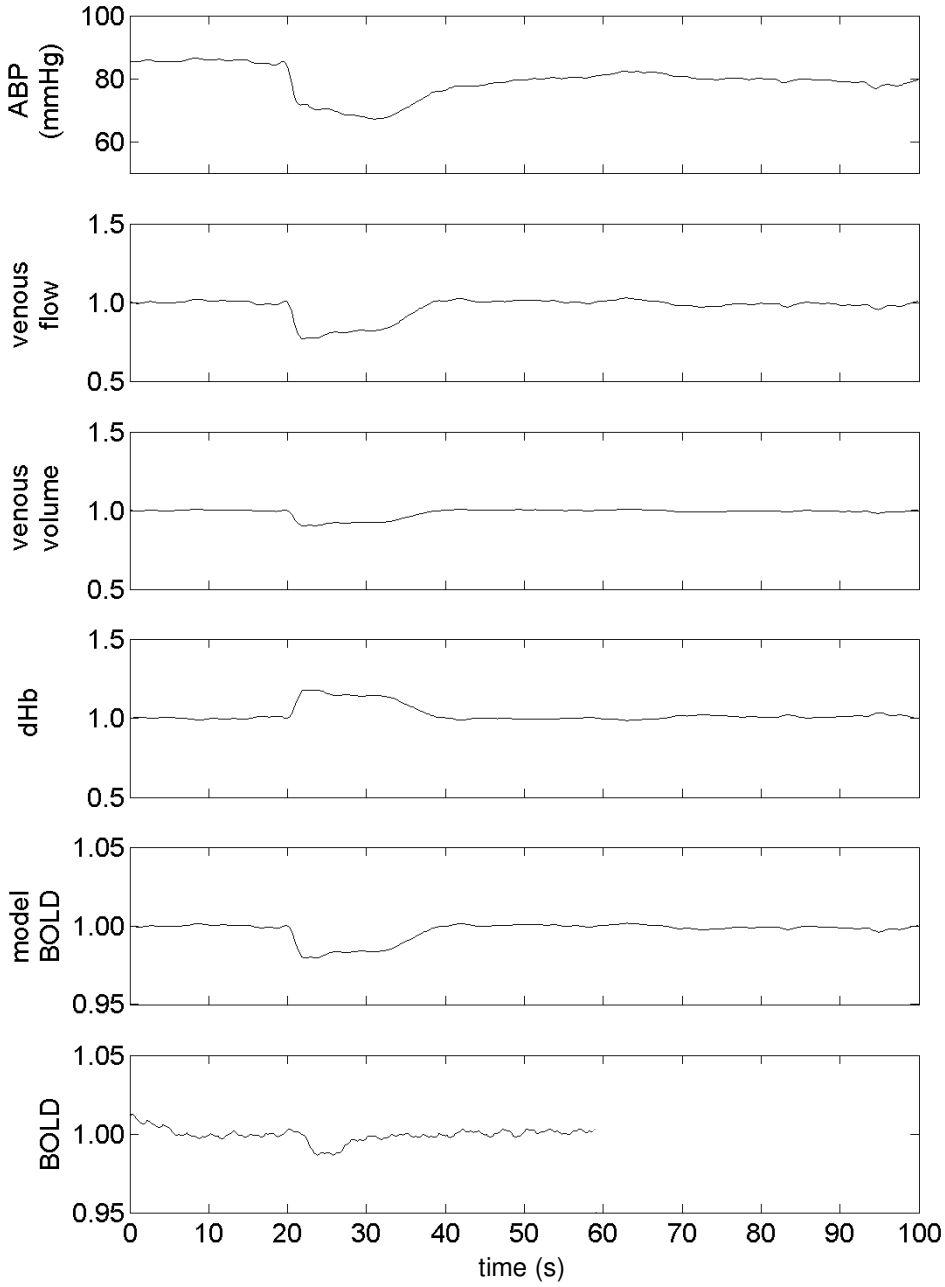

Figure 46: Mean BOLD related modelling results for thigh cuff deflation (dHb – deoxyhaemoglobin).

These results show some similarity between averaged BOLD data from nine subjects and averaged model predictions of the BOLD signal. The primary measures made of this data are the drop in signal after thigh cuff deflation and the time taken for the signal to recover to its baseline value. The mean drop in BOLD signal measured from the BOLD model data is 2.04% ± 1.36%, whereas the equivalent mean drop measured from the experimental BOLD data is 1.30% ± 0.53%; this was not found to be significantly different when tested using a two-sample t-test at a significance level of $p < 0.05$. The mean time taken for recovery of the BOLD signal to a baseline value (from the time of thigh cuff deflation) is 17.29 s ± 2.99 s in the modelled BOLD data and 12.21 s ± 4.69 s in the experimental BOLD data; this difference was found to be statistically significantly different.

The mean drop in flow measured from the BOLD model is 27.2% ± 11.1%. The mean time taken for recovery of the flow is 17.17 s ± 3.02 s in the model. The mean drop in venous volume measured from the BOLD model is 12.2% ± 6.5%. The mean time taken for recovery of the flow is 17.19 s ± 3.04 s. The mean increase in deoxyhaemoglobin measured from the BOLD model is 22.2% ± 11.5%. The mean time for deoxyhaemoglobin to fall to the baseline level is 17.40 s ± 3.17 s.

This data is summarised in the table below:

	Mean change	SD
ABP drop	21.9%	7.6%
ABP recovery time	28.6 s	8.6 s
JVP drop	17.0%	6.6 %
JVP recovery time	21.6 s	3.3 s
BOLD signal drop from model	-2.04%	1.36%
BOLD signal drop from experiment	-1.30%	0.53%
BOLD signal recovery time from model	17.29 s	2.99 s
BOLD signal recovery time from experiment	12.21 s	4.69 s
Venous flow decrease	-27.2%	11.1%
Venous volume decrease	-12.2%	6.5%
Deoxyhaemoglobin increase	22.2%	11.5%
Time for flow to recover to baseline	17.19 s	3.04 s
Time for deoxyhaemoglobin to fall to baseline	17.40 s	3.17 s

Table 1: Summary of BOLD model output and experimental data for thigh cuff deflation

The largest percentage decrease of all the model parameters was seen in venous flow, which dropped by 27.2% ± 11.1%. This is proportionally greater

than the 17% decrease seen in ABP. A similar time course is seen in the venous volume data, but with a smaller percentage decrease. The deoxyhaemoglobin data follows an approximately inverse relationship to the flow data, and increased by 22.2% ± 11.5%. There was a corresponding decrease in venous volume of 12.2% ± 6.5%. These results have implications for the origin of the BOLD signal change, which are dominated by the deoxyhaemoglobin change arising predominantly from the changes in flow. The impact of venous volume changes is much smaller. The time taken for recovery of the flow, volume, deoxyhaemoglobin and BOLD model data are all similar, and this recovery occurs ahead of the ABP recovery. These results are considered in more detail in the discussion chapter.

7.1.2 ICP modelling and TMD results

This set of plots (figure 47) shows parameters relevant to ICP changes during the thigh cuff deflation. The parameters that are shown are arterial blood pressure, jugular venous pressure, JVP (derived from cross-sectional images of the internal jugular vein), ICP changes predicted by the Ursino model and TMD measurements acquired during thigh cuff deflation. The plots again show average data from all nine volunteers. Absolute values of all these parameters are plotted. Only qualitative comparisons are made between these datasets.

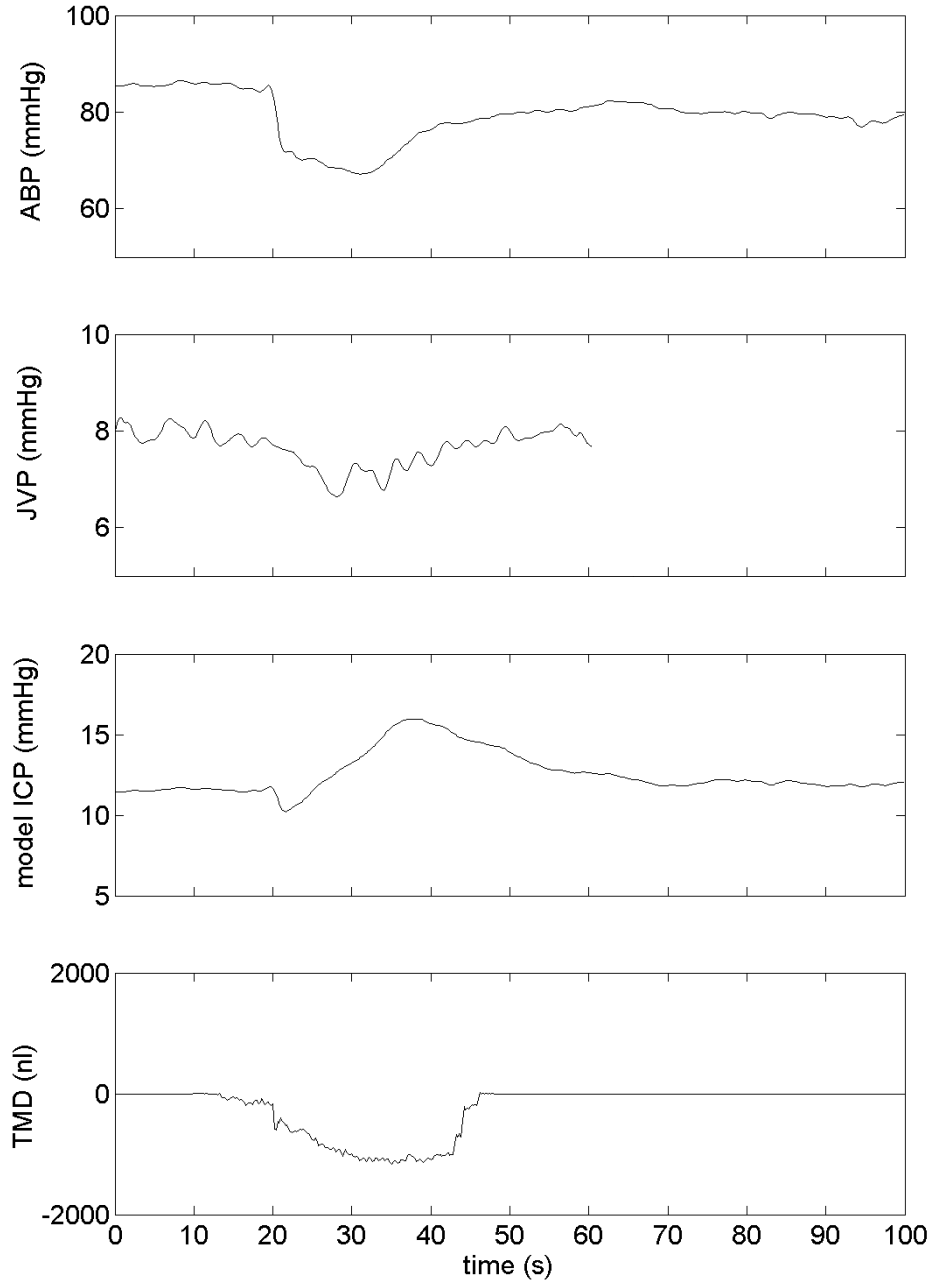

Figure 47: Mean ICP related modelling results for thigh cuff deflation.

There is a large difference between the model-predicted ICP changes seen after the thigh cuff deflation and the TMD changes observed after the same event. In the model results, ICP decreases for a short while after the point of thigh cuff deflation, before increasing for approximately 20 seconds, when it then decreases back to baseline levels. The TMD, on the other hand, shows a steep drop with thigh cuff deflation, followed by a further slower decrease for 15 seconds before appearing to start to recover. The increase in ICP shown in the model occurs when ABP and JVP are still below their resting values. This reflects a cerebral arterial vasodilation in response to the reduced cerebral blood flow. It is possible that the impact of this on intracranial pressure has been exaggerated in the model due to an underestimate of the term for intracranial compliance or an overestimate of the change in arterial volume.

There is some similarity between TMD measurements and venous blood pressure measurements, i.e. a decrease is seen after the point of thigh cuff deflation, and this decrease takes a few seconds to reach a minimum. An accurate assessment of the recovery of the TMD signal cannot be made as the measurement epoch ends at 45 seconds. It might be expected that TMD would continue increasing gradually back to baseline levels after this time point, as observed in the venous pressure measurements.

7.2 Valsalva manoeuvre

7.2.1 BOLD modelling results

The following graphs show the same corresponding results from the modelling work and experimental results, but this time in response to the Valsalva manoeuvre. These plots (figure 48) show parameters relevant to the BOLD modelling aspects of the project. The parameters that are shown are arterial blood pressure (ABP), taken from Finapres measurements; venous flow and venous volume, derived from Ursino's model; deoxyhaemoglobin (dHb), derived from these flow and volume estimates; the resulting BOLD signal in response to the arterial pressure change, predicted by the Buxton model; and the BOLD signal change measured in the Valsalva manoeuvre experiment. Again, these plots show the average data from all nine subjects and all data is normalised apart from ABP, where absolute values are shown.

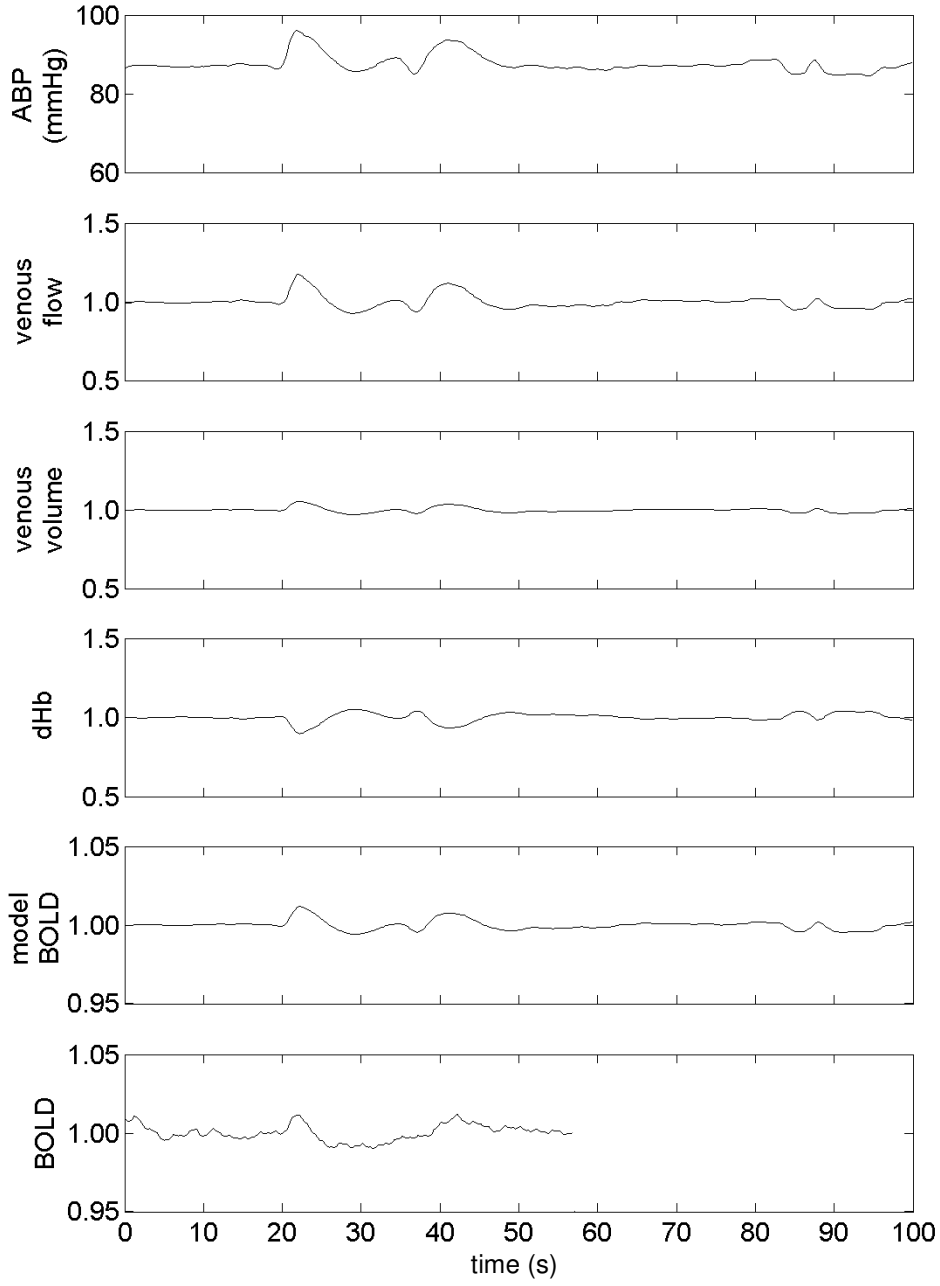

Figure 48: Mean BOLD related modelling results for the Valsalva manoeuvre (dHb – deoxyhaemoglobin).

These results show similarity between averaged BOLD data from nine subjects and averaged modelled predictions of the BOLD signal. The primary measures made of this data are the same as those measured from the arterial blood pressure data, the change from baseline during phase II and phase IV of the manoeuvre (see figure 31, Section 6.1.2). The mean change in BOLD signal during phase II measured from the BOLD model data is –0.77% ± 1.05%, whereas the equivalent mean drop measured from the experimental BOLD data is –0.93% ± 2.45%. The mean change in BOLD signal during phase IV is 1.02% ± 0.75% in the modelled BOLD data and 1.20% ± 1.06% in the experimental BOLD data. There were no statistically significant differences found between the BOLD modelling results and the BOLD experimental results, for changes during either phase II or phase IV of the Valsalva manoeuvre (using a two-sample t-test at a significance level of $p<0.05$).

The mean change in venous flow during phase II measured from the BOLD model is –9.0% ± 11.8%. The mean change in flow during phase IV is 15.9% ± 13.7%. The mean change in volume during phase II measured from the BOLD model is –3.8% ± 5.0%. The mean change in volume during phase IV is 4.8% ± 3.8%. The mean change in deoxyhaemoglobin during phase II measured from the BOLD model is 6.8% ± 9.2%. The mean change in deoxyhaemoglobin during phase IV is –8.8% ± 6.9%.

This data is summarised in the table below:

	Mean change	SD
ABP change during phase II	-1.87%	10.81%
ABP change during phase IV	7.23%	9.75%
Maximum increase in JVP during VM	86.5%	60.4%
BOLD signal change during phase II in model	–0.77%	1.05%
BOLD signal change during phase II from experiment	–0.93%	2.45%
BOLD signal change during phase IV in model	1.02%	0.75%
BOLD signal change during phase IV from experiment	1.20%	1.06%
Venous flow change during phase II	–9.0%	11.8%
Venous flow change during phase IV	15.9%	13.7%
Venous volume change during phase II	–3.8%	5.0%
Venous volume change during phase IV	4.8%	3.8%
Deoxyhaemoglobin change during phase II	6.8%	9.2%
Deoxyhaemoglobin change during phase IV	–8.8%	6.9%

Table 2: Summary of BOLD model output and experimental data for the Valsalva manoeuvre

The greatest percentage changes are seen in the flow data, and during phase IV of the Valsalva manoeuvre. Similarly to the thigh cuff results, the flow changes were proportionally greater than the corresponding ABP changes. The volume changes follow the ABP and flow changes, but with a smaller magnitude. Again, deoxyhaemoglobin data follows an approximately inverse relationship to the flow data, and the changes are larger than the corresponding changes in venous volume. This leads to a similar conclusion to that drawn from the thigh cuff data; that deoxyhaemoglobin is the overriding factor in determining the BOLD signal changes. This will be discussed further in Chapter 8.

7.2.2 ICP modelling and TMD results

The second set of plots (figure 49) shows parameters relevant to ICP changes during the thigh cuff deflation. The parameters that are shown are arterial blood pressure, jugular venous pressure, JVP (derived from cross-sectional images of the internal jugular vein), ICP changes predicted by the Ursino model and TMD measurements acquired during thigh cuff deflation. The results show the averaged data from all nine volunteers. As with the thigh cuff data, absolute values of all these parameters are plotted. Only qualitative comparisons are made between these datasets.

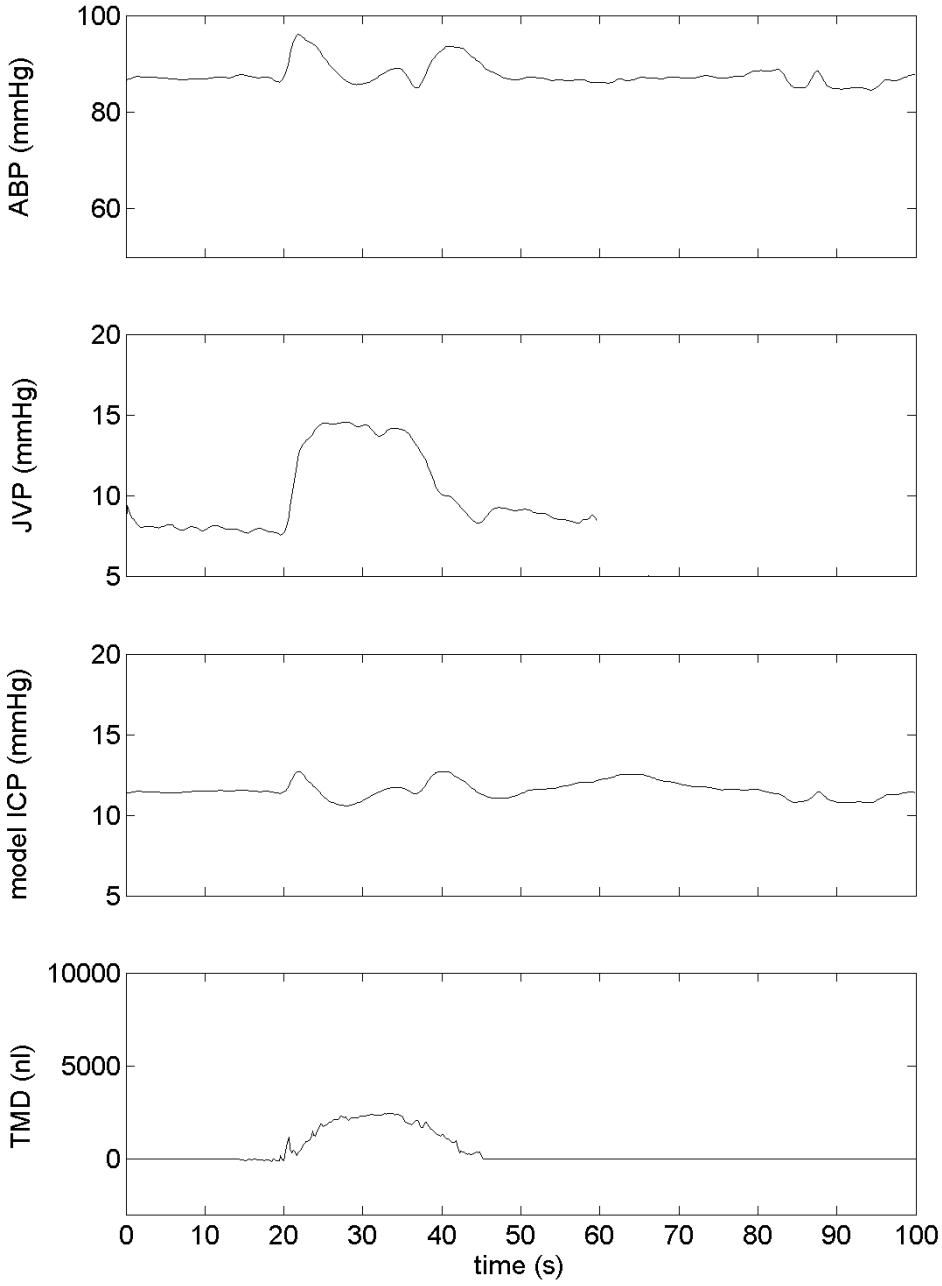

Figure 49: Mean ICP related modelling results for the Valsalva manoeuvre.

There is no similarity between the model-predicted ICP changes seen during the Valsalva manoeuvre and the TMD changes observed during the same event. ICP changes follow arterial blood pressure changes whereas TMD changes are more similar to the jugular venous pressure changes that have been observed. The subtle changes in the shape of the jugular vein data can also be seen in the TMD data, i.e. a fairly sharp increase at the start of the manoeuvre, a plateau and then a gradual decrease once the Valsalva manoeuvre has been released.

Chapter 8 Discussion, conclusions and further work

8.1 Introduction

The objective of this project has been to elucidate the BOLD signal changes that are observed in response to rapid alterations in arterial blood pressure. The motivation for this is two-fold; to try and account for errors in functional MRI data from such variations in arterial blood pressure if they exist, and to use the resulting changes in the BOLD signal to infer information about blood flow regulation across the whole brain. The dynamic vascular physiology relating the BOLD response to blood pressure changes has not been considered in great detail in the literature and it is hoped that this piece of work will help to demonstrate and explain these changes.

The key finding from this project is that BOLD signal changes are influenced by arterial blood pressure changes, which is borne out by modelling the BOLD response to a change in arterial blood pressure, induced by thigh cuff deflation and the Valsalva manoeuvre.

This discussion provides an in depth consideration of each element involved in this piece of work. The discussion will start with the implementation of the Ursino model and the inputs (both experimental and model-derived) that were used in this model to eventually provide inputs for the Buxton model. This will lead on to the discussion of the implementation of the Buxton model of BOLD signal changes in response to a blood pressure change. Various matters regarding this model will be discussed, including the data inputs, assumptions that have been made to enable certain parameters to be calculated, outputs that contribute to the BOLD signal estimation and the output of this BOLD signal, which can then be compared to the experimental data that has been collected. The next section will then discuss the experimental data that has been acquired, firstly in relation to the model prediction of what the BOLD signal should resemble. Various factors will influence these signal changes and these will be discussed, particularly in relation to the acquisition technique and the artefacts associated with this, and the analysis and post-

processing of the data. The signal changes that are observed will be related to the physiological changes taking place during the blood pressure challenges, particularly those concerning the venous vasculature. Other findings pertinent to these results will also be discussed. The next section will discuss the implications of these findings for functional MRI studies. Resting state functional MRI will also be considered in light of the findings in this project. The physiological changes in the brain that occur during such blood pressure provocations and their relationship to the BOLD signal changes will also be taken into account. The importance of the autoregulation mechanism will be introduced at this stage and related to the findings, as well as to outputs from the modelling work. The impact of these results on conditions where the autoregulation mechanism may be impaired will also be discussed. There will also be a discussion regarding the intracranial pressure changes predicted by the modelling and how these compare to the tympanic membrane displacement measurements. The final section will look towards the further work that may be carried out to take this project forward. This will include expanding the study to include a greater number of subjects (and maybe patients), development and optimisation of the BOLD technique, refinement of the modelling techniques, the use of different methods of blood pressure provocation, development of analysis techniques to include more sophisticated region of interest analysis and post-processing of data, and eventually to try and provide new vascular physiological imaging information. Development of the modelling aspects of the work could also be carried out in the future.

8.2 Implementation of the Ursino model

The first stage of the modelling work was to implement a model of the cerebral vascular system, which would then provide physiological inputs to the Buxton model for the BOLD signal. Deoxyhaemoglobin time series and venous volume time series are required as inputs for the Buxton model. As

these quantities cannot be measured directly they must be estimated or derived from other measurements. A model of the cerebral vasculature is required to derive these inputs (deoxyhaemoglobin and venous volume), from measurements and estimates that have been made of arterial blood pressure and jugular venous pressure respectively. The model that has been used is based on work by Ursino[50] and has been taken from Liu[211], as described in Chapter 4. There are a vast number of models of the cerebrovascular system, as discussed in Section 4.2.2, each with varying amounts of detail and each considering different aspects of the system[151,152,153,154,155,163,164,165,166,169]. The Ursino model provides a good approximation of the cerebral vasculature and incorporates CSF as well as blood flow dynamics, and autoregulatory components. This is a complex representation of the vascular system that was written to improve understanding of cerebral haemodynamics and ICP pathology and this is the first time, to our knowledge, that it has been used to aid interpretation of experimental BOLD data. Most MRI based approaches to this area of work have used a simple Windkessel[65,179,180] model of the venous vasculature; they do not provide a detailed representation of the various vascular compartments of the brain and cannot therefore estimate BOLD dynamics from ABP and jugular vein pressure inputs. There have been very recent developments, however, of similar BOLD models with expanded multi-compartment Windkessel models[212] and the use of a vascular anatomic network[213], which takes into account oxygen saturation distributions and arteriolar diameters in response to neuronal activity.

Autoregulation has been included in a model by Diamond *et al*[214], which attempts to link cerebrovascular responses to functional neuroimaging data. This is a biophysical model of systemic and cerebral circulation, which includes gas exchange and dynamic cerebral autoregulation. The model comprises seven systemic compartments, five cerebral and two neck compartments. This is a lumped parameter model comprising both systemic (i.e. blood circulation excluding cerebral and pulmonary circulation) and

cerebral regions. The systemic region contains chambers representing the large arteries, small arteries, arterioles, capillaries, venules, small veins and large veins. The cerebral region contains chambers representing pial arteries, arterioles, capillaries, venules and pial veins. Cerebrospinal fluid circulation and intracranial pressure are also accounted for in the cerebral region. Arteriolar compliance is determined by the autoregulation state variable, which is derived from flow changes and an autoregulation gain and CO_2 reactivity time constant. The model also incorporates parameter estimates at the steady state, non-linear resistances, Windkessel compliances and a pressure input into the small systemic artery. The pressure input data is measured using a device similar to the Finapres device. The neuroimaging technique that has been linked to this model is near infrared spectroscopy (NIRS) rather than BOLD MRI. The model was validated by examining results from resting state NIRS data. The NIRS experimental data was found to correspond more closely to the biophysical model rather than just blood pressure variations. This paper is one of the first to discuss the value of acquiring neuroimaging data pertaining to the autoregulation mechanism, and the clinical potential of such an approach. Diamond has proposed a complex model, but this should be explored further and compared to the approach used in this project, particularly if the work is extended to include functional MRI biophysics in the model.

Certain aspects of Diamond's physiological model differ from the approach used by Ursino. For example, the model includes gas exchange and the addition of neck compartments and a whole systemic region. Although autoregulation is included, this is assumed to act in the arteriolar compartment, and is not divided into proximal and distal mechanisms. The autoregulation mechanism in Diamond's model is dependent on flow and CO_2 changes and pressure changes are not incorporated explicitly. A Starling resistor is not included in the Diamond model, but is incorporated into venous outflow in the Ursino model.

As is the case with all mathematical models, assumptions have been made in implementing the Ursino model[50], which may lead to uncertainties in the accuracy of the model's representation of true physiological processes. Compliance of the large intracranial veins is assumed to be inversely proportional to local transmural pressure, i.e. not constant, which would lead to a mono-exponential pressure-volume relationship. Another simplification is the inclusion of a Starling resistor. This represents the passive narrowing or complete collapse of the terminal intracranial veins and this mechanism results in intracranial venous pressure always being slightly higher than ICP and therefore large cerebral veins and venules upstream from this resistor remain open during intracranial hypertension. CSF production at the cerebral capillaries and its subsequent outflow at the dural sinuses is assumed to be passive and in one direction, and proportional to the transmural pressure at these points. For the short duration measurements performed in this study, CSF flow is negligible.

Ursino and Liu[211] include CO_2 as a variable that affects arterial resistance. Nonetheless, in the implementation of the model, CO_2 is assumed to be constant and it is only arterial pressure that influences arterial resistance. This is most probably not the case, especially during the Valsalva manoeuvre, although reasonably constant CO_2 levels have been measured during the manoeuvre in some studies[137]. The model divides the autoregulating arterial system into two segments, the large pial arteries (proximal segment) and the small pial arteries (distal segment). It is appropriate to split the system into two segments due to differences in the autoregulation mechanism between the two segments[50]. However, this distinction is not thought to be that significant to the results from this project as signal is being detected downstream from the autoregulating compartment.

Four constants had to be defined before running the model in this project: a gain and a time constant of the smooth muscle response to blood pressure and flow alterations, for each of the two segments of the arterial system (proximal and distal). Only the flow response component (relating to the

distal arteries) was activated and the gain and time constant for this were set to reflect values corresponding to normal autoregulation, as this was assumed in all subjects. The assumptions made in setting up these autoregulation parameters may be another source of inaccuracy in the model. A large number of other constants were incorporated into the model, but these were not changed when implementing the model in this study. These described the resistances and compliances of the various vascular compartments. For all these constants, the values provided by Ursino were used in this study.

Notwithstanding these assumptions, the Ursino model has been used in other pieces of work as a good approximation of cerebral vascular physiology and has been validated in a number of experiments[211,171].

The starting point and driving input to this model is a time series of arterial blood pressure measurements made using a Finapres non-invasive blood pressure monitor. Under appropriate physiological conditions, results from the Finapres have been found to agree well with invasive blood pressure monitoring (the gold standard). However, as mentioned in Section 4.3.3, there are errors associated with this measurement if calibration is not carried out properly, for example measurements are more temperamental if the hands are cold. Peripheral vasoaction could also cause erroneous readings from the Finapres, this causes changes in light transmission through the finger which would then cause changes in finger cuff pressure that are not due to changes in central arterial pressure. In one study[80], it was found that blood pressure drops further and recovery is slower following thigh cuff deflation when measured with the Finapres than when measured with a tonometry device. This inaccuracy in the blood pressure measurements would influence the final results of the modelling work; this will be discussed later. Despite these problems the Finapres measurement is still assumed to give a reasonable approximation of arterial blood pressure. The magnitude of blood pressure changes induced by thigh cuff deflation is large, and thus, this

large non-physiological change will dominate over any individual variability in blood pressure within subjects.

The other experimental input to this model was that of jugular vein pressure. This pressure was derived from cross sectional area measurements of the internal jugular vein (this methodology has been described in Section 5.3.2). There are a number of assumptions that have been made in this calculation, the first being that venous pressure is directly proportional to cross-sectional area of the vein. This is most probably not the case, it is more likely a more complex monotonic relationship, but this approach was used for simplicity in this project. The cross sectional area of the left and right jugular veins is averaged and used to calculate a normalised change. These normalised changes in cross sectional area were multiplied by a mean baseline jugular vein pressure which was assumed to be 8 mmHg for all subjects. This provided an approximate time series of absolute jugular vein pressure changes. A more complex relationship has been described between cross sectional area changes and pressure changes[194], however only a relative change in pressure can be derived. Future work could use this approach to improve the accuracy of jugular vein pressure estimates.

The other variable in these experiments is the consistency of the performance of the Valsalva manoeuvre, for the three repeats in the scanner and the three repeats outside the scanner environment. It is assumed that each individual carries out the manoeuvre in a repeatable manner each time, but this may not be the case, and it is difficult to assess this. No measurement of airway pressure during the manoeuvre was made; this would improve both intra and inter-subject repeatability of the technique. The action of the thigh cuff inflation and deflation is thought to be more consistent in each repeat of the experiment.

Venous flow and venous volume changes, in response to the measured arterial and venous blood pressure changes, are the outputs from this model that have been used in the implementation of the Buxton model. However

other outputs, such as ICP, have also been derived to allow comparison to TMD data. These will be discussed in a later section.

8.3 Implementation of the Buxton model

A modified version of the BOLD signal changes described in the original Balloon model proposed by Buxton[51] (1998) has been implemented as described by Obata[52] (2004). The two variables in this model are deoxyhaemoglobin and venous volume and these are used as normalised values. There are a number of assumptions that have been made in deriving the equation that is used to describe the BOLD signal changes, as well as in the derivation of the time series for the variables that in the equation.

Firstly, the assumptions and approximations in the derivation of the BOLD signal equation need to be considered. There are two main contributions to signal changes; signal arising from intravascular and extravascular spins. In deriving these contributions, exponential terms are expanded into linear approximations, for small changes in relaxation rate, which should be the case in this piece of work. The constant relating to extravascular signal changes, i.e. the constant linking transverse relaxation times to oxygenation, (ν_0) is derived from theoretical equations (based on a simple tube-like model of the vasculature, and relating to large vessels) whereas the corresponding constant for intravascular signal changes (r_0) is determined empirically using experimental data[177], which is more likely to lead to inaccuracies in the final model. This experimental data has been obtained from a pig model as opposed to healthy human volunteers and assumes linearity of R_2* over a range of oxygen saturation levels of blood. Other assumptions include the value of the ratio of intravascular to extravascular signal at rest, which is an estimate from the same pig model, and the resting oxygen extraction fraction. It is thought that all these assumptions are likely to have a minimal effect on the accuracy of the model, which is borne out by experimental results from

the same paper by Obata[52]. Other studies have used the full Buxton model, which provides more validation of the model[23,184,185,186,187,188,189].

Larger uncertainties exist in the methods used to estimate venous volume and in particular deoxyhaemoglobin changes. Venous volume changes are derived directly from parameters in the Ursino model, whereas deoxyhaemoglobin changes are derived from blood flow and volume changes predicted by the Ursino model, and this derivation is described in Section 5.5.2. There are a number of assumptions in this derivation, the main ones being that there is constant metabolism during the experiments and that there exists a steady state at the start of the experiments. These may lead to inaccuracies in the final output from this model and differences between the model data and the experimental data. If metabolism is not constant, then values of deoxyhaemoglobin will vary both due to these changes in metabolism as well as blood flow and volume changes. This would be the case in activation studies, but the stimulus in this project is primarily to induce blood pressure changes. If blood pressure changes do induce neuronal activation as a result of neural components of a baroreceptor response or other cognitive responses, then this may produce metabolism changes, which is the basis of other work in this field[17,18,19,118,120]. There may also be spontaneous changes in metabolism, during the 'resting state' state of the brain, i.e. the default mode of brain function[215,216].

Other models have been devised to predict the BOLD response and many have used a similar approach to the Windkessel[179,180] method used to represent venous vasculature changes, which then control the resulting BOLD signal changes. Although these changes are reasonably accurately characterised by such models (which often include hypothetical inputs rather than real data), the vascular changes driving these changes may not be so well represented by such simple one, two or three compartment models. In this project, the main interest is the effect that real vascular changes have on the BOLD response (as opposed to neuronal activation) so it is important to try and increase the accuracy of this aspect of the modelling by using a more

complex vascular model such as the one proposed by Ursino. As mentioned previously, a recent model has been described that combines cerebral vascular responses and autoregulation with the biophysics of near infrared spectroscopy (Diamond *et al*[214]). Diamond states that one of the limitations of this model is the use of a lumped parameter approach to predict spatially distributed haemodynamics, which would be problem if the model was used to simulate changes on a voxel-by-voxel basis, for example with functional MRI data. As such, they suggest that their model could only be used to examine whole-brain signal dynamics in functional MRI. This is a similar drawback to the model employed in this project, as it is assumed that all the signal changes in the specified region of interest are due to changes in the properties of venous blood. A model has also been proposed by Payne, which predicts the response of the cerebral vasculature to changes in arterial blood pressure, arterial CO_2 concentration and neuronal activation[23] and combines Ursino's model with Buxton's equation for BOLD signal changes. However, no experimental data has been incorporated into the model or compared to the model outputs.

The output from the model proposed in this project is the predicted BOLD signal change in response to imposed blood pressure changes due to thigh cuff deflation and the Valsalva manoeuvre. This has then been compared to the experimental data and this is discussed in a later section.

8.4 Experimental data

The results that have been presented compare the BOLD signal changes predicted by the modelling to the experimentally acquired BOLD data. In addition, the arterial blood pressure data is shown as well as the flow, volume and deoxyhaemoglobin time series derived from this data using the Ursino model. The mean results from nine subjects are shown.

The results show that in the thigh cuff deflation experiments the mean drop in BOLD signal measured from the BOLD model data is 2.04% ± 1.36%,

whereas the equivalent mean drop measured from the experimental BOLD data is 1.3% ± 0.53%. The mean time taken for recovery of the BOLD signal is 17.29 s ± 2.99 s in the modelled BOLD data and 12.21 s ± 4.69 s in the experimental BOLD data.

The results from the thigh cuff deflation experiments show that there is good general agreement between the model prediction and these results. However, there are some discrepancies that need to be explored. The maximum drop in signal intensity predicted from the model is greater than that measured from the data, but this was not found to be statistically significantly different. Also, the time taken for recovery of the BOLD signal is less in the experimental data than in the model prediction (which was found to be statistically significantly different). This would indicate that there are factors in the experiments that are not considered in the model or a disparity between the input variables measured outside the scanner environment and the actual changes occurring during the experiments. These are discussed later on in this section (see pages 240-244).

In the Valsalva manoeuvre experiments, the mean change in BOLD signal during phase II measured from the BOLD model data is -0.77 ± 1.05%, whereas the equivalent mean drop measured from the experimental BOLD data is -0.93% ± 2.45%. The mean change in BOLD signal during phase IV is 1.02 ± 0.75% in the modelled BOLD data and 1.20% ± 1.06% in the experimental BOLD data. There are similarities between the BOLD data acquired during the Valsalva manoeuvre and the changes predicted by the modelling. The opposite trend was seen compared to the signal changes during thigh cuff deflation, in that the magnitude of the changes predicted in the modelling was smaller than those observed in the experiments. However, the general shape of the two time series was observed to be similar and these differences were not found to be statistically significantly different.

Considering the mean data, averaged over all nine subjects, the main influence on the final BOLD signal changes (with both blood pressure stimuli)

is the relative change in deoxyhaemoglobin, itself derived primarily from flow, and to a lesser extent, volume changes. Changes in venous volume alone do not contribute to the BOLD signal change to the same extent as the deoxyhaemoglobin change, which can be predicted considering the constants in the model (~5 for the term relating to deoxyhaemoglobin, compared to ~1.3 for the term relating to venous volume). For example, in the case of the thigh cuff deflation experiments, a large increase in venous volume would have to occur for venous volume effects to be the dominant factor causing a decrease in BOLD signal, although venous volume increases would also increase deoxyhaemoglobin. Jugular vein pressure changes are particularly prominent during the Valsalva manoeuvre and such pressures might be expected to have a pronounced impact on the BOLD signal. However, the modelling shows that cerebral venous volume is not largely affected by jugular vein pressure changes. The resulting BOLD signal changes predicted by the modelling are supported by the experimental results.

There is a complex relationship between flow and oxygenation. The relationship between oxygen extraction fraction (OEF) and cerebral blood flow (CBF) has been modelled by Buxton and Frank[183], and for small changes in CBF there is approximately a linear inverse relationship. This would lead to a similar trend seen in the modelling results. For example in the case of thigh cuff deflation, if CBF decreases, OEF will increase, thus increasing the deoxyhaemoglobin content of the blood, which is what is seen in the modelling data for deoxyhaemoglobin levels after cuff deflation. A similar relationship is predicted by Rostrup *et al*[208] at low values for relative CBF (rCBF), i.e. decrease in deoxyhaemoglobin levels are seen as rCBF increases from low to intermediate values. However, flow seems to have less of an effect on deoxyhaemoglobin at higher values of flow. Measurements of arterio-jugular oxygenation difference ($AJDO_2$) show that as CBF decreases, $AJDO_2$ increases, which would indicate greater oxygen extraction[217]. This would result in increases in deoxyhaemoglobin, which fits with the deoxyhaemoglobin changes predicted by the modelling implemented in this

study. Metabolism is assumed to be constant in this project, but this may not be the case. If metabolism were not constant, then this would introduce errors into the estimation of deoxyhaemoglobin levels. This is an intricate relationship and the accuracy of modelling results will benefit from further investigation into this.

Another issue with the modelling is that of the input function, i.e. the arterial blood pressure data and the fact that this may not fully accurately represent the changes occurring during the experiments. A study by Birch *et al*[80] compared the measurements of blood pressure following thigh cuff deflation (using the same methodology used in this project) carried out using two devices, a tonometry device (the Colin® CBM-7000 system) and the Finapres. It was found that blood pressure drops further and recovery is slower following thigh cuff deflation when measured with the Finapres than when measured with the tonometry device; however it is not known which is more accurate. This would fit with the difference seen between the model BOLD predictions (driven by Finapres acquired blood pressure data) and the experimental BOLD data.

There may also be errors present in the jugular vein data, mainly due to the inaccuracies in the derivation of these pressures from area measurements. Additional errors could arise from the uncertainty of the jugular vein borders in some of the cross-sectional images, which would lead to inaccuracies in the time course data.

Certain assumptions have been made about the action of the autoregulation mechanism in the implementation of the Ursino model. It may be that normal autoregulation is not being fully represented by the model, or that autoregulation in all the volunteers is not normal, and this could be a factor in the differences seen between the modelled and experimental BOLD data.

Errors in the acquisition of the BOLD data and noise in the data may also contribute to the differences observed between the experimental data and the results predicted by the modelling. Head movement out of the imaging plane

may result in signal intensity changes, particularly at the time of cuff deflation or at the beginning and end of the Valsalva manoeuvre. This would most probably result in an increase in signal intensity due to spin-history effects[218], i.e. tissue with a higher signal intensity (containing spins that have not been previously excited) moving into the imaging plane. Motion correction of the images was carried out in the plane of image acquisition, however as only one slice was acquired it was not possible to correct for any movement in and out of the acquisition plane. The magnitude of movement out of the slice plane is not known, but the movement in the plane of the slice was always less then ± 1 mm, which is smaller than the dimension of a voxel. However, this movement could still have a deleterious effect at boundaries between different tissue types. Movement artefacts may be apparent in individual volunteer's data (volunteer 4 and volunteer 9) at the point of cuff deflation, as these variations are not seen in the ABP data. Similar errors may also be seen in the Valsalva manoeuvre data, particularly in volunteer 10, and maybe in other volunteers where large changes in BOLD signal intensity are seen at the start or end of the Valsalva manoeuvre, which do not correlate to blood pressure changes (volunteer 4). However, these data artefacts are largely averaged out of the final mean dataset. In addition, it is difficult to separate out signal increases due to ABP changes or movement if both could be the cause of such signal changes.

BOLD-EPI (echo planar imaging) is an inherently noisy technique and is also prone to artefacts, in part due to the fast acquisition times that are required. The main artefacts present in EPI data include Nyquist sampling errors, chemical shift artefacts, image distortion, T_2*-induced image blurring and intra-voxel dephasing and those due to physiological factors. All these factors lead to noise, spurious signals or signal loss in EPI images, which would not be accounted for in the modelling, and would contribute to differences between the modelling and experimental results. There is also the issue of thermal noise present in the data. This is as a result of stray currents in the body that produce spurious signals in the receiver coil. This is

manifest in the raw data, and is then reconstructed in the final image[5]. No smoothing was applied to the data collected in this project, as this may have diminished the signal changes that were trying to be detected.

As mentioned above other noise in the data may be related to physiological factors, many of them unavoidable. For example, it is known that respiratory[142,143] and cardiac[219,220] functions produce artefacts. Motion of the chest wall whilst breathing alters the homogeneity of the magnetic field[221] and changes in CO_2 levels during breathing result in low frequency variations in blood flow and oxygenation. Cardiac function can result in vessel pulsation, CSF movement and tissue deformation which all affect functional MRI data. Cardiac gating can be used reduce these artefacts but this a complex technique to implement consistently and it also increases acquisition time[222,223]. This methodology may also introduce errors in signal changes, due to varying amounts of T_1 relaxation during each TR period, as this varies with heart rate. This can be corrected for, but this requires a precise knowledge of each R-R interval, as well as the T_1 relaxation time of the tissue in each voxel, which can be difficult to estimate due to partial volume effects[103].

Inflow effects may also have an influence on the signal changes that are observed[224]. Although these were reduced by using a flip angle that was optimised for the TR that was employed[5,205,206], they may still have some influence on the signal changes that are observed. For example, in the BOLD data from the thigh cuff experiments, a faster recovery in signal is observed than predicted from the BOLD modelling data. This could be as a result of false increases in signal due to the inflow of unsaturated blood during this recovery time. Inflow of CSF in the voxels of interest (for example in the perivascular space) could also cause spurious increases in signal that are not due to oxygenation changes.

Regarding image analysis, a very simple region of interest approach was used where large regions representing white matter, grey matter and CSF

were drawn and time series produced from average pixel values within these regions at each time point. However, there are a number of disadvantages to this method, the main one being that each region does not solely contain tissue relating to white matter, grey matter or CSF, there will be some contamination from other types of tissue. An improvement to this would be to precisely segment (for example using a package such as SPM, Statistical Parametric Mapping[225]) high-resolution anatomical images of the brain into these corresponding regions and overlay these on to the BOLD images. This may be carried out a future point in time. Even with this segmentation, the relatively large voxel sizes used in this type of acquisition mean that there will always be some signal from different substances within each voxel.

How do these results compare to other work in the field? The BOLD signal response to a blood pressure alteration does seem to be influenced by the blood pressure changes imposed. It is difficult to compare this result to most of the literature, as the majority of other studies involve blood pressure changes occurring over a much slower timescale and involve other methods of applying the blood pressure changes. The other difficulty with relating these findings to the previous work is that many of the results reported in the literature are contradictory. However it is valuable to compare these results with published work. Early work in this field involved blood withdrawal in rats to alter blood pressure, but this was carried out over long timescales (of the order of minutes). In one of these studies (Zaharchuk *et al*[81]) no effect was seen whilst in another (Kalisch *et al*[113]) a decrease in signal was seen and this was thought to be due to venous dilation and a corresponding increase in venous volume. Another rat study concluded that autoregulation compensates for alterations in blood pressure and as such the BOLD signal is not affected (Luo *et al*[117]). Similarly, another study reports that small changes in blood pressure (over a long timescale) do not affect the BOLD signal in patients with healthy autoregulation, but care should be taken in interpreting results from patients with abnormal autoregulation (Tuor *et al*[116]). Other studies by Henderson[17], Wang[19] and Qiao[120] investigated the spatial

distribution of BOLD signal changes in response to blood pressure alterations, which is a slightly different aim to this project. They did however find that BOLD signal changes followed changes in blood pressure. Work by Liu[118] agreed with findings from Luo and Zaharchuk, i.e. that the BOLD signal is not affected by BP variations as a result of the autoregulation mechanism. So, although some papers report that the BOLD signal is not affected by changes in blood pressure, the timescale of blood pressure changes in these studies is much longer than that used in this study. Those that do report changes in BOLD signal are examining a slightly different outcome, which is more concerned with the function of the brain in response to such changes (i.e. a neuronal response) rather than a purely haemodynamic response. This questions the assumption that metabolism is constant during these experiments; a neuronal response is reported in reaction to blood pressure changes in certain areas of the brain, which would mean that metabolism is not constant in these regions. However, these regions are not coincident with the regions investigated in this study.

There is less work that reports on the specific effect of the Valsalva manoeuvre on the BOLD signal. Studies have been carried out using breath holding, acetazolamide administration and CO_2 changes, all of which act as vasodilators, rather than as direct mediators of BP, as stimuli for BOLD experiments. A study by Li *et al*[129] compared a deep inspiration of breath to an incomplete Valsalva manoeuvre and resulted in a biphasic change in BOLD signal (decrease then increase), due to an initial decrease in Pa_{CO2} and blood flow (as a result of venous pressure increases), followed by an increase in Pa_{CO2} after prolonged breath holding. A more relevant study by Gareffa[22] investigates the negative BOLD signal changes as a result of a stimulus similar to the Valsalva manoeuvre. These negative signal changes are attributed to reduced venous flow during the manoeuvre, which induces venous dilation and a resulting increase in deoxyhaemoglobin concentration. In this project, a more complex pattern of flow and volume changes during the Valsalva manoeuvre is predicted from the Ursino model (based on blood

pressure changes) and this results in deoxyhaemoglobin changes, which are approximately inversely related to the blood pressure and flow changes. The venous dilation and corresponding pressure increase seen in the jugular veins does not seem to have a large effect on the intracranial venous volume. This may be due to the action of the Starling resistor included in the Ursino model and the higher values of the resting ICP and cerebral venous pressure relative to the jugular venous pressure. However, in some subjects (Volunteers 4 and 8) a larger decrease in signal is seen during the Valsalva manoeuvre and this may be due to venous dilation effects, which are not predicted by the modelling. These changes are averaged out in the mean dataset. The model would predict a more profound change in venous volume in subjects where the maximum pressure of the Valsalva manoeuvre exceeds the resting intracranial venous pressure. This may have occurred in volunteers 4 and 8 but is not demonstrated in the modelling results due to an overestimate of initial venous pressure values in these subjects.

In conclusion, the BOLD signal changes that are observed follow those predicted by the modelling reasonably well, and these changes are mainly attributed to deoxyhaemoglobin changes, which in turn are found to be primarily as a result of flow alterations.

8.5 Physiological importance and questions

As well as the impact of these results on the technique of functional MRI, the experiments also provide information regarding the physiological changes occurring during these blood pressure challenges, particularly in the venous vasculature, which is poorly understood and under-investigated at the moment. The main questions that are addressed by this work are:

1) *Which physiological factors dominate the BOLD signal changes observed in response to rapid blood pressure changes?*
2) *What are the implications of these changes on functional MRI studies?*

3) *Can information about the physiological processes occurring (i.e. autoregulation) be deduced from these studies?*

4) *Can any information about intracranial pressure be derived from this data?*

Question 1

Which physiological factors dominate the BOLD signal changes observed in response to rapid blood pressure changes?

The modelling work that has been carried out in this project has attempted to answer this question by examining the blood flow, blood volume and deoxyhaemoglobin changes in response to arterial blood pressure changes. In many studies, the haemodynamics of the BOLD response to blood pressure alterations are not considered and it is purely the neuronal response that is of interest. However, it is valuable to examine these haemodynamic changes as they form the basis of BOLD signal changes and may provide new information about cerebral vasculature. In these experiments it is assumed that metabolism is constant and the only stimuli are due to blood pressure changes.

In each of the blood pressure challenges employed in this study, thigh cuff deflation and the Valsalva manoeuvre, there are different physiological changes occurring. The blood pressure alterations due to thigh cuff deflation are much simpler than those occurring during the Valsalva manoeuvre, particularly in relation to the venous vasculature. An important consideration in the venous vasculature is the venous volume change that takes place, as this change could have a large impact on the BOLD signal.

The sensitivity of the BOLD signal to different vascular compartments is a complex interaction, but the largest sensitivity is theoretically in the veins (in a gradient echo EPI acquisition), due to the oxygenation changes in this compartment during flow changes. Boxermann[106] used a model to quantify

the contribution of intravascular spins to the BOLD signal and found it to be a maximum of 70% of the total signal. This model also predicted that the intravascular contribution of venules and veins to the signal exceeded that of capillaries. This is because, assuming minimal dilution, the oxygenation of the venous blood after traversing the capillary bed is substantially less than the average capillary blood oxygenation, so there is a greater signal change in venous blood than in capillaries. Also, even at equivalent levels of oxygenation, spins within venules or larger venous vessels produce greater changes in T_2* than spins within capillaries (due to greater diffusion effects over larger distances in these larger vessels). The signal from capillaries is still significant, which means that signal from the larger vessels can be nulled and a signal can still be detected. This can be achieved by using bipolar gradients to remove signal from rapidly flowing spins in these larger vessels. An interesting and valuable extension to this project would be to see how signal from these two compartments (the micro and macrovasculature) varies in similar experiments, if signal from each of them can be separated and studied independently. This could be achieved by using bipolar gradients or spin echo and gradient echo EPI sequences, which are sensitive to signal from different vascular compartments[103].

Considering the action of thigh cuff deflation, Rosengarten *et al*[226] used a transcranial Doppler technique to observe a positive net effect (i.e. increase in cerebral blood volume) after thigh cuff deflation, where there was a relatively smaller decrease in blood inflow (arterial blood flow) than outflow (venous blood flow). This will result in an increase in intracranial blood volume, which is thought to increase blood oxygen extraction. This will result in increased levels of deoxygenated blood compared to oxygenated blood. However, this is a transient effect that does not last after the effective onset of cerebral autoregulation. As these measurements were made using transcranial Doppler rather than BOLD MRI, only blood flow has been considered and blood volume changes are inferred from the flow changes in the arterial and venous components of the vasculature. Such venous volume

changes were not apparent from the modelling implemented in this project; in fact the opposite effect was seen. This requires further investigation in the future.

Another model that has been proposed is by Hoge[227] who describes the Deoxyhaemoglobin Dilution Model. This model was mainly concerned with the coupling between cerebral blood flow and oxygen consumption (and oxygen consumption assumed to be constant in these experiments), however the paper highlighted some interesting observations regarding the regulation of cerebral blood flow and cerebral blood volume. They stated that cerebral blood volume is highly correlated with steady state perfusion, which is in turn regulated by the varying the diameter of the arterioles feeding a volume of tissue. They hypothesised that neurally mediated arteriolar dilation is the mechanism that regulates cerebral blood flow (i.e. the autoregulation mechanism). The influence of this on the BOLD signal is insignificant, as this comprises a small fraction of total cerebral blood volume and contains negligible amounts of deoxyhaemoglobin. However, they concluded that BOLD MRI relevant changes in total CBV are therefore mainly due to *passive* inflation of venules (as opposed to the *active* inflation of the arterioles) caused by the elevation of venous blood pressure when arteriolar resistance is lowered. They and others (Kannurpatti[147] *et al* and Iannetti[13] *et al*) consider the case of static autoregulation, and the increase in venous blood pressure and consequently venous volume during arterial vasodilation. During the dynamic changes taking place in the experiments in this project, there will be additional pressure dynamics before and during the volume changes that take place (due to autoregulation) and the dynamic time course of flow and volume changes are what is observed in this project.

Conversely, studies by Gozzi[119] and Zaharchuk[81] report that significant cerebral blood volume changes do not occur during blood pressure alterations within the range of autoregulation as these changes are only thought to occur in the arterioles. However, Zaharchuk found that during hypoperfusion, CBV changes occurred in both the microvasculature (the

arterioles) and the larger vessels (the veins), i.e. once the autoregulatory capacity of arterioles is exhausted, venous vasodilation is the source of the CBV changes in total CBV (as well as arteriolar dilation).

Aaslid[228] has found in transcranial Doppler measurements that the propagation of flow measurements takes place almost simultaneously between the arterial and venous systems in the cerebral circulation, and as such, arterial, capillary and venous measurements of blood flow are almost equivalent for the analysis of autoregulation responses. If this were the case, the venous volume change would be negligible and as a result, flow and autoregulation may be a more dominant factor (rather than venous volume changes) in the signal changes observed in these experiments. This disagrees with work by Rosengarten[226], who observed a difference between arterial and venous blood flow recovery after thigh cuff deflation. Rosengarten is considering the case of dynamic autoregulation during rapid changes in blood pressure, which is what is being imposed in this study. So, according to Aaslid's findings, flow and autoregulation will have a dominant effect on the BOLD signal and arterial blood flow changes will reflect flow in the venous vasculature and the corresponding BOLD signal. Looking at the modelling results for thigh cuff deflation, there is no overshoot of venous blood volume after recovery of blood flow, which would be in agreement of this study by Aaslid, indicating a minimal change in venous dilation and venous volume. There would have to be a large change in venous volume for this to be the dominant factor in the BOLD signal changes that the modelling predicts.

When considering the changes taking place during the Valsalva manoeuvre it is valuable to consider what is happening throughout the cerebral vasculature, in particular the venous vasculature both intra and extra-cranially. A signal change similar to those observed in response to the Valsalva manoeuvre in this project has been seen in other studies by Gareffa[22,138]. They hypothesise that negative signal changes resulting from the action of the Valsalva manoeuvre are due to a slowing down of venous

blood flow resulting in venous dilation and an increase in deoxyhaemoglobin. The manoeuvre results in a high intra-thoracic pressure, the consequence of which is that blood pools in the jugular veins, leading to high pressure in these vessels associated with this increase in volume. In our model, flow is not impeded because venous pressure is maintained above this threshold. In theory, venous flow should slow down, but it doesn't due to the effect of the simultaneous initial increase in arterial blood pressure. Venous dilation is seen in the measurements made in the jugular vein, but this seems to have minimal impact on the venous flow and intracranial venous volume changes derived from this model. This is due to the relative magnitude of intracranial venous pressure, which is greater than the blood pressure in a large draining vein such as the internal jugular vein throughout the Valsalva manoeuvre. This results in arterial pressure changes (rather than jugular pressure changes) still being the principal mediator of venous volume changes in response to the Valsalva manoeuvre, and characteristics relating to the ABP changes are observed in the BOLD response in this study (phase I and phase IV changes). The BOLD signal changes are predominantly affected by deoxyhaemoglobin changes which have been most influenced by venous flow, which is in turn altered by arterial pressure rather than venous pressure.

So, it is not venous volume changes that primarily affect the BOLD signal during these dynamic blood pressure challenges, but the changes in deoxyhaemoglobin levels and these changes are predominantly influenced by flow changes as a result of arterial blood pressure changes. These changes in deoxyhaemoglobin have an effect on the extravascular signal around the venous vasculature, resulting in BOLD signal changes.

Question 2

What are the implications of these changes on functional MRI studies?

The rapid changes in blood pressure imposed in this study do influence the corresponding BOLD signal. This is a new finding that concurs to a certain

extent with some other studies that have been published[17,19,120]. However, few studies have investigated the haemodynamics of this result; the main focus has been the neuronal response of such provocation and the resulting BOLD response. Results from this study would indicate that there would be some implications for functional MRI studies.

It has been found that blood pressure alterations do arise during some functional MRI experiments[9,10], although observations tend to be over a longer timescale than the blood pressure changes imposed in this study. In studies where blood pressure changes were found to have no impact on BOLD signal intensity changes, this is often attributed to the efficiency of the autoregulation mechanism, and if this were to become impaired, then signal changes may result which are not related solely to neuronal activation. The changes seen in this study become apparent when data is averaged from nine volunteers. It may be that on an individual basis effects from blood pressure variations are obscured as noise in the data and in addition become averaged out in a block design type of functional MRI experiment. However, if these changes are large and temporally correlated with the paradigm used in the experiment, then erroneous signal changes may result, leading to inaccurate maps of neuronal activation.

The detection of neuronal activation in the presence of blood pressure changes was investigated by Wang[19] and it was concluded that transient BP changes (greater than 10 mmHg over a 10 s period) do have implications for functional MRI studies, particularly in a state of transient hypertension, even in healthy brain. The widespread BOLD changes that were detected during hypertension were thought to be more likely due to increased blood flow rather than neuronal activation. It would be difficult to distinguish this pressure invoked effect from that of a neuronal effect if BP changes are coincident with the experimental paradigm, for example in stress studies[9]. Hypotension has less of an effect on the detection of neuronal activation.

The study by Henderson *et al*[17] showed different BOLD responses in specific areas of the brain associated with baroreceptor activity in barodenervated animals, compared to those with baroreceptors intact, in response to a blood pressure challenge. They concluded that signal changes were due to the effect of blood pressure changes on baroreceptors rather than global changes in blood flow. This is a different conclusion to that from Wang[19]. The time resolution of the images acquired in this study was 4 s, and the pharmacologically induced blood pressure changes were induced over an 8 s period, which makes direct comparison with the results in our study difficult.

Modelling work by Payne[23] indicates that arterial pressure changes do affect the BOLD signal but this has not been investigated experimentally. This study has used a similar modelling approach as used in our project, i.e. combining Ursino and Buxton's models to predict BOLD signal changes and also includes the effects of CO_2 changes and neuronal activation as well as ABP changes. An increase in ABP of 10 mmHg was stimulated for 1 s, which resulted in a peak 0.22% increase in BOLD amplitude and a 3.5% drop in deoxyhaemoglobin. The author also concludes that autoregulation status has an effect on the response of the brain to neuronal stimulation.

Neuronal changes in response to the Valsalva manoeuvre (similar to those investigated in the above study by Henderson) have been seen in several studies[20,137,21]. However, more pertinent changes, similar to those observed in response to the Valsalva manoeuvre in this project have been seen in other studies by Gareffa[22,138]. As discussed above, they hypothesise that negative signal changes resulting from the action of the Valsalva manoeuvre are due to a slowing down of venous blood flow resulting in venous dilation and an increase in deoxyhaemoglobin levels. Gareffa's studies have not considered the blood pressure changes taking place during this type of manoeuvre. Although a similar negative signal change is seen in this study, there are other characteristics of the signal change, which relate to arterial blood pressure changes (for example changes during phase I and IV of the manoeuvre). These signal intensity changes would impact on functional MRI

studies if Valsalva type events occurred during such experiments, especially if these are correlated with the functional MRI paradigm.

Other physiological factors may also induce BOLD signal changes in functional MRI experiments, the main ones being respiration and cardiac related. These functions may also invoke blood pressure alterations, which could affect the BOLD signal. There have been a number of studies that investigate respiratory related changes in BOLD signal, in particular using breath holding as a method for assessing cerebrovascular reactivity[127,128,129,130,131,133,134,135] by altering CO_2 levels. It could be questioned whether such tasks only change CO_2, as some studies have reported the similarity of such tasks to the Valsalva manoeuvre[129,135] which is known to have a strong effect on blood pressure (although conversely studies have reported that CO_2 levels do not change during the Valsalva manoeuvre[137]). Windischberger[144] found that different regions in the brain are affected by cardiac and respiratory functions, with artefacts at cardiac frequencies occurring in the arterial vasculature whilst the venous vasculature is affected by respiration, due to an alternating intra-thoracic pressure affecting central venous pressure and venous back-flow to the heart. This results in variations in cerebral venous oxygenation during inspiration and expiration. It is suggested that the arterial pressure wave generated during systole is propagated to the cerebral arterial vasculature and this high frequency fluctuation in cerebral perfusion pressure is not compensated for by the autoregulation mechanism, and this is why cardiac frequency noise is often present in functional MRI data. This would agree with findings from this study that fast dynamic changes in arterial blood pressure do induce signal intensity changed in BOLD data. Wise *et al*[145] found significant correlation between the partial pressure of end tidal CO_2 levels and BOLD signal changes, although these are not thought to have a significant effect on arterial blood pressure.

Although spontaneous fluctuations in blood pressure may cause artefacts in standard functional MRI studies, resting state functional MRI could be used to

investigate these fluctuations and provide information about the autoregulation mechanism, similar to the approach used in transcranial Doppler measurements[87]. These signal variations are due to a variety of factors, including those mentioned above. Other factors include low frequency variations due to vasomotion of the arteries and higher frequency variations in cerebrovascular resistance and cerebral perfusion. The significance of these types to measurements to the assessment of autoregulation is discussed in answer to the next question.

A point that has been made in many studies of the BOLD response to arterial blood pressure changes is the fact that even if a change in BOLD signal is not always apparent, this is reliant on a healthy autoregulation mechanism[81,116,117,118]. Various pathological states, such as tumour, vascular disease, stroke or brain injury[27,28,11,12,29,229,230] can cause impairment of this autoregulation mechanism. It is important to consider this with regard to functional MRI studies. A disturbed autoregulation mechanism would lead to blood flow variations (as a result of blood pressure changes during the functional MRI experiment) that are not related to neuronal activity, even if neurovascular coupling is intact. Some studies have found that impaired cerebrovascular reactivity or cerebral autoregulation does affect the BOLD signal, for example in stroke, in the vicinity of tumours or in the case of stenosis of the cerebral arteries[12,14,15,16,132].

It would be difficult to distinguish between flow changes in response to blood pressure alterations or neuronal activation, especially as the response times of such mechanisms are similar[228]. In the case of disrupted autoregulation, oxygen delivery may also be impaired, which could itself depress the neuronal activity of interest[13]. Impaired autoregulation may also result in uncoupling of cerebral blood flow and metabolism for more than a few seconds, i.e. a delay in this coupling occurs[15]. It has also been found that brain activity affects dynamic cerebral autoregulation[231,232], which provides further evidence for the close relationship between neurovascular coupling and autoregulation.

In conclusion, the blood pressure variations imposed in this study do affect the BOLD signal. If such changes were to occur in a functional MRI experiment, particularly if these changes were correlated with the task, there may be changes in BOLD signal intensity that are not purely due to neuronal activity. Spontaneous changes in blood pressure may also cause artefacts in functional MRI studies; however, these changes may also be employed to investigate the autoregulation mechanism. Abnormal blood flow regulation as a result of pathology may result in incorrect blood flow changes in functional MRI experiments and inaccurate mapping of true neuronal activation.

Question 3

Can information about the physiological processes occurring (i.e. autoregulation) be deduced from these studies?

Cerebral autoregulation is the mechanism that adjusts blood flow in the brain in response to blood pressure changes. It has been frequently mentioned in previous discussions as a reason for the BOLD signal not being affected by slow changes in blood pressure, as this mechanism maintains blood flow in response to these changes, thus keeping the BOLD signal constant. However, if blood pressure changes are rapid, the autoregulation mechanism may not be able to respond immediately, and it is thought that this is what is occurring in the experiments carried out for this study. If this is the case then it may be that this mechanism can be investigated using the BOLD response to BP changes.

It is valuable to compare the time series of ABP, flow and BOLD signal changes following thigh cuff deflation, as this may provide information about the autoregulation response and whether it can be measured using BOLD imaging. The time taken for recovery of signal back to baseline levels following thigh cuff deflation is a parameter that reflects efficiency of autoregulation. In healthy subjects, blood flow should recover ahead of blood pressure, as a consequence of autoregulation. If this recovery can be

observed in BOLD data, then this type of measurement could be used as an assessment of the autoregulation mechanism. However, blood pressure would also have to be accurately recorded during the measurement. There are methods of quantifying autoregulation; for example the one proposed by Tiecks *et al*[68] involves setting up a model of blood flow recovery (following thigh cuff deflation) resulting from differing levels of autoregulation, which generates different blood flow recovery curves. The curve which most closely matches measured blood flow data is identified and an autoregulation index (ARI) can be derived[68].

In the thigh cuff experiments in this study, arterial blood pressure took 28.6 s ± 8.6 s to recover back to baseline levels, whereas blood flow took 17.17 s ± 3.02 s and signal recovery took 17.29 s ± 2.99 s in the modelled BOLD data and 12.21 s ± 4.69 s in the experimental BOLD data. Despite the discrepancy between the modelling and experimental results, which may be due to an underestimated representation of the action of normal autoregulation mechanism in the model, inaccuracies in blood pressure data obtained from Finapres measurements or false inflow effects in the experimental data, the BOLD signal does recovery ahead of the blood pressure measurements and is influenced by flow changes. This would imply that some measure of the autoregulation response could be made from similar BOLD data. However, these results are from data averaged over nine subjects, and derived from large grey matter regions of interest. For this to be a useful assessment of autoregulation this kind of measure needs to be achieved on an individual subject basis, and even more ideally, on a pixel-by-pixel basis, in more than one slice; this is discussed in the further work section.

Alternative measures of autoregulation can be made using the response of the Valsalva manoeuvre[85]. In transcranial Doppler studies[85], autoregulation indices have been proposed relating to the blood flow response to the blood pressure decrease during phase II, and also the blood flow increase in response to the blood pressure increase in phase IV. If similar changes could

be detected in the BOLD signal response to the Valsalva manoeuvre then this could lead to measures of autoregulation. The advantage of this technique is that it is a much easier methodology to implement within the MRI scanner, and is painless and non-invasive. Once again, accurate measurements of the blood pressure changes that are occurring would have to also be made.

The Ursino model implemented in this study incorporates constants that reflect the efficiency of autoregulation mechanism, a gain and a time constant of the smooth muscle response to blood flow alterations. These were set to values that characterise a normal state of autoregulation, but these could be altered to represent differing levels of autoregulation. This would lead to changes in the model predicted BOLD response, and if the model is accurate, then the experimental result can be matched to the model output corresponding to a certain degree of autoregulation. This is a similar approach to that used by Tiecks[68] to generate an autoregulation index from transcranial Doppler data. Payne[23] has also suggested such an approach and had produced theoretical curves for CBF and deoxyhaemoglobin corresponding to varying states of autoregulation. This aspect of Payne's study concludes that the state of autoregulation impacts upon the brain's response to neural stimulus, which provides motivation for the development of such a technique.

Spontaneous alterations of blood pressure may also provide information regarding the patency of the autoregulation mechanism; this has already been investigated in relation to transcranial Doppler measurements[233]. In a similar vein, resting state functional MRI examines spontaneous fluctuations in the BOLD signal, primarily to identify 'resting state networks' in the brain at rest[215,216]. One study has examined the resting fluctuations in arterial carbon dioxide and the corresponding fluctuations in BOLD signal[145] and it is postulated that these fluctuations can be used to map regional vascular responsiveness to carbon dioxide (i.e. cerebrovascular reactivity). A similar approach could be used to map autoregulation by examining the BOLD response to spontaneous alterations in blood pressure.

Question 4

Can any information about intracranial pressure be derived from this data?

Another aspect of this project has been to investigate the intracranial pressure (ICP) changes that occur during thigh cuff deflation and the Valsalva manoeuvre, and relate these to arterial and venous blood pressure alterations and tympanic membrane displacement (TMD) measurements.

In the case of the thigh cuff deflations, a decrease is observed in arterial and venous blood pressure. A decrease in TMD is also seen, but this does not correspond to the ICP prediction from the modelling, which shows an initial decrease in ICP before an increase, which arises from autoregulatory dilation and the implementation of the Monro-Kellie doctrine. It is thought that TMD measurements correspond to ICP changes[202], but this has only been observed in one patient. The other uncertainty in this comparison is the measurement of jugular vein pressure and the assumed relationship (for this part of the study) to intracranial venous pressure; this may not be a good assumption, particularly when considering the action of the Starling resistor.

The Valsalva manoeuvre induced a much more complex variation of vascular and intracranial pressures. There are several issues to note in this data. Firstly, modelled intracranial pressure changes follow arterial blood pressure changes much more closely (this is not seen in the thigh cuff deflation results) and this is not what is reported in the literature[85]. Secondly, jugular vein pressure increases and follows a similar time course to the TMD measurements. The similarity between jugular vein and TMD measurements is an interesting result. This is the first time such TMD measurements have been made, so this provides a useful starting point for further investigation.

8.6 Further work

This was initially conceived as a pilot study to investigate the effects of rapid changes in blood pressure on the BOLD signal. As such, there are a number

of improvements and developments that can be made to the methodology to take these investigations forward, concerning both the modelling and experimental aspects of the work.

Although the modelling has provided some valuable results, both the Ursino and Buxton model warrant further investigation. Investigation of the autoregulation mechanism and the action of the Starling resistor in the Ursino model would be beneficial. In particular the constants that define the actions of these mechanisms need to be explored and optimised. Refinement of the estimation of input parameters for the Buxton model, in particular the estimate of deoxyhaemoglobin would provide more accurate modelling results. There may be other physiological factors that could also be included in these models (either by estimate or measurement), such as CO_2 levels and metabolism changes.

It would be beneficial to carry out these experiments on a much larger subject group. As this was a pilot study, a small subject group was thought to be sufficient. Unfortunately there were certain issues with some subjects (for example movement artefacts), but as this was such a small subject group, it was thought not to be appropriate to disregard this data. Higher quality data could be obtained with a larger subject group as a result of being able to discount any erroneous datasets. In addition, a larger group of subjects may amplify the magnitude of the signal changes that are observed when the datasets averaged as random noise will be reduced. To minimise movement artefacts better head support should be employed, for example the use of a bite bar. More sophisticated motion correction could also be employed to take into account spin history effects.

Another important development of the methodology would be to employ different and more consistent blood pressure challenges, such as lower body negative pressure changes or square wave breathing paradigms. This would further strengthen the findings from this study and provide new information if

the results from these challenges were combined with different methods of data analysis.

There are much more sophisticated methods of image analysis that could be utilised with this data, and data that is acquired in the future. Previous studies have used Statistical Parametric Mapping[225] (SPM) to investigate correlations between blood pressure changes and BOLD signal changes on a spatial basis. This is a slightly different focus to that used in this particular study, but it would be a valuable extension of this work. For this kind of analysis to be used, careful consideration of the paradigm used to impose blood pressure changes would be required. Periodic changes in blood pressure would be a suitable methodology and this could be implemented by using either a square-wave breathing device to alter blood pressure (similar to the Valsalva manoeuvre) or a lower body negative pressure vacuum box, imposing square wave changes on the lower body to alter blood pressure.

Independent component analysis has been used to interrogate resting state functional MRI data[141,142,145] and could be used to investigate spontaneous changes in blood pressure and the corresponding effect on the BOLD signal. However, due to the magnitude of signal changes (caused by noise in the data), it may be difficult to detect signal changes, particularly on an individual case basis. Investigations at higher field strengths would improve the signal-to-noise-ratio (SNR) of the data. However, this may increase other EPI related artefacts in the data and in particular those related to magnetic susceptibility artefacts.

The development of the pulse sequence used in these studies could provide better quality data, free from artefacts from pulsations and minimise physiological noise in the data. A single-shot, spiral, k-space data acquisition method is less likely to be affected by brain pulsations and would reduce this type of cardiac induced physiological noise[127]. Any artefacts from inflow effects could be minimised by either further reducing the flip angle, by using spatial pre-saturation pulses[6] or diffusion sensitising (velocity nulling)

gradients[103]. It may be valuable to investigate the vascular specificity of the signal changes taking place by employing both spin-echo and gradient-echo EPI techniques. One major limitation of the sequence used in this project was that only one image slice could be acquired per time point. Using a more advanced EPI sequence, for example in conjunction with parallel imaging would result in greater brain coverage, whilst maintaining good or even improving temporal resolution[234,235]. It may also be possible to reduce susceptibility related artefacts using such techniques[236]. There should be careful consideration of the frequency of blood pressure changes (and other physiological changes) and the associated MRI sampling frequency, i.e. the repetition time of the sequence. Optimisation of the echo time of the sequence for this particular application would be beneficial. Mapping of static magnetic field inhomogeneities to enable correction of these would improve the quality of the EPI data.

An aim of this project was to investigate the potential of assessing autoregulation across the brain using BOLD MRI, and this may be possible if more sophisticated analysis of the data is carried out. For this aim to be achieved, analysis on a pixel-by-pixel basis would be preferable, rather than a region of interest based approach, in a similar way that whole brain maps are obtained in perfusion and diffusion imaging. This would require high SNR data, which could be optimised and obtained using the methods described above.

If such maps of autoregulation could be produced, then this may provide extremely valuable information for a wide range of neurological conditions, including stroke, epilepsy, dementia, sub-arachnoid haemorrhage and tumours (see Section 1.3). As well as possibly identifying abnormally autoregulating regions of the brain, which may not be picked up by standard perfusion imaging methods, this information would be valuable as a pre-surgical planning tool, and for improved interpretation of functional MRI studies.

8.7 Final conclusions

This study has provided new information about the BOLD response to two dynamic blood pressure provocations in healthy volunteers; thigh cuff deflation and the Valsalva manoeuvre. This type of study has not been carried out previously. By combining two models, the Ursino model of the cerebral vasculature and part of the Buxton model describing BOLD signal changes, BOLD signal changes were predicted in response to these two blood pressure alterations. Reasonable similarity was demonstrated between the BOLD modelling results and the experimental data when averaged over nine subjects. This provided information for the basis of the signal changes that have been observed and these are hypothesised to be primarily due to deoxyhaemoglobin changes as a result of flow, and to a lesser extent, volume changes induced by the blood pressure alterations.

This information has significant implications for BOLD studies where blood pressure alterations may be invoked, particularly if these alterations are concurrent with the functional MRI paradigm. This is also important in functional MRI studies in patients who exhibit impaired cerebral autoregulation, as blood pressure changes may cause spurious blood flow alterations that are interpreted as being due to neuronal activity.

The eventual benefit of these findings could be the development of an MRI technique that enables the mapping of autoregulation function across the brain; this is currently investigated in the middle cerebral artery using a transcranial Doppler technique and thus has very limited spatial specificity. This would be valuable in the management of a variety of neurological conditions and it could also improve the accuracy of functional MRI studies.

A final investigation as part of this study was to explore the intracranial pressure changes occurring during the two blood pressure challenges using tympanic membrane displacement. This has not been carried out before and although it was difficult to match these changes to those predicted by the modelling; the initial results provided a foundation for further studies.

References

[1] Lassen N A (1959) Cerebral blood flow and oxygen consumption in man. *Physiol. Rev.* **39**:183-238.

[2] Panerai RB (1998) Assessment of cerebral pressure autoregulation in humans – a review of measurement methods. *Physiological Measurement* **19**: 305-338.

[3] Ogawa S, Lee TM, Kay AR, Tank DW (1990) Brain magnetic resonance imaging with contrast dependent on blood oxygenation. *Proceedings of the National Academy of Sciences* **87**: 9868-9872.

[4] Detre JA, Zhang W, Roberts DA, Silva AC, Williams DS, Grandis DJ, Koretsky AP, Leigh JS (1994) Tissue specific perfusion imaging using arterial spin labelling. *NMR in Biomedicine* **7**: 75-82.

[5] Buxton RB (2002) *Introduction to functional magnetic resonance imaging: principles and techniques*. Cambridge University Press.

[6] Frahm J, Merboldt K-D, Hanicke W, Kleinschmidt A, Boecker H (1994) Brain or Vein - Oxygenation or Flow? On Signal Physiology in Functional MRI of Human Brain Activation. *NMR in Biomedicine* **7**: 45-53.

[7] Chalela JA, Alsop DC, Gonzalez-Atavalez JB, Maldjian JA, Kasner SE, Detre JA (2000) Magnetic resonance perfusion imaging in acute ischemic stroke using continuous arterial spin labeling. *Stroke* **31**: 680-687.

[8] Jezzard P and Ramsey NF (2004) Functional MRI. In *Quantitative MRI of the Brain: Measuring changes caused by disease.* Edited by Tofts P. John Wiley & Sons Ltd, Chichester, pp 420-428.

[9] Carter JR, Kupiers NT, Ray CA (2005) Neurovascular responses to mental stress. *Journal of Physiology* **564**: 321-327.

[10] Critchley HD, Corfield DR, Chandler MP, Mathias CJ, Dolan RJ (2000) Cerebral correlates of autonomic cardiovascular arousal: a functional neuroimaging investigation in humans. *Journal of Physiology* **563(1)**: 259-270.

[11] Holodny AI, Schulder M, Liu WC (2000) The effect of brain tumors on BOLD functional MR imaging activation in the adjacent motor cortex: implications for image guided neurosurgery. *American Journal of Neuroradiology* **21(8)**: 1415-1422.

[12] Hsu Y-Y, Chang C-N, Jung S-M, Lim K-E, Huang J-C, Fang S-Y, Liu H-L (2004) Blood oxygenation level-dependent MRI of cerebral gliomas during breath holding. *Journal of Magnetic Resonance Imaging* **19**: 160-167.

[13] Iannetti GD, Wise RG (2007) BOLD functional MRI in disease and pharmacological studies: room for improvement? *Magnetic Resonance Imaging* **25**: 978-988.

[14] Carusone LM, Srinivasan J, Gitelman DR, Mesulam MM, Parrish TB (2002) Hemodynamic response changes in cerebrovascular disease: Implications for functional MR imaging. *American Journal of Neuroradiology* **23**: 1222-1228.

[15] Röther J, Knab R, Hamzei F, Fiehler J, Reichenbach JR, Buchel C, Weiller C (2002) Negative dip in BOLD fMRI in caused by blood flow-oxygen consumption uncoupling in humans. *NeuroImage* **15**: 98-102.

[16] Hamzei F, Knab R, Weiller C, Röther J (2003) The influence of extra- and intracranial artery disease on the BOLD signal in FMRI. *NeuroImage* **20**: 1393-1399.

[17] Henderson LA, Richard CA, Macey PM, Runquist ML, Yu PL, Galons J-P, Harper RM (2004) Functional magnetic resonance signal changes in neural structures to baroreceptor reflex action. *Journal of Applied Physiology* **96**: 693-703.

[18] Kimmerley DS, O'Leary DD, Menon RS, Gati JS, Shoemaker JK (2005) Cortical regions associated with autonomic cardiovascular regulation during lower body negative pressure in humans. *Journal of Physiology* **569**: 331-345.

[19] Wang R, Foniok T, Wamsteeker J, Qiao M, Tomonek B, Vivanco RA, Tuor UI (2006) Transient blood pressure changes affect the functional magnetic resonance imaging detection of cerebral activation *NeuroImage* **31**: 1-11.

[20] King AB, Menon RS, Hachinski V, Cechetto DF (1999) Human forebrain activation by visceral stimuli. *Journal of Comparative Neurology* **413**: 572-582.

[21] Henderson LA, Macey PM, Macey KE, Frysinger RC, Woo MA, Harper RK, Alger JR, Yan-Go FL, Harper RM (2002) Brain responses associated with the Valsalva manoeuvre revealed by magnetic resonance imaging. *Journal of Neurophysiology* **88**: 3477-3486.

[22] Garreffa G, Colonnese C, Macri MA, Modugno N, Rocco R, Calistri V, De Cesare E, Venditti E, Maraviglia B (2003) BOLD signal sign and transient vessels volume variation. *Magnetic Resonance Imaging* **21**: 1207-1212.

[23] Payne SJ (2006) A model of the interaction between autoregulation and neural activation in the brain. *Mathematical Biosciences* **204**: 260-281.

[24] Fulesdi B, Limburg M, Bereczki D, Michels RPJ, Neuwirth G, Legemate D, Valikovics A, Csiba L (1997) Impairment of cerebrovascular reactivity in long-term type 1 diabetes, *Diabetes* **46**: 1840-1845.

[25] Fulesdi B, Limburg M, Bereczki D, Kaplar M, Molnar C, Kappelmayer J, Neuwirth G, Csiba L (1999) Cerebrovascular reactivity and reserve capacity in type II diabetes mellitus. *Journal of Diabetes Complications* **13**: 191-199.

[26] Edvinsson L, Mackenzie ET, McCulloch J (1993) *Cerebral blood flow and metabolism*. Raven Press Ltd, New York, pp 565-580.

[27] Steiner LA, Coles JP, Johnston AJ, Chatfield DA, Smielewski P, Fryer TD, Aigbirhio FI, Clark JC, Pickard JD, Menon DK, Czosnyka M (2003) Assessment of cerebrovascular autoregulation in head-injured patients: a validation study. *Stroke* **34**: 2404-2409.

[28] Panerai RB, Kerins V, Fan L, Yeoman PM, Hope T, Evans DH. (2004) Association between dynamic cerebral autoregulation and mortality in severe head injury. *British Journal of Neurosurgery* **18(5)**: 471-479.

[29] Haubrich C, Kohnke A, Diehl RR, Möller-Hartmann W, Klötzsch C. (2005) Impact of vertebral artery disease on cerebral autoregulation. *Acta Neurol Scand* **112**: 309-316.

[30] Reinhard M, Roth M, Guschlbauer A, Harloff J, Timmer M, Czosnyka M, Hetzel A (2005) Dynamic cerebral autoregulation in acute ischaemic stroke assessed from spontaneous blood pressure fluctuations. *Stroke* **36**: 1684-1689.

[31] Dütsch M, Devinsky O, Doyle W, Marthol H, Hilz MJ (2004) Cerebral autoregulation improves in epilepsy patients after temporal lobe surgery. *Journal of Neurology* **251**: 1190-1197.

[32] Cowan F, Eriksen M, Wertheim DPF (1989) Regulation of cerebral blood flow in the newborn preterm human infant. *Journal of Physiology* **417** 13P.

[33] Panerai RB, Kelsall AWR, Rennie JM, Evans DH (1995) Cerebral autoregulation dynamics in premature newborns. *Stroke* **26**: 74-80.

[34] Younkin DP, Reivich M, Jaggi JL, Obrist WD, Delivoria-Papadopoulos M (1987) The effect of hematocrit and systolic blood pressure on cerebral blood flow in newborn infants. *Journal of Cerebral Blood Flow and Metabolism* **7**: 295-299.

[35] Ramaekers VT, Casaer P, Daniels H, Marchal G (1992) The influence of blood transfusion on brain blood flow autoregulation among stable preterm infants. *Early Human Development* **30**: 211-220.

[36] Strandgaard S, Olesen J, Skinhoj E, Lassen NA (1973) Autoregulation of brain circulation in severe arterial hypertension. *British Medical Journal* **1**: 507-510.

[37] Fu CH, Yang CCH, Kuo TBJ (2005) Effects of different classes of antihypertensive drugs on cerebral hemodynamics in elderly hypertensive patients. *American Journal of Hypertension* **18**: 1621-1625.

[38] Nishizawa H and Kudoh I (1996) Cerebral autoregulation is impaired in patients resuscitated after cardiac arrest. *Acta Anaesthesiol. Scand.* **40**: 1149-53.

[39] Diehl RR, Linden D, Lucke D, Berlit P (1995) Phase relationship between cerebral blood flow velocity and blood pressure: a clinical test of autoregulation. *Stroke* **26**: 1801-1804.

[40] Newell DW, Aaslid R, Lam A, Mayberg TS, Winn HR (1994) Comparison of flow and velocity during dynamic autoregulation testing in humans. *Stroke* **25**: 793-797.

[41] White RP and Markus HS (1997) Impaired dynamic cerebral autoregulation in carotid artery stenosis. *Stroke* **28**: 1340-1344.

[42] Strauss G, Hansen BA, Kirkegaard P, Rasmussen A, Hjortrup A, Larsen FS (1997) Liver function, cerebral blood flow autoregulation and hepatic encephalopathy in fulminant hepatic failure. *Hepatology* **25**: 837-839.

[43] Hanon O, Haulon S, Lenoir H, Seux ML, Rigaud AS, Safar M, Girerd X, Forette F (2005) Relationship between arterial stiffness and cognitive function in elderly subjects with complaints of memory loss. *Stroke* **36**: 2193-2197.

[44] Qiu CX, Winblad B, Viitanen M, Fratiglioni L (2003) Pulse pressure and risk of Alzheimer disease in persons aged 75 years and older – a community-based, longitudinal study. *Stroke* **34**: 594-599.

[45] Niwa K, Kazama K, Younkin L, Younkin SG, Carlson GA, Iadecola C (2002) Cerebrovascular autoregulation is profoundly impaired in mice overexpressing amyloid precursor protein. *American Journal of Physiology* (*Heart Circulation Physiology)* **283**: H315–H323.

[46] Kennelly SP, Lawlor BA, Kenny RA (2009) Blood pressure and the risk for dementia – a double edged sword? *Ageing Research Reviews* **8(2)**: 61-70.

[47] Wierenga CE, Bondi MW (2007) Use of functional magnetic resonance imaging in the early identification of Alzheimer's disease. *Neuropsychology Reviews* **17(2)**: 127–143.

[48] Van der Zande FHR, Hofman PAM, Backes WH (2005) Mapping hypercapnia-induced cerebrovascular reactivity using BOLD MRI. *Neuroradiology* **47**: 114-120.

[49] Mandell DM, Han JS, Poublanc J, Crawley AP, Stainsby JA, Fisher JA, Mikulis DJ (2008) Mapping cerebrovascular reactivity using blood oxygen level-dependent MRI in patients with arterial steno-occlusive disease comparison with arterial spin labeling MRI. *Stroke* **39**: 2021-2028.

[50] Ursino M and Lodi CA (1998) Interaction among autoregulation, CO_2 reactivity, and intracranial pressure: a mathematical model. *American Journal of Physiology* **274** (*Heart Circulation Physiology* **43**): H1715-H1728.

[51] Buxton RB, Wong EC, Frank LR (1998) Dynamics of Blood Flow and Oxygenation Changes During Brain Activation: The Balloon Model. *Magnetic Resonance in Medicine* **39(6)**: 855-864.

[52] Obata T, Liu TT, Miller K, Luh W-M, Wong EC, Frank LR, Buxton RB (2004) Discrepancies between BOLD and flow dynamics in primary and supplementary

motor areas: application of the balloon model to the interpretation of BOLD transients. *NeuroImage* **21**: 144-153.

[53] Seeley RR, Stephens TD, Tate P (1995) *Anatomy and Physiology*, 3rd Edition, Mosby-Year Book Inc.

[54] Soloman EP, Schmidt RR, Adragna PJ (1990) *Human Anatomy and Physiology*, 2nd Edition. Saunders College Publishing.

[55] This article was published in Gray H, Standring S, Ellis H, Berkovitz BKB, *Gray's Anatomy: the anatomical basis of clinical practice*, 39th Edition, pp298-299, Copyright Elsevier Churchill Livingstone, Edinburgh (2005).

[56] Auer LM and Loew F (1983) The cerebral veins. An experimental and critical update. Springer-Verlag, Vienna.

[57] http://www.brain-aneurysm.com/ba1.html. Accessed 08/08/2007

[58] Guyton AC and Hall JE (2005) *Textbook of Medical Physiology.* 11th Edition, Elsevier Saunders, Philadelphia.

[59] Barakat AI, Lieu DK (2003) Differential responsiveness of vascular endothelial cells to different types of fluid mechanical shear stress. *Cell Biochemistry and Biophysics* **38(3)**: 323-343.

[60] Pfitzner J (1976) Poiseuille and his law. *Anaethesia* **31**: 273-275.

[61] Nichols WW and O'Rourke MF (1998) *McDonald's Blood Flow in Arteries.* 4th Edition, Oxford University Press, Oxford.

[62] Hudetz AG (1997) Blood flow in the cerebral capillary network: a review emphasizing observations with intravital microscopy. *Microcirculation* **4(2)**: 233-252.

[63] Stewart GN (1894) Research on the circulation time in organs on the influences which affect it, parts I-III. *Journal of Physiology (London)* **15**: 1.

[64] Grubb RL, Raichle ME, Eichling JO, Ter-Pogossian MM (1974) The effect of changes in pCO_2 on cerebral blood volume, blood flow and vascular mean transit times. *Stroke* **5**: 630-639.

[65] Mandeville JB, Marota JJA, Kosofsky BE, Keltner JR, Weissleder R, Rosen BR, Weisskoff RM (1998) Dynamic functional imaging of relative cerebral blood volume during rat forepaw stimulation. *Magnetic Resonance in Medicine* **39**: 615-624.

[66] Buijs J, van Bel F, Nandorff A, Hardjowijono R, Stijnen T, Ottenkamp J (1992) Cerebral blood flow pattern and autoregulation during open-heart surgery in infants and young children: a transcranial Doppler ultrasound study. *Critical Care Medicine* **20**: 771-777.

[67] Strebel S, Lam AM, Matta B, Mavberg TS, Aaslid R, Newell DW (1995) Dynamic and static cerebral autoregulation during isoflurane, desflurane, and profopol anesthesia. *Anesthesiology* **83:** 66-76.

[68] Tiecks FP, Lam AM, Aaslid R, Newell DW (1995) Comparison of static and dynamic cerebral autoregulation measurements. *Stroke* **26**: 1014-1019.

[69] Aaslid R, Lindegard K-F, Sorteberg W, Nornes H. (1989) Cerebral autoregulation dynamics in humans. *Stroke* **20(1)**: 45-52.

[70] Paulson OB, Strandgaard S, Edvinsson L (1990) Cerebral autoregulation. *Cerebrovascular and Brain Metabolism Reviews* **2(2)**: 161-192.

[71] Kontos HA, Wei EP, Navari RM, Levassuer JE, Rosenblum WI, Patterson JL (1978) Responses of cerebral arteries and arterioles to acute hypotension and hypertension. *American Journal of Physiology* **234**: H371-383.

[72] Bayliss WM (1902) On the local reaction of the arterial wall to changes of internal pressure. *Journal of Physiology* **28**: 220-231.

[73] McPherson RW, Koehler RC, Traystman RJ (1988) Effect of jugular venous pressure on cerebral auto-regulation in dogs. *American Journal of Physiology* **255(6)**: H1516-H1524.

[74] Faraci FM and Heistad DD (1998) Regulation of the cerebral circulation: role of endothelium and potassium channels. *Physiological Reviews* **78(1)**: 53-97.

[75] Edvinsson L, Nielsen KC, Owman C, West KA (1973) Evidence of vasoconstrictor sympathetic nerves in brain vessels of mice. *Neurology* **23**: 73-77.

[76] MacKenzie ET, Farrar JK, Fitch W, Graham DI, Gregory PC, Harper AM (1979) Effects of hemorrhagic hypotension on the cerebral circulation: part 1-cerebral blood flow and pial arteriolar calibre. *Stroke* **10**: 711-718.

[77] White RP, Vallance P, Markus HS (2000) Effect of nitric oxide synthase on dynamic cerebral autoregulation in humans. *Clinical Science (London)* **99(6)**: 555-560.

[78] Kety SS, Schmidt CF (1945) The determination of cerebral blood flow in man by use of nitrous oxide in low concentrations. *American Journal of Physiology* **143**: 53-66.

[79] Obrist WD and Wilkinson WE (1990) Regional cerebral blood-flow measurement in humans by Xe-133 clearance. *Cerebrovascular and Brain Metabolism Reviews* **2(4)**: 283-327.

[80] Birch AA, Morris SL (2003) Do the Finapres (TM) and Colin (R) radial artery tonometer measure the same blood pressure changes following deflation of thigh cuffs? *Physiological Measurement* **24(3)**: 653-660.

[81] Zaharchuk G, Mandeville JB, Bogdanov AA. (1999) Cerebrovascular Dynamics of Autoregulation and Hypoperfusion: An MRI study of CBF and changes in total and microvascular cerebral blood volume during hemorrhagic hypotension. *Stroke* **30**: 2197-2205.

[82] Aaslid R, Markwalder TM, Nornes H (1982) Non-invasive transcranial Doppler ultrasound recording of flow velocity in basal cerebral arteries. *Journal of Neurosurgery* **57 (6)**: 769-774.

[83] Czosnyka M, Guazzo E, Iyer V, Kirkpatrick P, Smielewski P, Whitehouse H, Pickard JD (1994) Testing of cerebral autoregulation in head injury by waveform analysis of blood flow velocity and cerebral perfusion pressure. *Acta Neurochir.* **60** (Supplement): 468-471.

[84] Smielewski P, Czosnyka M, Kirkpatrick P, McEroy H, Rutkowska H, Pickard JD (1996) Assessment of cerebral artery autoregulation using carotid artery compression. *Stroke* **27**: 2197-2203.

[85] Tiecks FP, Lam AM, Matta BF, Strebel S, Douville C, Newell DW (1995) Effects of the Valsalva maneuver on cerebral circulation in healthy adults: A transcranial Doppler study. *Stroke* **26**: 1386-1392.

[86] Birch AA, Dirnhuber MJ, Hartley-Davies R, Iannotti F, Neil-Dwyer G (1995) Assessment of autoregulation by means of periodic changes in blood pressure. *Stroke* **26**: 834-837.

[87] Panerai RB, Rennie JM, Kelsall AW, Evans DH (1998) Frequency-domain analysis of cerebral autoregulation from spontaneous fluctuations in arterial blood pressure. *Med Biol Eng Comput* **36(3)**: 315-322.

[88] Tsuji M, Saul JP, du Plessis A, Eichenwald E, Sobh J, Crocker R, Volpe JJ. (2000) Cerebral intravascular oxygenation correlated with mean arterial pressure in critically ill premature infants. *Pediatrics* **106**: 625-632.

[89] Munro MJ, Walker AM, Barfield CP (2004) Hypotensive extremely low birth weight infants have reduced cerebral blood flow. *Pediatrics* **114**: 1591-1596.

[90] Morren G, Naulaers G, Lemmerling P, Van Huffel S, Casaer P, Devlieger H. (2003) Quantitation of the concordance between cerebral intravascular oxygenation and mean arterial blood pressure for the detection of impaired autoregulation. *Adv Exp Med Biol* **510**: 403-408.

[91] Wagner BP, Pfenninger J (2002) Dynamic cerebral autoregulation responses to blood pressure rise measured by near-infrared spectroscopy and intracranial pressure. *Critical Care Medicine* **30(9)**: 2014-21.

[92] Bloch F, Hansen WW, Packard ME. (1946) Nuclear Induction. *Phys Rev* **69**: 127.

[93] Purcell EM, Torrey HC, Pound RV (1946) Resonance absorption by nuclear magnetic moments in a solid. *Phys Rev* **69**: 37-38.

[94] Damadian R (1971) Tumour detection by NMR. *Science* **171**: 1151-1153.

[95] Lauterbur P (1973) Image formation by induced local interaction: examples employing nuclear magnetic resonance. *Nature* **241**: 190-191.

[96] Damadian R, Minkoff L, Goldsmith M, Stanford M, Koutcher J. (1976) Tumour imaging in a live animal by field focussing NMR (FONAR). *Physiol Chem Phys* **9**: 61-5.

[97] Damadian R, Goldsmith, Minkoff L (1977) NMR in cancer XVI: FONAR imaging of the live human body. *Physiol Chem Phys* **9**: 97-100.

[98] Edelstein WA, Hutchison JMS, Johnson G, Redpath T (1980) Spin warp NMR imaging and applications to human whole body imaging. *Physics in Medicine and Biology* **25**: 751-756.

[99] Hutchison JMS (1996) MSc Course Notes, *NMR Deeper Study*. Department of Bio-Medical Physics and Bio-Medical Engineering, University of Aberdeen.

[100] Mansfield P (1977) Multi-planar image formation using NMR spin echoes. *Journal of Physics* **C10**: L55-58.

[101] Mansfield P (1984) Real time echo planar imaging by NMR. *British Medical Bulletin* **40**: 187-190.

[102] Zhou XJ (2004) Echo train pulse sequences. In *Handbook of MRI pulse sequences*. Edited by Bernstein MA, King KF, Zhou XJ. Elsevier Academic Press, London, pp 702-740.

[103] Jezzard P, Matthews PM, Smith SM (Editors) (2001) *Functional MRI: an introduction to methods.* Oxford University Press.

[104] Elster AD (1994) *Questions and Answers in Magnetic Resonance Imaging*. Mosby – Year Book, Inc.

[105] van Zijl PCM, Eleff SM, Ulatowski JA, Oja JME, Ulug AM, Traytsman RJ, Kaupinnen RA (1998) Quantitative assessment of blood flow, blood volume and blood oxygenation effects in functional magnetic resonance imaging. *Nature Medicine* **4(2)**: 159-167.

[106] Boxerman JL, Bandettini PA, Kwong KK, Baker JR, Davis TL, Rosen BR, Weisskoff RM (1995) The Intravascular Contribution to fMRI Signal Change - Monte Carlo Modeling and Diffusion-Weighted Studies In-Vivo. Article; 108. *Magnetic Resonance in Medicine* **34**: 4-10.

[107] Haacke EM, Lai S, Yablonskiy DA, Lin WL (1995) In Vivo Validation of the Bold Mechanism - a Review of Signal Changes in Gradient-Echo Functional MRI in the Presence of Flow. Article 29. *International Journal of Imaging Systems and Technology* **6**:153-163.

[108] Righini A, Pierpaoli C, Barnett AS, Waks E, Alger JR (1995) Blue blood or black blood: R_1 effects in gradient-echo echo-planar functional neuroimaging. *Magnetic Resonance Imaging* **13(3)**: 367-378.

[109] Vorstrup S, Paulson OB (1984) Effect of acetazolaminde on cerebral blood flow and cerebral metabolic rate for oxygen. *Journal of Clinical Investigation* **74**: 1634-1639.

[110] Meyer JS, Gotoh F (1961) Interaction of cerebral haemodynamics and metabolism. *Neurology* **11**: 46-65.

[111] Cotev S, Lee J, Severinghaus JW (1968) The effects of cerebral haemodynamics and metabolism. *Anesthesiology* **29(3)**: 471-477.

[112] Mukherjee B, Preece M, Houston GC, Papadakis NK, Carpenter TA, Hall LD, Huang CL-H (2005) Mapping the cerebral response to acetazolamide using graded asymmetric spin echo EPI. *Magnetic Resonance Imaging* **23**: 907-920.

[113] Kalisch R, Elbel G-K, Gossl C, Czisch M and Auer DP (2000) Blood pressure changes induced by arterial blood withdrawal influence BOLD signal in anaesthetized rats at 7 Tesla: implication for pharmacological MRI. *NeuroImage* **14**: 891-898.

[114] Auer LM, Ishiyama N, Pucher R (1987) Cerebrovascular reponse to intracranial hypertension. *Acta Neurochirurgica* **84(3-4)**: 124-128.

[115] Weiskoff RM (1999) Basic theoretical models of BOLD signal change. In *Functional MRI.* Edited by Moonen C and Bandettini PA. Springer, Berlin, Heidelberg, pp 115-123.

[116] Tuor UI, McKenzie E, Tomanek B (2002) Functional magnetic resonance imaging of tonic pain and vasopressor effects in rats. *Magnetic Resonance Imaging* **20**: 707–712.

[117] Luo F, Wu G, Li Z, Li S-J (2003) Characterisation of effects of mean arterial blood pressure induced by cocaine and cocaine methiodide on BOLD signals in the rat brain. *Magnetic Resonance in Medicine* **49**: 264-270.

[118] Liu H, Rainey C, Lauer KK, Piacentine L, Bloom A, Risinger R, Ward BD, Stein E, Li S-J (2006) Peripheral blood pressure changes induced by dobutamine do not alter BOLD signals in the human brain. *NeuroImage* **30**:745-752.

[119] Gozzi A, Ceolin L, Schwarz A, Reese T, Bertani S, Crestan V, Bifone A (2007) A multimodality investigation of cerebral haemodynamics and autoregulation in pharmacological MRI. *Magnetic Resonance Imaging* **25**: 826-833.

[120] Qiao M, Rushforth D, Wang R, Shaw RA, Tomanek B, Dunn JF, Tuor UI (2006) Blood-oxygenation-level-dependent magnetic resonance signal and cerebral oxygenation responses to brain activation are enhanced by concurrent hypertension in rats. *Journal of Cerebral Blood Flow and Metabolism* **27**: 1280-1289

[121] Bruhn H, Kleinschmidt A, Boecker H (1994) The effect of acetazolamide on regional cerebral blood oxygenation at rest and under stimulation as assessed by MRI. *Journal of Cerebral Blood Flow and Metabolism* **14**: 742-748.

[122] Kleinschmidt A, Steinmetz H, Sitzer M, Merboldt K-D, Frahm J (1995) Magnetic resonance imaging of regional cerebral blood oxygenation changes under acetazolamide in carotid occlusive disease. *Stroke* **26**: 106-110.

[123] Righini A, Orsi M, Tadeo CS (1998) fMRI changes in the brain associated with the carotid compression Test. *Journal of Computer Assisted Tomography* **22(4)**: 509-513.

[124] Lythgoe DJ, Williams SC, Cullinane M (1999) Mapping of Cerebrovascular Reactivity Using BOLD Magnetic Resonance Imaging. *Magnetic Resonance Imaging* **17(4)**: 495-502.

[125] Vesely A, Sasano H, Volgyesi G, Somogyi R, Tesler J, Fedorko L, Grynspan J, Crawley A, Fisher JA, Mikulis D (2001) MRI mapping of cerebrovascular reactivity using square wave changes in end tidal PCO_2. *Magnetic Resonance in Medicine* **45**: 1011-1013.

[126] Cohen ER, Ugurbil K, Kim SG (2002) Effect of basal conditions on the magnitude and dynamics of the blood oxygenation level-dependent fMRI response. *Journal of Cerebral Blood Flow and Metabolism* **22**: 1042-1053.

[127] Kastrup A, Li TQ, Takahashi A. (1998) Functional magnetic resonance imaging of regional cerebral blood oxygenation changes during breath holding. *Stroke* **29(12)**: 2641-2645.

[128] Kastrup A, Kruger G, Glover GH, Neumann-Haefelin T, Moseley ME (1999) Regional variability of cerebral blood oxygenation response to hypercapnia. *NeuroImage* **10**: 675-681.

[129] Li T-Q, Kastrup A, Takahashi AM, Moseley M (1999) Functional MRI of human brain during breath holding by BOLD and FAIR techniques. *NeuroImage* **9**: 243-249.

[130] Liu H-L, Huang J-C, Wu C-T, Hsu Y-Y (2002) Detectability of blood oxygenation level-dependent signal changes during short breath hold duration. *Magnetic Resonance Imaging* **20**: 643-648.

[131] Shiino A, Morita Y, Tsuji A, Maeda K, Ito R, Furukawa A, Matsuda A, Inubushi T (2003) Estimation of cerebral perfusion reserve by blood oxygenation level dependent imaging: comparison with single photon emission computed tomography. *Journal of Cerebral Blood Flow and Metabolism* **23**: 121-135.

[132] Krainik A, Hund-Georgiadis M, Zysset S, von Cramon YD (2005) Regional impairment of cerebrovascular reactivity and BOLD signal in adults after stroke. *Stroke* **36**: 1146-1152.

[133] Kannurpatti SS, Biswal BB (2004) Effect of anaesthesia on CBF, MAP and fMRI-BOLD signal in response to apnea. *Brain Research* **1011**: 141-147.

[134] Handwerker DA, Gazzaley A, Inglis BA, D'Esposito M (2007) Reducing vascular variability of fMRI data across aging populations using a breathholding task. *Human Brain Mapping* **28**: 846-859.

[135] Thomason M, Glover GH (2008) Controlled inspiration depth reduces variance in breath-holding induced BOLD signal. *NeuroImage* **39(1)**: 206-214.

[136] Bright MG, Bulte DP, Jezzard P, Duyn JH (2009) Characterization of regional heterogeneity in cerebrovascular reactivity dynamics using novel hypercapnia task and BOLD fMRI. *NeuroImage* **48**: 166-175.

[137] Harper RM, Bandler R, Spriggs D, Alger JR (2000) Lateralized and widespread brain activation during transient blood pressure elevation revealed by magnetic resonance imaging. *Journal of Comparative Neurology* **417**: 195-204.

[138] Garreffa G, Ken S, Macri MA, Giulietti G, Giove F, Colonnese C, Venditti E, De Cesare E, Galasso V, Maraviglia B (2003) BOLD signal and vessel dynamics: a hierarchical cluster analysis. *Magnetic Resonance Imaging* **24**: 411-418.

[139] Shmuel A, Yacoub E, Pfeuffer J, Van de Moortele PF, Adriany G, Hu X Urgubil K (2002) Sustained negative BOLD, blood flow and oxygen consumption response and its coupling to the positive response in the human brain. *Neuron* **36**: 1195-1210.

[140] Smith AT, Williams AL, Singh KD (2004) Negative BOLD in the visual cortex: evidence against blood stealing. *Human Brain Mapping* **21**: 213-220.

.

[141] Shmueli K, van Gelderen P, de Zwart JA, Horovitz SG, Fukunaga M, Jansma JM, Duyn JH (2007) Low-frequency fluctuations in the cardiac rate as a source of variance in the resting state fMRI BOLD signal. *NeuroImage* **38**: 306–20.

[142] Birn RM, Diamond JB, Smith MA, Bandettini PA (2006) Separating respiratory-variation-related fluctuations from neuronal-activity related fluctuations in fMRI. *NeuroImage* **31**: 1536–1548.

[143] Birn RM, Smith MA, Jones TB, Bandettini PA (2008) The respiration response function: The temporal dynamics of fMRI signal fluctuations related to changes in respiration. *NeuroImage* **40**: 644-654.

[144] Windischberger C, Langenberger H, Sycha T, Tschernko EM, Fuchsjager-Mayerl G, Schmetterer L, Moser E (2002) On the origin of respiratory artefacts in BOLD-EPI of the human brain. *Magnetic Resonance Imaging* **20**: 575-582.

[145] Wise RG, Ide K, Poulin MJ, Tracey I (2008) Resting fluctuations in arterial carbon dioxide induce significant low frequency variations in BOLD signal. *NeuroImage* **21**: 1652-1664.

[146] Auer DP (2008) Spontaneous low frequency blood oxygenation level-dependent fluctuations and functional connectivity analysis of the 'resting' brain. *Magnetic Resonance Imaging* **26**: 1055-1064.

[147] Kannurpatti SS, Biswal BB, Kim YR, Rosen BR (2008) Spatio-temporal characteristics of low-frequency BOLD signal fluctuations in isoflurane-anesthetised rat brain. *NeuroImage* **40**: 1738-1747.

[148] Razavi M, Eaton B, Paradiso S, Mani M, Hudetz AG, Bolinger L (2008) Sources of low frequency fluctuations in functional MRI signal. *Journal of Magnetic Resonance Imaging* **27**: 891-897.

[149] Monro A (1783) Observations on the structure and function of the nervous system. W Creech, Edinburgh.

[150] Kellie G (1824) Appearances observed in the dissection of two individuals; death from cold and congestion of the brain. *Trans. Med. Chir. Soc. Edinb.* **1**: 84-169.

[151] Fincham W and Tehrani FT (1983) On the regulation of cardiac output and cerebral blood flow. *Journal of Biomedical Engineering* **5**: 73-75.

[152] Hillen B (1986) The variability of the Circle of Willis: univariate and bivariate analysis. *Acta Morphologica* **24**: 87-101.

[153] Perktold K and Rappisch G (1995) Computer simulation of local blood flow and vessel mechanics in a compliant carotid artery bifurcation model. *Journal of Biomechanics* **28**: 845-856.

[154] Zagzoule M and Marc-Vergnes JP (1986) A global mathematical model of the cerebral circulation in man. *Journal of Biomechanics* **19(12)**: 1015-1022.

[155] Bekker A, Wolk S, Turndorf H, Kristol D, Ritter A (1996) Computer simulation of cerebrovascular circulation: assessment of intra-cranial hemodynamics during induction of anesthesia. *Journal of Clinical Monitoring* **12**: 433-444.

[156] Ursino M (1988) A mathematical study of human intracranial hydrodynamics. Part 1 – the cerebrospinal fluid pulse pressure. *Annals of Biomedical Engineering* **16**: 379-401.

[157] Ursino M (1988) A mathematical study of human intracranial hydrodynamics. Part 2 – simulation of clinical tests. *Annals of Biomedical Engineering* **16**: 403-416.

[158] Ursino M, Di Giammarco P (1988) A mathematical model of the relationship between cerebral blood volume and intracranial pressure changes: the generation of plateau waves. *Annals of Biomedical Engineering* **19**: 15-42.

[159] Ursino M, Magossa E (2001) Role of tissue hypoxia in cerebrovascular regulation: a mathematical modelling study. *Annals of Biomedical Engineering* **29**: 563-574.

[160] Lodi CA, Ter Minassian A, Beydon L, Ursino M (1998) Modeling cerebral autoregulation and CO_2 reactivity in patients with severe head injury. *American Journal of Physiology* **274** (*Heart Circulation Physiology* **43**): H1729-H1741.

[161] Ursino M, Lezzi M, Stocchetti N (1995) Intracranial pressure dynamics in patients with acute brain damage: a critical analysis with the aid of a mathematical model. *IEEE Transaction in Biomedical Engineering* **42**: 529-536.

[162] Ursino M and Giulioni M (2003) Quantitative assessment of cerebral autoregulation from transcranial Doppler pulsatility: a computer simulation study. *Medical Engineering and Physics* **23**: 655-666.

[163] Czonyka M, Pickard J, Whitehouse H, Piechnick S (1992) The hyperaemic response to a transient reduction in cerebral perfusion pressure – a modelling study. *Acta Neurochirugica (Wien)* **115**: 90-97.

[164] Czonyka M, Piechnick S, Richards HK, Kirkpatrick P, Smielewski P, Pickard JD (1997) Contribution of mathematical modelling to the interpretation of bedside tests of cerebrovascular autoregulation. *Journal of Neurology, Neurosurgery and Psychiatry* **63**: 721-731.

[165] Olufsen MS, Nadim A, Lipsitz LA (2001) Dynamics of cerebral blood flow regulation explained using a lumped parameter model. *American Journal of Physiological Regulatory Integrative Computation Physiology* **282**: R611-R622.

[166] Banaji M, Tachtsidis I, Delpy D, Baigent S (2005) A physiological model of cerebral blood flow control. *Mathematical Biosciences* **194**: 125-173.

[167] Olufsen MS (1999) Structured tree outflow condition for blood flow in larger systemic arteries. *American Journal of Physiology (Heart Circulation Physiology)* **276**: H257-H268.

[168] Olufsen MS, Peskin CS, Kim Y, Pedersen EM, Nadim EM and Larsen J (2000) Numerical simulation and experimental validation of blood flow in arteries with structured-tree outflow conditions. *Annals of Biomedical Engineering* **28**: 1281-1299.

[169] Stergiopulos N, Young DF and Rogge TR (1992) Computer simulation of arterial flow with applications to arterial and aortic stenosis. *Journal of Biomechanics* **25**: 1477-1488.

[170] Westerhof N, Bosman F, DeVries CJ and Noordergraaf A (1969) Analog studies of the human systemic arterial tree. *Journal of Biomechanics* **2**: 121-143.

[171] Jung A, Faltermeier R, Rothoerl R, Brawanski A (2005) A mathematical model of cerebral circulation and oxygen supply. *Journal of Mathematical Biology* **51**: 491-507.

[172] Marmarou A, Shulman K, LaMorgese J (1975) Compartmental analysis of compliance and outflow resistance of the cerebrospinal fluid system. *Journal of Neurosurgery* **43**: 523-534.

[173] Ogawa S, Menon RS, Tank DW, Kim S-G, Merkle H, Ellerman JM, Ugurbil K (1993) Functinal brain mapping by blood oxygenation level-dependent contrast magnetic resonance imaging: a comparison of signal characteristics with a biophysical model. *Biophysics Journal* **64**: 803-812.

[174] Davis TL, Kwong KK, Weisskoff RM, Rosen BR (1998) Calibrated functional MRI: mapping the dynamics of oxidative metabolism. *Proceeding of the National Academy of Sciences USA* **95**: 1834-1839.

[175] Buxton RB, Uludag K, Dubowitz DJ, Liu T (2004) Modelling the hemodynamic response to brain activation. *NeuroImage* **23**: S220-S233.

[176] Yablonsky DA, Haacke EM (1994) Theory of NMR signal behaviour in magnetically inhomogeneous tissues: the static dephasing regime. *Magnetic Resonance in Medicine* **32**: 749-763.

[177] Li D, Waight DJ, Wang Y (1998) In vivo correlation between blood T_2* and oxygen saturation. *Journal of Magnetic Resonance Imaging* **8**: 1236-1239.

[178] Friston KJ, Mechelli A, Turner R, Price CJ (2000) Nonlinear responses in fMRI: The balloon model, volterra kernels, and other hemodynamics. *NeuroImage* **12**: 466-477.

[179] Zheng Y, Johnston D, Berwick J, Chen D, Billings S, Mayhew J (2005) A three-compartment model of the hemodynamic response and oxygen delivery to the brain. *NeuroImage* **28**: 925-939.

[180] Huppert TJ, Allen MS, Benav H, Devor A, Jones P, Dale A, Boas D (2007) A multi-compartment vascular model for inferring arteriole dilation and cerebral metabolic changes during functional activation. *Journal of Cerebral Blood Flow and Metabolism* **27(6)**: 1262-1279.

[181] Kong Y, Zheng Y, Johnston D, Martindale J, Jones M, Billings S, Mayhew J (2004) A model of the dynamic relationship between blood flow and volume changes during brain activation. *Journal of Cerebral Blood Flow and Metabolism* **24(12)**: 1382-92.

[182] Zheng Y, Martindale J, Johnston D, Jones M, Berwick J, Mayhew J (2002) A model of the hemodynamic response and oxygen delivery to the brain. *NeuroImage* **16**: 617-637.

[183] Buxton RB and Frank LR (1997) A model for the coupling between cerebral blood flow and oxygen metabolism during neural stimulation. *Journal of Cerebral Blood Flow and Metabolism* **17**: 64-72.

[184] Behzadi Y, Liu TT (2005) An arteriolar compliance model of the cerebral blood flow response to neural stimulus. *NeuroImage* **25**: 1100-1111.

[185] Aubert A, Costalat R (2002) A model of the coupling between brain electrical activity, metabolism, and hemodynamics: application to the interpretation of functional neuroimaging. *NeuroImage* **17**: 1162-1181.

[186] Toronov V, Walker S, Gupta R, Choi JH, Gratton E, Hueber D, Webb A. (2003) The roles of changes in deoxyhaemoglobin concentration and regional cerebral blood volume in the fMRI BOLD signal. *NeuroImage* **19**: 1521-1531.

[187] Steinbrink J, Villringer A, Kempf F, Haux D, Boden S, Obrig H. (2006) Illuminating the BOLD signal: combined fMRI-fNIRS studies. *Magnetic Resonance Imaging* **24**: 495-505.

[188] Vazquez AL, Cohen ER, Gulani V, Hernandez-Garcia L, Zheng Y, Lee GR, Kim S-G, Grotberg JB, Noll DC (2006) Vascular dynamics and BOLD fMRI: CBF level effects and analysis considerations. *NeuroImage* **32**: 1642-1655.

[189] Emir UE, Ozturk C,and Akin A (2007) Multimodal investigation of fMRI and fNIRS derived breath hold BOLD signal with an expanded balloon model. *Physiological Measurement* **29**: 49-63.

[190] Sotero RC, Trujillo-Barreto (2008) Biophysical model for integrating neuronal activity EEG, fMRI and metabolism. *NeuroImage* **39**: 290-309.

[191] http://en.wikipedia.org/wiki/Valsalva_maneuver. Accessed on16/09/2009.

[192] Peñáz J (1973) Photoelectric measurements of blood pressure, volume and flow in the finger. *Digest 10th International Conference on Medical and Biological Engineering,* Dresden, Germany, p 104.

[193] Imholz BPM, Wieling W, van Montfrans GA, Wesseling KH (1998) Fifteen years experience with finger arterial pressure monitoring: assessment of the technology. *Cardiovascular Research* **38**: 605-616.

[194] Berczi A, Molnar AA, Apor A, Kovacs V, Ruzics C, Varallyay C, Huttl K, Monos E, Nadasy GL (2005) Non-invasive assessment of human large vein diameter, capacity, distensibility and ellipticity in situ: dependence on anatomical location, age, body position and pressure. *European Journal of Applied Physiology* **95**: 283-289.

[195] Beddy P, Geoghegan T, Ramesh A, Buckley O, O'Brien J, Colville J, Torreggiani WC (2006) Valsalva and gravitational variability of the internal jugular vein and common femoral vein: Ultrasound assessment. *European Journal of Radiology* **58**: 307-309.

[196] Lobato EB, Florete OG Jr, Paige GB, Morey TE (1998) Cross-sectional area and intravascular pressure of the right internal jugular vein during anaesthesia: effects of Trendelenburg position, positive intrathoracic pressure, and hepatic compression. *Journal of Clinical Anaesthesia* **10**: 1-5.

[197] Marchbanks R (1984) Measurement of Tympanic Membrane Displacement Arising form Aural Cardiovascular Activity, Swallowing, and Intra-aural Muscle Reflex. *Acta Otolaryngol (Stockh)* **98**: 119-129.

[198] Marchbanks RJ, Reid A, Martin AM, Brightwell AP, Bateman D (1987) The effect of raised intracranial pressure on intracochlear fluid pressure: three case studies. *British Journal of Audiology* **21**: 127–30.

[199] Marchbanks RJ (2003) Measurement of inner ear fluid pressure and clinical applications. In *Textbook of Audiological Medicine: Clinical aspects of hearing and balance*. Edited by Luxon L, Martin Dunitz Ltd, pp 289-307.

[200] Lang EW, Paulat K, Witte C, Zolondz J, Mehdorn M (2003) Noninvasive intracranial compliance monitoring. *Journal of Neurosurgery* **98**: 214-218.

[201] Doumoto Y, Oizumi T, Mizoi K, Matsuyama M, Ohira T, Toya S (1994) A trial of intracranial pressure measurement from external auditory canal – clinical analysis. *In: Intracranial Pressure IX*. Edited by Nagai H, Kamiya K, Ishii S. Springer-Varlag Tokyo.

[202] Lin J-P, Rosenthal E, Marchbanks R (2005) Non-invasive assessment of intracranial arterial and respiratory pressure waves via the trans-aural route. *Proceedings of the Physiological Society published in Journal of Physiology* **565**: C19.

[203] http://www.dim.hcuge.ch/osiris/01_Osiris_Presentation_EN.htm. Accessed on 20/09/2009.

[204] Bland JM and Altman DG (1986) Statistical methods for assessing agreement between two methods of clinical measurements. *The Lancet* February 8 1986: 307-310.

[205] Shen Q, Hongxia R, Duong TQ (2008) CBF, BOLD, CBV, and $CMRO_2$ fMRI signal temporal dynamics at 500-msec resolution. *Journal of Magnetic Resonance Imaging* **27**: 599-606.

[206] Silva AC and Lim S-G (1999) Pseudo-continuous arterial spin labeling technique for measuring CBF dynamics with high temporal resolution. *Magnetic Resonance in Medicine* **42**: 425-429.

[207] Woods RP, Cherry SR, Mazziotta JC (1992) Rapid automated algorithm for aligning and reslicing PET images. *Journal of Computer Assisted Tomography* **16**: 620-633.

[208] Rostrup E, Knudsen GM, Law I, Holm S, Larsson HBW, Paulson OB (2005) The relationship between cerebral blood flow and volume in humans. *NeuroImage* **24**: 1-11.

[209] ImageJ 1.40g, Wayne Rasband, National Institutes of Health, USA, http://rsb.info.nih.gov/ij/

[210] Ursino M, Giulioni M, Lodi CA. (1998) Relationship between cerebral perfusion pressure, autoregulation and transcranial Doppler waveform: a modeling study. *Journal of Neurosurgery* **89**: 255-266.

[211] Liu Y (2003) A study of mathematical modelling and signal processing of cerebral autoregulation. *PhD Thesis,* Institute of Sound and Vibration Research, University of Southampton.

[212] Huppert TJ, Allen MS, Diamond SG, Boas DA (2009) Estimating cerebral oxygen metabolism from fMRI with a dynamic multi-compartment windkessel model. *Human Brain Mapping* **30(5)**: 1548-1567.

[213] Boas DA, Jones SR, Devor A, Huppert TJ, Dale AM (2009) A vascular anatomic network model of the spatio-temporal response to brain activation. *NeuroImage* **40(3)**: 1116-1129.

[214] Diamond SG, Perdue KL, Boas DA (2009) A cerebrovascular response model for functional neuroimaging including dynamic cerebral autoregulation. *Mathematical Biosciences* **220**: 102-117.

[215] Biswal BB, Van Kylen J, Hyde JS (1997) Simultaneous assessment of flow BOLD signals in resting-state functional connectivity maps. *NMR in Biomedicine* **10**: 165-170.

[216] Lowe MJ, Mock BJ, Sorenson JA (1998) Functional connectivity in single and multislice echoplanar imaging using resting-state fluctuations. *NeuroImage* **7**: 119-132.

[217] Zanier ER, Rossi S, Conte V, Colombo A, Nicolini R, Caironi P, Stochetti N, Gattinoni L (2006) *Minerva Anesthesiol* **72**: 543-549.

[218] Friston KJ, William S, Howard R, Fracowiak RS, Turner R (1996) Movement-related effects in fMRI time-series. *Magnetic Resonance in Medicine* **35(3)**: 346-355.

[219] Dagli MS, Ingeholm JE, Haxby JV (1999) Localization of cardiac-induced signal change in fMRI. *NeuroImage* **9**: 407-415.

[220] Bhattacharyya PK and Lowe MJ (2003) Cardiac-induced physiologic noise in tissue is a direct observation of cardiac-induced fluctuations. *Magnetic Resonance Imaging* **22**: 9-13.

[221] Raj D, Anderson AW, Gore JC (2001) Respiratory effects in human functional magnetic resonance imaging due to bulk susceptibility changes. *Physics in Medicine and Biology* **46**: 3331-3340.

[222] Zhang W-T, Mainero C, Kumar A, Wiggins CJ, Benner T, Purdon PL, Bolar DS, Kwong KK, Sorensen AG (2006) Strategies for improving the detection of fMRI activation in trigeminal pathways with cardiac gating. *NeuroImage* **31**: 1506-1512

[223] Guimaraes AR, Melcher JR, Talavage TM, Baker JR, Ledden P, Rosen BR, Kiang NYS, Fullerton BC, Weisskoff RM (1999) Imaging subcortical auditory activity in humans. *Human Brain Mapping* **6**: 33-41.

[224] Duyn JH, Moonen CTW, van Yperen GH, de Boer RW, Luyten PR (1994) Inflow versus deoxyhaemoglobin effects in BOLD functional MRI using gradient echoes at 1.5 T. *NMR in Biomedicine* **7**: 83-88.

[225] Statistical Parametric Mapping: http://www.fil.ion.ucl.ac.uk/spm/

[226] Rosengarten B, Ruskes D, Mendes I, Stolz E (2002) A sudden arterial blood pressure decrease is compensated by an increase in intracranial blood volume. *Journal of Neurology* **249**: 538-541.

[227] Hoge RD, Atkinson J, Gill B, Crelier GR, Marrett S (1999) Investigation of BOLD Signal Dependence on Cerebral Blood Flow and Oxygen Consumption: The Deoxyhemoglobin Dilution Model. *Magnetic Resonance in Medicine* **42**: 849-863.

[228] Aaslid R, Newell DW, Stooss R, Sorteberg W, Lindegaard KF (1991) Assessment of cerebral autoregulation dynamics from simultaneous arterial and venous transcranial Doppler recordings in humans. *Stroke* **22**: 1148-1154.

[229] Dawson SL, Panerai RB, Potter JF (2003) Serial changes in static and dynamic cerebral autoregulation after acute ischaemic stroke. *Cerebrovasc.Dis*. **16:** 69–75.

[230] Golding EM, Robertson CS, Bryan RM Jr (1999) The consequences of traumatic brain injury on cerebral blood flow and autoregulation: a review. *Clinical Experimental Hypertension* **21**: 299-332.

[231] Rosengarten B, Hecht M, Kaps M (2007) Brain activity affects dynamic but not static autoregulation. *Experimental Neurology* **205**: 201-206.

[232] Panerai RB, Moody M, Eames PJ, Potter JF (2005) Dynamic cerebral autoregulation during brain activation paradigms. *American Journal of Physiology – Heart and Circulatory Physiology* **289**: H1202-H1208.

[233] Panerai RB, Rennie JM, Kelsall MR, Evans DH (1998) Frequency-domain analysis of cerebral autoregulation from spontaneous variations in blood pressure. *Med. Biol. Eng. Comput.* **36**: 315-322.

[234] Golay X, de Zwart JA, Ho YC, Sitoh YY (2004) Parallel imaging techniques in functional MRI. *Topics in Magnetic Resonance Imaging* **15(4)**: 255-265.

[235] de Zwart JA, van Gelderen P, Golay X, Ikonomidou VN, Duyn JH (2006) Accelerated parallel imaging for functional imaging of the human brain. *NMR in Biomedicine* **19**: 342-351.

[236] Winter JD, Poublanc J, Crawley AP, Kassner A (2009) Comparison of spiral imaging and SENSE-EPI at 1.5 and 3.0 T using a controlled cerebrovascular challenge. *Journal of Magnetic Resonance Imaging* **29(5)**: 1206-1210.